PONTIFICIA UNIVERSIDAD CATOLICA DE CHILE

ESCUELA DE INGENIERIA

GENOME-SCALE RECONSTRUCTION OF THE METABOLIC NETWORK IN *OENOCOCCUS OENI* AND ITS FUNCTIONAL ANALYSIS IN MALOLACTIC FERMENTATION

PABLO MARTÍN CAÑÓN AMENGUAL

Thesis submitted to the Office of Graduate Studies in partial fulfillment of the requirements for the Degree of Doctor in Engineering Sciences

Advisor:

EDUARDO AGOSÍN TRUMPER

Santiago de Chile, January 2021

PONTIFICIA UNIVERSIDAD CATOLICA DE CHILE

SCHOOL OF ENGINEERING

GENOME-SCALE RECONSTRUCTION OF THE METABOLIC NETWORK IN *OENOCOCCUS OENI* AND ITS FUNCTIONAL ANALYSIS IN MALOLACTIC FERMENTATION

PABLO MARTÍN CAÑÓN AMENGUAL

Members of the Committee:

EDUARDO AGOSÍN

JOSE RICARDO PÉREZ

EDMUNDO BORDEU

MARÍA ANGÉLICA GANGA

PATRICK LUCAS

GUSTAVO LAGOS

Thesis submitted to the Office of Graduate Studies in partial fulfillment of the requirements for the Degree of Doctor in Engineering Sciences

Santiago of Chile, January, 2021

¿En qué reino, en qué siglo, bajo qué silenciosa
conjunción de los astros, en qué secreto día
que el mármol no ha salvado, surgió la valerosa
y singular idea de inventar la alegría?

Con otoños de oro la inventaron. El vino
fluye rojo a lo largo de las generaciones
como el río del tiempo y en el arduo camino
nos prodiga su música, su fuego y sus leones.

En la noche del júbilo o en la jornada adversa
exalta la alegría o mitiga el espanto
y el ditirambo nuevo que este día le canto

otrora lo cantaron el árabe y el persa.
Vino, enséñame el arte de ver mi propia historia
como si ésta ya fuera ceniza en la memoria.

Soneto del vino
Jorge Luis Borges

ACKNOWLEDGEMENTS

I want to express my particular gratitude to my advisor, Prof. Eduardo Agosín, for his support, guidance and great patience throughout these professional and personal processes, and who allowed me to develop myself in many professional areas, beyond concerning my doctoral thesis.

I would like to give special thanks to the members of the committee, Professors José Ricardo Pérez, Edmundo Bordeu, María Angélica Ganga, Patrick Lucas and Gustavo Lagos, for their time to correct the final manuscript and the thoughtful comments on it.

I would like to give special thanks to *O. oeni* teamwork, Sebastián Mendoza, Dra. Ángela Contreras, Magdalena Ribbeck and Vicente Herrera, who spent many years studying malolactic fermentation together with me, and I also want to thank to Dr. Waldo Acevedo (Pontificia Universidad Católica de Valparaiso), Dr. Daniel Aguayo, Felipe Gomez y Jaime Huerta (Center for Bioinformatics and Integrative Biology, Universidad Andrés Bello), who were fundamental for the modeling and molecular dynamics of the malolactic enzyme.

Moreover, this thesis would not have been possible without the help of my Lab's friends; María Carolina Zúñiga, Isabel Moenne, Javiera López, Nicole Werner, Marcelo Orellana, Felipe Aceituno, Benjamin Sanchez, Martín Cárcamo, Francisco Saitua and Vicente Cataldo, as well as the School of Engineering, who were present not only throughout the development of my thesis, but also in the most difficult moment of my life.

I would like to thank my family, Alex, Verónica, Juan José, Felipe y Fernanda, without whose love and support none of this would have been possible.

Financial support: I really appreciate the financial support of the CONICYT through the Human Capital Formation Advanced Program National Doctoral Fellowship 2012 (Folio 21121015), FONDEF Grant D11i1139, Vice-rectory of Research UC (VRI), and the School of Engineering of Pontificia Universidad Católica de Chile to carry out my PhD studies.

LIST OF PAPERS

This thesis is based on the following papers, referred in the text by respective chapters:

Chapter I: Mendoza, S. N.[1], **Cañón, P. M.**[1], Contreras, A., Ribbeck, M., Agosín, E. (2017). **Genome-Scale Reconstruction of the Metabolic Network in *Oenococcus oeni* to Assess Wine Malolactic Fermentation.** *Frontiers in Microbiology* 8, 534.

Chapter II: Contreras, A., Ribbeck, M., Gutiérrez, G. D., **Cañon, P. M.**, Mendoza, S. N., and Agosin, E. (2018). **Mapping the Physiological Response of *Oenococcus oeni* to Ethanol Stress Using an Extended Genome-Scale Metabolic Model**. *Frontiers in Microbiology* 89, 291.

Chapter III: Acevedo, W., **Cañón, P. M**., Gómez-Alvear, F., Huerta, J., Aguayo, D., and Agosin, E. (2020). **L-Malate (-2) protonation state is required for efficient decarboxylation to L-lactate by the malolactic enzyme of *Oenococcus oeni*.** *Molecules* 25, 3431

[1] Sebastián Mendoza and Pablo Cañón are first authorships.

PROCEEDINGS

Parts of this work have also been presented at international congresses under the following references:

Pablo Cañón, Sebastián Mendoza, Magdalena Ribbeck, Ángela Contreras and Eduardo Agosín.
Genome-scale Metabolic Model of Oenococcus oeni.
In: *Macrowine* 2018.
Zaragoza, Spain.
May 2018 **(Oral Presentation).**

Pablo Cañón, Sebastián Mendoza, Magdalena Ribbeck, Ángela Contreras and Eduardo Agosín.
Genome-scale reconstruction of the metabolic network in Oenococcus oeni and its functional analysis.
In: *39th World Congress of Vine and Wine*
Bento Gonçalves, Brazil.
October 2016 **(Oral Presentation).**

Sebastián Mendoza, **Pablo Cañón** and Eduardo Agosín.
Genome-Scale metabolic model of Oenococcus oeni and its application to the analysis of the malolactic fermentation.
In: *OENOS 2015, 10e édition du Symposium International d´Oenologie*.
Bordeaux, France.
June 2015 **(Oral Presentation).**

FIGURE INDEX

TABLE INDEX

ABBREVIATION INDEX

AF: Alcoholic Fermentation.

COBRA: Constraint-Based Reconstruction and Analysis models.

Cx: Biomass concentration.

EFMA: Elementary Flux Mode Analysis

FBA: Flux Balance Analysis.

FVA: Flux variability analysis.

GENRE: Genome-Scale Metabolic Reconstructions.

GPR: Gene-Protein-Reaction relationship.

GSMM: Genome-Scale Metabolic Model.

HPLC: High-Performance Liquid Chromatography.

IPTG: Isopropyl β-D-1-thiogalactopyranoside.

ITC: Isothermal titration calorimetry.

LAB: Lactic Acid Bacteria.

lb: Lower bounds of the exchange reactions.

LDH: Lactate dehydrogenase.

m: Number of measured variables.

$m_{ATP:}$ ATP maintenance.

MAL: L-malic acid.

MAL^{-} : L-malate (−1).

MAL^{2-}: L-malate (−2).

MD: Molecular Dynamics.

MDH: L-malate dehydrogenase.

ME: Malic Enzyme.

MFA: Metabolic Fluxes Analysis.

MLE: Malolactic Enzyme.

MLF: Malolactic Fermentation.

MM/GBSA: Molecular Mechanics/Generalized Born Surface Area.

MW: Molecular weight [g/mmol].

n: Number of measurements per variable.

NGAME: Non-Growth Associated Maintenance Energy.

OADC: Oxaloacetate decarboxylase.

OD: Optical density.

PCR: Polymerase Chain Reaction.

QPLD: Quantum Polarized Ligand Docking.

S: Stoichiometric Matrix (m x n).

SSN: Sequence Similarity Network.

t: Time [h].

Greek Letter:

μ: Growth rate in [1/ h].

LIST OF CONTENT

PONTIFICIA UNIVERSIDAD CATÓLICA DE CHILE
ESCUELA DE INGENIERÍA

GENOME-SCALE RECONSTRUCTION OF THE METABOLIC NETWORK IN *OENOCOCCUS OENI* AND ITS FUNCTIONAL ANALYSIS IN MALOLACTIC FERMENTATION

Thesis submitted to the Office of Graduate Studies in partial fulfillment of the requirements for the Degree of Doctor in Engineering Sciences by

PABLO MARTÍN CAÑÓN AMENGUAL

ABSTRACT

Oenococcus oeni is the main agent in Malolactic fermentation (MLF) in wines, responsible for the decarboxylation of L-malic into L-lactic acid. MLF is a key process in winemaking, reducing the acidity of wine and contributing with flavor complexity and microbiological stability, but is erratic and unpredictable. Despite its pivotal role, the whole process is not yet fully understood. Aiming to improve the comprehension of this bacterium and this process, we constructed and exhaustively curated the first genome-scale metabolic model (GSMM) of *Oenococcus oeni* PSU-1 strain (iSM454). Then, we studied its growth under different ethanol conditions, determining the redistribution of intracellular metabolic fluxes, and ultimately, we generated a malolactic enzyme (MLE) homology model.

In silico experiments revealed that nutritional requirements are predicted by the iSM454 GSMM with an accuracy of 93%. Then, the model was applied to determine the non-growth associated maintenance. Results showed that *O. oeni* cultured at 12% ethanol concentration spent thirtyfold more ATP to stay alive than in the absence of ethanol. Most of this ATP was employed for extruding protons outside the cell.

In vitro experiments were performed in MaxOeno, a wine-like defined culture medium developed and optimized by us. The integration of experimental data with iSM454

model allowed to determine the redistribution of intracellular metabolic fluxes, under different ethanol conditions (0 to 12% v/v). Four growth phases were clearly identified during the batch cultivation of *O. oeni* PSU-1 strain, according to the consumption of malic and citric acids, sugars and amino acids uptake, and biosynthesis rates of metabolic products – biomass, erythritol, mannitol, and acetic acid, among others. We found that, under increasing ethanol conditions, *O. oeni* favors anabolic reactions related with cell maintenance, as the requirements of $NAD(P)^+$ and ATP augment.

Finally, a MLE homology model, together with quantum polarized ligand docking (QPLD), was used to describe the MLE binding pocket and pose of L-malic acid (MAL) and it deprotonates states MAL^- and MAL^{2-}. MAL^{2-} has the lowest $\Delta G_{binding}$, followed by MAL^- and MAL, with values of −23.8, −19.6, and −14.6 kJ/mol, respectively, consistent with those obtained by isothermal titration calorimetry (ITC) assays. Furthermore, molecular dynamics and MM/GBSA results suggest that only MAL^{2-} displays an extended open conformation at the binding pocket, satisfying the geometrical requirements for Mn^{2+} coordination, a critical component of MLE activity.

We expect that the GSMM (iSM454) and MLE homology model described here, supply unique tools to understand and predict the successful completion of wine malolactic fermentation carried out by *O. oeni*, as well as the difficulties the process can eventually face in any particular physico-chemical condition.

Members of the Doctoral Thesis Committee:

Eduardo Agosín Trumper
José Ricardo Pérez Correa
Edmundo Bordeu Schwarze
María Angélica Ganga Muñoz
Patrick Lucas
Gustavo Lagos Cruz-Coke

Santiago, September 2020

PONTIFICIA UNIVERSIDAD CATÓLICA DE CHILE
ESCUELA DE INGENIERÍA

RECONSTRUCCIÓN A ESCALA GENÓMICA DE LA RED METABÓLICA EN *OENOCOCCUS OENI* Y SU ANÁLISIS FUNCIONAL EN LA FERMENTACIÓN MALOLÁCTICA

Tesis enviada a la Dirección de Postgrado en cumplimiento parcial de los requisitos para el grado de Doctor en Ciencias de la Ingeniería por

PABLO MARTÍN CAÑÓN AMENGUAL

RESUMEN

Oenococcus oeni es el agente principal de la fermentación maloláctica en vinos, responsable de la descarboxilación del ácido L-málico a ácido L-láctico. Es un proceso clave en la vinificación, reduciendo la acidez y aportando complejidad aromática y estabilidad microbiológica, pero es errático e impredecible Pese a su rol crucial, el proceso no es aún entendido del todo. Para mejorar la comprensión de la bacteria y el proceso, se construyó y curó el primer modelo metabólico a escala genómica de *O. oeni* cepa PSU-1 (iSM454). Luego, se estudió su crecimiento bajo distintas condiciones de etanol, determinando la redistribución de los flujos metabólicos intracelulares, y, por último, se generó un modelo por homología de la enzima maloláctica.

Los experimentos *in silico* revelaron que el modelo iSM454 predice los requerimientos nutricionales con una exactitud del 93%. Luego, éste se aplicó para determinar la energía de mantención no asociada a crecimiento. Los resultados mostraron que el *O. oeni* cultivado al 12% de concentración de etanol gastaba treinta veces más ATP para mantenerse vivo que en su ausencia. La mayor parte de este ATP era empleado en la extrusión de protones fuera de la célula.

Los experimentos *in vitro* se llevaron a cabo en MaxOeno, un medio de cultivo definido y similar al vino, desarrollado y optimizado para el estudio. La integración de los datos

experimentales con el modelo permitió determinar la redistribución de los flujos metabólicos intracelulares bajo diferentes condiciones de etanol (0 a 12% v/v). Se identificaron claramente cuatro fases de crecimiento durante el cultivo por lote de la cepa PSU-1 del *O. Oeni*, según el consumo de los ácidos málico y cítrico, la absorción de azúcares y aminoácidos, y las tasas de biosíntesis de productos metabólicos – biomasa, eritritol, manitol y ácido acético, entre otros. Se halló que, bajo condiciones de etanol crecientes, el *O. oeni* favorece reacciones anabólicas relacionadas con el mantenimiento celular, mientras los requerimientos de $NAD(P)^+$ y ATP aumentan.

Finalmente, se usó un modelo por homología de la enzima maloláctica y la técnica de *quantum polarized ligand docking* para describir el sitio de unión y ubicación del ácido L-málico (MAL) y sus estados desprotonados MAL^- y MAL^{2-}. MAL^{2-} tuvo el más bajo $\Delta G_{binding}$, seguido por MAL^- y MAL, con valores de −23.8, −19.6 y −14.6 kJ/mol, respectivamente, consistente con los valores obtenidos en los ensayos de titulación de calorimetría isotérmica (ITC). Los resultados de dinámica molecular y de MM/GBSA sugieren que sólo el MAL^{2-} exhibe una conformación abierta extendida en el sitio de unión, que cumple los requerimientos geométricos para la coordinación con Mn^{2+}, componente crítico de la actividad de la enzima maloláctica.

Se espera que iSM454 y el modelo de homología para la enzima maloláctica descritos aquí, provean herramientas únicas para comprender y predecir la compleción de la fermentación maloláctica en el vino por *O. Oeni*, así como los inconvenientes que el proceso puede eventualmente afrontar en cualquier condición físico-química particular.

Miembros de la Comisión de Tesis Doctoral:

Eduardo Agosín Trumper

José Ricardo Pérez Correa

Edmundo Bordeu Schwarze

María Angélica Ganga Muñoz

Patrick Lucas

Gustavo Lagos Cruz-Coke

Santiago, Septiembre 2020

1. INTRODUCTION

1.1 Motivation

Chile is the sixth wine producer and the fourth wine exporter worldwide. The international market is dominated by three main exporters (Spain, Italy and France), which together account for over 50% of volume and 59% of value share (OIV, 2019). In this highly competitive scenario, Chile is year after year fighting with other producers for its positioning in the global market right after the three main producers.

Both, quality and quantity of wine are critical for maintaining and hopefully increasing our participation in these changing and competitive markets, urging producers and researchers for continuous process improvement and optimization of wine organoleptic properties.

Besides Alcoholic Fermentation (AF), mainly conducted by yeast, the production of some wines also involves Malolactic Fermentation (MLF), conducted by lactic acid bacteria. MLF is a key secondary fermentation for the production of most red wines and some white and sparkling wines. It is critical for developing certain organoleptic features, such as reduced acidity and flavor complexity; as well as for increasing microbiological stability (Henick-Kling et al., 1994; Zoecklein et al., 1999). Since red wine varieties account for 65% of Chilean wine production (SAG, 2018), optimal management of MLF is critical; furthermore, Chardonnay, the fourth wine grape variety cultivated in Chile (SAG, 2018), is also frequently subjected to MLF. Altogether, MLF is involved in the production of 3 in 4 wines of the country.

This secondary fermentation involves the NAD^+ and manganese-dependent decarboxylation of L-malate to L-lactate (Kunkee, 1974; Williams et al., 1984). *Oenococcus oeni* is the main LAB species involved in MLF. Consequently, the success of this secondary fermentation depends on the ability of *O. oeni* to grow under the hostile conditions prevailing in wine (Gockowiak & Henschke, 2003; Le Marrec et al., 2007). Unfortunately, *O. oeni* is not always able to achieve this task under these harsh environments, often generating sluggish or even, stuck malolactic fermentations. For this reason, this process is considered one of the most difficult to manage in

winemaking, involving unpredictable timings and results. Often, MLF inconveniently delays the overall process of winemaking and therefore results in significant economic losses. Several studies have been carried out with the aim of understanding the metabolism of *O. oeni* under oenological culture conditions (Bourdineaud et al., 2003; Cafaro et al., 2014; Carreté et al., 2002; da Silveira et al., 2003; Grandvalet et al., 2005, 2008; Olguín et al., 2009). However, MLF still remains mostly an unpredictable, capricious and precarious operation in the winemaking process.

The present research seeks to contribute to the understanding of *O. oeni* metabolism under oenological conditions and its role in MLF. The first chapter of the thesis deals with the construction of the first Genome-Scale Metabolic Model (GSMM) for *O. oeni* strain PSU-1. The latter was exhaustively curated after comparing *in silico* experiments with experimental cultures, focusing on the production of metabolites with either organoleptic, microbiological, or oenological interest. In the second chapter, we focused on the metabolic response of the malolactic bacterium under increasing ethanol contents. Finally, the third chapter presents a completely different approach to understanding malolactic fermentation. Here, we explored the question of the reaction mechanism of the malolactic enzyme. Indeed, the reaction mechanism of the malolactic enzyme is not fully understood yet, and three different pathways for the decarboxylation of malic acid have been proposed, so far (Flesch, 1969; Korkes & Ochoa, 1948; Schümann et al., 2013). For this purpose, we first built a structural model of the malolactic enzyme (MLE), which was then employed for identifying the binding sites and estimating the binding free energies of potential substrates, via molecular docking. Measurements of the MLE affinity with potential substrates using a calorimetric essay was employed to validate *in silico* results.

1.2 Hypothesis

The construction of a genome-scale metabolic model of *Oenococcus oeni* (strain PSU-1) and the three-dimensional modeling of the malolactic enzyme would allow a better comprehension of its metabolism and growth capabilities under different ethanol levels, giving a more precise understanding of malolactic fermentation in winemaking.

1.3 Objectives

The main objective of this thesis is to contribute to a better comprehension, at the systemic level, of the metabolism of *Oenococcus oeni* under oenological conditions. For this purpose, the specific objectives of this work were the following:

a) To construct and curate the first Genomic Scale Metabolic Model (GSMM) for *O. oeni* strain PSU-1, using the available genomic sequence.

b) To develop a defined culture medium and characterize the kinetic parameters of *O. oeni* cultures grown under increasing ethanol content.

c) To uncover the molecular reaction mechanism of the malolactic enzyme by structural modeling and thermodynamic essays.

1.4 Approach

We first developed several tools, either computational or experimental, that allow addressing, from a systemic perspective, the control of malolactic fermentation led by *O. oeni* in wines. Two different approaches were undertaken. The first one seeks to develop, curate and validate a genome-scale metabolic model (GSMM) for *O. oeni* strain PSU-1, including the description of its metabolic network and growth rate under increasing ethanol concentrations. The second aimed to generate a three-dimensional structural model of malolactic enzyme (MLE), for identifying which of the three reaction mechanisms proposed in the literature, fit better with the binding free energies of potential substrates estimated *in silico*. Calorimetric measurements of the MLE affinity with potential substrates were then employed to validate these *in silico* results.

1.5 General Introduction

1.5.1 The winemaking process

Wine is the product of a diverse microbiota, comprising several yeasts, bacteria and fungi, interplaying in a highly complex and nutrient rich ecological niche, the grape must (Piao et al., 2015). During its transformation, the latter continuously evolves to new physico-chemical conditions, consuming some nutrients, particularly nitrogenous compounds and sugars, and producing new ones, such as ethanol, fermentative aromas and glycerol, to name a few. These medium modifications differentially impact the microbial populations at different stages and generate both, promoting and stressful conditions, in a highly complex and delicate balance, easily perturbed and strongly determining the final quality of wine (Cappello et al., 2017; Chidi et al., 2018; Piao et al., 2015).

During winemaking, the participating microorganisms can be either indigenous or introduced exogenously, *i.e.,* starter cultures. They can impact the quality of the final product, either positively (lactic acid bacteria, like *Oenococcus oeni* and *Lactobacillus plantarum*) or negatively (*Brettanomyces bruxelensis* or *Acetobacter aceti*) (Bokulich et al., 2013; du Toit & Pretorius, 2000; Piao et al., 2015; Renouf et al., 2006). Besides the microorganisms inhabiting the grape berries, winery resident microbiota also acts as a potential reservoir for microbial transfer between fermentations, and seasonally fluctuating populations of bacteria and fungi have been detected and characterized in winery surfaces and machinery (Bokulich et al., 2013).

Two major types of fermentation can be distinguished during winemaking: alcoholic fermentation (AF) and malolactic fermentation (MLF). AF is the essential process by which grape must is transformed into wine. It is led by different yeasts and, to some extent, by bacteria, but mainly by the budding yeast *Saccharomyces cerevisiae* (Chidi et al., 2018). Besides ethanol, CO_2 and glycerol, other secondary volatile metabolites, e.g. fusel alcohols, ethyl and acetate esters, carbonyls and volatile fatty acids are also synthesized, that contribute to the final organoleptic properties of wine (Cordente et al., 2012; da Mota et al., 2017; Suomalainen & Lehtonen, 1979; Swiegers

et al., 2005). Most fermentative aromas are formed during this step (Mateo et al., 2001; Sumby et al., 2010).

While all wines require AF, some of them also endure malolactic fermentation (MLF). This second fermentation improves organoleptic features of the final product, adding new flavors and aromas during the transformation of malic acid into lactic acid (Olguín et al., 2019; Pozo-Bayón et al., 2005; Sumby et al., 2010). The whole quality of wine is also improved by the consequent pH increase (Bartowsky, 2005; Bartowsky et al., 2015; Bauer & Dicks, 2004). Lactic acid bacteria (LAB) are responsible for this secondary process, the most important one being *Oenococcus oeni* (Chidi et al., 2018; da Mota et al., 2017; Mills et al., 2005; Olguín et al., 2019).

AF and MLF can occur either simultaneously or sequentially. However, MLF normally occurs after AF, as LAB are only present in limited numbers during AF (da Mota et al., 2017; Fleet, 1993). Even though the wine industry mostly prefer the sequential AF-MLF approach (Bartowsky et al., 2015), current research is contributing evidence in favor of simultaneous fermentations, using co-inoculation of yeasts and new strains of LAB able to cope AF conditions (Bleve et al., 2016; Howell, 2016; Izquierdo-Cañas et al., 2015; Tristezza et al., 2016; Zapparoli et al., 2006).

As pointed out above, either native microorganisms present in grape surfaces, leaves and winery machinery can carry out AF and MLF (Bokulich et al., 2013; Carre et al., 1983; Kunkee, 1974; Renouf et al., 2006); or commercial starters can be inoculated. Though native microorganisms are said to have the advantage of producing higher flavor complexity (Fleet, 1993; Olguín et al., 2019; Renouf et al., 2006), they are difficult to control for achieving the desired results in terms of quality, and involve less predictable timings and higher risk of spoilage than inoculated cultures (Bauer & Dicks, 2004; Howell, 2016). On the contrary, inoculation with a starter culture optimizes timings and reduces risks and delays, by favoring the proliferation of the desired strain. Furthermore, the latter could possess some desirable characteristics (da Mota et al., 2017; Howell, 2016; Zamora, 2009), such as tolerance to high initial sugar concentration (Mateo et al., 2001), or minimization of biogenic amines production

(Henríquez-Aedo et al., 2016; Howell, 2016; Martuscelli et al., 2018; Restuccia et al., 2018; Toledo et al., 2018).

Although helpful to control MLF onset and completion, wine inoculation with malolactic starters has not been always successful (da Mota et al., 2017; Iorizzo et al., 2016; J. C. Nielsen & Richelieu, 1999). Its interest remains limited due to its costs, rapid decrease in cell viability (Bauer & Dicks, 2004), and lesser geographical adaptation (Iorizzo et al., 2016).

Since indigenous microorganisms are considered to enhance the complexity of wine through the production of a broader spectrum of sensory-active compounds than those produced from a pure inoculum (Bokulich et al., 2013; Garofalo et al., 2015; Olguín et al., 2019), the exclusive use of inoculated starters has been thought to impoverish diversity and homogenize wine styles, with potentially detrimental effects to local oenological patrimonies. Also, some evidence supports the use of autochthonous yeasts and bacteria for reducing the risks of spoilage by contamination with *Brettanomyces bruxellensis* (Berbegal et al., 2017).

The impact of indigenous microflora on the wine characteristics and style has become a focus for research, reflecting the traditional concept of *terroir*, since the specificity of certain strains in different geographical estates persists year after year (Renouf et al., 2006). Different cellars had diverse strains of *S. cerevisiae* and *O. oeni*, and a very specific mix of microorganisms. Renouf et al. (2006) found qualitative and quantitative differences in bacteria and yeast populations across four estates in Bordeaux region, whereas Bokulich et al. (2013) described their spatial and chronological distribution in winery surfaces prior, during and after the harvest. In conclusion, combination of vineyard indigenous flora associated with oenological practices currently used may be determinant in specific *terroir* characteristics (Garofalo et al., 2015; Renouf et al., 2006).

The development of new starters using selected autochthonous strains is a new trend, promoted by the rise of more affordable and scalable genetic techniques (Alegría et al., 2004; Bravo-Ferrada et al., 2013; Garofalo et al., 2015; Sun et al., 2016). Directed evolution of more efficient strains also promotes these developments (Betteridge et al.,

2015, 2018; Jiang et al., 2018; N. Li et al., 2015; Marengo et al., 2015), looking for higher expression of stress related genes or desired properties, such as psychrotrophy for example (Bordas et al., 2015; Olguín et al., 2019; Vigentini et al., 2016) The use of indigenous starter cultures, best adapted to a specific wine-producing area has been recommended to maintain the wine regional characteristics (Berbegal et al., 2017; Brizuela, Bravo-Ferrada, et al., 2018; du Toit et al., 2011; Garofalo et al., 2015).

1.5.2 Organic Acids in Wine

Organic acids and total acidity play a pivotal role in wine sensory perception, and directly influence the overall organoleptic character of wines (Chidi et al., 2018). Whereas too much acidity will make the wine to taste excessively sour and sharp, too little can result in flabbiness, flatness, and a less-defined flavor profile (Mato et al., 2005). Organic acids concentrations in grape musts are primarily a function of grape maturity and variety (Conde et al., 2007); however, both alcoholic and malolactic fermentations change the concentration and content of wine acidity (Volschenk et al., 2017; Yabaya et al., 2016). Malic, citric and tartaric acids are the primary acids in wine grapes, contributing the highest proportion of acidity to the final product, known as *titratable acidity* (Defilippi et al., 2009). During fermentation, yeasts and bacteria synthesize several other important organic acids, such as succinic, pyruvic, lactic and acetic acids, respectively associated with the fresh, tart, sour and metallic taste of wines (Chidi et al., 2018).

Organic acids also contribute to wine stability (Kučerová & Široký, 2011; Tita et al., 2006) and preservation of desired organoleptic features (Darias-Martín et al., 2000). Acidity is also a primary driver in managing contamination risks (Akin et al., 2008). Indeed, lower acidity generally supports microbial growth, including several unwanted or spoilage species (Bisson & Walker, 2015).

L-malic acid is commonly found in many fruits, including green apples and grapes (Krueger, 2012). In grapes, L-malic acid declines with maturation, from up to 25 g L^{-1} to 2.0-6.5 g L^{-1} (Ribéreau-Gayon et al., 2006), but significant higher amounts can be found in cooler climatic regions and in certain varieties, such as Barbera, Carignan and Sylvaner (Chidi et al., 2018). Since it can be rough on the palate,

winemakers usually prefer its transformation into lactic acid, whose concentrations normally average from 1 to 3 g L^{-1} in wines, increasing through MLF (Boulton et al., 1996).

1.5.3 Malolactic Fermentation (MLF): a biochemical approach

MLF consists in the conversion of the dicarboxylic L-malic acid into the monocarboxylic L-lactic acid; in fact, it is this reaction - decarboxylation of malic acid - which is known as malolactic fermentation. As a consequence, pH increases between 0.1 and 0.2 units, and titratable acidity decreases (Bartowsky et al., 2015; Bauer & Dicks, 2004; Kunkee, 1968, 1991; Versari et al., 1999). These two changes result in a softer wine, more agreeable and appealing in mouth (Chidi et al., 2018; J. C. Nielsen & Richelieu, 1999). During MLF, several aroma compounds are biosynthesized, the most relevant being diacetyl, with a buttery attribute, easily perceived in Chardonnay. Other MLF compounds affecting flavor are acetic acid and acetoin, produced by citrate degradation (Bartowsky & Henschke, 2004; Lonvaud-Funel, 1999); diethyl succinate, related to buttery notes; and ethyl lactate, contributing creamy ones (Tristezza et al., 2016).

Additionally, MLF increases microbial stability in wines, as it removes remaining carbon sources available for spoilage bacteria (Bartowsky, 2005; Bartowsky et al., 2015; Bauer & Dicks, 2004; da Mota et al., 2017; Kunkee, 1968). In addition, lactic and acetic acids synthesized during MLF, and in some extent, other metabolites such as diacetyl, have proven to have antimicrobial activity (De Vuyst & Vandamme, 1994; Jay, 1982).

In spite of its key relevance, MLF is not yet fully understood and remains difficult to predict and manage (da Mota et al., 2017; Guzzo et al., 2000; Versari et al., 1999). Spontaneous MLF can be triggered as early as a few days after the completion of AF (Lonvaud-Funel, 1999), after bacterial population has reached about 10^6 CFU ml^{-1} (Versari et al., 1999); nonetheless, its triggering can be a real challenge and delayed even for months, increasing risks of spoilage and immobilizing the volume capacity of the winery (da Mota et al., 2017; Iorizzo et al., 2016). Its completion takes normally a few weeks after the harvest, but it remains an unpredictable process of

winemaking, often taking much longer than expected (da Mota et al., 2017; Iorizzo et al., 2016; Kunkee, 1991).

Wine temperatures under 12 ºC, associated with pH below 3.2 and free SO_2 above 15 mg L^{-1}, have been identified as inhibiting or lengthening MLF after the lysis of yeast cells (da Mota et al., 2017). High alcohol and residual sugar content also delay the process, as described in winter wines (da Mota et al., 2017); high alcohol concentration reduces bacterial growth, but not bacterial activity, the latter being impaired by free SO_2 concentrations higher than 15 mg L^{-1} and pH < 3.5 (Lasik, 2013; Sun et al., 2016). Total SO_2 concentration below 30 mg L^{-1}, initial temperatures of 20 °C to 25 °C, and the availability of nutrients in the sediment of yeast cells are also fundamental in the equation (da Mota et al., 2017; Lasik, 2013). Other compounds, such as acetaldehyde and medium-chain fatty acids released by yeasts, (Carreté et al., 2002; Lasik, 2013), the presence of copper and the fungicide dichlofluanid (Cabras et al., 1999; Carreté et al., 2002), high amounts of tannins, and pesticide residues (Cabras et al., 1999; Lasik, 2013; Wells & Osborne, 2012) may impair LAB growth and reduce its activity.

Although highly desirable for most red wines, MLF could affect negatively some others. Grapes produced under warmer climates tend to be less acid and reducing its acidity could be detrimental for its microbiological stability (Bauer & Dicks, 2004; Versari et al., 1999). On the other hand, wines from cooler regions need MLF to decrease the excess of malic acid and its organoleptic effects (Bauer & Dicks, 2004; Chidi et al., 2018; Kunkee, 1991; S.-Q. Liu, 2002).

Not only dealing with late or stuck MLF is a problem; its lengthening is also undesirable. When it happens, excessive reduction of acidity leads to discoloration (Bauer & Dicks, 2004; du Toit & Pretorius, 2000). It might also indirectly encourage microbial spoilage, resulting from more favorable growth conditions for species that are less acid tolerant than *O. oeni* (du Toit & Pretorius, 2000). Furthermore, a too early onset of MLF has been associated with sluggish and stuck alcoholic fermentations, as the acetic acid generated inhibits *Saccharomyces* spp (du Toit & Pretorius, 2000).

The simultaneous co-inoculation of resistant strains of lactic acid bacteria with yeast has been proposed as an alternative to reduce MLF duration (Bleve et al., 2016; Howell, 2016; Lerena et al., 2016; Suriano et al., 2015). Other researchers have explored LAB replacement of MLF. For example, Benito et al. (2015) proposed two yeasts species instead of LAB, namely *Schizosaccharomyces pombe* and *Lachancea thermotolerans*. *S. cerevisiae* and other yeast species have also been genetically engineered to conduct MLF themselves (Ansanay et al., 1996; Bony et al., 1997; Husnik et al., 2006, 2007; Volschenk et al., 1997), though only in experimental settings because in most countries, GMOs for wine production are strictly prohibited (Vaudano et al., 2016).

1.5.4 Lactic Acid Bacteria and wine

Lactic acid bacteria (LAB) are responsible for MLF in wine. They are a group of Gram-positive, catalase negative, non-spore forming, facultative anaerobic bacteria (du Toit & Pretorius, 2000), functionally related by their general ability to produce lactic acid during homofermentative and/or heterofermentative metabolism (Duar et al., 2017; O'Sullivan et al., 2009). They have been isolated from sources as diverse as plants, animals and humans (Duar et al., 2017; Makarova et al., 2006; Makarova & Koonin, 2007; O'Sullivan et al., 2009; Stefanovic et al., 2017).

LAB can be classified into 7 phylogenetic clades: *Lactococcus, Lactobacillus, Enterococcus, Pediococcus, Streptococcus, Leuconostoc* and *Oenococcus* (O'Sullivan et al., 2009). This group of bacteria has been extensively exploited in food industry, playing crucial roles in the fermentation of dairy products, meat and vegetables, as well as in the production of wine, coffee, cocoa and sourdough, with some LAB having demonstrated probiotic functions (Ljungh & Wadström, 2006).

Over 30 LAB species can be found in wine, although not all are of oenological interest or utility, some being even potentially harmful for the final quality of wine (Cappello et al., 2017). Its diversity has been linked with aroma and flavor richness in wine, with a wide spectrum of wine sensory outcomes due to specific enzymatic activities, transcending MLF (Cappello et al., 2017). These species belong mainly to five genera: *Lactobacillus*, *Pediococcus*, *Leuconostoc*, *Oenococcus* and *Weissella*.

Leuconostoc, *Weisella* and *Oenococcus* spp are obligate heterofermentative; conversely, *Pediococcus* spp are homofermentative, and *Lactobacillus* spp can be either homofermentative (*Lactobacillus vini*), facultative heterofermentative (*Lactobacillus plantarum*) or obligate heterofermentative (*Lactobacillus brevis*) (Bauer & Dicks, 2004; du Toit & Pretorius, 2000; König et al., 2009; S.-Q. Liu, 2002; Lonvaud-Funel, 1999; Mills et al., 2005).

Among the many species found in wine, the most oenological relevant for MLF are *Oenococcus oeni* and *Lactobacillus plantarum*, recently renamed as *Lactiplantibacillus plantarum* (Zheng et al., 2020) They can synthesize antimicrobial peptides which might help prevent the production of undesired compounds, by inhibiting other indigenous LAB microflora (du Toit & Pretorius, 2000). Currently, *O. oeni* is the main species used in MLF as LAB starter (Brizuela, Bravo-Ferrada, et al., 2018; Brizuela, Tymczyszyn, et al., 2018; Garofalo et al., 2015; Jiang et al., 2018; Sun et al., 2016). However, some *Lb. plantarum* strains can also survive the harsh conditions of wine (Alegría et al., 2004; Bravo-Ferrada et al., 2013; Howell, 2016; Iorizzo et al., 2016; Izquierdo-Cañas et al., 2015; Lee et al., 2012; Lerm et al., 2011) and possess many other favorable characteristics, such as faster growth rates, lower nutritional requirements and higher ability to consume malic acid than *O. oeni* (Bravo-Ferrada et al., 2016; Brizuela, Bravo-Ferrada, et al., 2018; Brizuela, Tymczyszyn, et al., 2018). *Lb. plantarum* has shown to be a good choice for pre-AF or co-inoculation with yeasts to grape must (Brizuela, Bravo-Ferrada, et al., 2018; Brizuela, Tymczyszyn, et al., 2018; Howell, 2016; Lerena et al., 2016). *Lb. plantarum* strains have a more diverse enzymatic profile than *O. oeni,* and therefore could significantly modify the wine aroma profile (du Toit et al., 2011; Lerm et al., 2011; Matthews et al., 2006; Mtshali et al., 2010); in addition to malolactic enzyme, it displays other relevant enzymes influencing wine flavor, like glycosidases, β-glucosidases, esterases, phenolic acid decarboxylases, and citrate lyases (Brizuela, Tymczyszyn, et al., 2018; Grimaldi et al., 2005a, 2005b; S.-Q. Liu, 2002; Matthews et al., 2004). When employed as a starter, *Lb. plantarum* increases the concentration of key aroma compounds, such as

esters and terpenes, providing a richer flavor profile to the resulting wine (Howell, 2016).

Besides *Lb. plantarum*, other *Lactobacilli* species have been studied as starters with overall positive results, such as *Lb. mali*, *Lb. paracasei* and *Lb. satsumensis* (Lucio et al., 2017). Finally, some authors have also proposed blend cultures of native *Lb. plantarum* and *O. oeni* strains, a promising strategy that could support longer microbial survival, therefore increasing the overall consumption of L-malic acid, and enhance the aroma complexity of the final wine (Brizuela, Bravo-Ferrada, et al., 2018; Brizuela, Tymczyszyn, et al., 2018).

1.5.5 *O. oeni* and its metabolic features relevant for winemaking

Oenococcus oeni is an acidophilic, microaerophilic bacterium, member of the *Leuconostocaceae* family of LAB, indigenous to wine and similar environments (Iorizzo et al., 2016). This species dominates the scene in wines with low pH, *i.e.* 3.0-3.5 (Bartowsky, 2005; Maicas et al., 2002; Mills et al., 2005); in fact, *O. oeni* is the bacterium that mainly drive MLF and more successfully proliferates as it runs, whilst other competing population progressively diminish (Versari et al., 1999). Conversely, *Lactococcus* and *Pediococcus* spp are more related with defects in wine (Bartowsky, 2005; Bauer & Dicks, 2004; Zapparoli et al., 2009) and have a lesser contribution to MLF (Bartowsky, 2005; Bartowsky & Borneman, 2011). Altogether with other bacteria, they threat the final quality of wine, especially when MLF is slowed down or stuck (Davis et al., 1986).

Garvie (1967a) was the first to propose a separate species for wine-related LAB, classified as belonging to the *Leuconostoc* genus, named *Leuconostoc oenos*. Its high tolerance to acid conditions and a peculiar growth enhancement in media containing tomato juice led to its differentiation as a new species (Garvie, 1967a, 1967b). Dicks et al. (1995) proposed a new genus, *Oenococcus*, for reclassification of *Leuconostoc oenos* almost three decades later, when a study based on 16S r-DNA and 23S r-DNA showed genetic deep differences with *Leuconostoc mesenteroides*. Originally thought to be a genus composed by a sole member, *Oenococcus oeni*, three new species have been discovered since its definition: *O. kitaharae* (Endo & Okada, 2006), *O.*

alcoholitolerans (Badotti et al., 2014), and *O. sicerae* (Cousin et al., 2019; Verce et al., 2020) the last one recently identified in french cyder and water kefir. For a graphical, brief description of its history, see Figure 1-1.

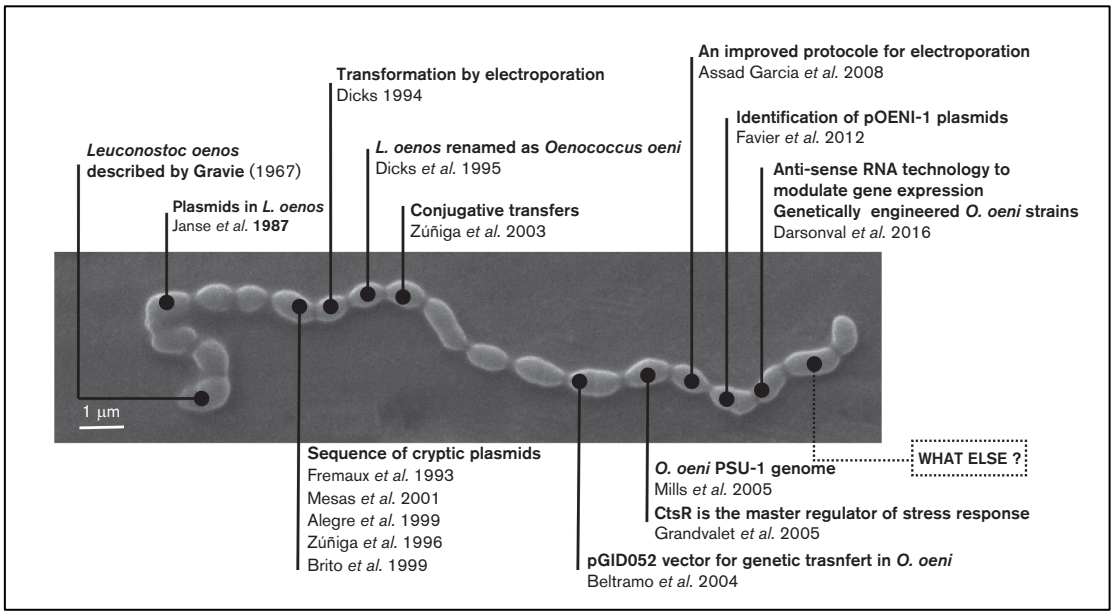

Figure 1-1: Evolution of *O. oeni* genetics. Timeline of the history of genetic research on *O. oeni* from the first description of the species by Gravies in 1967 to sequencing of the genome by Mills et al. (2005), and the last major advances thanks to the application of anti-sense technology to modulate gene expression (Darsonval, Msadek, et al., 2016).

Oenococcus phylogenetic relationships with other genera have been reported (Figure taken from Grandvalet, 2017). Also, its genetic diversity has been studied inside geographic-specific or broader populations (Björkroth & Holzapfel, 2006; Chelo et al., 2007) and pan-genome analyses have been carried out comparing strains (Bridier et al., 2010; Campbell-Sills et al., 2015; de las Rivas et al., 2004; Delaherche et al., 2006; Guerrini et al., 2003; Lechiancole et al., 2006; H. Li et al., 2006; Marques et al., 2011; Renouf et al., 2009; Sato et al., 2001). These advances provide a promising basis for new developments in genetic engineering and biotechnology, with genetically engineered strains already being designed (Ilabaca et al., 2014; Romero et al., 2018; Toledo et al., 2018); however, extensive discussion should take place before their introduction for industrial utilization, since currently international regulation forbids

the use of genetically modified organisms in commercial wine production. For the time being, the research on its genetic variability and diversity, and the characterization of indigenous population is being used in the selection of new strains with specific desired features via directed evolution (Darsonval, Alexandre, et al., 2016; Grandvalet, 2017).

Although not the only bacterium performing MLF in wine, *O. oeni* is preferred for oenological use because of its unique properties: high acid-tolerance (Betteridge et al., 2015, 2018; Jiang et al., 2018; N. Li et al., 2015; Marengo et al., 2015), resistance to high ethanol (>10% v/v) and SO_2 concentrations (<50 ppm) (Bauer & Dicks, 2004; Chu-Ky et al., 2005; Liu, 2002; Versari et al., 1999), low production of acetic acid (Bartowsky et al., 2015; Bauer & Dicks, 2004), and scant occurrence of the ropy phenotype (Ribéreau-Gayon et al., 2006). Furthermore, it develops unique flavor compounds via enzymatic activity (Ribéreau-Gayon et al., 2006; Torriani et al., 2011), adding to the wine buttery and nutty notes; it is able to produce smoother tannins, as well as (Liu, 2002).

The capacity for synthesizing lactic and acetic acids represents an important competitive advantage for *O. oeni* and other LAB, since these weak acids have antimicrobial activity (Salema et al., 1996). Their undissociated form can move freely across the cell membrane and cause acidification by releasing a proton into the cell cytoplasm during acids dissociation due to the difference between the pH of the growth medium and the cytoplasmic one, the latter being generally higher than the former (De Vuyst & Vandamme, 1994). This acidification results in a disruption of cytoplasmic anion pool, damaging the integrity of purine bases, and therefore denaturizing essential enzymes of cell metabolism and survival (Cotter & Hill, 2003).

Besides malic acid, *O. oeni* also ferments the remaining sugars present in the wine through the phosphoketolase pathway, also known as heterolactic fermentation (HLF) (Wu et al., 2014). This metabolic pathway generates ATP and NAD(P)H by catabolizing sugars into carbon dioxide, ethanol, acetic acid or acetaldehyde, and lactic acid as by-products (Bartowsky, 2005; Maicas et al., 2002).

Numerous studies have demonstrated that *O. oeni* can reach higher specific growth rates in a medium including alternative electron acceptors such as fructose

(Bartowsky, 2005; Grimaldi et al., 2005b) or pyruvate (Maicas et al., 1999). These compounds are employed to oxidize NAD(P)H, allowing to metabolize acetyl-P into acetate instead of ethanol, with consequential higher yield of ATP (Maicas et al., 2002). Fructose can be either metabolized through HLF or transformed into mannitol (Gänzle, 2015) or erythritol (Gänzle, 2015). Pyruvate can be reduced into lactate (Maicas et al., 2002; Wagner et al., 2005). $NAD(P)^+$ is regenerated in both processes.

1.5.5. *Oenococcus oeni* PSU-1 strain

The *Oenococcus oeni* PSU-1 strain was initially isolated from a spontaneous malolactic fermented wine in Pennsylvania in 1972 (Bordas et al., 2015). Very similar to the previously described strain ML-34 from California (Beelman et al., 1977), the main advantage of PSU-1 over the latter was its ability to start MLF faster in red wines (Ingraham et al., 1960). Because of this property, it was once a common starter culture, though replaced today by more recently selected and efficient strains (Beelman et al., 1977).

As early as the late 1990s, PSU-1 strain was intensively studied and mapped (Guzzon et al., 2009; Semon et al., 2001; Torriani et al., 2011; Ugliano & Moio, 2005). Its complete genome sequence was released for public access during the first decade of the 21th century (Zé-Zé et al., 1998, 2000, 2008), being the first *O. oeni* strain to be sequenced. PSU-1 strain has a single circular chromosome of 1.780.517 nucleotides, and a GC content of 38% (Mills et al., 2005). Consistently with its classification as an obligate heterofermentative lactic acid bacterium, the PSU-1 genome encodes all the enzymes for the phosphoketolase pathway (Mills et al., 2005).

This genomic annotation opened the gate for the study of its metabolic pathways and *O. oeni* phylogenetic tree. Borneman et al. (2012) analyzed *O. oeni* pan genome, using PSU-1 strain as reference, and found relevant differences between strains. Each strain was predicted to contain 1800 ± 52 ORFs and 104 ± 25 potential pseudogenes, in average. The *O. oeni* pan genome comprises 2846 ORFs, while the core genome contains 1165 (Borneman et al., 2012).

To date, there are sequences of more than 250 different strains of *O. oeni*, grouped into 4 phylogenetic groups (Lorentzen & Lucas, 2019).

1.5.6 Malolactic Enzyme

O. oeni metabolizes L-malic acid via the malolactic enzyme (MLE) (Borneman et al., 2012). MLE is not privative of *O. oeni*, as it has been shown by its purification from several LAB species (Bartowsky & Borneman, 2011; Kunkee, 1991).

The gene encoding MLE (*mleA*) has been cloned, sequenced and mapped on the *O. oeni* chromosome, as well as the genes encoding the related malate permease (*mleP*) and a proposed regulatory protein (*mleR*) (Caspritz & Radlert, 1983; Lonvaud-Funel & Strasser de Saad, 1982; Naouri et al., 1990; Spettoli et al., 1984). *O. oeni* strains differ in their ability to metabolize malic acid efficiently (Labarre, Diviès, et al., 1996; Labarre, Guzzo, et al., 1996; Mills et al., 2005; Zé-Zé et al., 2008).

It has been suggested that MLE is less sensitive to ethanol content than the mechanisms regulating cell growth, associating MLF arrest with growth inhibition rather than the inhibition of enzymatic activity (Bartowsky, 2017). Wang et al. (2014) undertook the production, purification and characterization of malolactic enzyme from *Oenococcus oeni* strain SD-2a. The purified enzyme had a nominal molecular mass of 59 kDa and a theoretical pI of 4.76. It exhibited maximum enzyme activity at 35°C and pH 6.0, retaining over 50% of its initial activity in the presence of 14% (v/v) ethanol (2014). Mn^{+2} was proven to be the most effective divalent cation to promote enzyme activity. Under 30°C and pH 6.0, the K_m and V_{max} parameters of MLE on L-malic acid were 12.5×10^{-3} M and 43.86 μmol min^{-1} mg^{-1}, respectively (Wang et al., 2014).

The reaction mechanism involved in MLF remains speculative. Three possible pathways for decarboxylation have been proposed (Wang et al., 2014):

1) Korkes and Ochoa (Schümann et al., 2013) hypothesized a pathway through a malic enzyme, followed by L-lactate dehydrogenase, transforming first malate to pyruvate, and then to lactate.
2) Flesch (1948) proposed a three-step reaction mediated by a L-malate dehydrogenase, oxaloacetate decarboxylase and then a L-lactate dehydrogenase.
3) Finally, the third mechanism was proposed by Caspritz and Radley (1969): a direct conversion of L-malate into L-lactate, through a reaction carried out in

the presence of NAD^+ and Mn^{+2}, but without reduction of NAD^+ neither detection of free reaction intermediates (1983).

Similarly, little is known about the three-dimensional structure of the protein. Molecular docking has not been conducted yet for establishing its exact physicochemical mechanism. Several authors have proposed that MLE was a homo-dimeric enzyme, composed of two identical subunits of 60 kDa (Bartowsky & Borneman, 2011; Groisillier & Lonvaud-Funel, 1999; Schümann et al., 2013).

1.5.7 Genomic Scale Metabolic Reconstructions (GENRE) and Models (GSMM)

Metabolic networks at the genome scale or genome-scale metabolic reconstructions (GENRE**)** are collections of biochemical reactions of a target organism and their associated genes describing its metabolism (Ahmad et al., 2017). They are built using genome annotation, databases, *omics* studies, and primary literature (Thiele & Palsson, 2010). This input information is integrated in a structured, mathematical representation that can be translated into computational models, called genome-scale metabolic models (GSMM). GSMM allow the phenotype of an organism to be studied *in silico*, performing computational quantitative queries to answer questions about the capabilities of its metabolism and its most probable phenotypic states. All this information is integrated using various algorithms to simulate the status of the cell as a whole (Park et al., 2009).

Several methods have been developed for GSMM since its beginnings in the late ‘90s of the last century (Bartowsky & Borneman, 2011). Their scope has also been expanded, addressing an increasingly broader spectrum of basic and practical applications in metabolic engineering, model-directed discovery, interpretations of phenotypic manifestations, analysis of network properties, and studies of evolutionary processes (Feist & Palsson, 2008). A meticulous protocol of 96 steps to construct high quality GENREs has been established by Thiele and Palsson (2009), leading to more accurate predictions of the metabolism of the studied organism.

These genome-scale models have led to novel insights and guidance of further experiments. For example, they have allowed to identify antimicrobial and anti-cancer drug targets (Feist & Palsson, 2008; McCloskey et al., 2013), to discover mechanisms

underlying other diseases (Angione, 2018; Folger et al., 2011; Frezza et al., 2011; Ho Sui et al., 2012; Kim et al., 2014; Lewis & Abdel-Haleem, 2013; Nilsson & Nielsen, 2017; Shen et al., 2010; Yizhak et al., 2015), to understand the impact of medicines and the microbiota interspecies interactions in intestinal flora (Cook & Nielsen, 2017; Dunphy & Papin, 2018; Geng & Nielsen, 2017; Lewis et al., 2010; Mardinoglu et al., 2014), and to design improved strains of microorganisms (Magnúsdóttir et al., 2017; Magnúsdóttir & Thiele, 2018; Rosario et al., 2018; van der Ark et al., 2017), among many other applications (Cardoso et al., 2018). The clinical use of GSMM is a new trend in medical treatments and pharmacological developments, opening new exciting opportunities in medicine (Bordbar et al., 2014; Gudmundsson et al., 2017; W. J. Kim et al., 2017; Xu et al., 2018).

Some highly refined genome-scale metabolic models (GSMM) of well-known bacteria, such as *Escherichia coli*, has also been used in the study of interspecies interactions (Feist & Palsson, 2008; Oberhardt et al., 2009) and microbial consortia (McCloskey et al., 2013). The current developments and efforts in bioinformatics are enabling researchers and bioengineers with a solid comprehension of genotype-phenotype mechanistic links for diverse cells metabolism (Hanly et al., 2012), including eukaryote and cells in multicellular organisms.

Metabolic models can be roughly divided into two types, structural and kinetic. Whereas structural models define systems in terms of reaction stoichiometry and direction, kinetic models explicit rate equations for each reaction (Agren et al., 2014; J. Nielsen, 2017; Raškevičius et al., 2018). Due to practical reasons, studies including large number of reactions (>≈50–100) tend to be structural; that is the case of GSMM (Ahmad et al., 2017).

GSMMs require substantial theoretical validation before being applied to the desired scenarios to be queried (Lewis et al., 2012). Curation and experimental validation are essential for the refinement of the initial, automatically-driven draft model, generally obtained using public databases. The modeler's task can be simplified by automation of error detection and model validation processes (Poolman et al., 2006),

but the throughout and meticulous curation by hand remains an unavoidable, although significantly time consuming, key step (Gevorgyan et al., 2008; Poolman et al., 2006).

Initially, only highly characterized microorganisms, such as *Escherichia coli* and *Saccharomyces cerevisiae*, were reconstructed *in silico*. Nowadays, these models are widely used in a larger range of organisms, including *Lactococcus lactis* (Opdam et al., 2017), the first LAB to be reconstructed at the genome scale.. It was followed by *Lactobacillus plantarum* (Flahaut et al., 2013; Oliveira et al., 2005; Verouden et al., 2009), *Streptococcus thermophilus* (Teusink et al., 2006) and, more recently, *Enterococcus faecalis* (Pastink et al., 2009), *Lactobacillus casei* (Veith et al., 2015), *Streptococcus pyogenes* (Xu et al., 2015), *Lactobacillus rhamnosus* (Levering et al., 2016) and *Leuconostoc mesenteroides* (Magnúsdóttir et al., 2017).

Constraint-based reconstruction and analysis (COBRA) is the most widely used framework for GSMM analysis (Koduru et al., 2017). First COBRA models at the genome scale were implemented very shortly after the first whole-genome sequences were released (Lewis et al., 2012; Stefanovic et al., 2017). Thus, the first GSMM was reconstructed for *Haemophilus influenza* just four years after its genome sequence (Fleischmann et al., 1995).

The COBRA approach is based on three fundamental concepts (Magnúsdóttir et al., 2017), which corresponding steps are illustrated in Figure 1-2:

1. **The imposition of physicochemical constraints that limit computable phenotypes** (Figure 1-2 a-d). The reaction occurrence is limited by three primary constraints: substrate and enzyme availability, mass and charge conservation, and thermodynamics. Substrates must be present in cell environment or produced from other reactions, and enzymes must be available. Mass conservation further limits the possible reaction products and their stoichiometry, and thermodynamics constrains reaction directionality. This information is obtained from biochemical and genetic studies about the specific organism or it can be inferred from related ones, and then catalogued in metabolic reconstruction knowledge databases (Lewis et al., 2012). The metabolic reconstruction is then converted into an *in silico* model by mathematically describing the reactions and adding network inputs and outputs

(Feist et al., 2009; Thiele & Palsson, 2010) (Figure 1-2 a-b). A matrix representing the stoichiometric coefficients of each reaction mathematically describes the physicochemical constraints. Known upper and lower bounds on each reaction flux are imposed as additional constraints. Mathematically, these constraints define a multi-dimensional 'solution space' of allowable reaction flux distributions, and the actual expressed flux state resides in this solution space. Additional constraints can further reduce the solution space to focus in on the actual flux state of the network (Figure 1-2 c). These additional constraints may include enzyme capacity, spatial localization, metabolite sequestration, and multiple levels of gene, transcript and protein regulation (Figure 1-2 d).

2. **The identification and mathematical description of evolutionary selective pressures, via defining an objective function** (Figure 1-2 e). The objective function is an important part of the COBRA framework. In non-biological chemical networks, the material flow through pathways can be predicted in a cause and effect manner, using mathematical models that describe the associated physical laws. This description is time invariant, as reproducing the physical conditions will always drive flux through the same pathways. By contrast, causation in biology is time variant. Diverse chemical reactions may occur inside a cell, and many pathways can link a starting molecule to a given product. However, regulatory mechanisms have evolved to select when and where pathways will be used in an organism under given conditions. If the cellular objectives that drive evolution are understood or can be inferred, optimal flux states of biochemical reaction networks can be predicted. In the COBRA framework these cellular objectives are described mathematically and used to compute phenotypic states. Many cellular objectives can be defined in the context of metabolism; for instance, a biomass function can be defined as a proxy for growth, containing all the necessary precursors for synthesizing the cell components (Lewis et al., 2012).
3. **A genome-scale perspective of cell metabolism that accounts for all metabolic gene products in a cell** (Figure 1-2 f). Genome annotations provide the genetic basis for the reconstruction of metabolic network of the target organism, defining

the relationships between genes, enzymes and the reactions that they catalyze (Figure 1-2 f). When this database is converted into a GSMM, the mathematical representation provides constraints, and the objective function represents the optimal biological functions that the organism strives to achieve. Together, they allow to simulate phenotypes. The genome-scale view of metabolism in these models has two primary implications. First, the models account for all known metabolic genes in a cell and their functions. When used in the analysis of genome-scale data sets, they provide novel insight because they account for real chemical connections between components. Second, as metabolic genes are associated with the biochemical functions of their gene products, simulations of metabolite flow through the network can provide mechanistic predictions of how each gene product affects the metabolic network function. Cell phenotypes can be computed, and data can be interpreted with GSMMs, providing mechanistic insight into how the cell genotype may contribute to the cell phenotype.

COBRA methods have evolved and diversified over the past two decades, with more than 100 different methods currently available. Many of them have been implemented in software packages, allowing to a more-or-less automated processing of data.

Finally, a range of cellular functions have been predicted with this framework, including cell capacity to grow in various substrates, the effect of gene knockouts on product synthesis, antibiotic design, and organismal and enzyme evolution (Edwards & Palsson, 1999).

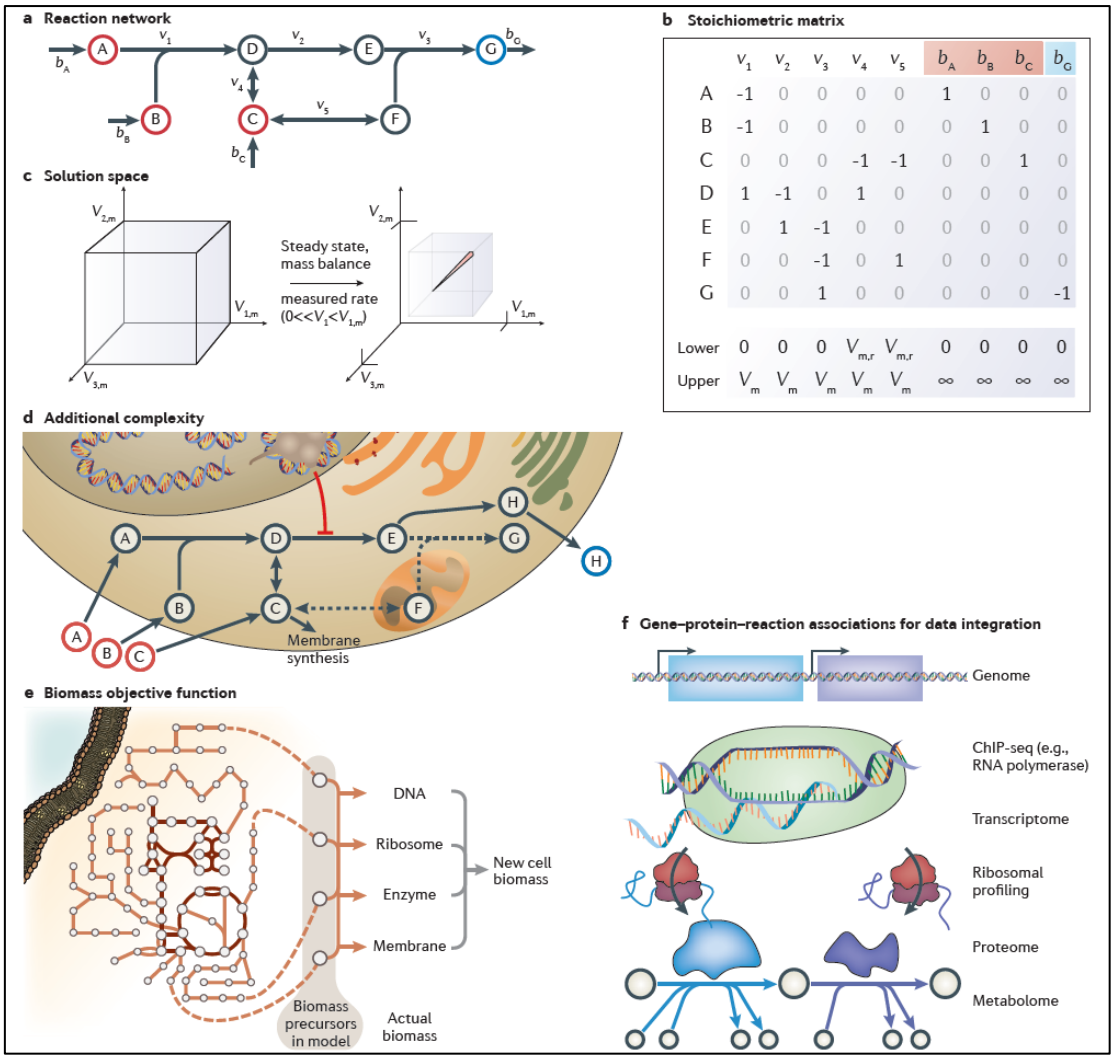

Figure 1-2: Fundamentals of the genome-scale metabolic genotype–phenotype relationship. The constraint-based reconstruction and analysis (COBRA) approach is based on three primary fundamental concepts: network constraints (parts a–d), objective functions (part e) and the association of reactions with the genome (part f) (Lewis et al., 2012).

2. CHAPTER I: GENOME-SCALE RECONSTRUCTION OF THE METABOLIC NETWORK IN *OENOCOCCUS OENI* TO ASSESS WINE MALOLACTIC FERMENTATION.

2.1 Introduction

Malolactic fermentation (MLF) is a key step in the production of most red wines, as well as some white and sparkling wines. This process is primarily responsible for lowering the acidity of wine, and also generates other benefits, such as improving aroma and flavor complexity; as well as increasing the biological stability of the resulting wines (Bartowsky et al., 2002; Davis et al., 1985; Henschke, 1993). This secondary fermentation, mainly carried out by lactic acid bacteria (LAB), involves the NAD^+ and manganese-dependent decarboxylation of L-malate to L-lactate and CO_2 (Kunkee, 1974; Williams et al., 1984). Failures in the onset and completion of malolactic fermentation are commonplace worldwide, which inconveniently delays the overall process of winemaking and therefore results in significant economic losses.

Oenococcus oeni is the main species involved in MLF due to its ability to grow in harsh environments, such as wine. This bacteria species is characterized by its high ethanol content (>13% v/v), low pH (< 3.5), limited nutrient availability and high sulphite concentration (<50 ppm) (Bartowsky, 2005; Bauer & Dicks, 2004; Zapparoli *et al*, 2009). Consequently, the success of this secondary fermentation depends on the ability of *O. oeni* to cope with these hostile conditions (Gockowiak & Henschke, 2003; Le Marrec *et al*, 2007) . Several studies have been conducted to understand the metabolism of *O. oeni* under oenological culture conditions. Despite these efforts, MLF remains an unpredictable, capricious and precarious operation of the winemaking process. Indeed, its onset and completion can take weeks or even months (Bartowsky et al., 2015).

Genome sequencing has paved the way to a deeper understanding of this microorganism. Mills et al. (2005) reported that the circular chromosome of *O. oeni* strain PSU-1 contained 1,780,517 nucleotides, with a guanine–cytosine (GC) content of 38%. Borneman *et al*. (2012) found important genomic differences among several O. *oeni* strains through a comparative analysis of the *O. oeni* pan genome, employing *O. oeni* PSU-1 strain as a reference. More recently, Campbell et al. (2015) reviewed the

population structure of many *O. oeni* strains using comparative genomics, and confirmed that the distribution of 50 strains can be divided into two major groups, according to their ecological niche: wine or cider. Transcriptomic and proteomic analyses of *O. oeni* strains cultivated under wine-simulated conditions showed that the environment strongly affects *O. oeni* stress-responses at both levels (Costantini et al., 2015; Olguín et al., 2015). Despite the bioinformatic tools employed for these studies, a full systemic understanding of the metabolic capabilities and behavior of this malolactic bacterium under extreme environments would strongly benefit from the reconstruction of a genome–scale metabolic model able to integrate the current knowledge of this LAB.

Genome annotation, databases and primary literature (Feist et al., 2009), along with specific collection of biochemical reactions and associated genes that describe the cell metabolism of a specific organism, can be employed for the reconstruction of the metabolic network at the genome scale (Thiele & Palsson 2010) . A genome-scale metabolic model (GSMM) is a mathematically structured format of different types of biological knowledge that is used to perform computational and quantitative queries to answer questions about the capabilities of an organism and its likely phenotypic states. GSMMs have primarily focused on six applications: (1) metabolic engineering, (2) model-driven discovery, (3) prediction of cellular phenotypes, (4) analysis of biological network properties, (5) studies of evolutionary processes, and (6) models of interspecies interactions (McCloskey et al., 2013). Initially, these models only considered well - characterized organisms; nevertheless, the interest in the generation of metabolic models of less characterized and complex biological systems has progressively increased, including the GSMMs of several lactic acid bacteria, such as *Lactococcus lactis* (Flahaut et al., 2013; Oddone et al., 2009; Oliveira et al., 2005; Verouden et al., 2009), *Lactobacillus plantarum* (Teusink et al., 2006) and *Streptococcus thermophilus* (Pastink et al., 2009).

In this work, we constructed the first genome-scale metabolic model of an *O. oeni* strain (named iSM454 model) to provide a tool for simulating the metabolism, nutritional requirements, and specific growth rate of this microorganism under the harsh conditions of winemaking. Here we report the general features of the model, as well as its prediction

performance. The resulting metabolic model was employed to assess the metabolic capabilities, limitations and potential of this LAB to successfully accomplish malolactic fermentation in wine**.**

2.2 Materials and Methods

2.2.1 Construction of the GSMM

The model was constructed following the protocol described by Thiele & Palsson (2010) (Figure 2-1). As a starting point, we generated a draft reconstruction with Pathway Tools™ version 16.5 (Karp et al., 2002) from the genomic sequence of *O. oeni* PSU-1. The model was then manually curated consulting scientific literature and the online databases KEGG™ [2] (Kyoto Encyclopedia of Genes and Genomes, Kanehisa, 2000), MetaCyc™ [3](Caspi et al., 2014) and TransportDB™ [4](Membrane Transport Database, Ren *et al*, 2007). Comparison with other genome annotations such as RAST[5], as well as with previous models MG1363 (Flahaut et al., 2013) and WCFS1 (Teusink et al., 2006) from *Lactococcus lactis* and *Lactobacillus plantarum* respectively, was conducted in order to find missing reactions (Table 2-1). The presence of the enzyme(s) responsible for carrying out these reactions in the genome were subsequently checked using the online available version of Basic Local Alignment Tools[6] (BLAST™, Madden 2002).

For proper network visualization, the model was then manually exported into Omix™ version 1.8 (Droste et al., 2011). Then, it was exported to MATLAB™ version 2013b, as an SBML file, and curated using Cobra Toolbox version 2.0. FBA, FVA, single gene deletion and single reaction deletion were performed to explore the metabolic capabilities of the network.

---

[2] http://www.genome.jp/kegg/

[3] https://metacyc.org/

[4] http://www.membranetransport.org/transportDB2/index.html

[5] http://blog.theseed.org/servers/

[6] https://blast.ncbi.nlm.nih.gov/Blast.cgi

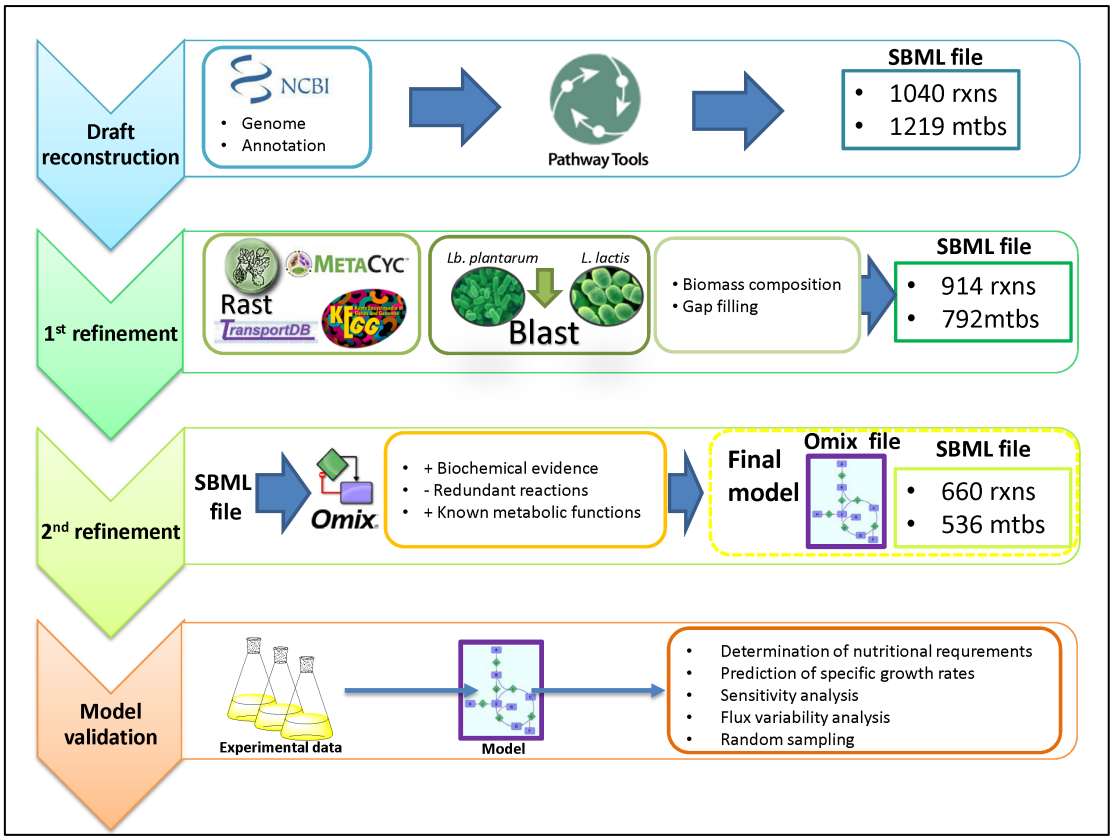

Figure 2-1: Genome-scale reconstruction of the metabolic network in *Oenococcus oeni* PSU-1, and model validation.

Table 2-1: Comparison between GSMM of *Oenococcus oeni* PSU-1, *Lactobacillus plantarum* WCFS1 and *Lactococcus lactis* IL1403. The table shows common reactions between models, unique reactions, and total reactions in the model of O. oeni. Figures in parentheses indicate uncommon reactions in the model respect to Lb. plantarum or Lc. lactis models.

	Common reactions with				**Unique reactions**	**Total reactions**
	Lb. plantarum		***Lc. lactis***		**both models**	**in *O. oeni***	**in *O. oeni***
Amino acids metabolism	39	*(21)*	40	*(20)*	32	13	60
ATP maintenance	1	*(0)*	1	*(0)*	1	0	1
Beta-oxidation	0	*(8)*	3	*(5)*	0	5	8
Biomass assembly	0	*(1)*	0	*(1)*	0	1	1
Carbohydrates metabolism	49	*(26)*	43	*(32)*	34	17	75
Citrate degradation	5	*(2)*	7	*(0)*	5	0	7
Exchange reactions	66	*(44)*	55	*(55)*	44	33	110
EPS biosynthesis	5	*(5)*	4	*(6)*	4	5	10
Fatty acid biosynthesis	40	*(23)*	4	*(59)*	2	21	63
Glycolipids metabolism	10	*(9)*	13	*(6)*	9	5	19
Glutathione redox reactions	1	*(3)*	1	*(3)*	1	3	4
Inorganic metabolism	5	*(7)*	2	*(10)*	1	6	12
Macromolecules assembly	2	*(4)*	4	*(2)*	2	2	6
Malolactic fermentation	1	*(0)*	1	*(0)*	1	0	1
Menaquinol metabolism	2	*(3)*	1	*(4)*	1	3	5
Nucleotides metabolism	53	*(19)*	53	*(19)*	47	13	72
Peptidoglycan biosynthesis	9	*(4)*	10	*(3)*	7	1	13
Terpenes biosynthesis	9	*(6)*	11	*(4)*	9	4	15
Thioredoxin redox reactions	0	*(1)*	0	*(1)*	0	1	1
Transport	30	*(101)*	24	*(107)*	15	92	131
Ubiquinol metabolism	0	*(3)*	0	*(3)*	0	3	3
Vitamins metabolism	27	*(16)*	20	*(23)*	15	11	43
TOTAL	**354**	***(306)***	**297**	***(363)***	**230**	**239**	**660**

2.2.2 Mathematical formulation

Flux balance analysis (FBA) is a widely used approach for studying biochemical networks. Among its many uses, FBA has been applied for predicting gene essentiality, quantifying the cellular growth under cultivation conditions and identifying by-product secretion (Park et al., 2009). This approach allows us to calculate the flow of metabolites through the network (Orth et al., 2010). Specifically, FBA quantifies the flux distribution by linear programming (LP) on the basis of stoichiometry of metabolic reactions and mass balances around metabolites under the pseudo-steady state, or stationary assumption (Park et al., 2009).

We employed FBA to calculate the optimal distribution of metabolic fluxes of an under -determined system of stoichiometric equations (Orth et al., 2010). Following formal procedures, the GSMM iSM454 was represented by a stoichiometric matrix *S*,

in which the row *i* represents the *i*th reaction and the column *j* the *j*th metabolite of the network. Under a pseudo-steady state assumption, the concentration of metabolites was considered to be constant, which is stated by the equation $S \times v = 0$, where v is the vector of reaction fluxes. To determine the flux distribution, biomass formation was defined as the objective function and optimized through LP (Equation 1). Gurobi 6.5 [7](Gurobi Optimization Inc., 2016) was chosen as the optimization solver.

(1) $Max\ \mu$

$Subjet\ to\ S \times v = 0$

$v_l \leq v_i \leq v_u\ \forall\ i = 1 \ldots n$

Where μ is the specific growth rate [1/h], v_i is the flux through reaction i, v_l and v_u are the lower and upper bounds for that reaction, and n is the number of reactions of the reconstruction.

2.2.3 Network evaluation

2.2.3.1 Determination of nutritional requirements

We ran *in silico* single omission experiments to determine the nutritional requirements of the *O. oeni* PSU-1 strain. For this purpose, we defined the restrictions required to simulate the nutrients included in the minimum culture medium described by Terrade et al. (2009); *i.e.* we allowed carrying flux only for exchange reactions corresponding to those nutrients that were present in the medium. Otherwise, lower and upper bounds of exchange reactions representing substrate uptake were set to zero (Supplementary material S1-1). Then, each nutrient was removed, one by one, and an optimization run was carried out each time. Nutrients that inhibited growth when removed were considered to be essential. We considered that growth was inhibited when the specific growth rate of the auxotrophic mutant was less than 20% that of the wild type. Results were classified as true positives (non-essential nutrients both *in silico* and *in vivo*), true negatives (essential nutrients both *in silico* and *in vivo*), false positives (essential

[7] http://www.gurobi.com/company/news/highlights-of-gurobi-optimizer-6.5

nutrients *in vivo* but not *in silico*) and false negatives (essential nutrients *in silico* but not *in vivo*).

From these predictions, we calculated critical statistical parameters that define model performance, *i.e.* sensitivity, specificity, precision, negative predictive value, accuracy, and the F-score, as follows:

(2) $Sensitivity = TP/(TP + FN)$

(3) $Specificity = TN/(TN + FP)$

(3) $Precision\ (PPV) = TP/(TP + FP)$

(4) $Negative\ predicted\ value\ (NPV) = TN/(TN + FN)$

(5) $Accuracy = (TP + TN)/(TP + TN + FP + FN)$

(6) $F - score = 2(precision \times sensitivity)/(precision + sensitivity)$

2.2.3.2 Prediction of ATP-maintenance

Following standard procedures, we added an equation (equation 7) to represent non-growth associated maintenance (NGAM).

(7) $ATP + H_2O \rightarrow ADP + P_i + H^+$

The values of NGAM were determined from the model for each experimental condition. For this purpose, we first fixed the consumption and production rates of different metabolites and then we progressively increased the NGAM from 0 to 5 mmol $gDW^{-1}\ h^{-1}$. At each iteration, the growth rate was maximized and the error between the experimental and predicted growth rate was calculated. The value that minimized the error between the experimental and predicted growth rate was chosen as the ATP required for maintenance of cellular processes.

The experimental rates included in the model were specific consumption rates of glucose, fructose, citrate, L-malate, L-cysteine, L-serine, L-threonine; it also included specific production rates of D-mannitol, L-lactate, D-lactate, acetate, erythritol and ethanol (Contreras et al, in preparation). They were calculated from experimental data of three batch cultures containing 0% and 12% ethanol, respectively, run in duplicate (see below).

2.2.3.3 Experimental determination of specific growth rates and consumption/production rates

An *O. oeni* PSU-1 preculture was prepared from a frozen stock by inoculating 100-ml Erlenmeyer flasks containing 75 ml MRS (Man, Rogosa and Sharpe) medium (De Man et al., 1960), supplemented with 0.5 g L^{-1} of cysteine. Before inoculation, the cells were subjected to ethanol adaptation. For this purpose, we serially passaged every culture, starting from 1% ethanol (v/v) to reach 0 or 12% ethanol concentration (v/v) in each culture.

The adapted cells were inoculated in 50 mL flasks containing 35 mL of a chemically defined, wine-like, culture medium to achieve an initial optical density at 600 nm (OD600) of approximately 0.2. We employed the modified culture medium described by Terrade *et al*., (2009), at an initial pH adjusted to 4.8.

The flasks were incubated at 25 °C, without stirring. OD600 was periodically measured to calculate the specific growth rate. At the same time, the content from each flask was centrifuged, the supernatant was collected, and an aliquot was injected in a Lachrom L-700 HPLC system (Hitachi, Japan) equipped with a Diode Array and a Refractive Index detector (Merck Hitachi, Japan). Organic acids, alcohols and sugars were separated using an Aminex HPX-87H ion exchange carbohydrate-organic acid column (Bio-Rad, USA) and quantified, as described previously (Varela et al., 2003).

2.2.3.4 Amino acids essentiality assay

An *O. oeni* PSU-1 preculture was prepared from a frozen stock as described above. The cells (not pre-adapted in ethanol) were inoculated in 50 mL flasks containing 35 mL of the same chemically defined, wine-like, culture medium, but lacking the amino acids evaluated for essentiality (glutamate, glutamine, asparagine, and threonine), one amino acid per flask, in duplicate. The flasks were incubated at 25°C for 13 days, without stirring, and OD600 was periodically measured to calculate the specific growth rate.

2.2.3.5 Sensitivity analysis

For each optimization using experimental data, non-zero reduced costs were extracted from the solver solution and employed for quantifying the impact of changing a capacity constraint on the objective flux. Scaled reduced costs were calculated as follows:

(8) $$W_i = w_i \times q_i/\mu$$

Where w_i represents the reduced cost, q_i the flux through exchange reaction *i,* and μ the specific growth rate. W_i, the scaled reduced cost of the exchange reaction *i,* represents the fractional change in biomass obtained by a fractional variation in compound *i*. Reactions that showed both, a non-zero reduced cost and a non-zero scaled reduced cost, were further analyzed.

2.2.3.6 Flux Variability Analysis

Flux variability analysis (FVA) was carried out by minimizing and maximizing the flux through each reaction, under either unconstrained or constrained conditions. Span range was sorted by magnitude and plotted.

Reactions unable to carry flux were considered blocked. For each of these, the cause of the obstruction was investigated by finding dead-end metabolites; these were determined searching for those metabolites that were only consumed or produced in the stoichiometric matrix. Additionally, we determined dead-ends by adding a demand (maximizing the flux) or a sink (minimizing the flux) reaction for each metabolite. Metabolites were considered dead-ends if the model was unable to produce, nor consume them.

2.2.3.7 Random Sampling

We conducted a random sampling analysis using optGpSampler (Megchelenbrink et al., 2014), an efficient algorithm based on the Monte Carlo procedure *hit and run* (Smith, 1984). For each experimental condition, we set the algorithm parameters in order to sample 100.000 points using 500 steps between each point.

We applied the algorithm to explore the solutions at an optimal specific growth rate for each experimental condition. For this purpose, the model was restricted with

the calculated optimal growth rate and the corresponding experimental consumption/production rates. Then, we applied the algorithm for determining the 100,000 flux distributions that accomplished these restrictions. For every condition, we found the 50 reactions that showed the greatest flux variations among the distributions. We classified these reactions according to pathways and then we sorted pathway frequency.

We also applied this algorithm to explore the solutions near the optimal specific growth rate, by following the same procedure described above. For this purpose, the lower bound for specific growth rate was fixed at 90% of the optimal, and the upper bound, at the optimal specific growth rate.

2.3 Results

2.3.1 General features of the GSMM of *Oenococcus oeni* PSU-1 strain

The iSM454 model (Supplementary material S2-2) consists of 660 reactions, 536 metabolites and 454 genes. 24% of the 1864 genes described in the genome annotation (Makarova et al., 2006) were included in the model. 68% of the reactions are associated at least to one gene. The model includes 132 transport reactions, 110 exchange reactions, 3 extracellular reactions (dextran synthesis, heteropolysaccharide synthesis and cellulose degradation) and 411 intracellular reactions. It contains 148 blocked reactions, *i.e.* reactions that do not carry flux, including 107 that contain dead-ends (Table 2-2).

Connectivity corresponds to the number of reactions where a metabolite participates. As shown in Table 2-3, the iSM454 model presents a similar connectivity, in relation to key metabolites, with WCFS1 (*Lb. plantarum*), IL1403 (*Lc. Lactis*) and Yeast 7 (*S. cerevisiae*) models (Aung et al., 2013; Oliveira et al., 2005; Teusink et al., 2006). The connectivity analysis (Supplementary material S2-3) indicates that 240 out of the 536 metabolites included in the iSM454 model participate in two metabolic reactions: 100 in three reactions, and only 40 in more than seven reactions. 100 dead - end metabolites were also found.

Table 2-2: Main features of genome scale metabolic model of *O. oeni* PSU-1.

Total Genes	**1864**
Included genes	454
Total Pathways	**91**
Total Reactions	**660 (448) [a]**
Intracellular	413 (340) [a]
Extracellular	3 (2) [a]
Transport	133 (106) [a]
Exchange	111
Spontaneous	8
Assembly	7
Non-genes associated [b]	101
Blocked	148
With dead-ends	107
Without dead-ends [c]	41
Total Metabolites	**536**
Intracellular	434
Extracellular	102

[a] In brackets, number of reactions associated to genes
[b] Exchange reactions are not considered
[c] Without dead-ends, but associated to reactions with dead-ends

Table 2-3: Comparison of key metabolites connectivity between SM454 model (*O. oeni*), WCFS1 (*Lb. plantarum*), IL1403 (*Lc. lactis*) and Yeast 7(*S. cerevisiae*) models.

	Connectivity			
	O. oeni **iSM454**	***Lb. plantarum*** **WCFS1**	***Lc. lactis*** **IL1403**	***S. cerevisiae*** **Yeast 7**
NADPH	32	34	37	58
$NADP^+$	33	35	39	58
NADH	39	57	36	36
PPi	43	63	50	69
NAD^+	43	62	40	42
Pi	96	93	101	155
ADP	111	113	113	121
ATP	128	148	130	158
H_2O	162	165	141	269
H^+	230	382	110	433

2.3.2 Metabolic Refinement of the iSM454 model

The metabolism of carbohydrates, amino acids, and fatty acids, as well as macromolecular assembly, transport, and ATP production, were thoroughly checked at this stage, as described below.

Carbohydrates metabolism. *O. oeni* is a heterofermentative bacterium. It consumes hexoses through the 6-phospho-gluconate pathway and produces carbon dioxide, D-lactate, acetate and/or ethanol. The main metabolized hexoses are glucose and fructose. The latter can also be transformed into mannitol or erythritol to fulfill the demand for NAD^+ required in the heterolactic fermentative pathway. Even though the genes related to mannitol and erythritol biosynthetic pathways were not found in the PSU-1 genome, these pathways were included in the model to account for reported experimental data (Beelman et al. 1977, Contreras et al, in preparation). The membrane transporters of these and other carbohydrates - arabinose, ribose, melibiose, mannose, fucose, xylose and galactose - were found using PathoLogic (Dale et al., 2010), which is provided by Pathway Tools, and included in iSM454.

Meanwhile, as *O. oeni* synthesizes exopolysaccharides (EPS) (Ciezack et al., 2010; Dimopoulou et al., 2012, 2014), we included 7 reactions responsible for EPS biosynthesis, associated with 22 genes annotated in the genome.

Finally, we also curated the pathways related to peptidoglycan biosynthesis. The draft reconstruction contained three alternative pathways to synthesize peptidoglycan (pathways I, III or V). We only left pathway I in the model because it was the most complete, *i.e.,* 9 out of the 10 reactions of this pathway were associated with genes.

Amino acids metabolism. The iSM454 model contains the whole biosynthetic pathways for 6 amino acids (alanine, aspartate, glutamine, lysine, proline and glycine), as arisen from gene annotation (Mills et al., 2005). The biosynthetic pathways of the remaining 14 amino acids are incomplete however (arginine, asparagine, cysteine, glutamate, histidine, isoleucine, leucine, methionine, phenylalanine, serine, threonine, tryptophan, tyrosine, and valine), in accordance with genomic analysis (Mills et al., 2005).

Fatty acids metabolism. *O. oeni* does not store triglycerides as an energy reserve. Instead, fatty acids are mainly utilized for the construction of the cytoplasmic

membrane. The lipid fraction of *O. oeni* is mainly composed by saturated fatty acids (laurate, myristate, palmitate, stearate), unsaturated fatty acids (palmitoleate, oleate, cis-vaccenate) and cyclopropane fatty acids (lactobacillate and dihydrosterculate) (Garbay et al., 1995; Guerrini et al., 2002; Lonvaud-Funel & Desens, 1990; Tracey & Britz, 1989b). Biosynthesis of saturated fatty acids was automatically included into the model by Pathway Tools. Meanwhile, the biosynthesis of unsaturated and cyclopropane fatty acids were manually added to the model with their respective gene associations.

The synthetic routes for cardiolipin, 3-D-glucosyl-1,2-diacylglycerol, L-1-phosphatidyl-glycerol, and lysophosphatidylglycerol, starting from dihydroxyacetone phosphate, were also included.

In relation to β-oxidation of fatty acids, Pathway Tools assigned two genes, *OEOE_1366* and *OEOE_1263*, to the same acyl-CoA synthetase (EC number 6.2.1.3) associated with a generic acyl fatty acid. We therefore manually included these genes and reactions for the canonical catabolism of the above-mentioned saturated fatty acids.

Assembly of macromolecules. A modified version of the reported biomass equation of *L. lactis* (Oliveira et al., 2005) was included in iSM454, according to some unique features reported in the literature for *O. oeni*. For example, deoxyribonucleotide content was taken from the genomic analysis for *O. oeni* PSU-1 (Makarova et al., 2006). Fatty acid composition was determined as the average of each individual molecule (Garbay et al., 1995; Guerrini et al., 2002; Lonvaud-Funel & Desens, 1990; Tracey & Britz, 1989b). Amino acids, ribonucleotides and lipids composition correspond to *L. lactis* biomass composition (Oliveira et al., 2005). Similarly, macromolecular elements (proteins, lipids, DNA and RNA) were included (Oliveira et al., 2005). Finally, the lipoteichoic acid (LTA) synthetic pathway present in the *L. lactis* genome was eliminated because the genes for its synthesis were absent in the *O. oeni´s* genome and its presence has not been described in this microorganism (Ribéreau-Gayon et al., 2006).

Energy. Malate metabolism was added to the model, considering the transformation of malic acid to lactic acid by the malolactic enzyme (malate decarboxylase), codified by

the *OEOE_1564* gene. In this reaction, a cytosolic proton is consumed, and lactic acid diffuses outside of the cell (Figure 2-2) (Konings et al, 1997; Salema et al, 1996). The net result of this process is a decrease in the concentration of intracellular protons, contributing to the formation of an electrochemical gradient. Additionally, the citrate lyase complex was lumped into one reaction, directly allowing the conversion of citrate to oxaloacetate. A stoichiometric equation to account for the diffusion of citrate inside *O. oeni* was also added. The model also contains a functional ATP synthase system.

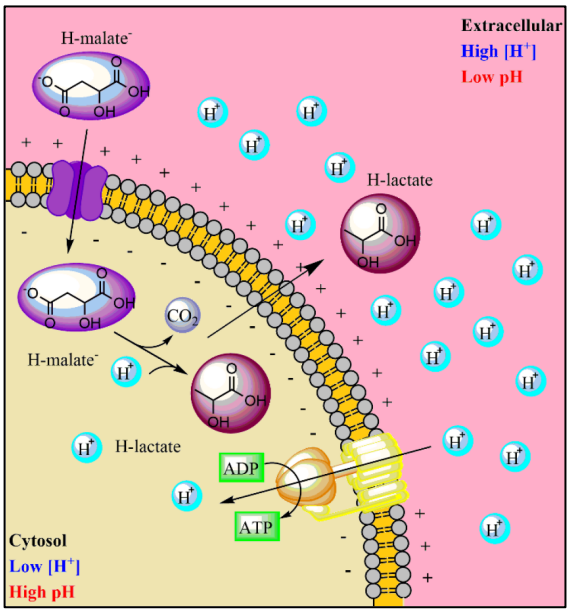

Figure 2-2: Electrochemical gradient formation in *Oenococcus oeni* towards the malolactic fermentation.

2.3.3 Model Validation

With the aim of determining the functionality of the model, we contrasted the results predicted by iSM454 with experimental data.

2.3.3.1 Determination of *in vivo* amino acids requirements

Model outputs of the essentiality of some amino acids differed from literature data (Fourcassie et al., 1992; Garvie, 1967b; Mills et al., 2005; Terrade & Mira de Orduña, 2009; Tracey & Britz, 1989a). Therefore, we addressed these differences by experimentally evaluating their role on cell growth (Figure 2-3).

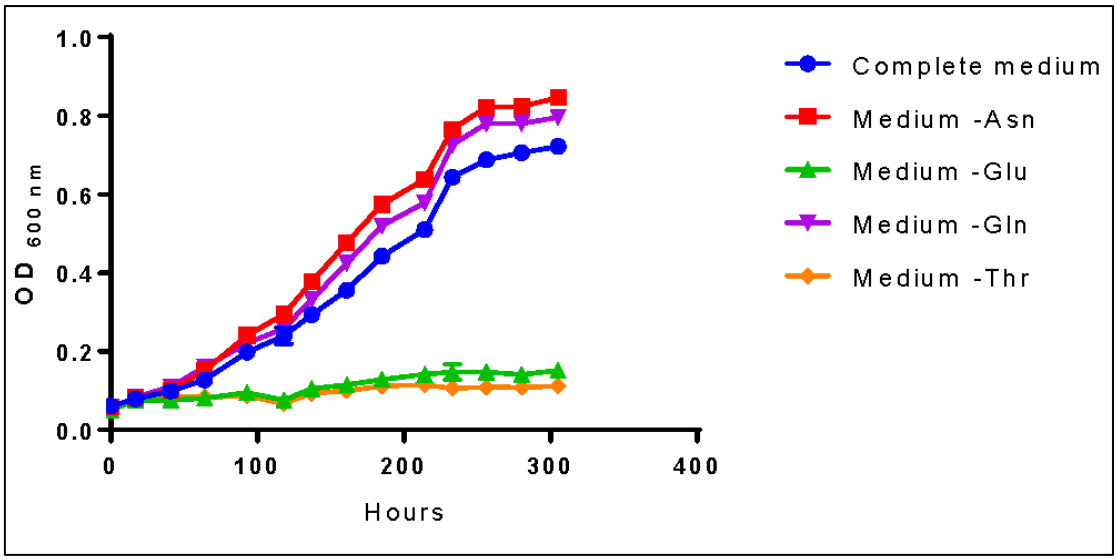

Figure 2-3: Amino acids essentiality analysis of *O. oeni* PSU-1. The amino acids studied are those with controversy with literature. Bacterial growth was compared with the complete medium (and the medium lacking asparagine (- Asn), glutamate (- Glu), glutamine (- Gln) and threonine (- Thr).

For example, Mills *et al*, (2005) reported that the genes related to the threonine biosynthetic pathway were all present in PSU-1. However, we identified a pseudogene within this pathway and experimentally demonstrated its essentiality for *O. oeni* PSU-1. On the contrary, even though several genes of the asparagine biosynthetic pathway were not found in the genomic sequence, our experimental results confirmed that *O. oeni* PSU-1 could synthesize this amino acid (Figure 2-3); and the whole pathway was included in the reconstructed model. In the case of glutamine, both our experimental results and model reconstruction confirmed that this amino acid is not essential, at least for this strain. Finally, *O. oeni* PSU-1 showed auxotrophy for glutamate, in agreement with previous results (Fourcassie et al., 1992; Garvie, 1967b; Mills et al., 2005; Terrade & Mira de Orduña, 2009; Tracey & Britz, 1989a).

2.3.3.2 Determination of *in silico* nutritional requirements

First, we carried out an *in silico* single omission experiment to compare the nutritional requirements predicted by the model with the experimental data obtained after growth of *O. oeni* in the culture medium of Terrade et al. (2009) (Table 2-4). Additionally, a

confusion matrix was constructed to measure the performance of our predictions (Figure 2-4). This approach has been used before to assess the GSMM quality of *S. cerevisiae* iIN800 (Nookaew et al., 2008) and iLL672 (Kuepfer et al., 2005), as well as for *L. plantarum* (Teusink et al., 2006) and *Y. lypolitica* (Loira et al., 2012)).

The *in-silico* analysis of nutritional requirements showed that at least one carbon source is required for growth. Thus, one out of the 9 following carbon sources could be employed to sustain growth: glucose, fructose, ribose, galactose, arabinose, cellobiose, trehalose, melibiose or gluconate. Additionally, the model predicted that 14 amino acids are essential for growth (arginine, cysteine, histidine, isoleucine, methionine, phenylalanine, tryptophan, tyrosine, valine, leucine, threonine, serine, glutamate, and asparagine), and that the 6 remaining ones (alanine, aspartic acid, glutamine, glycine, lysine, and proline) were not.

Table 2-4: Experimental validation of the iSM454 metabolic model. We compared 61 *in vivo* experiments with *in silico* simulations under different media conditions. From the 61 experiments, we obtained 30 true positives (TP), 27 true negatives (TN), 1 false positive (FP) and 3 false negative (FN). + growth is achieved by *O. oeni* when the nutrient is removed, *i.e.*, the nutrient is not essential; - growth is not achieved by *O. oeni* when the nutrient is removed, *i.e.*, the nutrient is essential.

Nutrient	***In vivo***	***In silico***	**Result**	**References**	**Nutrient**	***In vivo***	***In silico***	**Result**	**References**
Carbon sources					**Amino acids**				
D-Glucose	+	+	TP	1	L-Alanine	+	+	TP	2
Fructose	+	+	TP	1	L-Arginine	-	-	TN	2,3,4,5
D-Ribose	+	+	TP	1,2	L-Asparagine	-	-	TN	2
Threhalose	+	+	TP	1	L-Aspartic acid	+	+	TP	2,3,4,5
Cellobiose	+	+	TP	1	L-Cysteine	-	-	TN	2,3,4,5
D-Deoxyribose	-	-	TN	1	L-Glutamic acid	-	+	FP	2,3,4,5
D-Xylose	-	-	TN	1	L-Glutamine	+	+	TP	2
L-Arabinose	-	+	FP	1	L-Glycine	+	+	TP	2,3,4,5
L-Rhamnose	-	-	TN	1	L-Histidine	-	-	TN	2,3,4,5
D-Mannose	-	-	TN	1	L-Isoleucine	-	-	TN	2,3,4,5
Esculin	+	-	FN	1	L-Leucine	-	-	TN	2,3,4,5
Salicin	+	-	FN	1	L-Lysine	+	+	TP	2,3,4,5
Glycerol	-	-	TN	1	L-Methionine	-	-	TN	2,3,4,5
D-Mannitol	-	-	TN	1	L-Phenylalanine	-	-	TN	2,3,4,5
L-Sorbitol	-	-	TN	1	L-Proline	+	+	TP	2,3,4,5
L-Malic acid	-	-	TN	1	L-Serine	+	-	FN	2,3,4,5
Citric acid	-	-	TN	1	L-Threonine	-	-	TN	2,3,4,5
Fumaric acid	-	-	TN	1	L-Tryptophan	-	-	TN	2,3,4,5
Nucleotides					L-Tyrosine	-	-	TN	2,3,4,5
Adenine	+	+	TP	2	L-Valine	-	-	TN	2,3,4,5
Guanine	+	+	TP	2	**Vitamins**				
Xanthine	+	+	TP	2	4-Aminobenzoic acid	+	+	TP	2
Cytosine	+	+	TP	2	Biotin	+	+	TP	2
Thymine	+	+	TP	2	Choline	+	+	TP	2

Uracil	+	+	TP	2	Cyanocobalamin	+	+	TP	2
Minerals					Folic acid	+	+	TP	2
$MnSO_4 \cdot 4 H_2O$	-	-	TN	2	Nicotinic acid	-	-	TN	2
$MgSO_4 \cdot 7 H_2O$	+	+	TP	2	D-Pantothenate	-	-	TN	2
K_2HPO_4	-	-	TN	2	Pyridoxine	+	+	TP	2
$CaCl_2$	+	+	TP	2	Riboflavin	+	+	TP	2
$CuSO_4 \cdot 5 H_2O$	+	+	TP	2	Thiamine	+	+	TP	2
$FeSO_4 \cdot 7 H_2O$	+	+	TP	2					
$ZnSO_4 \cdot 7 H_2O$	+	+	TP	2					

References: 1 (Beelman et al., 1977), 2 (Terrade & Mira de Orduña, 2009), 3 (Garvie, 1967b), 4 (Fourcassie et al., 1992), 5 (Remize et al., 2006).

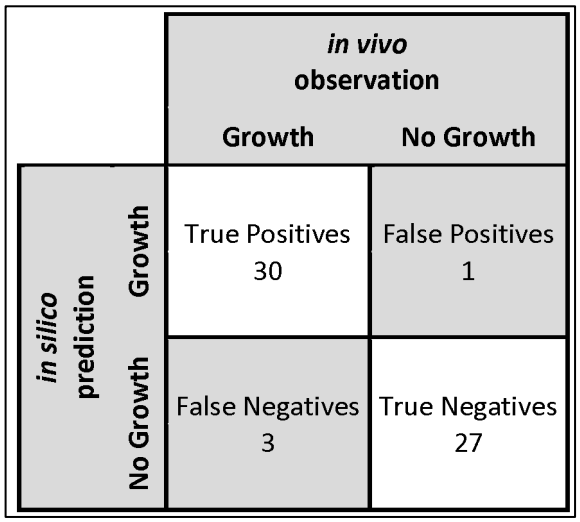

Figure 2-4: Confusion matrix used to measure the performance of predictions in the determination of *in silico* nutritional requirements. The statistical parameters that define model performance are: sensibility of 97%, specificity of 90%, precision 91% negative predictive value of 96%, accuracy of 93% and F-score of 94%.

Single nucleotide omission experiments of iSM454 showed that these metabolites were not essential for *O. oeni.* On the other hand, nicotinic acid and pantothenate were predicted to be essential nutrients. Moreover, several vitamins, such as biotin, folic acid, pyridoxine, riboflavin, and thiamin were not essential.

The model was able to identify that *O. oeni* was able to grow in 97% of those cases (sensitivity); whereas it identified 90% of the cases where the *O. oeni* did not grow (specificity). Furthermore, 91% of the experiments in which *O. oeni* were

predicted to grow, *O. oeni* actually grew (precision). Additionally, 96% of the experiments in which *O. oeni* was not predicted to grow, *O. oeni* actually did not grow (NPV). The accuracy of the model was 93%*, i.e.,* the proportion of correct results to total predictions. By comparison, the GS model of *L. plantarum* presents an accuracy of 86% (Teusink et al., 2005); and the iIN800 model of *S. cerevisiae*, 89% (Nookaew et al., 2008). Finally, the F-score, a measure of the accuracy that can be interpreted as a weighted average of the sensitivity and the precision, was 94%, indicating that overall the model has a very good performance.

We obtained one false positive related to prediction of growth in the absence of L-glutamate, because of the presence of transamination reactions in the network, which artificially allowed the production of this amino acid. On the other hand, we obtained three false negatives related to growth in the absence of L-serine, and growth with esculin and salicin as sole carbon sources.

2.3.5 Applications

The reconstructed GSMM can be employed to study metabolic fluxes, as well as to identify gene or nutrient essentiality *in silico*. In the following, we exemplify some potential uses of the iSM454 model.

2.3.5.1. Prediction of Non-Growth Associated Maintenance (NGAM)

In order to predict the NGAM values for each experimental data set, we optimized the growth rate considering a range of possible NGAM values. The value of NGAM that allowed the minimal error at each specific growth rate prediction was selected, reaching an average error in the biomass formation of 0.14% in the two conditions analyzed. These NGAM values accounted for 0.07 and 2.3 mmol of ATP gDW^{-1} h^{-1} at 0 and 12% ethanol, respectively. Thus, when exposed to 12% ethanol, *O. oeni* PSU-1 spends 30 times more ATP to maintain the cellular machinery than in the absence of ethanol.

2.3.5.2. Impact of ethanol concentration on the redistribution of intracellular fluxes

Flux Balance Analysis (FBA) of experimental data showed that a significant redistribution of intracellular fluxes occurs in the cell when *O. oeni* is grown in the absence of ethanol or under 12% ethanol content. To compare these two conditions, fluxes were standardized by growth rate. The glucose uptake rate is similar for 0% and 12% ethanol (Figure 2-5). On the contrary, significant changes occur in the consumption rates of fructose, malate, and citrate. The uptake rate of these compounds increases 102%, 169% and 127%, respectively, when the bacterium is cultivated with 12%v/v ethanol. The net result is an increase in the fluxes through the heterolactic pathway. Consequently, a higher production rate of D-lactate (279%), L-lactate (144%), acetate (150%), mannitol (39%) and erythritol (7%), was achieved.

Despite the fructose uptake rate more than double in cultures with 12% ethanol, the mannitol production rate only increased by 39%. Indeed, in the absence of ethanol, $Y_{mannitol/fructose}$ was 0.82; meanwhile, at 12% ethanol, this yield decreased to 0.56. Thus, fructose in cultures with ethanol is preferentially transformed to fructose-6-phosphate - and then to glucose-6-phosphate – compared to those without ethanol, which subsequently leads to a higher production of D-lactate and acetate. In fact, considering total carbon source as the sum of glucose, fructose, citrate and L-malate, resulting $Y_{D-lactate/total\ C}$ and $Y_{acetate/total\ C}$ were 0.044 and 0.35 in the absence of ethanol; and 0.086 and 0.46 at 12% ethanol, respectively.

The flux through the malolactic reaction was also much faster in ethanol-containing cultures. The uptake rate of L-malate increased 169%, and the concomitant production rate of L-lactate, 144%. It is worthy to note that in both cases, not all the L-malate was transformed to L-lactate. A minor fraction is transformed to oxaloacetate through the malate dehydrogenase. Interestingly, $Y_{L-lactate/L-malate}$ slightly decreased from 0.79 to 0.71, suggesting that for cells grown at 12% ethanol, a higher part of L-malate is destined to oxaloacetate.

Ethanol content significantly impacts the production rate of diacetyl, which increases from 0 to 4.23 mmol gDW^{-1} h^{-1}. Regarding erythritol, even though its production remains almost the same in both conditions $Y_{erythritol/glucose+fructose}$ decreased from 0.36 to 0.25, suggesting that a higher extent of fructose and glucose is transformed into other metabolites than erythritol.

As expected from the higher carbon flow through the heterolactic pathway in ethanol-containing cultures, the corresponding ATP specific production rate was three-fold faster than in the absence of ethanol, passing from 0.74 to 1.98 mmol gDW^{-1} h^{-1} for 0 and 12% ethanol, respectively. These were calculated by adding the fluxes of acetate kinase (EC 2.7.2.1), pyruvate kinase (EC 2.7.1.40) and phosphoglycerate kinase (EC 2.7.2.3); and subtracting the fluxes through hexokinase (EC 2.7.1.1/E.C 2.7.1.2) and fructokinase (EC 2.7.1.4). On the other hand, by using the usual method for ATP determination through heterolactic fermentation, which consists of adding the total D-lactate and acetate produced, the resulting ATP production rates were 1.38 and 2.12 mmol gDW^{-1} h^{-1}, for 0% and 12% ethanol-containing cultures, respectively.

Total ATP production increases as the concentration of ethanol in the medium increases (Figure 2-6). The model includes ATP generation by both, heterolactic fermentation and ATP synthase. At high ethanol content, the percentage of ATP produced via ATP synthase slightly decreases, from 48% to 45%; while the ATP formed through the heterolactic fermentation increases, correspondingly.

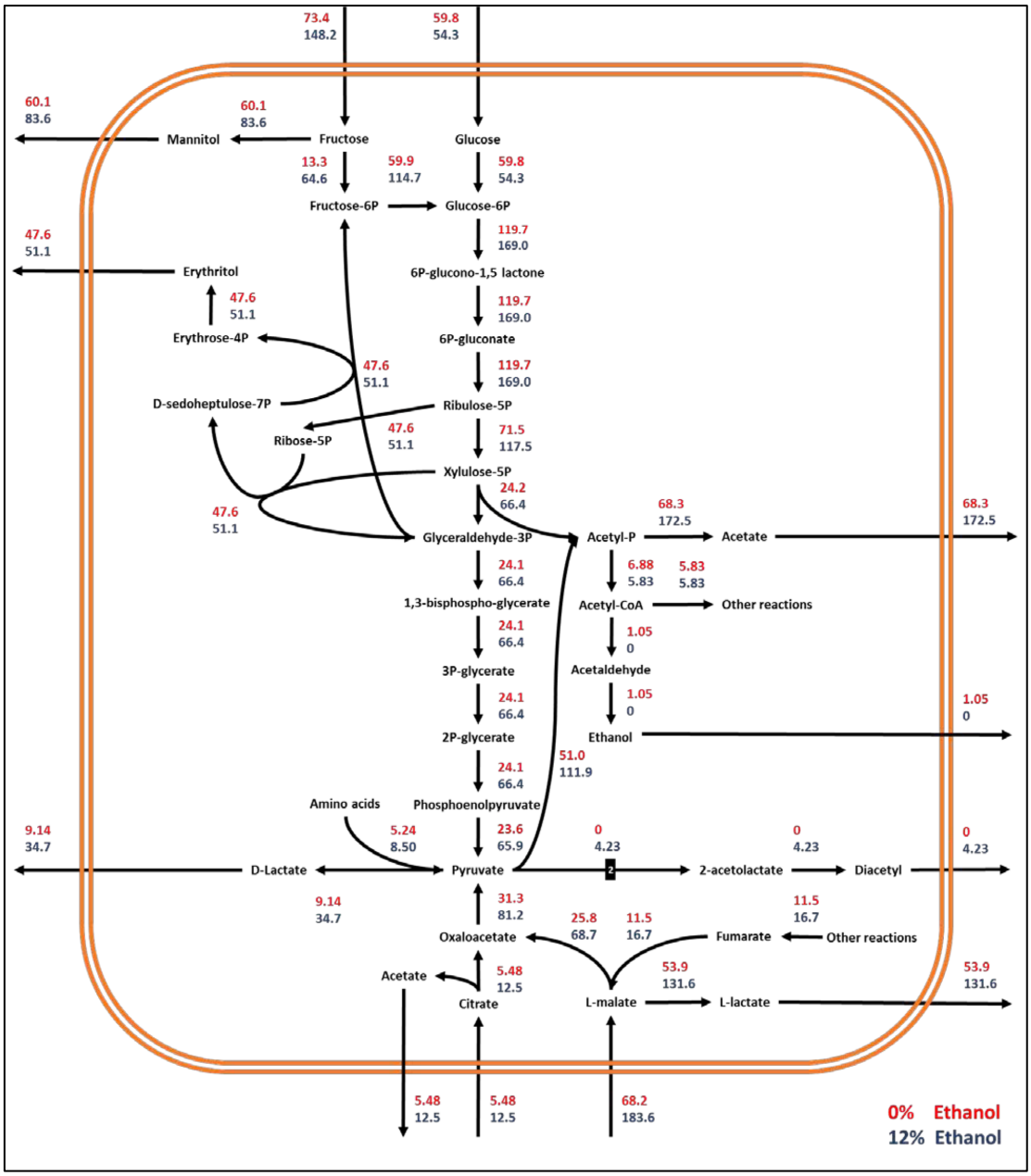

Figure 2-5: Metabolic flux redistribution of the central carbon metabolic pathways of *O. oeni* PSU-1 upon cultivation in a culture medium with 0% (red), and 12% (blue) ethanol concentration. The number "2" in the reaction pyruvate to 2-acetolactate means that two moles of pyruvate generate one mole of 2-acetolactate.

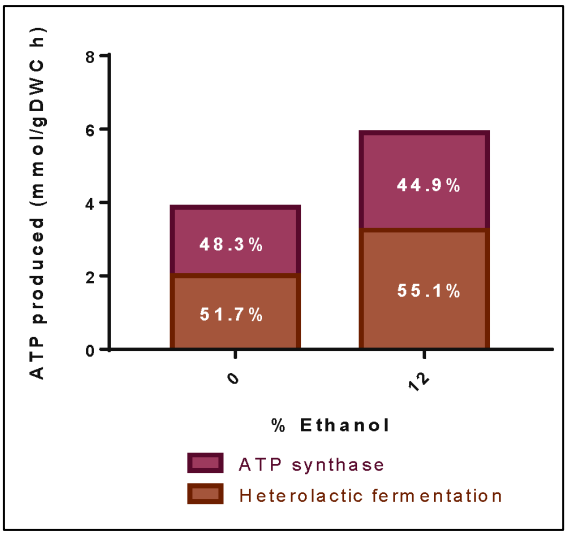

Figure 2-6: Production of ATP at different ethanol concentrations. The figure illustrates the total ATP produced during simulation of experimental data at pH 4.8 and at different ethanol concentrations. Numbers indicate the ATP production either by heterolactic fermentation (dark bars) or ATP Synthase (light bars).

2.3.5.3 Sensitivity Analysis

We assessed the impact of exchange reactions on the growth of *O. oeni*, by conducting a sensitivity analysis (Table 2-5) through estimation of the reduced costs, as well as of the scaled reduced costs, associated with these constrained fluxes. This methodology has been used before to assess the impact of metabolic reactions on ATP formation in the lactic acid bacterium *Lactobacillus plantarum* (Teusink et al., 2006). Reduced costs allow quantifying how much the objective flux could be improved by changing a capacity constraint. Scaled reduced costs represent the reduced cost normalized by the current biomass flux and the flux associated with the constraint. They allow computing the relative effect of a change in a parameter to the whole system.

The increase of sugar uptake rate - fructose or glucose - had a positive effect on the specific growth rate (scaled reduced costs of 2.59 and 1.67, respectively) as well as the transport of acids -malate or citrate uptake- (scaled reduced costs of 0.86 and 0.03, respectively), and the export of acetate, L- and D-lactate (0.47, 0.34, 0.09 respectively). The specific uptake rate of cysteine, serine and threonine also showed a positive effect on the specific growth rate (scaled reduced costs of 0.05, 0.01 and 0.06, respectively).

On the contrary, the production rate of D-mannitol and D-erythritol had a negative effect on the specific growth rate, which showed scaled reduced cost of -2.67 and -1.48, respectively.

2.3.5.4. Exploring the solution space.

To evaluate the robustness of our results, we employed random sampling and Flux Variability Analysis (FVA) to identify and explore the different phenotypes achieved at optimal specific growth rate.

Table 2-5: Sensitivity Analysis of the model using experimental data at pH 4.8. Reactions analyzed correspond to exchange reactions of the model. Reduced cost quantifies how much the objective flux (specific growth rate) improves by changing a capacity constraint, and scaled reduced cost is the reduced cost normalized by the current biomass flux and the flux associated to the constraint. Positive value indicates an improvement in the specific growth rate, and negative value indicates a decrease.

Reaction	Direction	Reduced cost	Scaled reduced cost
β-D-fructose [ex]	consumed	0,023 ± 0,007	2,585 ± 0,824
α-D-glucose [ex]	consumed	0,031 ± 0,007	1,670 ± 0,433
D-mannitol [ex]	produced	-0,035 ± 0,008	-2,671 ± 0,817
Citrate [ex]	consumed	0,005 ± 0,008	0,033 ± 0,066
(R)-lactate [ex]	produced	0,003 ± 0,005	0,089 ± 0,154
(S)-lactate [ex]	produced	0,003 ± 0,005	0,338 ± 0,586
(S)-malate [ex]	consumed	0,009 ± 0,005	0,860 ± 0,502
L-Cys [ex]	consumed	0,012 ± 0,003	0,054 ± 0,013
L-Ser [ex]	consumed	0,005 ± 0,005	0,011 ± 0,012
L-Thr [ex]	consumed	0,022 ± 0,002	0,057 ± 0,009
Ethanol [ex]	produced	-0,005 ± 0,009	-0,005 ± 0,009
Acetate [ex]	produced	0,003 ± 0,002	0,468 ± 0,482
D-erythritol [ex]	produced	-0,032 ± 0,010	-1,488 ± 0,412

FVA revealed some important differences between unconstrained and constrained networks (Figure 2-7). 485 and 419 reactions were able to carry flux in the unconstrained and constrained network, respectively. The larger differences were found for reactions with a narrow flux range (less than 1 mmol gDW^{-1} h^{-1}, *i.e.,* a negative value for the logarithm of the flux range in Figure 2-7). We found only 30 reactions with a flux range of less than 1 mmol gDW^{-1} h^{-1} in the unconstrained network; meanwhile, this value increased to 370 in the constrained network. Moreover, 99% of

the reactions in the constrained network showed a flux range lower than 3 mmol gDW^{-1} h^{-1}, suggesting that the constraints applied (uptake and production rates) strongly delimit the solution space. Thus, applying these constraints, the phenotype is well defined.

Additionally, random sampling in the constrained network revealed that the solution space was tight and alternative pathways were limited. Except in the case of reactions of isomer interconversions which could result in a futile cycle, none of the reaction rates analyzed changed more than 1.1 mmol gDW^{-1} h^{-1}.

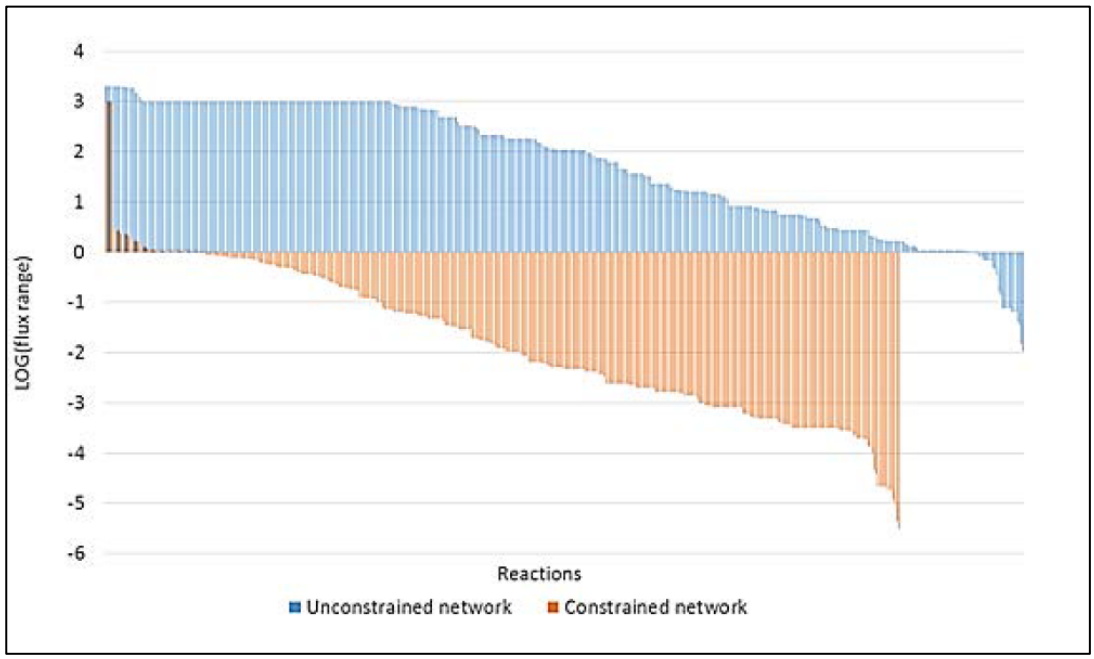

Figure 2-7: Flux Variability Analysis for unconstrained and constrained networks. The figure illustrates the flux range in mmol gDW-1 h-1 for every non-blocked reaction of the unconstrained (blue) and constrained (orange) network expressed as base 10 logarithm. Flux range of the constrained network was calculated as the average flux ranges of networks applying constraints for 0 and 12% of ethanol content.

Interestingly, when constrained by experimental rates, FVA shows that *O. oeni* requires oxygen to achieve growth at all ethanol levels. Moreover, the oxygen consumption rates needed for growth increase as the concentration of ethanol increases, ranging from 0.8-1.2 and 4.1- 4.2 mmol gDW^{-1} h^{-1} for 0% and 12% ethanol, respectively.

2.3.5.5 *In silico* reaction deletion analysis

The essential reactions of *O. oeni* were predicted by *in silico* simulations of reaction knockouts – inhibiting the activity of the enzyme(s) carrying away the respective reaction. This was conducted by further constraining the model, *i.e.*, fixing the flux of the corresponding reaction to zero.

132 essential reactions were found by reaction deletion analysis, which represent 20% of the 660 total reactions of the model; of these, 28% correspond to fatty acid biosynthesis, and 14% to unsaturated fatty acid biosynthesis. The other main essential pathways include the biosynthesis of peptidoglycan (10%), glycerolipids (8%) and amino acid biosynthesis (8%) (Figure 2-8).

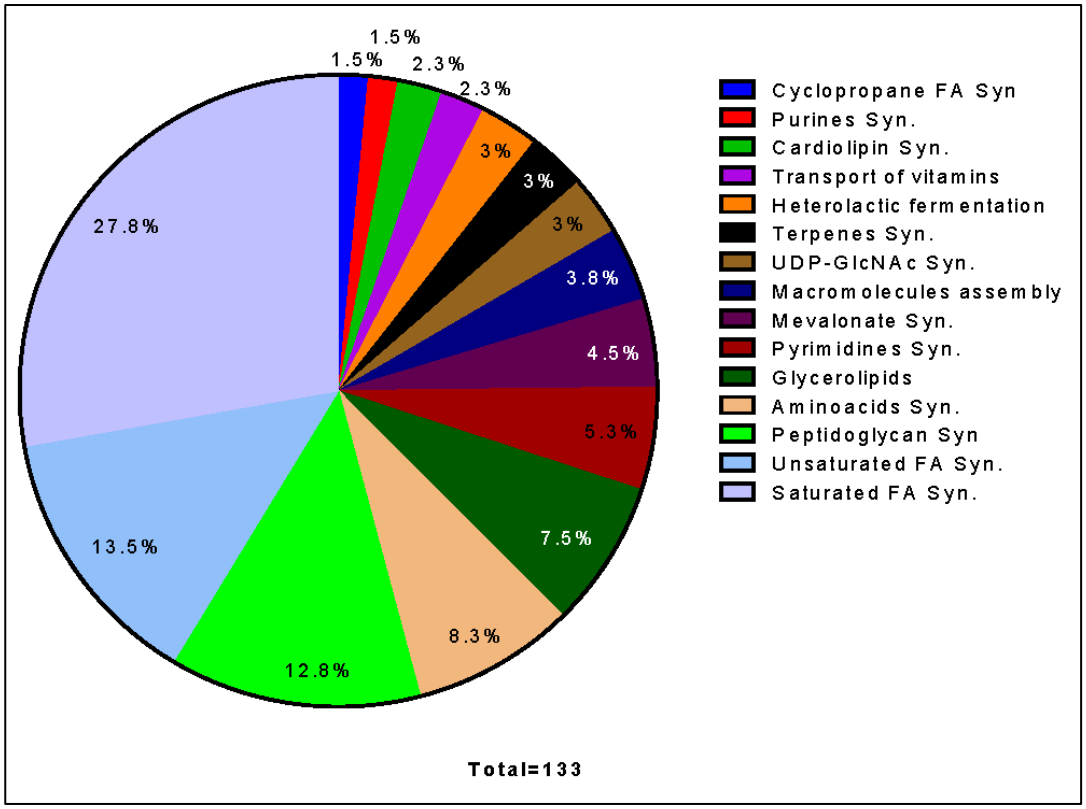

Figure 2-8: Pathway distribution of 133 out of 164 essential reactions determined by Reaction Deletion on an *in-silico* simulation. Reactions were classified as essential if growth was affected by at least 80%. Reactions corresponding to non-classified reactions, exchange reactions or pathways that have only one reaction as essential were not considered.

2.4 Discussion

In this work, we reconstructed, curated and validated the first genome-scale metabolic model of *O. oeni* PSU-1. The resulting iSM454 comprises 660 reactions, 536 metabolites and 454 genes, and is able to predict growth under different culture conditions with 93% accuracy. An accurate prediction depends largely on the refinement process. The draft reconstruction was thoroughly curated pathway by pathway, evaluating the stoichiometry, direction, and reversibility of each reaction. After an exhaustive literature search, several pathways were modified in the draft reconstruction, while others were completed, removed, or added to the iSM454 model. Several metabolisms (fatty acids, exopolysaccharides, amino acids and energetic) were thoroughly curated in the model.

Regarding biosynthesis of unsaturated and cyclopropane fatty acids, we included the reactions for the biosynthesis of palmitoleate (C16:1 Δ9), cis-vaccenic acid (C18:1 Δ11), lactobacillic acid (C19:0 cyΔ11) and dihydrosterculic acid (C19:0 cyΔ9). Moreover, we discovered that the reactions for generating cyclopropane bounds were associated with *OEOE_1176*, a gene related to a generic reaction of cyclization of unsaturated fatty acids. We identified dihydrosterculic acid, which derives from oleic acid under stress conditions (Guerrini et al., 2002; Lonvaud-Funel & Desens, 1990; Tracey & Britz, 1989b), as an essential nutrient in the model. Therefore, an equation for the transport of oleic acid was included.

EPS biosynthesis has been related to the survival of *O. oeni* under stress conditions, such as those prevailing in wine during malolactic fermentation (MLF). Moreover, these polysaccharides have been implicated in ropiness, a wine spoilage process (Dimopoulou et al., 2012). Therefore, we included in the model the detailed biosynthesis of EPS based on the pathways described by Dimopoulou et al. (2012, 2014), which consist of two main products: heteropolysaccharide (glucosyl-rhamnosyl-galactoside) and homopolysaccharide (dextran).

Moreover, the iSM454 model was able to correctly predict most essential amino acids, in agreement with the analysis of amino acids pathways reported by Mills et al. (2005). The model predicts that 14 amino acids are essential and that *O. oeni* is only

able to synthesize 6 amino acids, which is supported by previous evidence (Fourcassie et al., 1992; Garvie, 1967b; Remize et al., 2006; Terrade & Mira de Orduña, 2009). Mills et al. (2005) found that the biosynthesis pathway of cysteine was complete, which agrees with our reconstruction. However, cysteine has been experimentally found as an essential amino acid in most cases (Fourcassie et al., 1992; Garvie, 1967b; Remize et al., 2006; Terrade & Mira de Orduña, 2009). Hence, although its biosynthesis pathway is complete, missing pathways for sulfur assimilation could explain its essentiality for *O. oeni* cells.

Another important feature of the model is the representation of different proton extrusion/energy generation pathways employed by *O. oeni,* particularly the transformation of malic into lactic acid, using the malolactic enzyme (malate decarboxylase). Likewise, a lactic acid transporter that allows this compound to cross the cytoplasmic membrane was added. Citrate metabolism, another important system of energy generation in *O. oeni,* was also included. Both processes allow proton extrusion, which relates to ATP synthase, allowing more ATP to be synthesized. These three added metabolic processes were critical for accurate model performance, especially for the prediction of specific growth rates. Thus, simulations strongly suggest that proton transport is the most important process for the survival of *O. oeni* under these harsh cultural conditions.

We found that accurate proton balancing, and cofactor utilization was fundamental for the successful prediction of *O. oeni* phenotype by iSM455 model. For this purpose, we ensure that the only reactions for extrusion of protons were those related to heterolactic fermentation (efflux of lactate and carbon dioxide); in those cases, the network properly described the proton motive force needed to generate energy from the ATP synthase located in the cell membrane. Additionally, a careful revision of the metabolism was performed to account for proper cofactor utilization. This feature was recently reported as a critical step in improving phenotypic predictions by genome-scale metabolic models (Pereira et al., 2016). Therefore, we manually curated all reactions by forcing the use of NADPH/$NADP^+$ in anabolic reactions, e.g., fatty acid biosynthesis, and NADH/NAD^+ for catabolic reactions.

The total ATP production rate calculated by the model was 26% less, on average, than the ATP production rate estimated using the approach of other authors (Salou et al, 1994; Zhang et al, 2005, 2006). This difference could result from several reasons: i) pyruvate, the precursor of D-lactate, can be produced either from oxaloacetate, malate or even from some amino acids, such as cysteine, serine, or threonine or consumed for the synthesis of diacetyl and ethanol; ii) acetate can be directly produced from citrate or acetaldehyde, not yielding any ATP; and iii) production of erythritol requires that some carbon leaves the heterolactic pathway to generate its precursor, erythrose 4 phosphate; therefore, the ATP consumed by the hexokinase could not be regenerated downstream. Mink et al., (2015) showed that diacetyl production could be induced by exogenous pyruvate; the authors concluded that any substrate increasing intracellular pyruvate could induce the synthesis of diacetyl, as observed in a manner consistent with our results.

In general, microorganisms colonizing extreme ecological niches need higher energetic requirements for cell maintenance, which is not reflected in biomass formation (Russell & Cook, 1995). Therefore, a relevant applied use of iSM454 was the determination of m-ATP, which represents non-growth associated maintenance (NGAM) requirements. Using our experimental data, the model was able to predict m-ATP of 0.07 and 2.3 mmol gDW^{-1} h^{-1} for *O. oeni* PSU-1 grown under 0% and 12% v/v ethanol, respectively. These m-ATP values allowed predicting biomass with an average error of 0.14%. Despite the remarkable importance of m-ATP for visualization of cell behavior under stress conditions, there is scarce information in the literature about this parameter for *O. oeni*. Zhang and Lovitt (2006) determined an NGAM of 0.6 mmol ATP g DW^{-1} h^{-1} for *O. oeni* 11648 strain, when growing in continuous culture at pH 4.5 with glucose and fructose as carbon sources and in the absence of ethanol. We determined that the stress produced by 12% ethanol in the medium required a 30-fold increment in the m-ATP needed, compared to the cultivation without ethanol. Interestingly, growth associated maintenance (GAM) was on average 0.25 mmol ATP gDW^{-1}, pointing out that under ethanol stress (12%v/v), *O. oeni* spends in total almost

nine times more energy in cell maintenance than under non-stress conditions, *i.e.,* absence of ethanol in the medium.

To the best of our knowledge, this is the first report determining the ATP required for maintaining cells of *O. oeni* growing in a medium with ethanol. It is worthy to note that model predictions were performed using experimental data obtained in a wine-simulated environment, where this microorganism commonly develops. As a consequence, the model can effectively be used to predict internal fluxes in cases where there is scarce growth. This is relevant for winemakers because many strains are able to perform MLF in spite of achieving scarce growth in wine. The model is particularly useful in this case because it predicts MLF, whereas other mathematical models of *O. oeni* cannot (Brandam et al., 2016; Fahimi et al., 2014). Furthermore, the model is able to predict internal metabolic fluxes, determining the production of mannitol, erythritol, acetate, diacetyl, acetoin, among other compounds that could have significant organoleptic impacts on the resulting wine.

As expected for the effect of variations in the constrained fluxes, the sensitivity analysis showed positive reduced costs associated with the uptake rate of D-glucose, D-fructose, and D-malic acid, as well as an increase in the production of DL-lactate and acetate. It is expected that a higher rate for these reactions leads to a higher specific growth rate because more ATP can be obtained directly through heterolactic – from D-glucose and D-fructose – and indirectly through malolactic fermentation – from D-malic acid. Interestingly, the uptake of D-fructose has higher scaled reduced cost, meaning that it has the greatest effect on growth rate, probably because of the importance of the regeneration of redox factors. Zhang et al. (2005) reported that the specific growth rate of *O. oeni* NCIMB 11648 increased when the ratio among glucose and fructose concentrations in the medium was reduced from 0.5 to 0.3, supporting our results related to the impact on the specific growth rate of increasing fructose uptake rate. On the other hand, an increase in the uptake rate of citric acid and some amino acids such as L-cysteine, L-serine and L-threonine also leads to a higher growth rate, in accordance with the essentiality of these amino acids. All these metabolites have

been identified as important contributors to energy metabolism in lactic acid bacteria (Teusink et al., 2006), which support their role in the specific growth rate.

Sensitivity analyses demonstrated that an increase in the production of D-mannitol or D-erythritol has a negative effect on growth rate. At first sight, this could be counterintuitive. Nevertheless, *O. oeni* needs reduced redox cofactors for anabolic processes and biomass formation, which are regenerated during the biosynthesis of mannitol and/or erythritol.

The iSM454 model allowed finding a direct relationship between several metabolic fluxes and ethanol content in the medium. Fructose and amino acid consumption rates increased concomitantly with ethanol content. Moreover, erythritol, D-lactate and acetate production rates also increased in ethanol-containing cultures. As expected, the metabolic fluxes related with malic acid consumption and L-lactic production rates increased with ethanol. These compounds are critical for regeneration of redox cofactors such as NADH/NAD^+, which restore the redox balance inside the cell. Our results therefore confirm previous studies that point to redox balancing as a survival strategy for *O. oeni* (Maicas et al., 1999; Salou et al., 1994; D. S. Zhang & Lovitt, 2005).

Moreover, a redistribution of intracellular fluxes occurred when ethanol content increased in the culture medium. FVA revealed that *O. oeni* requires oxygen to grow at all ethanol levels. Furthermore, oxygen requirements increase concomitantly with ethanol concentration. Although the calculated oxygen specific consumption rates were low, they had a similar value (6.25 mmol gDW^{-1} h^{-1}) to those determined by Aceituno et al. (2012) for the wine yeast strain *Saccharomyces cerevisiae* EC1118, grown in nitrogen–limited continuous cultures, sparged with 1.2 µM of oxygen. These results confirm the microaerophilic behavior of *O. oeni.* Oxygen is mainly used for pyruvate oxidation by pyruvate oxidase (E.C.1.2.3.3), threonine degradation by aminoacetone:oxygen oxidoreductase (E.C. 1.4.3.21) and spontaneous diacetyl formation by acetoin oxidation.

The overall good performance of the metabolic model evidences the correct distribution of metabolic fluxes, with or without 12% ethanol content and pH 4.8.

However, it is worthy to mention that the information about *O. oeni* is still scarce; the physiological as well as proteomic and transcriptomic responses of the bacterium grown under different environmental perturbations are necessary to further improve the model. These might include determination of biomass composition, exhaustive electronic and proton balancing of stoichiometric equations and integration of transcriptomic and proteomic data. On the other hand, dynamic flux balance analysis (dFBA) has emerged as a promising strategy to study batch cultures of several strains (Hanly et al., 2012; Sainz et al., 2003; Sánchez et al., 2014). Indeed, this methodology has been already applied to understand the behavior of industrial *Saccharomyces cerevisiae* strains in wine-like medium (Vargas et al., 2011). Therefore, a dFBA for *O. oeni* could be useful to simulate the kinetics of growth and industrial MLF extension.

Finally, a future challenge is the development of a more extended platform, based on the iSM454 model, allowing the simulation and prediction of the biological interactions occurring within the wine microbiome. For example, *E. coli's* GSMM has been successfully employed as a platform to model metabolite exchange between different organism under different environmental conditions(Jain & Srivastava, 2009; Klitgord & Segre, 2010; Wintermute & Silver, 2010).The consortium metabolic models could also be applied to winemaking to simulate and understand the interactions between *O. oeni* and other microorganisms that share this ecological niche, as *S. cerevisiae* and other LAB, like *Lb. plantarum, Lb. kunkeii, Pediococcus pentosaceus*; and even undesirable and detrimental wine microorganisms, like *Brettanomyces spp*. or *Acetobacter aceti*, responsible for acetic acid production spoilage. Consortium metabolic models might predict how each organism develops in a shared, not isolated, scenario (Tzamali et al., 2011). The iSM454 model would be a valuable tool to be employed for further modeling *O. oeni* in coexistence with other species.

3. CHAPTER II: MAPPING THE PHYSIOLOGICAL RESPONSE OF *OENOCOCCUS OENI* TO ETHANOL STRESS USING AN EXTENDED GENOME-SCALE METABOLIC MODEL.

3.1 Introduction

The winemaking of red wines, and of some white wines, involves two fermentation processes: alcoholic fermentation conducted by yeast, and malolactic fermentation (MLF) performed by lactic acid bacteria (LAB). MLF allows wine deacidification and improves flavor complexity and microbiological stability (Henick-Kling et al., 1994; Zoecklein et al., 1999). This process consists of the decarboxylation of L-malate into L-lactate, a reaction that decreases wine acidity. *Oenococcus oeni* is the main bacterial species that carries out the MLF, due to its ability to grow under the harsh conditions present in wine, such as high ethanol content (>13% v/v), low pH (< 3.2), and high sulphite concentration (< 50 ppm) (Bartowsky, 2005; Bauer & Dicks, 2004; H. Li et al., 2006; Zapparoli et al., 2009; G. Zhang, 2013). However, *O. oeni* is not always able to achieve this task under these hostile conditions, often generating sluggish or stuck MLFs. For this reason, this process is considered one of the most difficult to manage during winemaking. Several studies have been carried out with the aim of understanding the metabolism of *O. oeni* under winemaking conditions; however, MLF still remains mostly unpredictable (Bourdineaud et al., 2003; Cafaro et al., 2014; Carreté et al., 2002; da Silveira et al., 2003; Grandvalet et al., 2005; Olguín et al., 2009).

Survival of microorganisms under stress conditions requires the maintenance of the main functions of the cell membrane, which is essential to control ion permeability and to regulate solute exchange between the cell and the external medium. In wine, ethanol is considered the main stressor, because it can injure cell membrane integrity and impact cell viability.

Most studies on *O. oeni* survival in wine have focused on the deleterious effect of ethanol on the integrity of cell membrane and changes in the cell wall composition. Chu-Ky et al. (2005) reported that increasing ethanol content in the culture medium – from 10 to 14% v/v- increased membrane fluidity, resulting in significant loss of cell

viability, even after 30 min of cultivation. Da Silveira et al. (2004) noticed an increase in the level of proteins involved in cell wall biosynthesis. Dols-Lafargue et al. (2008) showed that *O. oeni* strains able to express a functional *gtf* gene - involved in exopolysaccharide synthesis - were more resistant to ethanol and other stressors. Other authors determined that cells grown in the presence of 8% v/v ethanol modified the membrane fatty acid profile, resulting in an increment of membrane cyclopropane fatty acids (CFAs) (Grandvalet et al., 2008; Teixeira et al., 2002). The biosynthesis of CFAs from unsaturated fatty acids is catalyzed by a CFA synthase, encoded by the *cfa* gene. The correlation between cfa induction and ethanol resistance has been demonstrated in *O. oeni* cells (Grandvalet et al., 2008).

Nevertheless, the central metabolism of *O. oeni* under winemaking conditions is still scarcely understood. Indeed, several related studies did not include ethanol in the culture medium (Fourcassie et al., 1992; Maicas et al., 1999, 2002; Salou et al., 1994). Others, although including ethanol, have employed complex culture media, with the aim of satisfying increasingly demanding nutritional requirements of this bacterium with increasing ethanol content (Arena & Manca De Nadra, 2005; Bravo-Ferrada et al., 2016; Capucho & San Romao, 1994; Olguín, 2010; Olguín et al., 2009; Tracey & van Rooyen, 1988).

Complex media contain plant and/or animal water-soluble extracts and sugars which result in solutions rich in minerals and organic nutrients, but where the exact composition is unknown. On the contrary, defined culture media are composed of well-known chemical compounds in previously determined concentrations. The latter are, therefore, best suited than the former to fully assess the metabolic responses of a microorganism under different perturbation conditions.

To the best of our knowledge, an optimized, defined culture medium is not available yet to allow a quantitative characterization of the growth and metabolism of *O. oeni* under wine-like culture conditions. The only defined medium currently available for *O. oeni* has been reported by Terrade and Mira de Orduña (2009). This is a non-selective, chemically defined medium for *O. oeni,* as well as for other LAB, that provides strong growth comparable to standard laboratory media used for LAB like the

MRS medium (De Man et al., 1960). However, Terrade´s medium does not include enological components, like malate, citrate, fructose or ethanol, among others.

Since the genome sequence of *O. oeni* PSU-1 was released by Mills et al. (2005), several -omic studies have significantly contributed to the understanding of the metabolic changes that occur in this microorganism during the malolactic fermentation (Bartowsky, 2017; Bordas et al., 2015; Costantini et al., 2015; Margalef-Català et al., 2016; Olguín, 2010; Olguín et al., 2009, 2015; Sternes et al., 2017). Bridier et al. (2010) constructed a phylogenetic tree comparing the sequences of the seven housekeeping genes presents in 258 *O. oeni* strains. Then, two major phylogenetic groups were observed. Moreover, a third putative group was proposed comprising one strain, which was isolated from cider. Likewise, Campbell et al. (2015) revised the population structure of 50 *O. oeni* strains, using comparative genomics and confirmed that it can be divided in two major groups, according to their ecological niche, wine or cider. In congruence with Bridier's work, a third group was proposed. Sternes and Borneman (2016) compared consensus pan-genome assemblies of the invariant (core) and variable (flexible) regions of 191 *O. oeni* strains. Genetic variation in amino acid biosynthesis and sugar transport and utilization was found to be common between strains. Moreover, other studies showed that *O. oeni* strains differed mainly in carbohydrate metabolism (Cibrario et al., 2016) and exopolysaccharide synthesis (Dimopoulou et al., 2014).

Besides, several studies have grouped *O. oeni* strains according to their capacity to perform the MLF or flavors production. Bon et al. (2009) observed the presence of eight stress-responsive genes in *O. oeni* strains that performed MLF more efficiently. El Khoury et al. (2017) reported the isolation, genotyping, and geographic distribution analysis of 514 *O. oeni* strains. Their phylogenetic relationships were evaluated using a method based on single nucleotide polymorphism (SNP) analysis. The results show that strains are not genetically adapted to regions but to specific types of wines. More recently, Sternes et al. (2017) found thirteen genes differentially expressed in the strains analyzed, which were associated with the production of diacetyl, a commercially valuable aroma compound. Finally, Campbell-Sills et al. (2017), studying the genomics

and metabolomics of 14 *O. oeni* strains isolated from Burgundy, identified two different *O. oeni* lineages associated to either red or white wines in this French region. Transcriptomic and proteomic analyses of *O. oeni* strains cultivated in wine-simulated cultures showed that the environment strongly affects *O. oeni* stress responses at this level. Costantini et al. (2015) found that under mild ethanol stress culture conditions, (8% v/v), genes codifying for chaperones with refolding activity were over-expressed; and at higher alcohol concentration (12%v/v), genes that codify for chaperones with proteolytic activity were induced. Olguín et al. (2015) performed transcriptomic and proteomic analyses which revealed that main genes affected by ethanol (12% v/v) were related with metabolite transport, as well as cell wall and membrane biogenesis; furthermore, they observed relocation of cytosolic proteins in the membrane, as a protective mechanism. More recently, Margalef-Catalá et al. (2016) also performed transcriptomic and proteomic analyses, showing that the amino acid metabolism and transport were altered and that several peptidases were up-regulated both at gene and protein levels. Moreover, the authors observed that genes related with malate and citrate uptake were up-regulated, while genes related with fructose consumption were down-regulated.

Otherwise, over the last 16 years, more than 80 genome-scale metabolic models (GSMM) have been reconstructed, which has been of substantial help in the study and applications of corresponding biological systems. Initially, GSMM have considered only highly characterized organisms, such as *Escherichia coli* and *Saccharomyces cerevisiae*; since then, its use has been expanded to other, less characterized species, as well as to complex biological systems. Nowadays, genome- scale models are widely used for studying the metabolism of numerous organisms, including LAB such as *Lactococcus lactis* (Flahaut et al., 2013; Oliveira et al., 2005; Verouden et al., 2009), *Lactobacillus plantarum* (Teusink et al., 2006), *Streptococcus thermophilus* (Pastink et al., 2009) and, more recently, Enterococcus *faecalis* (Veith et al., 2015) and *Streptococcus pyogenes* (Levering et al., 2016). These models have been employed for analyzing growth, auxotrophies and flavor formation; they have also assisted in the process of selection and development of strains with enhanced industrial utility. In a

previous work carried out by our group, we developed the first genome-scale metabolic model for an *O. oeni strain* (Mendoza et al., 2017). We reported the general features of the model, as well as its predictive capabilities. The genome sequence of *O. oeni* PSU-1 strain was employed for this purpose.

In this work, we first designed a defined culture medium simulating wine conditions, able to support *O. oeni*'s growth at different levels of ethanol; then, we characterized the evolution of different nutrients and metabolic products during the fermentation. Finally, taking advantage of the recently constructed genome-scale metabolic model (GSM) of *O. oeni* PSU-1 strain (named iSM454) (Mendoza et al., 2017), we predicted the metabolic behavior and the nutritional requirements of *O. oeni* at different growth phases, under increasing ethanol concentrations. The results clearly indicate that differential nutritional requirements of the PSU-1 strain are required when ethanol concentration increases. As a whole, this work contributes to a better understanding of *O. oeni* metabolism under oenological conditions, as well as to the identification of essential nutrients required for survival of this bacterium in the different stages of growth.

3.2 Materials and Methods

3.2.1 Microorganisms and media

Oenococcus oeni (Dicks et al., 1995; Garvie, 1967a) (PSU-1, ATCC®, BAA-331™) was obtained from the American Type Culture Collection (ATCC) (Virginia, USA). Cryogenically preserved (-80°C) strains were cultured and maintained on MRS plates (Man, Rogosa and Sharpe) (De Man et al., 1960) and stored at 4°C.

An *O. oeni* PSU-1 preculture was prepared from a frozen stock by inoculating 100 ml Erlenmeyer flasks containing 75 ml MRS medium supplemented with 0.5 g L^{-1} of cysteine. Before inoculation, the cells were subjected to ethanol adaptation. For this purpose, we serially passaged every culture, starting from 1% ethanol v/v to reach 0, 3, 6, 9 or 12% v/v ethanol concentration in each culture. *O. oeni*'s cells were inoculated in each culture medium to achieve an initial optical density at 600 nm (OD600) of

approximately 0.1. When the cultures reached OD600 = 0.2, they were transferred to other cultures containing higher ethanol content.

3.2.2 Design of a chemically defined culture medium

The developed chemically defined culture medium, named MaxOeno, was designed with the aim of simulating the wine environment, allowing *O. oeni* to grow in the presence of ethanol. However, the concentration of carbon and nitrogen used in MaxOeno was higher than that found in wine, because these concentrations allowed the growth of *O. oeni* avoiding its arrest or slowing. The vitamins and minerals were those of Terrade & Mira de Orduña (2009), but their concentration was increased threefold. Using literature data, we verified that these concentrations were not inhibitory for the bacterium growth (Mesas et al., 2004).

Carbon and energy sources were those normally found in wine, *i.e.,* glucose, fructose, malate and citrate. Glucose and fructose are the main residual sugars present in wine. Both were added in equal concentrations (12.5 g L^{-1}) with the aim of studying their metabolic fate in *O. oeni*. Meanwhile, malate and citrate, the main organic acids in wine, were included at a concentration of 5 and 1 g L^{-1}, respectively. We verified from the literature that these concentrations were not inhibitory for the bacterium, and that they also allow bacterial cells to grow in the presence of ethanol (Augagneur et al., 2007; Maicas et al., 2000; Mesas et al., 2004; Olguín, 2010; Saguir & Manca de Nadra, 1996; Salou et al., 1991).

The amino acids content was calculated using their yields in biomass. For this purpose, we employed the yields reported for *Lactobacillus plantarum* and *Lactococcus lactis* (Novak et al 1997; Teusink et al, 2006), because we did not find any reported data for amino acid yields in *O. oeni*.

3.2.2.1 *Composition of the MaxOeno culture medium*

The MaxOeno culture medium contained, in g L^{-1}: citrate 1, malate 5, calcium chloride (dihydrate) 0.4, magnesium sulfate 1.3, fructose 12.5, glucose 12.5, dipotassium phosphate 2.0. Tween 80 was also added at 1ml L^{-1}, as well as a nitrogenous bases

solution, 100 mL/L^{-1}; a mineral salts solution, 5 ml L^{-1}; and a vitamins solution, 1 ml L^{-1}.

The vitamin solution contained the following, in g L^{-1}: thiamine, 1; biotin, 1; nicotinic acid, 2; pyridoxine hydrochloride, 2; C-D-pantothenate, 2; folic acid, 1; choline chloride, 2; riboflavin, 1; 4-aminobenzoic acid, 0.1; cyanocobalamine, 0.1; and xanthine, 5. The nitrogenous bases solution contained: adenine sulphate, 0.5; uracil, 0.5; cytosine, 0.5; thymine, 0.5; and guanine, 0.5. Mineral salts solution contained: $MgSO_4*7H_2O$, 60; $FeSO_4*7H_2O$, 12; $CuSO_4*5H_2O$, 0.015; and $ZnSO_4*7H_2O$, 0.135. The vitamin solution was sterilized by membrane filtration (pore size < 0.22 μm, Millipore, USA).

Besides, the culture medium was supplemented with 1,060 mg L^{-1} of assimilable nitrogen prepared with the following amino acids, in g L^{-1}: L-arginine 0.4, L-serine 0.24, L-threonine 0.27, L-glutamic acid 0.33, L-aspartic acid 0.3, L-lysine 0.33, L-asparagine 0.3, L-leucine 0.30, L-glutamine 0.50, L-alanine 0.2, cysteine 0.54, glycine 0.27, histidine 0.53, isoleucine 0.30, methionine 0.34, phenylalanine 0.37, proline 0.67, tryptophan 0.46, tyrosine 0.41, and valine 0.27.
Before sterilization, the pH of the medium was adjusted to 4.8 using KOH.

3.2.3 *O. oeni* cultivation in different ethanol conditions

Ethanol-adapted cells were inoculated in 50 mL flasks containing 35 mL of MaxOeno culture medium to achieve an initial optical density at 600 nm (OD600) of approximately 0.2. The flasks were of glass, airtight and with a sampling port. The cultures were incubated at 25°C, without stirring. Samples were collected aseptically through the flask sampling port, and bacterial growth was estimated by OD600, the optical density of the culture measured at 600nm. At the same time, the content from each flask was centrifuged; the supernatant was collected and frozen at -20°C, for future chemical analyses.

The biomass was determined as dry weight of cells through a calibration curve of OD_{600} versus dry weight (g L^{-1}). The latter was previously carried out as described in Li and Mira de Orduña (2010) to obtain equation 1, where both parameters are related.

$$X\ (g\ DCW\ L^{-1}) = 0.8105 * (OD_{600}) + 0.0104 \quad (1)$$

3.2.4 Chemical analyses

L-lactate, D-lactate and amino acids were quantified by UHPLC/MS using a Dionex unit model Ultimate-3000 (Dionex Corp., Sunnyvale, CA, United States) coupled to a mass spectrometer Exactive™ plus (Thermo Fisher Scientific, San Jose, CA, United States). The UHPLC system was controlled using the Xcalibur™ 2.13 software (Thermo Fisher Scientific, San Jose, CA, United States). The methods utilized for compound identification and quantification are detailed below:

3.2.4.1 *L- and D- lactate*

Fifty microliter of sample were dried and then derivatized by adding 50 µl of (+)-*O,O´*-diacetyl-L-tartaric anhydride solution (≥97%) (DATAN) (Sigma-Aldrich, United States) [100 mg ml^{-1}, where DATAN was dissolved in dichloromethane:acetic acid (4 : 1, by volume)]. The samples were incubated for 40 min at 75°C, under agitation. Subsequently, the samples were dried and reconstituted in 200 µl of a solution of acetonitrile and water (1:2). L-lactate and D-lactate (≥98%) (Sigma-Aldrich, United States) were used as external standards. A 10 µl derivatized sample was injected in the equipment and separated using a UPLC BEH C18 (100 × 2.1 mm, 1.7 µm, Waters) analytical column at a flow of 0.5 ml min^{-1} and oven temperature of 31°C. Solvents used for separation were ammonium formate (1.5 mM, pH was adjusted at pH 3.6 using formic acid) as solvent A, and acetonitrile as solvent B.

3.2.4.2 *Amino acids*

A 10 µL sample was directly injected in the equipment and separated using a LiChrospher® 100 RP-18 (5µm) (Merck) analytical column with a flow of 0.35 ml min^{-1} and oven temperature of 30°C. Solvents used for separation were formic acid (0.1% v/v) as solvent A, and methanol as solvent B.

3.2.4.3 *Cysteine:*

A 50 µl sample was derivatized using 100 µl 5,5´-dithiobis(2-nitrobenzoic acid) (Ellman's reagent) (Sigma-Aldrich, United States). The reagent solution for derivatization was prepared using 4 mg Ellman's reagent dissolved in 10 ml buffer phosphate 0.01 M (pH 7.0). All samples were derivatized at the time of being taken. The chromatographic conditions were the same of those employed for amino acids analysis.

Sugars (glucose, fructose), organic acids (malate, acetate, citrate, total (L + D) lactate, and alcohols (ethanol, mannitol and erythritol) were separated and quantified in a Lachrom L-700 HPLC system (Merck Hitachi, Japan) equipped with Diode Array and Refractive Index detectors (Hitachi, Japan). An Aminex HPX-87H ion exchange column (Bio-Rad, United States) was used, as described previously (Varela et al., 2003). For s*ugars, malate, citrate, acetate and ethanol,* the mobile phase used was sulphuric acid 5 mM with a flow of 0.450 ml min^{-1} and oven at 35°C. For *mannitol and erythritol,* the mobile phase was milliQ™ water with a flow rate of 0.450 ml min^{-1} at a constant temperature of 75°C. External standards were used to quantify the required compounds in all cases.

3.2.5 Genome –scale metabolic model

Genome-scale metabolic models can be used to find flux distributions under the assumption of steady state. In steady state, the concentration of intracellular metabolites remains constant and all the mass produced must be consumed in order to fulfill the mass balances. No accumulation of intracellular metabolites is allowed. GSMMs can also be used to model the exponential phase (Figure 3-1, step 1) where a pseudo steady state is accomplished. Thus, we modeled each of the three differentiated growth phases observed during growth of *O. oeni* PSU-1 (Figure 3-1, step 2). However, experimental results suggested that intracellular accumulation of some metabolites occurred during growth, and thus the assumption of no accumulation could not be applied in this case (Figure 3-1, step 3).

In the most widely used approach, Flux Balance Analysis, a matrix S, which summarizes the biochemical reactions occurring in a metabolic network, is used. In this matrix, the stoichiometric coefficients are used to describe each reaction. The

assumption of steady state indicates that mass balances must be accomplished, which is equal to state S*v = 0, where v is a vector of reaction fluxes. As we observed experimental accumulation of metabolites, we decided to include that accumulation in the form of sink and demand reactions. In particular, accumulation reactions were added in the form of sink reactions for phases II and III, and demand reactions for phases I and II (Figure 3-1, step 5). To determine the variation range of these accumulation reactions, an extended model was built, able to simulate simultaneously the three growth phases, in which the assumption of S*v = 0 was still valid (Figure 3-1, step 4). This extended model was employed to calculate the maximum and minimum flux that these accumulation reactions were able to carry under the restrictions fixed by the experimental results. Then, these constraints were included in the iSM454 model and used for further analysis.

The GSMM of *Oenococcus oeni* PSU-1 recently developed by our group was employed in this work (Mendoza et al., 2017). GSMM allows to model the exponential phase of growth curves (Figure 3-1, step 1); thus, this approach was used here for modeling each of the four differentiated growth phases (three growth phases + stationary phase) observed during growth of *O. oeni* PSU-1 (Figure 3-1, step 2). However, experimental results suggested that intracellular accumulation of some metabolites occurred during growth, and thus the assumption of no accumulation, as well as the restriction S*v = 0, could not be applied in this case (Figure 3-1, step 3), unless the accumulation was represented in the model. Therefore, to include the latter in the S matrix, accumulation reactions were added in the form of sink reactions for phases II and III, and demand reactions for phases I and II (Figure 3-1, step 5). To determine the variation range of these reactions, an extended model was built, able to simulate simultaneously the three growth phases, in which the assumption of S*v = 0 was still valid (Figure 3-1, step 4). This extended model was employed to calculate the maximum and minimum flux that these accumulation reactions were able to carry carried out in the independent model described in 5), with the span determined in 6) for the accumulation reactions.

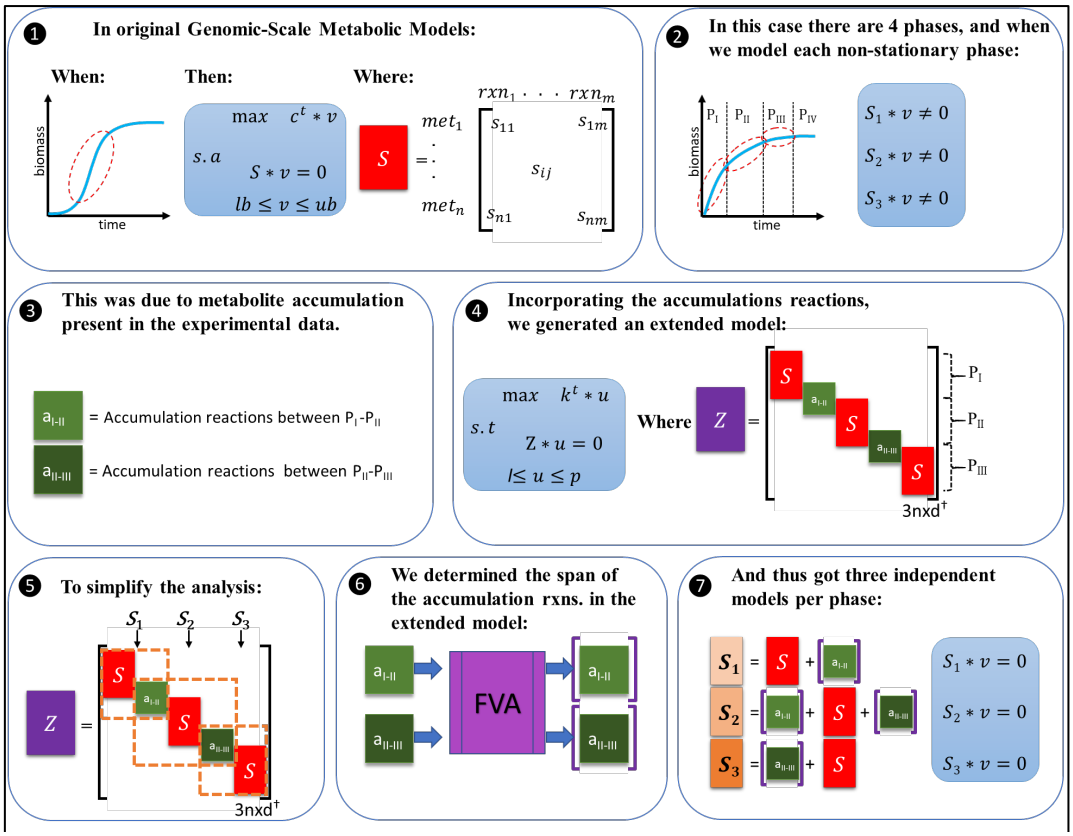

Figure 3-1: Framework for the incorporation of the experimental data. 1) General approach used to model exponential phase in GSMMs. 2) Our experimental results showed four phases: three growth phases and a fourth phase, corresponding to stationary phase. Growth phases couldn't be modelled individually as there was accumulation, as observed in the experimental results. 3) These accumulation compounds were: malate and mannitol, and the amino acids valine, phenylalanine, cysteine and threonine. Accumulation was observed between phases I to II, and II to III, and not from III to IV. 4) The extended model was constructed, which was able to simulate simultaneously the three phases identified for each ethanol level, and the accumulation observed experimentally. This matrix includes the following components: a matrix "Z" that contains three "S" matrix, one per phase, and 2 ''a" vectors (1x6), where "a" represents the accumulation reactions that allows interaction between phases; thus, matrix sigma has a size (3nxd), where d=3m+2*6. The extended model also includes vector "u" (1xd) of internal fluxes, limited by vector "l" and "p" (1xd), and a vector "k" of weights (1x3n). 5) To simplify the analysis, the extended matrix can be divided into three independent problems, one corresponding to each phase, and thus each one includes an S matrix, and a set of accumulation reactions as input of the system (accumulation in the previous phase) and/or output of the system (accumulation in the consecutive phase). 6) The span of these accumulation reactions was determined with flux variability analysis in the extended model, with the experimental data fixed in the model. 7) Estimations and further calculations were

carried out in the independent model described in 5), with the span determined in 6) for the accumulation reactions.

3.2.5.1 Construction of the Extended Model

An extended model was generated to allow simultaneous simulation of the three phases observed for each ethanol level (Figure 3-1, step 4). This model was used to determine the maximum and minimum fluxes required through the accumulation reactions so that each independent phase simulation was able to fulfill the S*v = 0 assumption. This extended model possesses a stoichiometric matrix Z, which contains three "S" sub matrices (Figure 3-1, step 4), each associated to a specific growth phase. These "S" sub matrices were taken from iSM454 and represent three independent problems solved simultaneously in the extended model. Then, to allow interaction between these three problems and thus lose independency, accumulation reactions were added, which allow flux to pass from $phase_n$ to $phase_{n+1}$. These were selected based on experimental results, and corresponded to the following compounds: mannitol, malate, cysteine, threonine, phenylalanine, and valine. These reactions had the following structure:

$$mannitol\_cytosol1 \rightarrow mannitol\_cytosol2$$

where *mannitol_cytosol1* represents cytosolic mannitol in growth phase I, and *mannitol_cytosol2* represents corresponding cytosolic mannitol in growth phase II.

3.2.5.2 Determination of the Constraints for the Accumulation Reactions

To determine the maximum and minimum values that the accumulation reactions were able to carry under the restriction of the experimental constraints, the following fluxes (mmol $gDCW^{-1}$ h^{-1}) were set in the extended model, according to the corresponding phase, with experimental values: the substrates glucose, fructose, citrate, malate, cysteine, threonine, valine, phenylalanine and serine; and the products mannitol, erythritol, L-lactate, D-lactate and acetate (Figure 3-1, step 4). To minimize experimental error, linear regressions were determined for each of the metabolites at each growth phase and used to predict the phase's final value. Initial values were taken

from the initial concentration of the experiment for phase I, and from the final values of the former phase for phases II and III.

Then, flux variability analysis (FVA) was carried out to determine the maximum and the minimum flux that each accumulation reaction was able to carry under these constrained conditions.

3.2.5.3 Generation of the Three S' Matrixes

When the ranges of the accumulation reactions were determined, the extended model was divided into three S' matrix, each one representing one of the growth phases. These were used to carry out all the further analysis. Each of these matrixes include the S matrix from iSM454, and also a set of the accumulation reactions as sink reactions for phases II and III, and demand reactions for phases I and II (Figure 3-1, step 5), to represent the mass difference observed experimentally as an input or/and output of the system. From now on in the text, every time the iSM454 model is mentioned, it will refer to the model in which the S' matrixes are included.

3.2.5.4 Flux Balance Analysis (FBA)

Flux balance analysis was carried out in the iSM454 model (with the S' matrixes) to analyze each of the different growth phases at each ethanol level. In order to do so, the following fluxes (mmol $gDCW^{-1}$ h^{-1}) were set with experimental values: the substrates glucose, fructose, citrate, malate, cysteine, threonine, valine, phenylalanine and serine; and the products mannitol, erythritol, L-lactate, D-lactate and acetate. The accumulation reactions were constrained with the ranges determined with the extended model. Also, experimental biomass and NGAM estimated in this work were fixed.

3.2.5.5 Prediction of Non-growth Associated Maintenance (NGAM)

Non-growth associated maintenance was estimated by setting the specific production and consumption rates of the experimentally measured compounds, as described above for FBA. Thereby, flux through the NGAM reaction was progressively increased from

0 to 4 mmol $gDCW^{-1}$ h^{-1}. In each cycle, biomass production rate was maximized, and the prediction error was assessed. The NGAM flux that allowed the lowest biomass prediction error was selected.

3.2.5.6 Sensitivity Analysis for NGAM

Sensitivity of estimated NGAM was assessed for each of the specific consumption/production rates set in the model. For this purpose, each rate was varied independently by increasing and decreasing its value in 1%, and then NGAM was recalculated each time.

3.2.5.7 Determination of Energetic and Redox Requirements

The flux distribution obtained through FBA was used to quantify ATP, and $NAD(P)^+$/NAD(P)H utilization. In *O. oeni*, ATP is produced through the F_0F_1-ATPase and/or through three reactions of the phosphoketolase pathway that involve the following enzymes: acetate kinase, pyruvate kinase and 3-phosphoglycerate kinase. To quantify the $NAD(P)^+$/NAD(P)H utilization, the reactions that produce NADH and NADPH were analyzed, that correspond to reactions that involve the following enzymes: malate dehydrogenase, glyceraldehyde-3P dehydrogenase, threonine dehydrogenase, NADH quinone reductase, $NAD(P)^+$ transhydrogenase and the pathway for methylglyoxal degradation for NADH formation; and Glucose-6P dehydrogenase, phosphogluconate dehydrogenase and GMP reductase for NADPH formation. This knowledge was considered for the determination of the maximum intracellular fluxes for $NAD(P)^+$ /NAD(P)H and ATP synthesis at different growth phases.

3.2.5.8 Flux Variability Analysis

Flux variability analysis was carried out by maximizing and minimizing the flux under the same constrained conditions used for FBA. This technique was applied to each of the accumulation reactions present in the extended model, and in iSM454 to analyze changes of production of ATP, NADH, NADPH; and separately, in F_0F_1-ATPase. To assess variation of ATP, NADH and NADPH, the sum of the reactions described above was subjected to FVA for each cofactor.

3.2.5.9 Elementary Flux Mode Analysis (EFMA)

As our culture medium mimics the wine composition, it contains different carbon sources and thus it is difficult to elucidate which substrate is being used to synthesize a particular product. Therefore, we used EFMA to find which metabolic products can be generated from each substrate, separately. EFMA was carried out with CellNetAnalyzer version 2017.4 (Klamt et al., 2007; Klamt & von Kamp, 2011; von Kamp et al., 2017). In order to do so, a reduced version of the iSM454 model was constructed. This model contained the central carbon metabolism of *O. oeni* PSU-1, that includes: phosphoketolase pathway, fructose reduction, citrate degradation and MLF. It also included energetic reactions such as F_0F_1-ATPase, NGAM, and the pathways for amino acid degradation present in *O. oeni* PSU-1, which correspond to serine, threonine and cysteine. A complete list of the reactions included is shown as Supplementary material S3-1.

3.2.5.10 Random Sampling Analysis

To determine the flexibility of the metabolic network under ethanolic conditions, a Random Sampling Analysis was conducted. In this analysis, the solution space is uniformly sampled, and flux distributions can be explored to assess the flexibility of different pathways. In contrast to EFMA, random sampling can be conducted in the range of minutes to hours for large metabolic network resulting in a valuable tool to explore the solution space without requiring the use of a reduced model.

Flux distributions were calculated using optGpSampler (Megchelenbrink et al., 2014). For each condition, the network was first constrained using uptake and production rates as well as sink reactions associated with metabolites accumulation. Then, 100.000 flux distributions were calculated for each constrained metabolic network using standard parameters (number of parallel threads = 4, number of steps between samples = 500, solver = gurobi 7.52). The flexibility of the network in each condition was assessed through the comparison of flux variations for 40 reactions belonging to phosphoketolase pathway. Standard deviations among the previously calculated 100.000 flux distributions were computed for each of the 40 reactions. Higher standard deviations were considered as indicators of higher network flexibility.

3.3 Results

3.3.1 Cell growth of *O. oeni* PSU-1 strain in defined wine-like culture medium.

The ability of *O. oeni* to grow in the defined, wine-like culture medium designed here, named MaxOeno, was followed by biomass concentration (measured as optical density, OD_{600nm}) and specific growth rates. Additionally, we compared the performance achieved in this medium with the defined medium previously described by Terrade & Mira de Orduña (2009). The growth in both media was evaluated either with (12% v/v of ethanol) and without ethanol; and at pH 3.5, in both cases. *O. oeni* PSU1 cultivated in MaxOeno´s grew more (OD_{600nm} = 0.75 vs OD_{600nm} = 0.25) and faster (μ= 0.012 h^{-1} vs. μ= 0.004 h^{-1}) than Terrade´s. Therefore, the MaxOeno culture medium was employed for all further experiments of this work.

3.3.2 Growth of *O. oeni* PSU-1 strain cultivated in the presence of increasing ethanol concentrations.

O. oeni PSU-1 was grown in MaxOeno culture medium with increasing ethanol concentrations (0, 3, 6, 9 or 12% v/v ethanol), at pH 4.8. Cell growth kinetics featured four clearly identifiable growth phases for all culture conditions, *i.e.,* phases I, II, III and stationary, ranging from 0 to 48 hours, 48 to 104 hours, 104 to 168 hours and 168 to 264 hours cultivation, respectively. These phases were characterized by different substrate consumption, e.g., during phase I, over 90% of malate and citrate were consumed; phase II presented a higher consumption rate of fructose and glucose, if compared to phase III; and phase III presented a slower specific growth rate, due to a strong decrease in sugar consumption rates (Supplementary material S3-2). It is worth mentioning that during growth, a lag phase was not observed in all cases (Figure 3-2). Besides, all cultures reached maximum biomass titers after 164 hours (6.8 days) cultivation; thereafter, growth arrested.

A clear, linear relationship (r^2 = 0.98) between ethanol concentration and cell growth was found, when considering each phase. Moreover, cultures with higher ethanol content showed slower specific growth rate and lower biomass production

compared to cultures without ethanol (Table 3-1). The maximum biomass production and specific growth rate were observed during phase I.

Stationary phase was not considered in further metabolic studies because neither growth, nor consumption or production of compounds was observed.

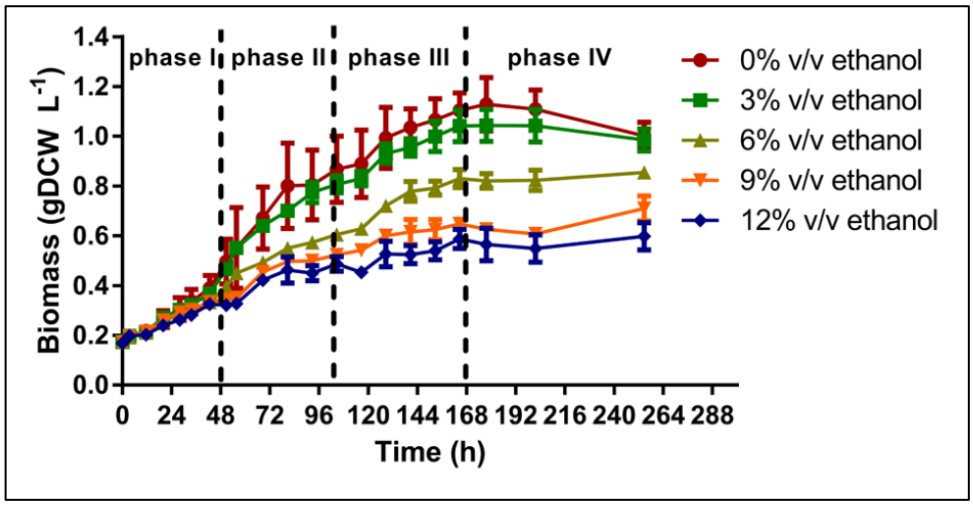

Figure 3-2: Effect of ethanol concentration on the growth of *O. oeni* PSU-1 strain cultivated in MaxOeno, a defined wine-like culture medium. Each growth phase is delimited by discontinued vertical lines. Phases I, II III and IV last between 0 to 48 hours, 48 to 104 hours and 104 to168 hours and 168 to 264 hours of cultivation, respectively.

Table 3-1: Maximum biomass production (gDCW/L^{-1}) and maximum specific growth rates (h^{-1}) of *O. oeni* PSU-1 cultivated in MaxOeno defined medium with increasing concentrations of ethanol.

Ethanol content (% v/v)	**Maximum biomass production (¥) (gDWC L^{-1})**	**Maximum specific growth rate (¥) (h^{-1})**
0	0.854[1]	0.021[1]
3	0.76[2]	0.018[2]
6	0.585[3]	0.016[3]
9	0.452[4]	0.014[4]
12	0.447[4]	0.013[5]

(¥) All assays were carried out in triplicate and its coefficients of variation (CV) were <20%. Shared superscript numbers in the same column indicate no significant difference between ethanol conditions (Mood test, $p < 0.05$).

3.3.3 Metabolism of sugars and organic acids by *O. oeni* PSU-1 strain.

Oenococcus oeni employs three metabolic pathways to obtain energy: phosphoketolase pathway (heterolactic fermentation), MLF and citrate degradation. The end-products of these catabolic pathways are D-lactate, L-lactate, acetate, ethanol, mannitol, erythritol and CO_2. To assess the metabolic response of *O. oeni* to ethanol concentration, we followed the consumption and production of the major metabolites of these pathways.

3.3.3.1 *Glucose and fructose consumption*.

As expected, the higher the ethanol concentration in the medium, the lower the sugar consumption. However, whatever the ethanol concentration was, the largest amounts of sugars were consumed during phase I. In this phase, total sugar consumption was similar for all culture conditions (Supplementary material S3-2), although specific consumption rates for fructose were twofold faster than for glucose, independently of ethanol concentration present in culture medium (Figure 3-3 A, B).

During phase II, both glucose and fructose consumption increased when ethanol content in culture medium was lower (Supplementary material S3-2). Furthermore, during this phase, *O. oeni* PSU1 consumed glucose faster than fructose. Specific

consumption rate of fructose was reduced by 50% compared to the previous phase, although specific glucose consumption rate decreased less, regardless of culture conditions (Figure 3-3 A, B).

Finally, in phase III, specific consumption rate of glucose was generally faster than fructose. Specific glucose consumption rates in cultures without and with 3% and 6% v/v ethanol were similar than phase II; but decreased significantly in cultures with 9% and 12% v/v ethanol (Figure 3-3 A and B). Besides, specific fructose consumption rates in cultures without and with 3% v/v ethanol decreased around 90 and 60%, respectively. Similar rates than in phase II were found for cultures with 6, 9 and 12% ethanol.

3.3.3.2 *Mannitol and erythritol production*.

These polyols are mainly produced through fructose catabolism - although they could also be synthesized from glucose. Again, the fastest production of mannitol and erythritol was achieved during phase I. The production of both metabolites increased concomitantly with ethanol content (Figure 3-3 C, D). Total mannitol concentration - the most abundant metabolite produced - was higher than erythritol concentration. In the absence of ethanol, specific production rates for mannitol and erythritol were 1.25 mmol $gDCW^{-1}$ h^{-1} and 0.95 mmol $gDCW^{-1}$ h^{-1}, respectively. Production rates of both polyols raised concomitantly with ethanol increment, during phase I (Figure 3-3 C, D). In phase II, production rates of both polyols dropped by half of the previous phase in the absence of ethanol in the culture medium. Once again, mannitol production increased with ethanol content, except for cultures with 6% ethanol (Figure 3-3 D). On the contrary, erythritol production sharply decreased in this phase for cultures containing 9 and 12%v/v ethanol (Figure 3-3 C).

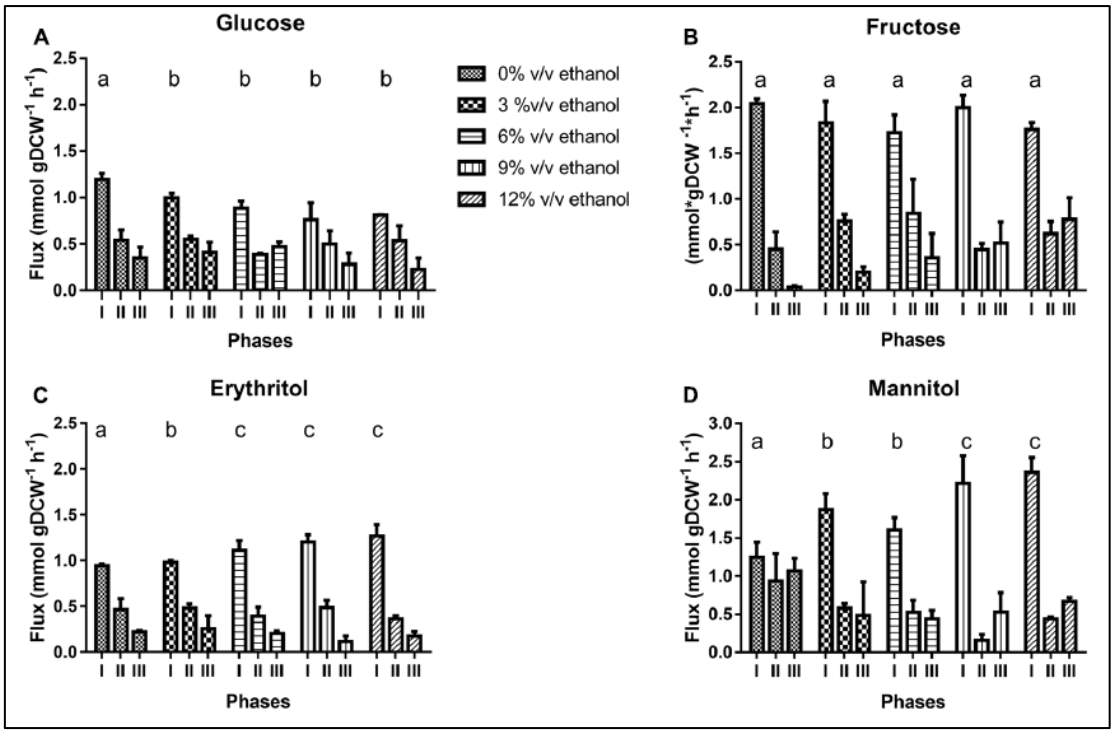

Figure 3-3: Specific consumption of glucose (A), and fructose (B) and concomitant specific production of the related products, erythritol (C) and mannitol (D) during cultivation of *O. oeni* PSU-1 under increasing ethanol contents. Statistical analysis only was performed in phase I and shared letters indicate no significant difference (Mood test, $p < 0.05$).

3.3.3.3 *L-malate and citrate metabolism.*

L-malate and citrate are the main organic acids in wine that support the growth of *O. oeni* under nutritional stress conditions. Lactate is synthesized by *O. oeni* as L- or D-enantiomers, according to its origin. L-lactate is produced in one step from L-malate through malolactic fermentation; and D-lactate towards the phosphoketolase pathway. L-malate and citrate were metabolized during phase I (Figure 3-4 A, B), their consumption being triggered at the very beginning of the cultivation. Total acid consumption, expressed in concentration units (g/L^{-1}), suggests that all cultures behaved similarly, both acids being completely consumed at the end of phase I, *i.e.,* after 48 h cultivation (Supplementary material S3-3). In relation to specific

consumption rates, L-malate was consumed faster when ethanol concentration was higher in culture medium; however, citrate was not differentially consumed.

Surprisingly, malate consumption was larger than L-lactate production; and the specific consumption rate of the former was *circa* 30 % faster than the latter, for all culture conditions (Figures 3-4 A, D). This suggests that one of these compounds is either accumulating intracellularly or being transformed into another metabolite (Figure 3-4 A, D).

Otherwise, the specific production rate of D-lactate (0.15 to 0.20 mmol $gDCW^{-1}$ h^{-1}) was more than tenfold slower than the corresponding one for L-lactate (1.5 to 3.0 mmol $gDCW^{-1}$ h^{-1}), at least during phase I. Also, during this phase D-lactate production is lower at 9 and 12% ethanol content. Contrary to L-lactate, D-lactate is still significantly synthesized in later phases, although at variable rates (Figure 3-4 D, E).

Acetate was the second most abundant metabolite produced, reaching a maximum of 50 mmol $gDCW^{-1}$ in cultures without ethanol. *O. oeni* produces acetate from citrate and from sugars through the phosphoketolase pathway. During phase I, citrate uptake and acetate synthesis rates were higher than other phases (Figure 3-4 B, C), suggesting that acetate was formed using all citrate consumed. However, acetate synthesis was faster than citrate uptake, which indicates that another pathway as phosphoketolase pathways was used additionally for its production. In later phases, however, acetate was mainly produced through phosphoketolase pathway, using other compounds, such as glucose.

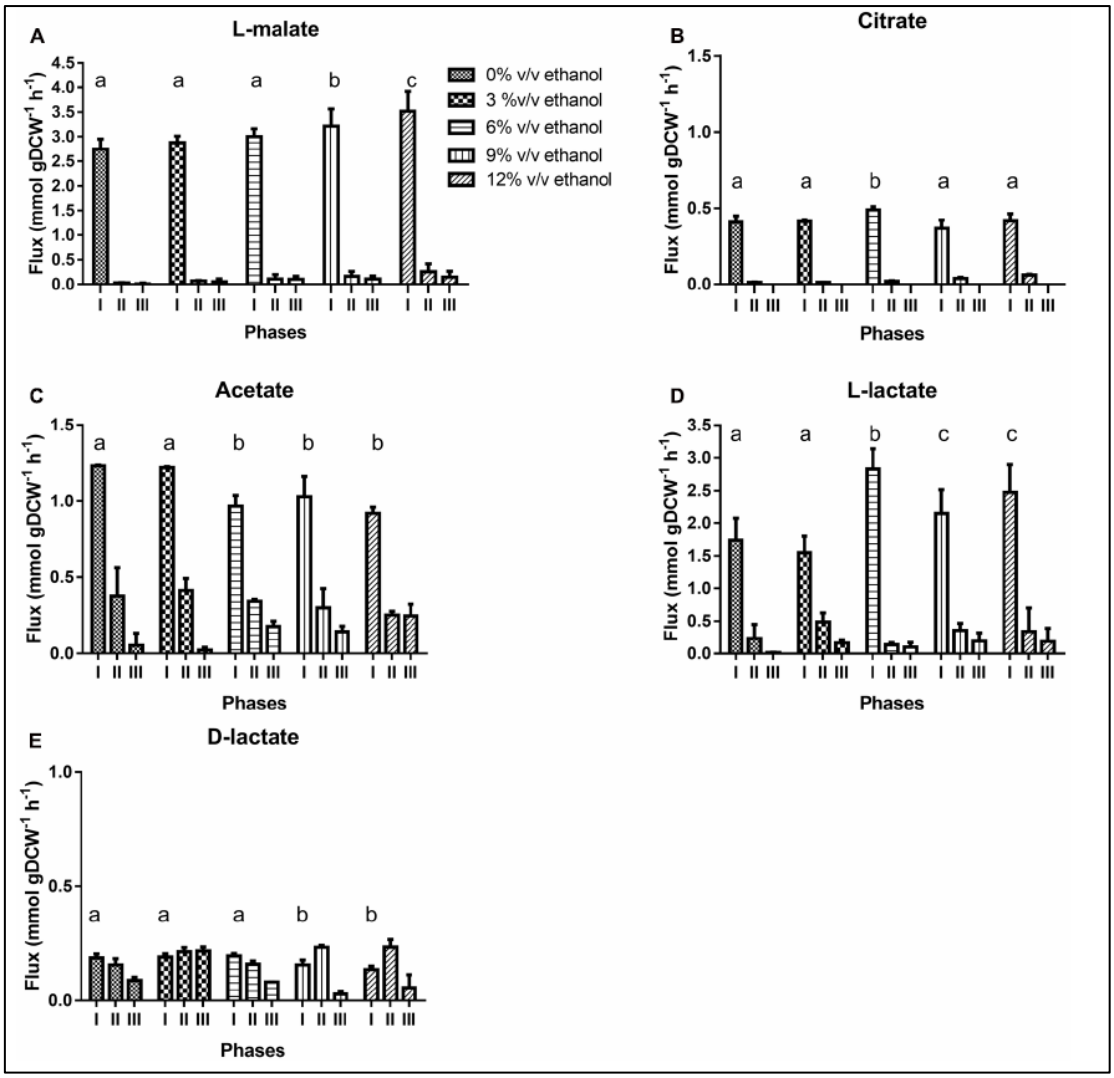

Figure 3-4: Specific consumption of L-malate (A) and citrate (B) and specific production of acetate (C) L-lactate (D) and D- lactate (E) during growth of *O. oeni* PSU-1, under increasing ethanol contents. Statistical analysis only was performed in phase I and shared letters indicate no significant difference (Mood test, $p < 0.05$).

3.3.4 Metabolism of Amino acids

All the amino acids were metabolized during the cultivation of *O. oeni* in MaxOeno culture medium at increasing concentrations of ethanol; however, none was totally consumed (Table 3-2). Histidine, cysteine, lysine and aspartic acid were the most consumed amino acids. The highest specific consumption rates were determined for histidine and proline (Figures 3-5 D, F) and their rates increased concomitantly with increasing ethanol contents in culture medium.

Table 3-2: Amino acid requirements by *O. oeni* PSU-1 cultured in medium with different ethanol content.

	Amino acid	Consumed amino acids [%] ¥ Ethanol (% v/v)				
		0%	**3%**	**6%**	**9%**	**12%**
	Histidine	72.1[a]	68.8b	82.9b	79.3c	67.8d
>50%	Lysine	77.6[a]	69.8a	74.7a	66.5a	64.9a
	Cysteine	67.9[a]	64.3a	68.2a	64.4a	64.4a
	Aspartic acid	65.0[a]	68.8a	62.1b	46.5c	24.7d
	Arginine	39.3[a]	39.3a	40.1a	36.4a	31.5b
	Methionine	32.7[a]	37.9a	37.0a	39.4a	36.8a
	Proline	36.3[a]	34.7ab	34.5ab	32.8ac	29.5c
30-50%	Alanine	31.7[a]	30.0b	30.2b	28.3c	25.5d
	Glutamic acid	41.3[a]	37.5a	36.4a	32.0b	25.5c
	Serine	46.6[a]	43.3ab	44.6ac	41.7ad	39.2d
	Glutamine	18.1[a]	21.4ab	22.4b	23.3bc	25.9c
	Valine	28.5[a]	27.2a	26.4a	23.7c	18.3d
	Tyrosine	13.4[a]	15.3b	17.4b	18.9b	16.4c
<30%	Leucine	6.8[a]	5.8a	13.5b	24.3c	19.5d
	Isoleucine	27.8a	21.0b	19.3b	16.9bc	14.3c
	Phenylalanine	24.8[a]	25.2a	25.0a	22.4b	18.7b
	Threonine	23.9[a]	20.9ab	17.0a	20.7b	19.3b
	Tryptophan	23.5[a]	23.2a	24.0a	23.4a	20.4a

¥ All assays were performed in triplicate and all coefficients of variation (CVs) were <10%. Shared superscript letters (a, b, c) in the same row indicate no significant difference (Mood test, $p < 0.05$). Consumption of amino acids highlighted in light gray are independent consumed of ethanol content present in the culture medium. Consumption of amino acids highlighted in dark gray are dependent consumed of ethanol content present in the culture medium.

Amino acids were mostly consumed (almost 90%), during phase I, with the exception of cysteine, which was consumed during both, phases I and II (Figure 3-5 and Supplementary material S3-4). Interestingly, specific consumption rate of cysteine was the only one that was higher for phase II than for phase I, even increasing with ethanol content (Figure 3-5A).

Threonine was consumed faster in cultures with 9 and 12% ethanol; and serine was consumed faster in cultures with 6% ethanol (Figures 3-5 C, E).

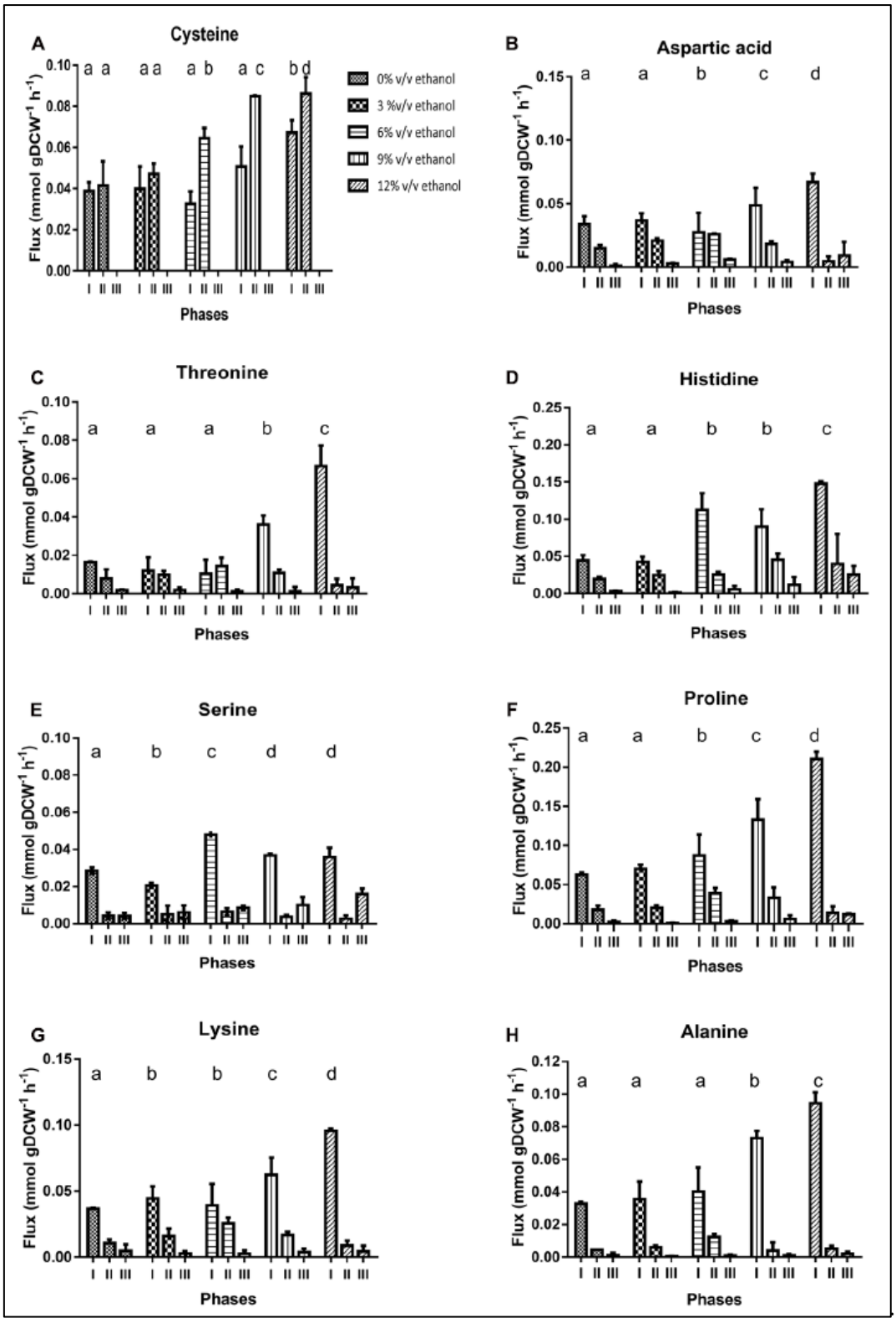
A
Cysteine
a a a a a b a c b d
Flux (mmol gDCW⁻¹ h⁻¹)
0.10
0.08
0.06
0.04
0.02
0.00
I II III
Phases
0% v/v ethanol
3 %v/v ethanol
6% v/v ethanol
9% v/v ethanol
12% v/v ethanol
B
Aspartic acid
a a b c d
0.15
0.10
0.05
0.00
C
Threonine
a a a b c
D
Histidine
a a b b c
0.25
0.20
0.15
E
Serine
a b c d d
F
Proline
a a b c d
G
Lysine
a b b c d
H
Alanine
a a a b c
0.12

Figure 3-5: Specific consumption rates of amino acids during cultivation of *O. oeni* PSU-1 under increasing ethanol contents. A) Cysteine. B) Aspartic acid. C) Threonine. D) Histidine. E) Serine. F) Proline. G) Lysine. H) Alanine. Statistical analysis was only performed for phase I and shared letters indicate no significant difference (Mood test, $p< 0.05$)

Besides, histidine and lysine consumption increased with ethanol. It is noteworthy that histidine was the most consumed amino acid in the cultures with 12% ethanol, reaching 18 mmol $gDCW^{-1}$.

Cysteine, lysine, methionine and tryptophan were up taken at similar amounts, whatever the ethanol concentration (Table 3-2). However, their specific consumption rates increased with ethanol content (Figure 3-5 A, G and Supplementary material S3-4). Alanine and aspartic acid were also consumed faster in cultures with higher ethanol content (Figures 3-5 B, H).

Finally, the consumption of aspartic acid, arginine, glutamic acid and isoleucine decreased as ethanol content was incremented in the culture medium.

3.3.5 Analysis of intracellular fluxes

3.3.5.1 *Non-Growth Associated Maintenance (NGAM).*

Flux balance analysis was carried out in iSM454 model to predict NGAM for each experimental data set. Thereby, a range of possible NGAM values was tested and biomass formation rate was predicted. The NGAM value that allowed the minimal biomass prediction error was selected for each data set. Biomass was predicted correctly, with an average biomass prediction error of 0.05%.

Estimated NGAM values significantly increased in all phases, although differently, depending on the ethanol content of the culture medium. In phase I, NGAM increased threefold in cultures with 3 and 6% ethanol; and 10- and 17-fold in cultures with 9 and 12% ethanol. In phase II, it sequentially increased from 6 to 11-fold in cultures from 3 to 12% ethanol, respectively. In phase III, a maximum NGAM increase of sevenfold was achieved for cultures with 12% ethanol content. Whatever the case, at any ethanol level, NGAM was the lowest for phase I and the largest for phase III (Figure 3-6A).

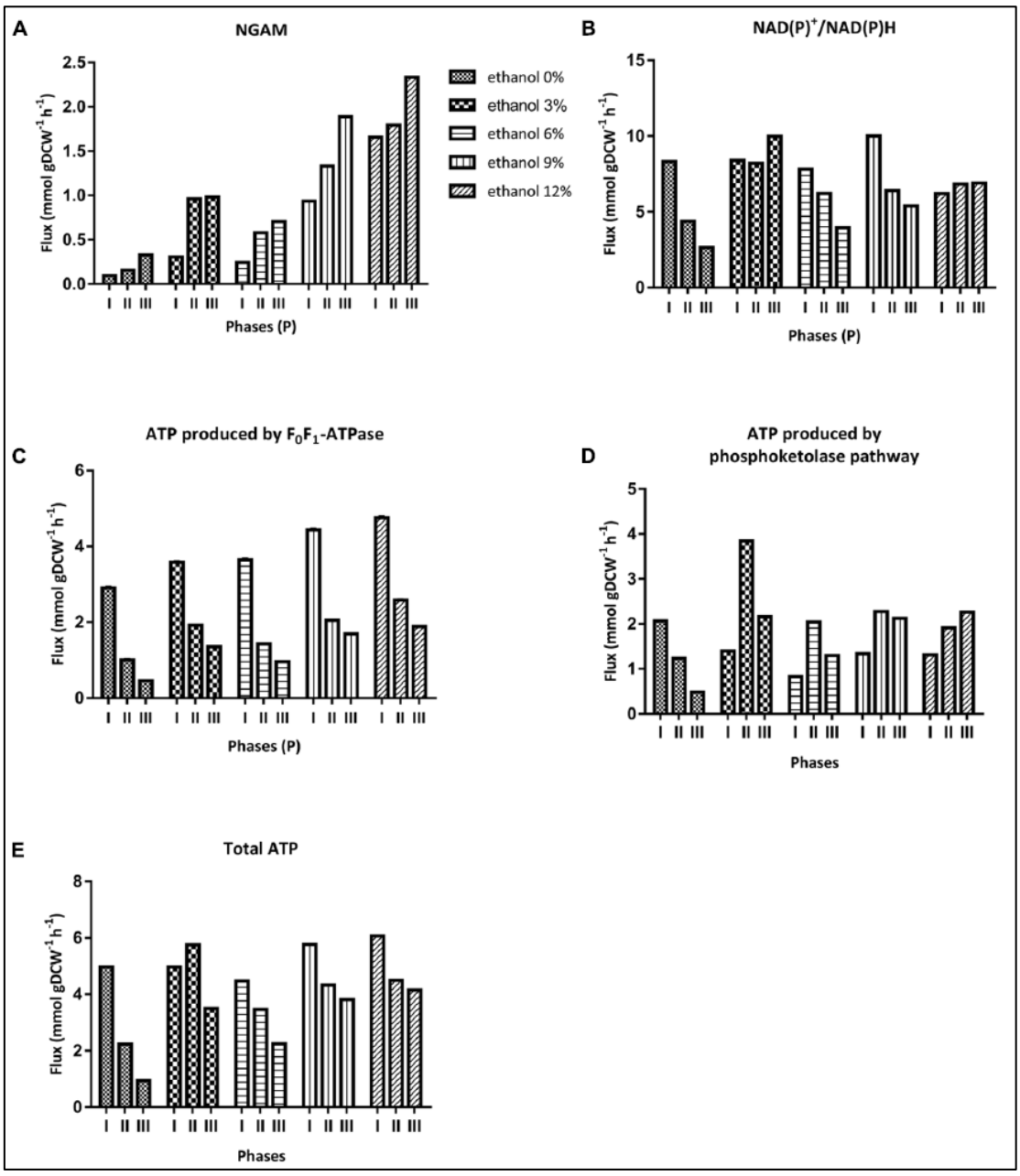

Figure 3-6: NGAM and *in silico* determined specific production rates of key metabolites of *O. oeni*. A) NGAM, B) $NAD(P)^+$/NAD(P)H, C) ATP produced by F_0F_1-ATPase, D) ATP produced by phosphoketolase pathway, E) Total ATP, (*i.e.*) ATP produced by both ATPase and phosphoketolase pathways.

3.3.5.2 *NGAM Sensitivity analysis.*

Sensitivity of NGAM values towards the experimental data was evaluated by varying each constrained flux independently in 1% of its value, and then repeating NGAM prediction. NGAM prediction variation was assessed by calculating the relative prediction error (in %), and the highest prediction error was taken as representative of the NGAM's sensitivity of the corresponding data set (Supplementary material S3-5). Phase I was the most sensitive phase at every ethanol level, reaching the highest NGAM prediction variation in the absence of ethanol (130%). The largest variations were obtained when fructose and mannitol fluxes were varied.

3.3.5.3 *Energetic requirements.*

The model predicted that ATP requirements increase with ethanol content at each phase. Higher ATP requirement is predicted during phase I, whatever the ethanol content.

ATP is synthesized either by F_0F_1-ATPase or phosphoketolase pathway. In phase I, the maximum specific production rate of ATP (rATP) produced by F_0F_1-ATPase was higher than ATP produced through the phosphoketolase pathway. In cultures with 0 to 12% ethanol, fluxes through F_0F_1-ATPase increased from 2.9 to 4.8 mmol $gDCW^{-1}$ h^{-1}, respectively; and fluxes through the phosphoketolase pathway decreased from 2.1 to 1.3 mmol $gDCW^{-1}$ h^{-1}, for the same cultures (Figures 3-6 C, D). In phase II, rATP occurring through F_0F_1-ATPase decreased by 50% in all cultures. On the contrary, r_{ATP} through the phosphoketolase pathway increased in all cultures with ethanol content. Finally, during phase III, r_{ATP} by F_0F_1-ATPase continues to decrease – by another 50% compared to phase II; and r_{ATP} through phosphoketolase pathway also decreased in cultures containing less than 6 % v/v of ethanol content but remained constant in cultures with higher ethanol contents (Figure 3-6 C, D).

Interestingly, during phase I, the ATP flux through F_0F_1-ATPase increased from 58% to almost 80% of total ATP flux in cultures without ethanol and cultures with ethanol content, respectively. Besides, during phases II and III there was a preference

for synthesis by the phosphoketolase pathway; on average, 56% of ATP was produced from this pathway (Figure 3-6 C-E).

3.3.5.4 *Cofactor Requirements*

We determined the impact of ethanol on the cofactor usage by analyzing the NAD(P)H flux during growth (Figure 3-6 B). The reactions that produce NAD(P)H involve the following enzymes: malate dehydrogenase, glyceraldehyde-3P dehydrogenase, threonine dehydrogenase, NADH quinone reductase, $NAD(P)^+$ transhydrogenase and the pathway of methylglyoxal degradation for NADH formation; and glucose-6P dehydrogenase, phosphogluconate dehydrogenase and GMP reductase for NADPH formation. A clear trend of the use of cofactors in relation to the presence of ethanol in the culture medium could not be found (Figure 3-6 B).

3.3.5.5 *Elementary Flux Mode Analysis*

As the MaxOeno medium contains several substrates, an EFMA was carried out to determine possible substrate-product relationships between the substrates present in the medium and the possible products, including but not limited to products measured experimentally (Table 3-3). Results showed that serine, threonine and cysteine can be used for diacetyl formation, as well as citrate, which can also be a precursor for acetate production. L-malate can be directed into either D- or L-lactate, and therefore it is the only substrate that can be used for L-lactate synthesis. Both glucose and fructose are able to generate all products but L-lactate.

3.3.5.6 *Random Sampling*

100.000 flux distributions were computed using optGpSampler for each ethanol level and each phase. In each of the 15 conditions, the network was constrained using uptake and production rates as well as sink reactions for simulating accumulations. We used these flux distributions to study the flexibility of the network in each condition.

Means and standard deviations were calculated for 40 reactions related to phosphoketolase pathway. Overall, standard deviations were higher in phase I and smaller in phase III for all ethanol levels. Thus, the metabolic network is more flexible in phase I than in phase III. This is expected from a biological perspective as at the

beginning of the fermentation there are more nutrients in the extracellular space – and with a higher concentration – than in later phases. Therefore, a higher number of reactions are expected to be available in order to catabolize these sugars. In contrast, at the end of the fermentation, citrate and malic acid are already depleted and other nutrients are almost exhausted resulting in a tighter metabolic network.

Table 3-3: Determination of possible substrate-product relationships by EFMA.

	D-mannitol	D-lactate	L-lactate	Diacetyl	Ethanol	Acetate	Erythritol
D-fructose	36	15	0	15	33	64	33
D-glucose	157	67	0	61	126	233	145
Citrate	0	0	0	2	0	2	0
L-malate	0	2	2	0	0	0	0
L-cysteine	0	0	0	3	0	0	0
L-serine	0	0	0	3	0	0	0
L-threonine	0	0	0	3	0	0	0

EFMA was carried out in a reduced version of the iSM454 model. Position *i,j* indicates the quantity of pathways that included consumption of only substrate *i* (other substrates in zero), and generation of the production *j*

3.3.5.7 *Metabolic flux distribution.*

Distribution of carbon intracellular fluxes was analyzed for all the growth phases, considering the major central metabolic pathways, which includes phosphoketolase pathway, fructose reduction, citrate degradation and MLF. FBA showed that a significant redistribution of intracellular fluxes occurred in *O. oeni* in response to ethanol content (Figure 3-7, 3-8 and 3-9). Fluxes were normalized over specific growth rates.

The model showed that fructose, the sugar that was most consumed, was mainly used – around 70% of the total – for mannitol biosynthesis during phase I; however, in later phases, fructose was redirected to glucose-6P synthesis, and then into the phosphoketolase pathway (Figure 3-7, 3-8 and 3-9).

Erythritol biosynthesis arises from ribulose-5P and glyceraldehyde-3P in almost all cases (Figure 3-7, 3-8 and 3-9). It was highest during phase I, and increased with ethanol content, from 42 to 84 mmol $gDCW^{-1}$ in cultures without and with 12% ethanol, respectively.

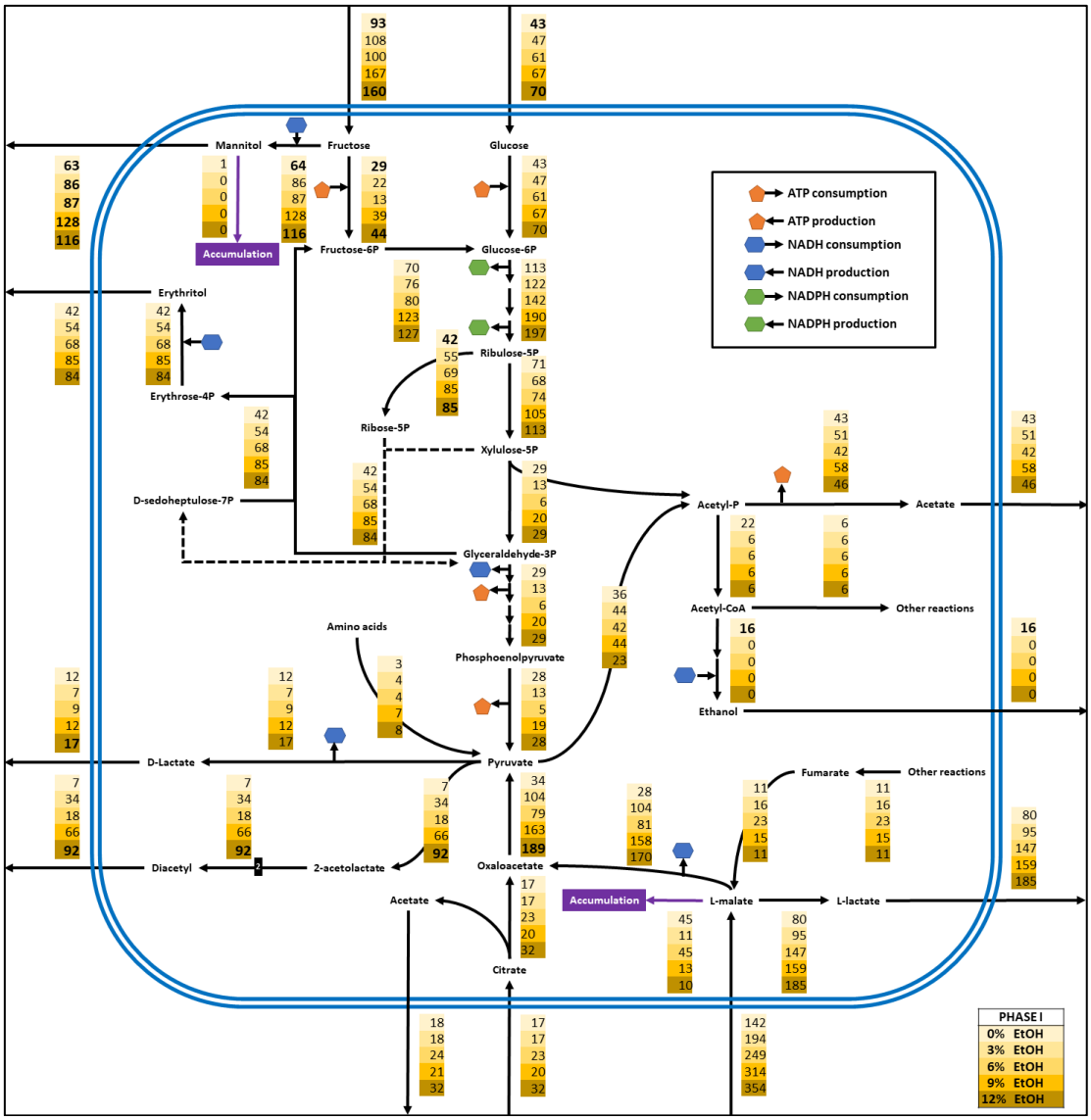

Figure 3-7: Metabolic flux redistribution of the central carbon metabolic pathways of *O. oeni* PSU-1 upon cultivation in a culture medium without and with 3, 6, 9 and 12% (yellow boxes, from top to bottom) ethanol concentration, during growth phase I. Polygons with colors orange, blue and green indicates consumption (or production) of ATP, NADH and NADPH, respectively.

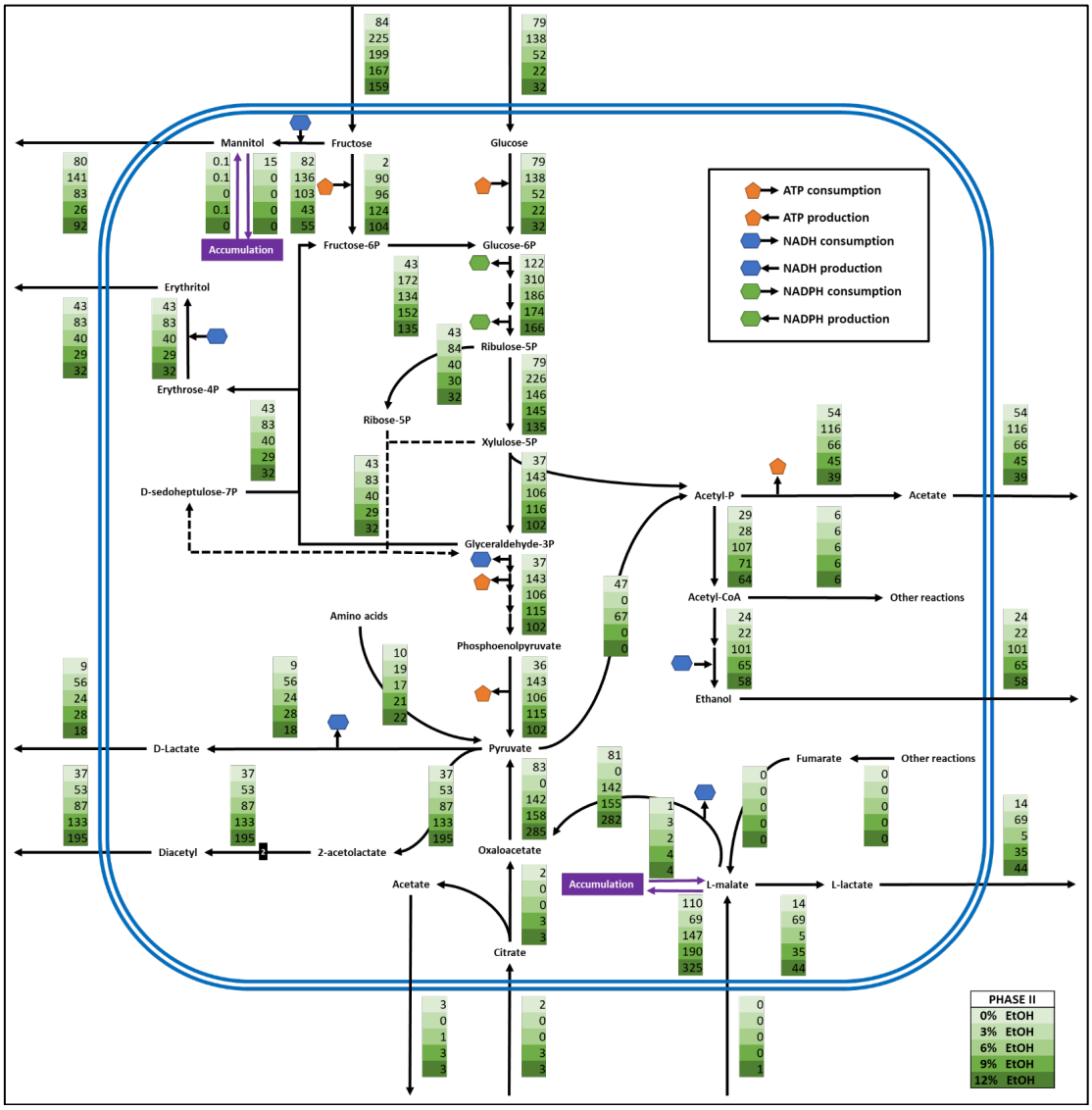

Figure 3-8: Metabolic flux redistribution of the central carbon metabolic pathways of *O. oeni* PSU-1 upon cultivation in a culture medium without and with 3, 6, 9 and 12% (yellow boxes, from top to bottom) ethanol concentration, during growth phase II. Polygons with colors orange, blue and green indicates consumption (or production) of ATP, NADH and NADPH, respectively.

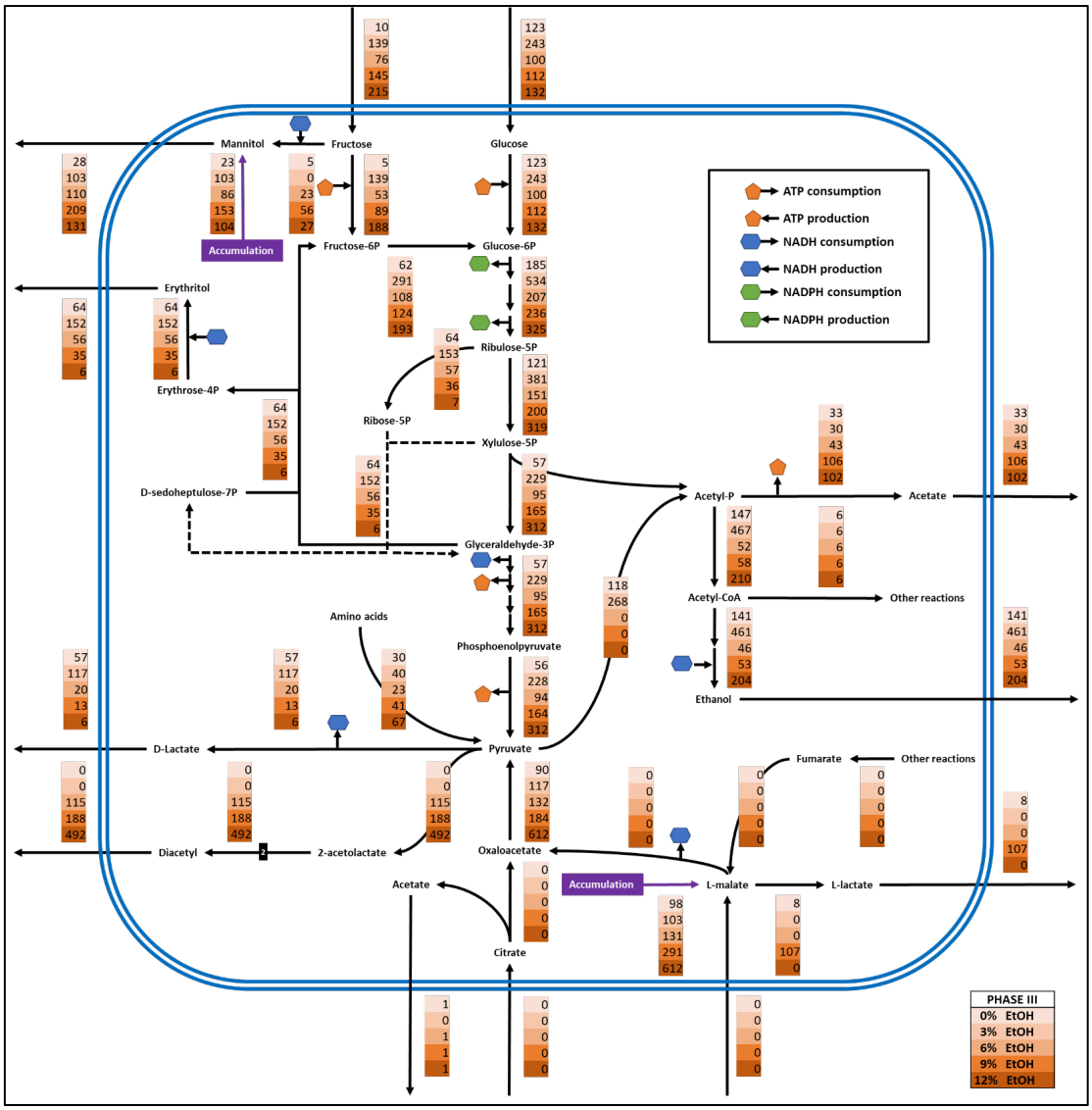

Figure 3-9: Metabolic flux redistribution of the central carbon metabolic pathways of *O. oeni* PSU-1 upon cultivation in a culture medium without and with 3, 6, 9 and 12% (yellow boxes, from top to bottom) ethanol concentration, during growth phase III. Polygons with colors orange, blue and green indicates consumption (or production) of ATP, NADH and NADPH, respectively.

The model also predicted diacetyl synthesis. This specific production rates incremented with ethanol content and thus were highest at 12% ethanol in all phases. This compound is produced from pyruvate.

Interestingly, pyruvate production increased in phase II, and even more in phase III by the following routes: amino acid degradation, citrate degradation, and L-malate conversion into oxaloacetate (Figure 3-7, 3-8 and 3-9). All of these fluxes also incremented as ethanol increased in the culture medium.

3.4 Discussion

In this work, we determined the effect of ethanol on nutritional and energetic requirements of *O. oeni* to ensure its growth. For this end, we cultivated *O. oeni* PSU-1 strain in a wine- like, defined culture medium spiked with 0, 3, 6, 9, or 12% v/v ethanol. Moreover, we took advantage of our recently constructed genome-scale metabolic model (Mendoza et al., 2017) that allowed assessing the redistribution of the intracellular metabolic fluxes and the energetic factors at increasing ethanol concentrations.

As expected, cell growth was closely related ($r2 = 0.98$) to ethanol content. Specific growth rate and maximal biomass content decreased progressively as ethanol concentration in the medium increased. Moreover, both decreased during the time course of the batch cultivation. In general, specific growth rates and biomass production were larger during phase I, which was coincident with the highest metabolic activity of *O. oeni* observed during this phase, for any culture condition.

Changes in ethanol level strongly impacted *O. oeni's* requirements of NGAM, $NAD(P)^+$ /NAD(P)H cofactors and energy, reflected in higher production of ATP by F_0F_1-ATPase.

Energetic demand for NGAM dramatically increased in *O. oeni* cells cultured under alcoholic stressful conditions. Indeed, cultures containing 9 and 12% ethanol required 10 and 17 times more NGAM during phase I, respectively, than cultures without ethanol. The latter indicates that the ATP produced was principally used to cope with cell maintenance resulting from this stress. This agrees with our previous work, where the genome scale metabolic model (GSMM) indicated that NGAM was

30-fold higher in cultures with 12% ethanol than in cultures without ethanol (Mendoza et al., 2017). Notably, the model predicted that the cells cultivated with 6% ethanol would require a lower NGAM than those grown at 3% ethanol. This agrees with Cavin et al. (1998) that reported that low concentrations of ethanol activate bacterial growth, *i.e.,* ethanol improves exchanges between the cell and the external medium. In addition, significant cellular changes normally occur when at least 8% ethanol is present in the medium, coinciding with changes in membrane lipid composition (da Silveira et al., 2003; Grandvalet et al., 2008; Teixeira et al., 2002). F_0F_1-ATPase is the favorite route employed for the synthesis of ATP during phase I. Indeed, even in the absence of ethanol in the culture, 58% of the total ATP is generated by this route. Moreover, to overcome the strong ATP demand for NGAM at higher ethanol concentrations, the model predicts that this pathway produces almost 80% of the required ATP. As F_0F_1-ATPase produces ATP at the expense of proton translocation to the inside of the cell, this indicates a higher requirement for proton extrusion. In this regard, the malolactic reaction is usually considered the major pathway for proton extrusion and ATP production in LAB (Tourdot-Maréchal et al., 1999; van de Guchte et al., 2002). In this process, one mole of malic acid is consumed and generates equivalent amounts of L-lactate and CO_2; and, because of pKa differences between the substrate and the products, a proton is consumed (Augagneur et al., 2007; Wil N. Konings, 2002; Marty-Teysset et al., 1996). This positive effect is augmented by L-lactate transport, a symporter that extrudes protons (Salema et al., 1996). We found that malic acid was almost totally depleted during phase I in each condition, in concordance with the higher F_0F_1-ATPase flux predicted by the model. Moreover, in this phase, specific consumption rates of malic acid were the fastest in cultures with 9 and 12% ethanol, as well as specific production rates of L-lactate. The key role of malic acid for proton extrusion is confirmed by the model, as it predicts that 74–95% of the protons translocated by F_0F_1-ATPase are extruded by MLF and L-lactate transport in all the experimental conditions; and that the flux through this reaction increases concomitantly with the ethanol content in the medium, to overcome higher energetic

requirements. This confirms that malolactic reaction is the main pathway for ATP synthesis in the presence of high ethanol content.

For reductive power regeneration, ethanol formation is the main pathway for reoxidation of $NAD(P)^+$ in *O. oeni,* although at high metabolic rates this process becomes limiting (Richter et al., 2003); therefore, other external electron acceptors are used for $NAD(P)^+$ reoxidation (Maicas et al., 2002; Richter et al., 2003; Versari et al., 1999). Several studies have reported that one of the main limitations in $NAD(P)^+$ regeneration through the ethanol biosynthetic pathway is the deficiency of D-pantothenate in the culture medium, an essential precursor for HSCoA in *O. oeni* (Richter et al., 2001; Terrade & Mira de Orduña, 2009). The latter is the cofactor of acetaldehyde dehydrogenase (Garvie, 1967a). Nevertheless, the MaxOeno culture medium employed in this work contains enough D-panthotenate to allow optimal growth of *O. oeni* and ethanol pathway activation. Another cause could be the limited availability of HSCoA due to its preferential use for fatty acid production, to overcome the damage of cell membrane that could result from ethanol.

When ethanol production pathway is non-functional, a lack of reduced cofactors occurs. Our results show that *O. oeni* PSU-1 uses fructose, glucose, and citrate as electron acceptors for cofactors reduction. In particular, the specific production rates of mannitol and erythritol incremented as ethanol concentration increased during phase I. However, fructose, which is the main precursor of mannitol and erythritol, showed similar specific consumption rates during phase I, whatever the culture conditions; and glucose, that can also be used in erythritol formation, displayed slower consumption rates at higher ethanol concentrations. This indicates that there is a preferential consumption of carbon sources toward mannitol and erythritol formation at higher ethanol concentrations rather than biomass formation, as a result of higher cofactor requirements. Indeed, the model predicts that cofactor regeneration due to mannitol and erythritol formation countervail for almost 50% of the cofactors used for sugar catabolism in conditions without ethanol, and for 51–57% of this usage in ethanol-containing cultures.

Citric acid consumption is also related with cofactor regeneration. Consumption of this chemical compound is used for pyruvate formation, which is then used for either production of D-lactate or diacetyl. D-lactate is used for $NAD(P)^+$ regeneration, while diacetyl is related with consumption of intracellular protons and thus increase of internal, as well as external pH, as diacetyl is less acidic than citric acid (Saguir & Manca de Nadra, 1996; Versari et al., 1999). Citric acid was mainly consumed during phase I at similar specific consumption rates, whatever the ethanol content. During this phase, D-lactate formation showed a different behavior: the highest flux toward D-lactate synthesis – which arises from both, citrate degradation and phosphoketolase pathway – was observed when ethanol was absent in the medium, where 72% of the consumed citrate was directed toward the synthesis of lactate, instead of the 38 and 58% observed at 9 and 12% v/v ethanol, respectively. On the contrary, the model predicted higher diacetyl production fluxes when ethanol was higher in the medium. As citric acid consumption was similar in all conditions, this indicates that, at high ethanol concentrations, citric acid consumption was not sufficient to supply all the pyruvate required for diacetyl synthesis. Indeed, in the absence of ethanol, 44% of the citrate consumed was used for diacetyl formation; however, at 9 and 12% ethanol, there were 3.2 and 2.9 moles of diacetyl produced per mole of consumed citrate. This clearly indicates that pyruvate was redirected to the formation of this compound. For this end, the required pyruvate is produced from L-malate, as at increasing ethanol conditions the flux through malic enzyme, which uses L- malic acid for oxaloacetate synthesis, increases. Thus, a 3.7-fold higher synthesis of oxaloacetate was achieved through this route in cultures containing 12% ethanol, as compared to those without ethanol.

Thus, citric acid was mainly used for internal ionic balance through diacetyl production under ethanolic conditions; and not for $NAD(P)^+$ cofactor regeneration. In LAB, diacetyl formation requires intracellular protons, resulting in an increase in the internal pH. In addition, its extrusion increases external pH because it is less acidic than citric acid. In general, D-lactate production is privileged with regards to diacetyl, probably to allow the cells to obtain NAD^+; however, when lactate dehydrogenase (LDH) function is reduced, pyruvate accumulates, and diacetyl is produced (García-

Quintáns et al., 1998; Tsakalidou & Papadimitriou, 2011). Thus, high ethanol content could limit the function of LDH, allowing diacetyl production, as demonstrated here. Another possible cause is that higher diacetyl formation results from the larger energetic requirements caused by higher NGAM requirements. As F_0F_1-ATPase generates ATP by translocating protons to the inside of the cell, higher ethanol concentrations imply a higher necessity to extrude these protons by alternative pathways. In fact, at the highest ethanol concentrations, diacetyl generation consumes 20 and 25%, respectively, of the protons introduced into the cell by F_0F_1-ATPase; opposite to only 5% for cells grown in the absence of ethanol. This shows that the increment of diacetyl formation and the resulting proton consumption in this reaction allows to increment the proton gradient. This gradient can then be used to produce, through F_0F_1-ATPase, the energetic requirements needed to overcome the challenging environment of this elevated ethanol concentration in the medium. From a biological perspective, proton consumption can also be used to compensate for the proton influx caused by the higher permeability of the plasmatic membrane at high ethanol concentrations.

Other authors have cultured *O. oeni* PSU-1 in the presence of 12% of ethanol, showing that genes related with malate and citrate consumption were up-regulated while genes related with fructose consumption were down-regulated, which was associated to mechanisms of ethanol resistance (Margalef-Català et al., 2016). We observed that malate and citrate were almost totally consumed during the first 48 h of culture (phase I), suggesting that both substrates were critical for *O. oeni* survival; although we did not find a clear relation between ethanol content and citrate consumption, we did observe an increment in fluxes related with citrate consumption. Moreover, we found that fructose and glucose were consumed faster during phase I, without any inhibition.

Additionally, the specific consumption rate of cysteine, one of the most consumed amino acids, increased with ethanol content in the medium. Genomic studies of *O. oeni* PSU-1 reported that this strain is unable to synthesize cysteine, because sulfur cannot be transported inside of the cell (Garvie, 1967a; Mills et al., 2005).

Cysteine can be used as a source for pyruvate formation, together with serine and threonine. The model predicted a 2.7-fold increase in pyruvate formation from these amino acids at 12% ethanol than in cultures without ethanol. Additionally, cysteine can be used in reactions of CoA synthesis, where this amino acid is added to D-4-P-phantothenate generating R-4-P-phantothenosyl-L-cysteine, and *O. oeni* does have the genes to this synthesize (Mills et al., 2005). CoA functions as an acyl group carrier and carbonyl activating group in numerous reactions central to cellular metabolism and provides the 40-phosphopantetheine prosthetic group incorporated by carrier proteins that play key roles in fatty acid and non-ribosomal peptides biosynthesis (Spry et al., 2008).

3.5 Conclusion

We found that under ethanol stress conditions, *O. oeni* favors anabolic reactions related with cell reconstruction pathways and/or production of stress protectors; consequently, the requirements of $NAD(P)^+$, NGAM and ATP increase with ethanol content, unrelated with biomass increment.

Finally, in this work we were able to integrate in the model specific consumption/production rates and specific growth rates for each of the determined growth phases, and thus, the model was able to represent the different phenotypes of *O. oeni* in each of the growth phases. To the best of our knowledge, this is the first report where experimental data from the entire exponential curve has been integrated to the model (Mendoza et al., 2017). Even if GSMM and FBA are usually applied to data obtained from steady state experiments, these strategies have been previously used to model data from batch growth, based on the assumption of a pseudo-steady state of the cellular metabolism (Pastink et al., 2009; Pereira et al., 2016; Teusink et al., 2005). The approach developed in this work allowed to characterize the physiological changes that occur in the metabolism of *O. oeni* PSU-1 during its growth in a culture medium containing various carbon sources, as the wine-like medium MaxOeno. The results highlight the flexibility of the metabolism of this bacterium, which could not have been carried out with a canonic approach (Mendoza et al., 2017); for example, we previously reported that at high ethanol concentrations, production of ATP was preferentially

carried out through the phosphoketolase pathway. In the present study, where dynamic changes were assessed, a similar result was found for phases II and III; however, the opposite was observed for phase I, a result that was previously lost due to the canonical analysis; the latter stresses the critical role of organic acids for ATP synthesis and, thus, for survival and adaptation in a medium with high ethanol concentrations. Furthermore, we were able to identify and include in our simulations the internal accumulation of compounds such as mannitol, which had an impact in the pathways used on each phase for cofactor regeneration.

Several perspectives derived from this study can be foreseen. For example, a similar approach can be employed to tackle the metabolic response to acidic conditions in this bacterium, which, together with alcohol and SO_2 stresses, are the most relevant conditions that affect the growth of *O. oeni.* For instance, Liu et al. (2017) recently showed, using RNA-seq, that in *O. oeni* SD-2a strain grown at pH of 4.8 and pH 3.0, several genes related with the metabolism of amino acids, carbohydrates, membrane transport and energy metabolism were differentially expressed. Therefore, the resulting quantitative transcriptomics can be incorporated into the iSM454 metabolic model as restrictions and, together with experimental data, could allow to simulate the redistribution of metabolic fluxes resulting from this environmental perturbation.

Moreover, important efforts have been made to identify the genetic characteristics of different communities of *O. oeni* from different geographical regions, which is particularly relevant to understand the relationship between the wines of a certain geographical location and what has been termed as the “terroir” (e.g., Capozzi et al., 2014). The characterization of these genomes is particularly relevant to determine different aspects of safety, tolerance to the harmful wine conditions and its contribution of the sensory quality of the wine. Thus, an approach like the one proposed in this paper, considering the genomic differences at the strain-specific level, would allow modeling the metabolic behavior of strains that are of interest for wines within a geographical location and to understand the physiological conditions in which a metabolic shift occurs. For example, the metabolic model used here is based on the PSU-1 strain, which does not produce biogenic amines, since the biosynthetic pathways

of these compounds have not been found in the genome of *O. oeni* PSU-1. However, it is known that most *O. oeni* strains produce these deleterious compounds (López et al., 2009; Lucas et al., 2008). Therefore, the inclusion of the related biosynthetic pathway in the *O. oeni*'s GSMM to simulate their biosynthesis under different cultural and environmental conditions, to understand and minimize their production will be particularly promising.

Finally, and in accordance with the above, determination of new ecotypes will permit to define new nutritional formulations that might be relevant for the wine industry, such as tolerance to alcohol, or resistance to SO_2 and pH, as well as efficient consumption of malic acid. For example, a recent study carried out in 16 wineries from different Chilean valleys showed that autochthonous strains present a unique number of genes with respect to commercial strains. Moreover, some of these strains do not contain some genes related to off-flavors, such as phenolic decarboxylase (Romero et al., 2018). Thus, physiological studies complemented with the GSMM of several indigenous *O. oeni* strains might unravel new organoleptic patterns, as well as environmental responses, which complement the current knowledge regarding the differences at genomic level and, eventually, discover new starter cultures.

4. CHAPTER III: L-MALATE (-2) PROTONATION STATE IS REQUIRED FOR EFFICIENT DECARBOXYLATION TO L-LACTATE BY THE MALOLACTIC ENZYME OF *OENOCOCCUS OENI*

4.1 Introduction

Most red wines, as well as some white and sparkling wines, are produced by two sequential fermentations: first, yeast alcoholic fermentation (AF) transforms grape must into wine; then, a secondary fermentation, called malolactic fermentation (MLF), is carried out by lactic acid bacteria (LAB). Contrary to AF, a mandatory process of winemaking, MLF is optional and depends on the desired wine style. MLF reduces the acidity of wine and improves flavor complexity and microbiological stability. MLF involves the NAD^+- and manganese-dependent decarboxylation of L-malate to L-lactate and CO_2 (Kunkee, 1974; Williams et al., 1984). Due to its monocarboxylic nature, lactic acid imparts a more elegant and round taste to the wine, as opposed to the astringent taste of the dicarboxylic, malic acid (Henick-Kling et al., 1994; S.-Q. Liu, 2002; Zoecklein et al., 1999). *Oenococcus oeni* is the main lactic acid bacterium involved in MLF, thanks to its ability to grow under the harsh conditions of wine, such as high ethanol content (>13% *v/v*), low pH (<3.5), and high sulphite concentration (>50 ppm) (Bartowsky, 2005; Bauer & Dicks, 2004; H. Li et al., 2006; Zapparoli et al., 2009; G. Zhang, 2013). MLF is considered one of the most difficult processes to manage during winemaking, because it is often delayed or simply not fully achieved.

Among the issues of malolactic fermentation (Grandvalet et al., 2005, 2008; Olguín et al., 2009), the mechanism involved in the enzymatic reaction is perhaps the most unpredictable to ensure efficient and reproducible malate decarboxylation. Three decarboxylation pathways have been proposed so far, as shown in Figure 4-1 (Schümann et al., 2013). The first one considers that a malic enzyme (ME), followed by a L-lactate dehydrogenase, transforms malate to pyruvate, and then to lactate (Korkes & Ochoa, 1948). A second mechanism postulates a three-step reaction, mediated by a L-malate dehydrogenase (MDH), an oxaloacetate decarboxylase and a L-lactate dehydrogenase, respectively (Flesch, 1969). Finally, the third mechanism

consists in the direct conversion of L-malate into L-lactate (Caspritz & Radlert, 1983), through a reaction carried out in the presence of NAD^+ and Mn^{2+}, and where neither reduction of NAD^+ nor detection of free reaction intermediates occurs (Groisillier & Lonvaud-Funel, 1999; Schümann et al., 2013). This mechanism is conducted by a protein different from a previously described malic enzyme, the "malolactic enzyme" (MLE) (Ochoa et al., 1948).

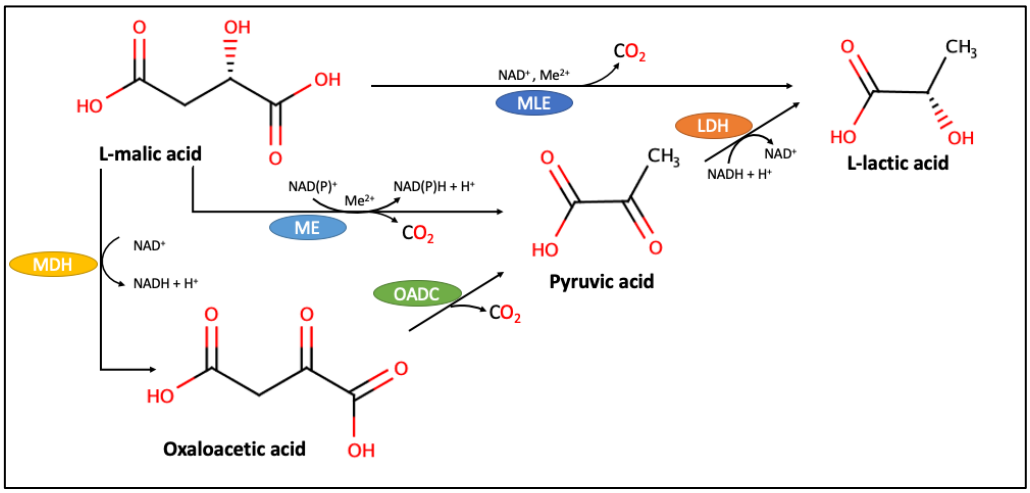

Figure 4-1: Possible decarboxylation pathways for the enzymatic conversion of L-malic acid to L-lactic acid. MDH, malate dehydrogenase; ME, malic enzyme; MLE, malolactic enzyme; OADC, oxaloacetate decarboxylase; LDH, lactate dehydrogenase. Adapted from Schümann et al. (2013).

The malolactic enzyme has been purified from several LAB, e.g., *Lactobacillus spp.*, *Lactococcus lactis,* and *O. oeni* (Bartowsky, 2005; Caspritz & Radlert, 1983; Lonvaud-Funel & Strasser de Saad, 1982; Spettoli et al., 1984). In all cases, the molecular mass of the MLE subunits range from 60 to 70 kDa, and the active form of the protein has been described either as a dimer or a tetramer of identical subunits (Ansanay et al., 1993; Battermann & Radler, 1991; Labarre, Guzzo, et al., 1996; Wang et al., 2014), although all subunits have an independent active site. Interestingly, MLE active sites have binding sites with different structural arrangements of the amino acids Asp, Lys, Ser, and Tyr that, altogether, satisfy the coordination of divalent cation and

cofactor positioning (Korkes & Ochoa, 1948). It is noteworthy that all described MLEs catalyze the same reaction.

Among LAB, *O. oeni* is the best adapted to the harsh conditions of wine. It is capable of carrying out spontaneous fermentation even at pH 3.2, a condition that could be found in some wines (Zapparoli et al., 2009). The objective of this study was to provide new insights on the reaction mechanism of the malolactic enzyme (MLE) of *O. oeni*, responsible for the transformation of L-malate into L-lactate in wine. To this end, we first expressed the MLE gene of *O. oeni* in *Escherichia coli* BL21. After purification of the protein, we measured the affinity of MLE for malic acid under several pH conditions by isothermal titration calorimetry. Then, we generated a MLE homology model, based on sequence similarity networking and phylogenetic analysis, in order to describe the MLE-malic acid molecular interaction at an atomic level, using molecular dynamics simulations. Finally, we explored the effect of pH on L-malate binding free energies and identified possible residues involved into malic acid binding by means of quantum polarized ligand docking and MM/GBSA calculations. To the best of our knowledge, this is the first study that explores the three-dimensional structure of the malolactic enzyme and its interaction with malic acid at the binding site, the first step of the reaction.

4.2 Materials and Methods

4.2.1 Analysis of Sequences and Construction of Phylogenetic Tree

The amino acid sequence of malolactic enzyme (MLE) from *Oenococcus Oeni* was retrieved from NCBI (accession number WP_002823502.1). Homologous amino acid sequences were found using the online available version of Basic Local Alignment Tools (BLAST™) (McGinnis & Madden, 2004). Twenty five sequences (accession number EEV40786.1, AMG48999.1, BAQ56789.1, AOO75947.1, BAP84672.1, ALJ31288.1, ANZ58780.1, ALO02977.1, CCC78515.1, ALG26877.1, CAI54742.1, AOO73522.1, ARE28303.1, KLK96319.1, API72025.1, ANZ71056.1, AMV69835.1, ABJ68638.1, AQP43157.1, ABV10389.1, CCF03237.1, CBY99983.1, AEH55110.1,

AEF25979.1, and ARC49389.1) of lactic acid bacteria were selected based on the e-value, the query coverage and its sequence identity with MLE, and were aligned using CLUSTAL OMEGA program (EMBL) (Sievers et al., 2011). The phylogenetic tree was built up using Interactive Tree Of Life (Letunic & Bork, 2006).

To perform the Sequence similarity Network, the MLE sequence from *O. oeni* (Uniprot ID: Q48796) was aligned to the closest sequences (>70% id) using all-by-all BLAST within InterProScan database performed by the web service EFI-Enzyme Similarity Tool (Gerlt et al., 2015; Zallot et al., 2019). Each sequence was labeled by its primary biological function and structural data availability as provided by UNIPROT. Even though all the function entries were cured manually, the lack of consistency of UNIPROT terminology could lead to ambiguous descriptions. Finally, 309,755 sequences were admitted to the SSN building.

4.2.2 Protein Modeling

4.2.2.1. Template Selection

The amino acid sequences of the malolactic enzyme from *O. oeni* strain DSM 20255 were retrieved from the NCBI (accession number ACX50963). The template was selected based on the e-value of the BLAST search, query coverage, and its sequence identity with MLE. Based on these criteria, malic enzyme from pigeon liver (PDB entry 1GQ2) was selected as a template to model MLE.

4.2.2.2 Modeling of Malolactic Enzyme

A comparative model for the malolactic enzyme was constructed using Prime from Schrödinger Suite 2019 using the PDB 1GQ2 and 6AGS as a template. Both enzyme cofactors, NAD^{+} and Mn^{+2}, were incorporated into the resulting models keeping the atomic coordinates from reference structure 1GQ2. The resulting model of the malolactic enzyme, including NAD^{+} cofactor and Mn^{+2} ion, was inserted in a water box and further neutralized with counter ions. Then MLE/NAD^{+}/Mn^{+2} complex was subjected to cycles of energy minimize as described elsewhere and equilibration for 200 nanoseconds under NPT conditions.

4.2.2.3 Ligand Preparation

L-malic acid three-dimensional structure was obtained from the PubChem database (Pubmed CID 222656) and prepared in Maestro (Schrödinger, LLC, New York, NY, USA) using the OPLS_2005 force field with default setting of the LigPrep package from Schrödinger. All molecules were visualized and pKa values were calculated using Epik at desire pH (Shelley et al., 2007).

4.2.2.4 Quantum Polarized Ligand Docking (QPLD)

L-malic acid and its other protonation states were docked with improved docking program of quantum polarized ligand docking (QPLD) of the Schrödinger Suite 2019 (Cho et al., 2005). The best poses obtained by flexible ligand docking using Glide (Friesner et al., 2004). Then QM calculations were done using Jaguar to calculate the partial charges were replaced on the ligand in the field of receptor for each ligand complex (Bochevarov et al., 2013). Single point electrostatic calculations were carried out with the 6-31G*/LACVP* base set and B3LYP density functional theory, using the "Ultrafine" SCF accuracy level (iacc = 1, iac-scf = 2) for the QM region. Finally, ligand was redocked with updated atomic charges with the help of Glide XP and QPLD of the Schrödinger Suite 2019.

4.2.2.5 Molecular Dynamics Simulation (MD)

MD simulations of malolactic enzyme and ligand complexes were carried out using Desmond and OPLS 2005 force field (Banks et al., 2005). The protein ligand complexes were solvated with TIP3 water molecules. Sodium counter ions were added to balance the system net charge. The systems were submitted to the default Desmond protocol, which contains a series of restrained minimizations and MD simulations. The minimized system was relaxed under NPT ensemble for 50 ns equilibration simulation period, and 150 ns production simulations were carried out. Long range electrostatic interactions were computed by particle-mesh Ewald method and van der Waals (VDW) cut-off was set to 9 Å.

4.2.3 Cloning and Expression of Recombinant Malolactic Enzyme

4.2.3.1 Microorganisms, Plasmids, and Media

Oenococcus oeni (Dicks et al., 1995; Garvie, 1967a) (PSU-1, ATCC® BAA-331™) was obtained from the American Type Culture Collection (ATCC) (Virginia, USA). Cryogenically preserved (−80 °C) strains were cultured and maintained on MRS plates (Man, Rogosa and Sharpe) (De Man et al., 1960) and stored at 4 °C.

Escherichia coli BL21 strain and plasmid pET28a were obtained from Novagen (Buenos Aires, Argentina). Transformants were grown at 37 °C in LB medium, with the addition of 50 µg/mL kanamycin. Agar plates were made of LB media, including 15 g/l agar.

4.2.3.2 Construction of the MLE Expression Vector

The malolactic enzyme gene was PCR amplified using genomic DNA from *O. oeni* strain PSU-1, extracted using the Wizard Genomic DNA purification kit (Promega). The 26 nt primers used for this amplification: 5'-GATATACCATGGGCAGCAGCATGACAGATCCAGTAAGTATTTTAAATGA-3 (forward) and 5′-CAGTGGTGGTGGTGGTGGTGGTATTTCGGCTCCCACC-3 (reverse), were designed based on the sequence of OEOE_RS07545 gene (1626 bp, NCBI). The linearized vector pET28a (5369 pb) was PCR amplified using the following 26 nt oligonucleotides: FWD 5′-ATACTTACTGGATCTGTCATGCTGCTGCCCATGG-3′; and 5′-TGAGGTGGGAGCCGAAATACCACCACCACCACCAC-3. Both pairs of primers were designed using SnapGene® software (Chicago, IL, USA), to be employed for Gibson Assembly.

All PCRs to amplify DNA fragments suitable for Gibson assembly were carried out in 35 PCR cycles, using Phusion High-Fidelity DNA polymerase (Thermo Scientific, Waltham, MA, USA), following the manufacturer's instructions. Gibson assembly was performed as previously described (Gibson et al., 2009) with pairs of primers for each fragment to be assembled containing segments of about ~40 bp homologous to the adjacent fragment to be linked. All PCR products were treated with

the DpnI enzyme to eliminate original vector residues and purified by gel extraction using the Qiaquick Gel Extraction kit from Qiagen, according to the manufacturer's instructions. The purified genes fragments and vectors were mixed based on their molar ratios in a final volume of 5 µL, containing 100 ng of total DNA. This DNA mix was added to 15 µL of 1.33X master mix (5X isothermal mix buffer, T5 exonuclease 1 U/µL, Phusion DNA polymerase 2 U/µL, Taq DNA ligase 40 U/µL and Milli-Q purified water), and the reaction mixture was incubated at 50 °C for 1 h. Finally, 10 µL reaction mix were used directly to transform chemically competent *E. coli* BL21 (DE3). The vector construct, designated pET28a-MLE, was verified by sequencing (Macrogen Inc., Seoul, Korea). The resulting map is shown in In Supplementary Material S2-2).

4.2.3.3 Expression and Purification of Recombinant Malolactic Enzyme of *O. oeni.*

E. coli BL21 (DE3) cells transformed with the pET28-MLE plasmid were grown at 37 °C and 140 rpm in 1 L shake flasks, containing 250 mL LB medium with 50 µL kanamycin. After 12 h incubation, MLE induction was performed by adding isopropyl β-D-1-thiogalactopyranoside (IPTG) to a final concentration of 0.5 mM. The cultures were incubated for another 12 h at 16 °C and 100 rpm. The resulting biomass was recovered from the fermentation broth by centrifugation (4000x g, 10 min, 4 °C) and the supernatant was discarded. Approximately 9 g of biomass were recovered from 1 L of fermentation broth. Subsequent cell disintegration was carried out in lysis buffer (Tris 20 mM pH 6.0, with 500 mM NaCl, 30 mM imidazole, and protease inhibitor cocktail complete™), at a concentration of 1 g of biomass in 10 mL of lysis buffer. The mix was distributed in 1.5 mL Eppendorf tubes with 250 µL of glass beads (Sigma-Aldrich®), and cell disruption was performed by agitation, three consecutive cycles of 30 s.

The crude extract was loaded onto immobilized metal affinity chromatography columns (HisTrap HP, 5 mL, Amersham Biosciences), operated with a peristaltic pump (with a flux 5 $mL \cdot m^{-1}$), and pre-equilibrated with binding buffer (HEPES 100 mM, KCl 100 mM, imidazol 20 mM, pH 6.0). The column was washed with 30 mL of binding buffer. The protein was eluted with 30 mL of stripping buffer (HEPES 100 mM, KCl 100 mM, imidazol 500 mM, pH 6.0), collecting fractions of 10 mL. The

active fractions were pooled, desalted, and lyophilized. For experimental purposes, the protein was resuspended in HEPES buffer (100 mM HEPES, 0.5 mM NAD^+, and 0.1 mM Mn^{2+}, pH 6.0).

4.2.4 Calorimetric Characterization

Enthalpy changes associated with MLE-substrate interactions were measured using a Nano ITC instrument (TA Instruments Ltd., Crawley, West Sussex, U.K.), at 25 °C. An amount of 170 μL of MLE solution (30 μM, HEPES buffer at desired pH) were placed in the sample cell of the calorimeter and buffered substrate solution (100 μM, HEPES buffer at desired pH) was loaded into the injection syringe. The substrates were titrated into the sample cell as a sequence of 20 injections of 2.5 μL aliquots. The time delay (to allow equilibration) between successive injections was 3 min. The contents of the sample cell were stirred throughout the experiment at 200 rpm to ensure thorough mixing. Raw data were obtained as a plot of heat (μJ) against injection number and featured a series of peaks for each injection. These raw data peaks were transformed using the instrument software Nano Analyze (version 3.11.0, TA Instruments, New Castle, DE, USA) to obtain a plot of observed enthalpy change per mole of injectant against molar ratio and were corrected by subtracting the mixing enthalpies of the substrate solutions into protein-free solution.

4.3 Results

4.3.1. Calorimetric Determination of Malic acid Binding Energies to Malolactic Enzyme

Malolactic fermentation in wine is usually carried out at a pH range between 3.2 and 3.5, allowing a small rise in pH as the malic acid is converted to lactic acid. Figure 4-2 illustrates the 2D-structure of L-malic acid (MAL) and its L-malate (−1) and (−2) protonation forms (MAL^- and MAL^{2-}, respectively). Isothermal calorimetry thermodynamic (ITC) data for malic acid interaction with MLE shows dissociation constant (K_d, Table 4-1) values in the micromolar range (Figure 4-3). MAL^{2-} has a

lower ΔG value than MAL^{1-}, suggesting this form as the most probable protonation state for malic acid at the binding site of MLE.

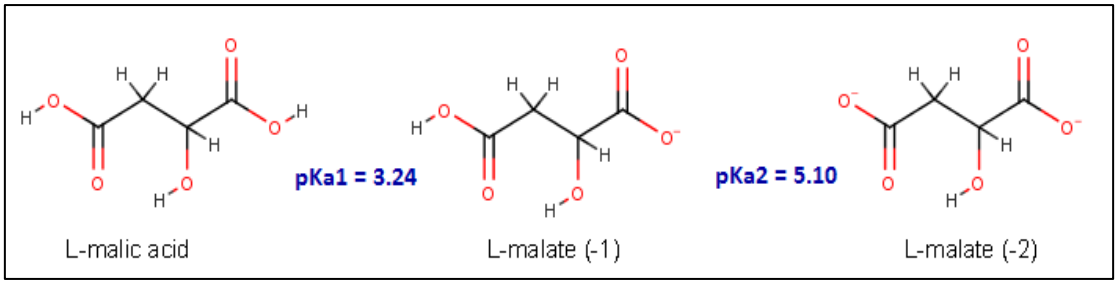

Figure 4-2: Chemical structure of L-malic acid and its protonation states.

Table 4-1: Binding energies (ΔG) of L-malate with malolactic enzyme using isothermal titration calorimetry.

Ligand	**Kd (M)**	**n**	**ΔG (kJ/mol)**	**Δ*H* (kJ/mol)**	***T*Δ*S* (kJ/mol)**
MAL^{-}	3.19×10^{-6}	2.7	−31.3	−30.0	1.3
MAL^{2-}	1.29×10^{-6}	1.5	−33.7	−14.5	19.2

Binding energies was calculated using an independent site interaction model. HEPES buffer (100 mM) was used to control pH and malic acid protonation form. Kd is dissociation constant, n correspond to non-integer stoichiometric values, Kd is the dissociation constant and ΔG is calculated as enthalpy (*ΔH*) minus *TΔS*.

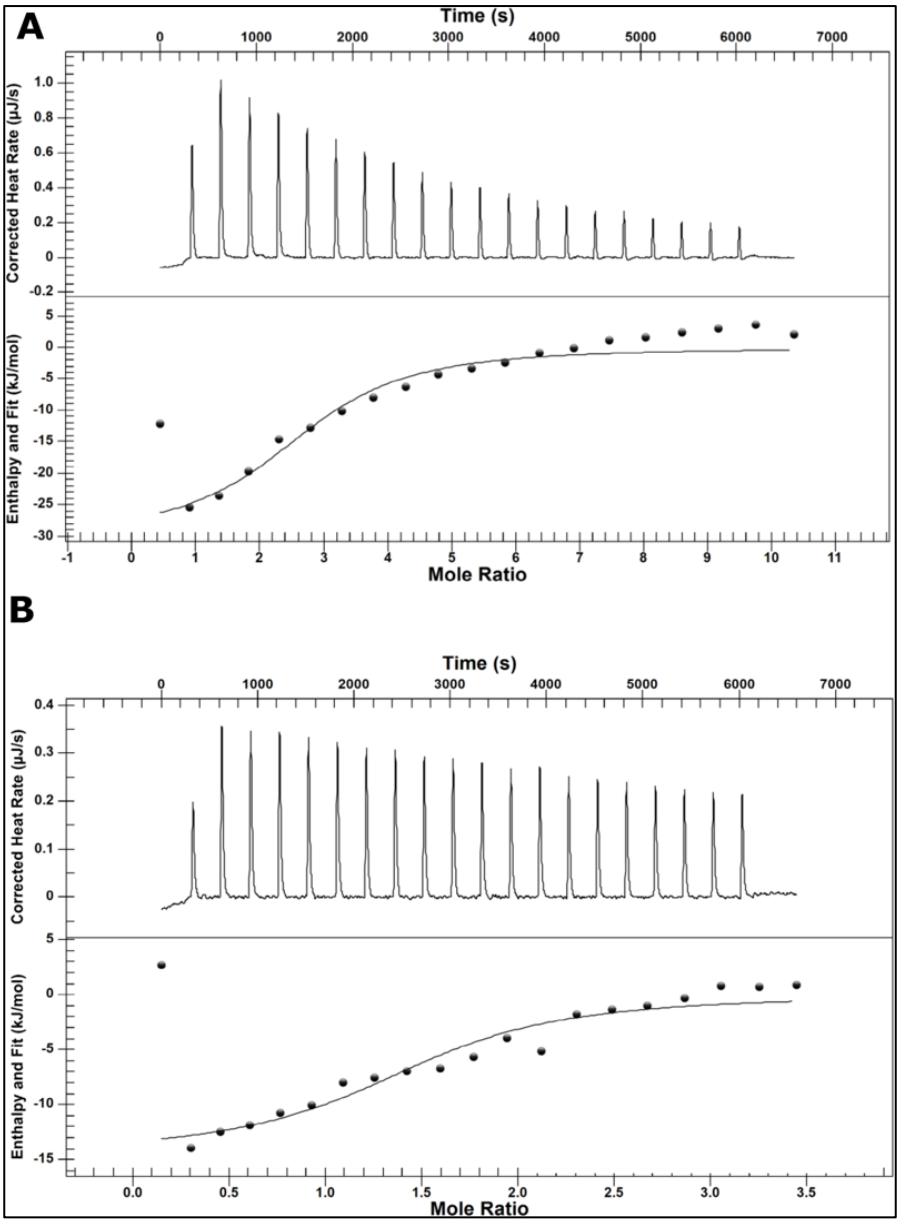

Figure 4-3: Binding isotherm curves of experimental calorimetric titrations of 0.3 mM L-malate (−2) (**A**) and (−1) (**B**) protonation states. Reaction was carried out by adding 30 mM malolactic enzyme to the reaction medium.

2.2. Sequence Similarity Networks of Malolactic Enzyme Family

To apprehend the impact of pH on *O. oeni* MLE activity, we performed an *in-silico* analysis by comparing its sequence with other MLF-related proteins, including malic enzyme and malate dehydrogenase. For this purpose, we generated a sequence similarity network (SSN), where nodes correspond to homologous proteins to MLE,

i.e., those containing at least 70% of sequence identity; and where connections allow to rapidly compute and visualize groups of proteins based on all-against-all sequence comparisons (Figure 4-4). The group that contains *O. oeni* MLE and its closest homologues from NCBI's non-redundant (nr) protein database are referenced as malate dehydrogenases, malic enzymes, and malolactic enzymes. Interestingly, most sequences of this group corresponding to malolactic enzymes and malic enzymes, therefore crystal structures of malic enzymes are the most adequate structural templates to model MLE as there is no structural data available for malolactic enzymes.

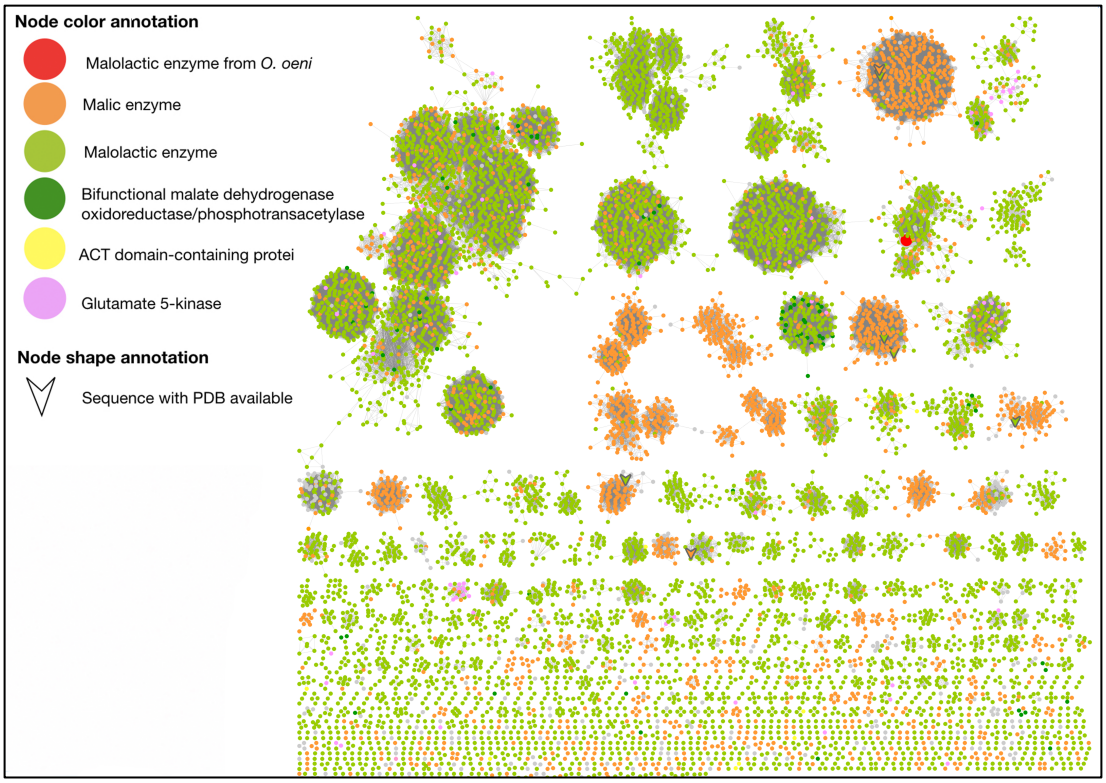

Figure 4-4: Sequence Similarity Network (SSN) of potential homologs to MLE of *O. oeni* with at least 70% identity of sequences. The nodes represent proteins and edges indicate similarity in amino acid sequence. Clustering by sequence identity is done with CD-HIT program. At values of sequence identity >70%, the nodes should contain sequences that share the same function; however, at lower values of sequence identity, the nodes may be functionally heterogeneous.

2.3. Phylogenetics of Malolactic Enzyme Family

Identification of a set of orthologs is a prerequisite for a robust genetic analysis of the evolution of a group of organisms (Koonin, 2005). We carried out multiple sequence alignment using CLUSTAL OMEGA to study the evolutionary relationships between different lactic bacteria in relation to the malolactic enzyme (Sievers et al., 2011). Most of the sequences homologous to the malolactic enzyme of *O. oeni*, correspond to proteins whose function has been assigned as malic enzymes by automatic annotation. However, some sequences have been experimentally reported as enzymes with malolactic activity. The latter were labelled with the abbreviation "MLE" below the name of the species, in the phylogenetic tree (Figure 4-5).

As illustrated in Figure 4-5, *O. oeni* is part of a monophyletic group, together with *Streptococcus spp, Lactococcus spp,* and *Enterococcus spp*. However, the evolution of the malic enzyme would be basal in *O. oeni* with respect to the rest of this clade. It is noteworthy that, within the clade representing the *Streptococcus* branch, the group of *Lactococcus* and *Enterococcus* are represented as sister groups of recent evolution. On the other hand, the branches of *Lactobacillus, Pediococcus,* and *Leuconostoc* constitute a paraphyletic group of basal character with respect to *Oenococcus* and *Streptococcus-Lactococcus-Enterococcus*; and they have a previous evolutionary origin.

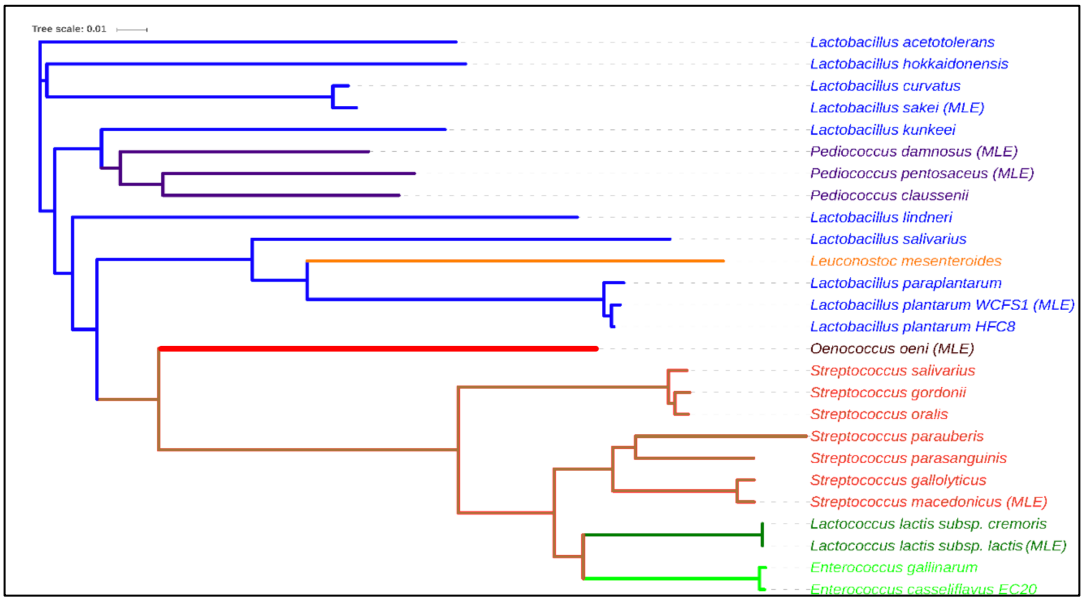

Figure 4-5: Phylogenetic tree of Lactobacillales constructed on the basis of multiple alignments of homologous sequences to *O. oeni* MLE, determined by Blastp. The multiple alignments and neighbor-joining tree were built using CLUSTAL OMEGA, and the visualization of the tree was done in iTOL.

2.4. Structural Modeling of the Malolactic Enzyme

The active site of the chain A of the malic enzyme from pigeon liver (PDB entry 1GQ2), the first malic enzyme described (Ochoa et al., 1947, 1948), was selected after SSN analysis as the best structural template for comparative modeling of MLE. The sequence alignment of both structures showed a sequence identity of 35.9% and a coverage of 98% against MLE (Figure 4-6).

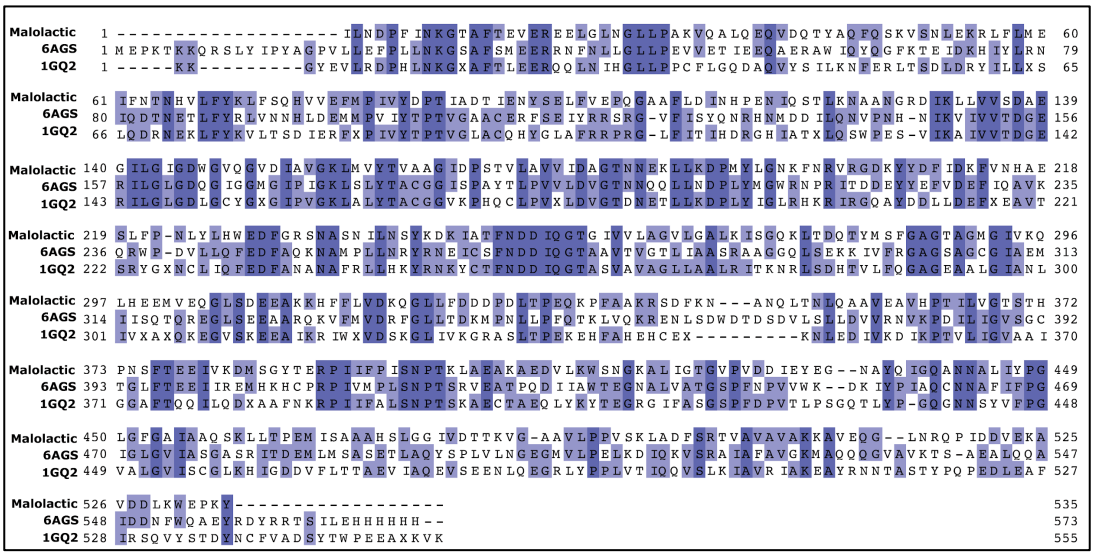

Figure 4-6: Sequence alignment of malolactic enzyme from *O. oeni*, malic enzyme from pigeon liver (PDB entry 1GQ2) and malic enzyme from *E. coli* (PDB entry 6AGS).

The crystal structure of the A chain contains an oxalate ion in the binding site and requires Mn^{2+} and $NADP^{+}$ as cofactors. Nevertheless, supported by the highly conserved structure of the active site in both proteins, we confirmed that the putative active binding site could correctly locate malate, after replacing the former cofactors with NAD^{+} and Mn^{2+}, and oxalate with malate, using SiteMap of Maestro suite (data not shown). It is worthy to mention that we also employed the malic enzyme from *E.*

coli (PDB entry 6AGS) (Figure 4-7) for these purposes; though only as secondary scaffold, because no experimental data is available for this protein crystal.

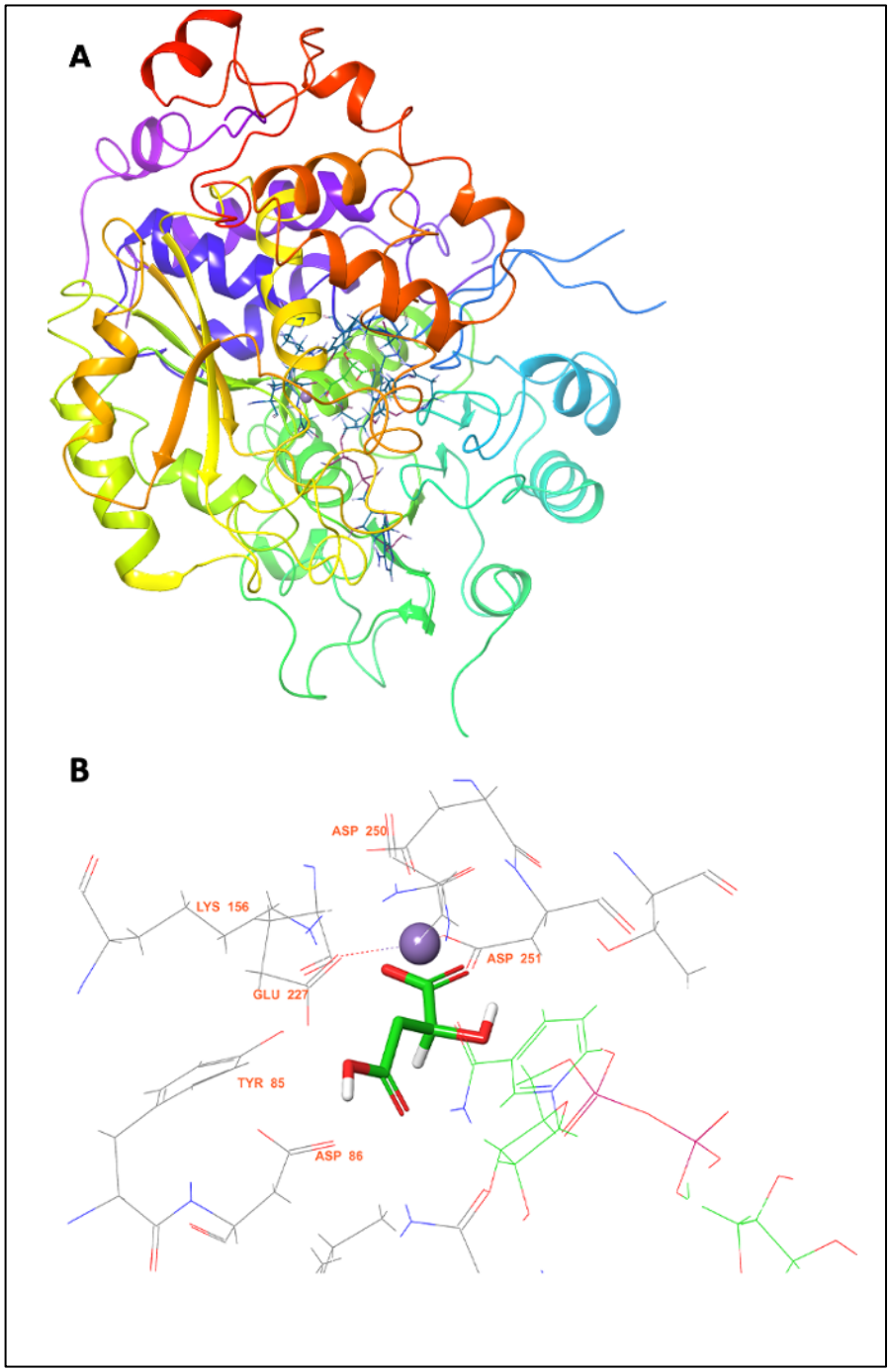

Figure 4-7: Homology model of *O. oeni* MLE. (**A**) Protein structure after 200 ns MD simulation. (**B**) MAL pose inside predicted MLE binding site.

Figure 4-7A shows the MLE homology model we obtained from the abovementioned templates and sequence alignments. This monomeric model was submitted to 200 ns simulation, reaching structural stability after 50 ns, by the structural rearrangement of the carboxyl-term (in Supplementary materials S4-1). Conversely, the pose of NAD^+ and Mn^{2+} reached stability after 20 ns, displaying an RMSD at or below 2 Å throughout simulation. Furthermore, putative MAL binding-site residues, based on previous reports, namely TYR85, ASP86, LYS156, ASP251, and ASP250 within MLE displayed movement of less than 2 Å (Figure 4-7 B). Then, MAL was oriented through molecular docking simulations (Figure 4-7 B).

2.5. Molecular Docking of Substrates of Malolactic Enzyme

Additionally, we evaluated the participation of the divalent cation on MLE mechanism by quantum polarized ligand docking (QPLD). Figure 4-8 illustrates the pose adopted by MAL inside the binding site of MLE. Malic acid interacts with MLE through coordination bonds with Mn^{2+}, one LYS protonated residue, and several ASP residues interacting through hydrogen bonds. MAL-MLE interacting residues on this pose correspond with equivalent residues proposed for divalent-cation-dependent MAL decarboxylation.

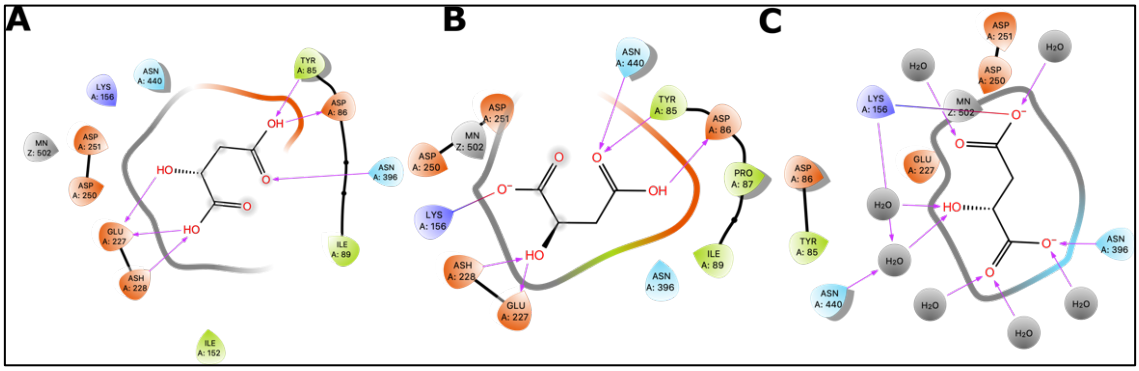

Figure 4-8: (A) L-Malic Acid and (B) L-Malate −1 and (C) L-Malate −2 pose into the MLE binding site predicted by the QLPD method.

We also calculated the most probable protonation state of MAL using the Epik module of the Schrödinger Suite. Results confirmed that MAL^{2-} is the most probable protonation state and thus interacting residues could be oriented differently to MAL^{-} and MAL.

Quantum polarized ligand docking (QPLD) was then employed to explore MAL^{2-} pose and binding energy ($\Delta G_{binding}$). Results showed that all malic acid protonation forms lie in the same binding cavity, sharing the same set of binding amino acid residues (Figure 4-8). The latter interact mainly by hydrogen bonding and hydrophobic interactions (in Supplementary material S4-2). MAL^{2-} has the lowest $\Delta G_{binding}$, followed by MAL^{-} and MAL, with values of −23.8, −19.6, and −14.6 kJ/mol, respectively (Table 4-2). Interestingly, MAL^{2-} displayed an extended conformation, when compared with the other protonation states. This open conformation better satisfies the geometrical requirements of Mn^{2+} coordination geometry and the mechanism described for malic enzymes (Soffritti et al., 2006).

Geometrical stability of MAL inside the binding site was assessed after 200 ns molecular dynamics simulations of the MLE/MAL/NAD^{+}/Mn^{2+} system. Of note, MAL does not remain on the site and exits the pocket at 25 ns. On the contrary, MAL^{-} and MAL^{2-} remain into the binding pocket throughout the whole simulation. Moreover, the average binding energy of the molecular interactions through the MM/GBSA rescoring method was calculated as it is relatively more accurate compared to single-structure theoretical determinations. MM-GBSA binding energies for MAL^{-} and MAL^{2-} showed binding affinity differences consistent with values from the ITC and QLPD experiments (Tables 4-1 and 4-2, respectively). Furthermore, energy decomposition of MAL^{-} and MAL^{2-} interactions within the MLE binding pocket allowed to identify that binding is mainly driven by the negative charge interactions of the MAL carboxyl group with the positive charge of the side chain-N of LYS156, (Figure 4-7); whereas MAL^{1-} interacts with ASP86 and ASN396 mainly by H-bonding; and MAL^{2-} with TYR85, ASP86, ASP228, ASN396, and ASN440 mainly through water bridges.

Table 4-2: MAL– and MAL2– interactions with malic enzyme through 200 ns simulations.

MAL^-	MAL^{2-}
QPLD $\Delta G_{binding}$ −19.6 kJ/mol	QPLD $\Delta G_{binding}$ −23.8 kJ/mol
MM/GBSA $\Delta G_{binding}$ −154.8 kJ/mol	MM/GBSA $\Delta G_{binding}$ −175.7 kJ/mol
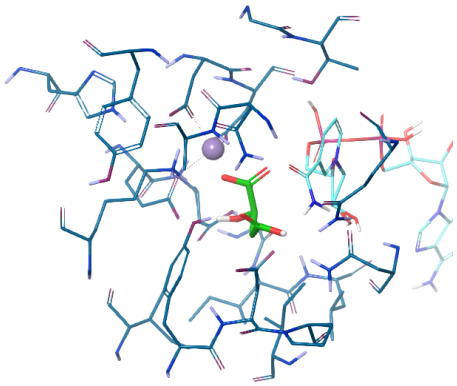	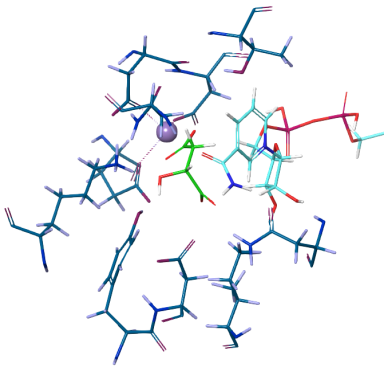
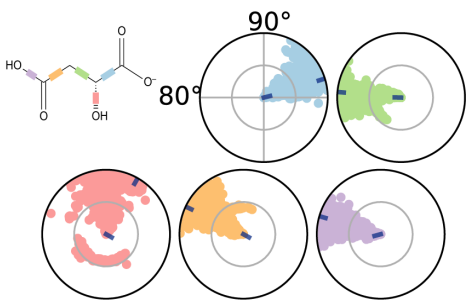	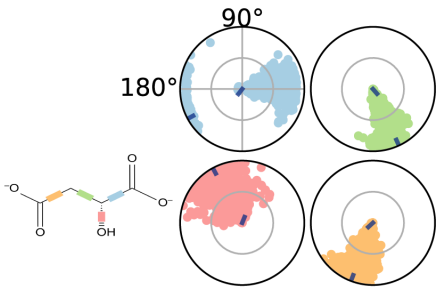
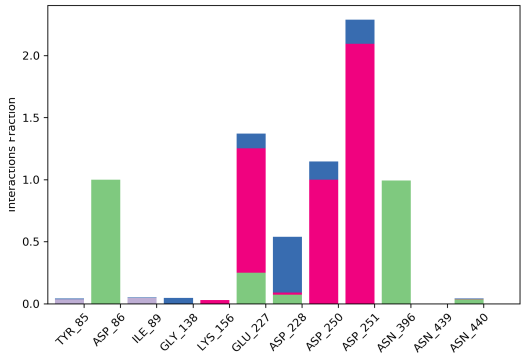	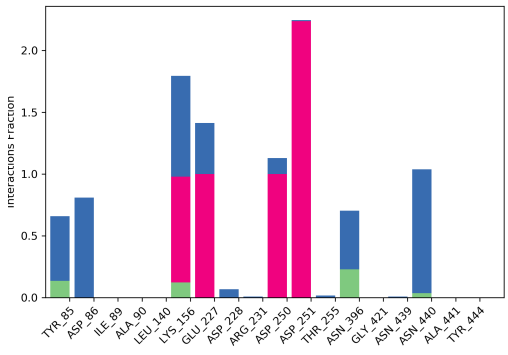

First row depicts MAL^- and MAL^{2-} representative conformations. Second row describes the conformation of the torsion throughout the course of the simulation. The beginning of the simulation is in the center of the radial plot and the time evolution is plotted radially outwards. Third row describes the kind of interactions both of MAL^{1-} and MAL^{2-} with amino acids of binding pocket, stacked bar charts are normalized over the course of the trajectory. Green represents H-bond, purple hydrophobic contacts,

magenta ionic contacts and blue water bridges. Only the last 150 ns were used for calculations.

4.4 Discussion

In silico analysis, MLE homology model together with QPLD and ITC experiments were carried out in the present study to determine the protonation state of L-malate required for its efficient decarboxylation to L-lactate by the malolactic enzyme of *Oenococcus oeni*.

The phylogenetic analysis showed that the evolution of the *O. oeni* malolactic enzyme is halfway between malic-malolactic enzymes of the genera Lactobacillus-*Pediococcus-Leuconostoc* and *Streptococcus-Lactococcus-Enterococcus*. The grouping of lactic acid bacteria in two clusters was in line with Makarova and Koonin (2007), which employed the sequence of ribosomal proteins and RNA polymerase subunits for their phylogenetic analysis. Our results indicated that *O. oeni MLE* is part of a monophyletic group, together with the branch *Streptococcus-Lactococcus-Enterococcus,* whereas *O. Oeni MLE* constitutes a paraphyletic group of the *Lactobacillus-Pediococcus* branch. These results point that the genera *Streptococcus, Lactococcus, Enterococcus,* and *Oenococcus* descended from a common evolutionary ancestor, whose malolactic enzyme could share similar structural characteristics.

Malolactic fermentation usually occurs at pH levels between the range of 3.2 and 3.5, allowing for a rise in pH as the malic acid is converted to lactic acid. At this pH, the MAL^- protonated L-malic acid form prevails (Figure 4-2). On the other hand, several LAB, including *O. oeni* have an intracellular pH ≈ 5.0 (Hutkins & Nannen, 1993; Salema et al., 1994), a condition where MAL^{2-} is the predominant protonated form. Several studies have reported that the malolactic fermentation reaction occurs in the *Oenococcus oeni* intracellular space, where pH is between 5.8 and 6.1; while in the extracellular medium, *i.e.*, the wine conditions, the pH is within a range of 3 to 4 (Augagneur et al., 2007; Salema et al., 1996). Additionally, Schümann et al. (2013) reported that *O. oeni* MLE has an optimum activity at pH 6.0 and 45 °C. Accordingly, we evaluated the effect of pH on L-malic acid interaction with the MLE active site. To this end, we measured the enthalpy of reaction of *O. oeni* MLE with both cofactors,

titrated with MAL at pH 4.5 and 5.3, using ITC. Our results showed a higher binding affinity for MAL^{2-} than for MAL^{-}, in agreement with Schümann et al. (2013). Under the *O. oeni* intracellular conditions, the presence of some residues, in the binding pocket or in its vicinity, could accept the proton from the MAL^{-} form, predominant in solution, to lead the most stable MAL^{2-}, such as Asp86 and Glu227 (see Figure 4-8 A). Although ITC experiments showed that pH significantly influences malic acid binding to *O. oeni* MLE, this method did not allow to extract structural information of the binding sites or enzymatic mechanisms, at atomic level. However, non-integer stoichiometric values indicated the formation or aggregation of dimers of higher quaternary structures, which was also observed by Dynamic Light Scattering measurements (data not shown). These results agree with the work of Schümann et al. (2012), where MLE of *O. oeni* was presented as a dimeric macromolecule, with each subunit having a functional binding site.

To give further structural insights and to understand the calorimetric results, we relied on the use of molecular docking and molecular dynamics methods. To this end, *O. oeni* MLE homology model was carried out, because the three-dimensional structure was not available. It is worth noting that SSN and phylogenetic analysis showed a close relation between malolactic and malic enzymes (Figure 4-4), although only four crystal structures are available as possible structural templates. Among these structures, malic enzyme from pigeon liver (PDB entry 1GQ2) and *E. coli* Malic enzyme (PDB entry 6AGS) were used as model templates, using the alignment shown in Figure 4-6. Both structures were identified as the closest related sequences according to the SSN; nevertheless, experimental data regarding 6AGS crystal is scarce, and was only used when no structural data from 1GQ2 were available. It is worth noting that NAD^{+}, Mn^{2+} were incorporated as model constraints, using the pose of cofactors found on the 1GQ2 crystal. The MLE model was submitted to 200 ns molecular dynamics simulations to further explore its dynamic and stability and to identify relevant residues for malic acid binding. The trajectory analysis showed that, overall, residues near cofactors have slow mobility and form cavities that are suitable to bind L-malic acid.

Interestingly, SSN and phylogenetic analysis suggest a closed relation between malate dehydrogenases, malic enzymes, and malolactic enzymes; however, their binding sites are not completely conserved and thus, substrate pose, and binding residues could be oriented differently. To correctly orientate malic acid and to calculate theoretical binding energies considering Mn^{2+}, we opted for the quantum polarized ligand docking (QPLD) method as it allows to properly calculate binding energies of metal-containing systems as it considers metal coordination, electronic polarization effect, among other missed terms in molecular-mechanics force fields. As can be seen in Table 4-2, QPLD results shown that MAL^- and MAL^{2-} have docking scores ($\Delta G_{binding}$) that correlate with ITC measurement results. Although both MAL protonation states bind into the same cavity and share a set of amino acids, MAL^{2-} adopts an extended conformation, supported by hydrogen bonding and coordination geometry with Mn^{2+} (Figure 4-7). Further, we explore the binding site dynamics of the MAL, MAL^-, and MAL^{2-} containing systems through molecular dynamics simulation. Of note, MAL^{2-} kept its orientation, as determined by the QLPD method, after 200 ns of molecular dynamics simulation, while MAL^- and MAL have more mobility inside the binding site. Furthermore, molecular dynamics provides a conformational ensemble that allows to calculate the average binding energy of the molecular interactions through the MM/GBSA rescoring method that is more accurate compared to single-structure theoretical determinations as it includes solvent effects. According to MM/GBSA results and ITC experiments, MAL^{2-} have the lowest binding energy ($\Delta G_{binding}$) and the major energetic contribution is the stabilization of the two carboxylic group charges that interacts with Mn^{2+}. Regarding ITC correlation with our molecular dynamics results, it should be noted that docking and MMGBSA calculations represent one of the steps of the reaction coordinates, that is pre-transition states without consider the diffusion pathways into the binding sites and omitting desolvation and other effects that directly impact the entropy variations observed by ITC measurements. This MAL^{2-} pose is in accordance with the mechanism described by Schümann et al. (2013), where Mn^{2+} act as an activator of the enzymatic catalysis and coordinate chemical reaction, while NAD^+ act as oxidizing agent for oxidation of L-malate.

4.5 Conclusion

In this work, we constructed a comparative model for MLE using the 3D structures of the malic enzyme from pigeon liver (PDB entry 1GQ2) and malic enzyme from *E. coli* (PDB entry 6AGS). Malic acid interactions within MLE binding pocket are mainly driven by hydrogen bonding and coordination with Mn^{2+}, both dependent on the protonation state of the substrate. Our experimental and theoretical studies demonstrated that MAL^{2-} stabilizes the pose that fulfills the geometrical requirements to favor the malic acid decarboxylation catalyzed by MLE. Further theoretical and experimental studies are currently underway to provide more detailed information about the contribution of each residue on the MLE proposed mechanism.

5. CONCLUSIONS AND FUTURE PERSPECTIVES

Both the results and knowledge obtained from this thesis allow to better understand the metabolism of *Oenococcus oeni* during the Malolactic Fermentation (MLF). They contribute to unveil the unpredictable, even capricious, development this crucial fermentative process usually has had in wineries. Then, maybe this lactic bacterium could be less a nightmare, still the queen of cellars, paraphrasing Grandvalet (2017).

First and foremost, we built the first Genome-Scale Metabolic Model (GSMM) for *O. oeni*, using the genome of PSU-1 strain, the only one completely sequenced when this research was started. This model, iSM454, was carefully curated in its biochemistry, reaching high standards of accuracy in predicting bacterial growth. Key metabolic pathways were included in the curation process, such as the synthesis of exopolysaccharides, participating in the response of the bacterium to stress conditions, as those that it finds in wine. We also focused on the synthesis of cyclopropane fatty acids, and on the pathways of aminoacids synthesis; it allowed us to determine which ones were essential for *O. oeni* survival.

On the energetic side, the model enabled us to define different proton extrusion/energy generation pathways employed by *O. oeni,* like the transformation of malic into lactic acid using the malolactic enzyme (MLE), the transportation of lactic acid through the plasmatic membrane, and the metabolism of citrate, all of them ATP-synthase related mechanisms, allowing more ATP to be synthesized. The m-ATP was also calculated, a key parameter for understanding the heightened energetic requirements cells need to colonize extreme ecological niches. Therefore, our work is the first reporting the ATP required for the maintenance of *O. oeni* growing in ethanol rich media, making the model a relevant tool for winemakers and researchers in that field. In such conditions, the model is able to predict the production of mannitol, erythritol, acetate, diacetyl, and acetoin, among other compounds that could have significant organoleptic impact on wine.

Nevertheless, iSM454 does not incorporate information about *O. oeni*'s transcriptomic and proteomic responses under different environmental conditions.

Indeed, it does embed limitations and diminish accuracy. Also, iSM454 uses a flux balance analysis based on the election of a single metabolic state in time; a dynamic flux balance analysis (dFBA) could be a more useful strategy to simulate the growth kinetics under industrial conditions. Finally, being a model built for a single isolated microorganism, it does not allow to represent the interactions that actually happen in the complex wine microbiome. A more extended platform development emerges as a necessity for the next steps in understanding the metabolic exchanges between different microorganisms.

Secondly, we developed a wine-like, defined culture medium (MaxOeno), and we characterized the kinetic parameters of *O. oeni* growing under increasing ethanol conditions. We found that under this stress conditions, *O. oeni* favors anabolic reactions allowing to reconstruct itself and to produce stress protecting factors. The requirements of $NAD(P)^+$, NGAM and ATP also augment, without any relation to biomass increase. The model allowed the integration of specific consumption/production rates during the different growth phases of *O. oeni*, reflecting the phenotypic changes it undergoes along them, for example, the change in the principal pathways to produce ATP under raising ethanol conditions. The simulations led us to detect the accumulation of compounds like mannitol, related to cofactors regeneration. On this matter, future research could address the effect of other stress factors as the medium acidity and SO_2 content in wine, both strongly conditioning the growth of *O. oeni*. These variables in the medium were not addressed in this work. Altogether, these approaches could help to define new nutritional formulations for reinforcing *O. oeni* tolerance to ethanol, pH or SO_2, fostering a more efficient consumption of malic acid.

Thirdly, we addressed the undetermined mechanism of MLF reaction. A comparative model of MLE was built using 3D structures of malic enzymes from pigeon liver and *E. coli*. The main interactions between malic acid and the enzyme binding pocket were found to correspond mainly to hydrogen bonds and coordination with Mn^{2+}. For these interactions, we proved that the protonation state MAL^{2-} was fundamental to stabilize the conformation that satisfies the geometric requirements, allowing the decarboxylating activity that catalyzes the MLE. This is consistent with

the pH conditions of *O. oeni*'s intracellular space (5.8 to 6.1), where malate decarboxylation takes place. The contribution of each residue of the binding pocket to the MLE reaction mechanism itself was not determined however, and it remains to be studied.

Future applications of this work include characterizing different strains of *O. oeni* from different geographical areas, which could be particularly interesting for understanding the relations between wine and its "terroir", finding possible answers to relevant aspects of wine production as safety, tolerance to harmful conditions, and organoleptic variability. In this way, the characterization of native and commercial strains, could provide enologists advanced tools for prediction, control of the final product, and differentiation. In the same vein, characterizing strains in regard to their production of some desired or undesired metabolites, e.g., biogenic amines, could be highly valuable for the industry. Our model revealed that PSU-1 strain does not have the ability to produce biogenic amines, but it is known that other *O. oeni* strains does.

6. REFERENCES

Aceituno, F. F., Orellana, M., Torres, J., Mendoza, S., Slater, A. W., Melo, F., & Agosin, E. (2012). Oxygen response of the wine yeast Saccharomyces cerevisiae EC1118 grown under Carbon-Sufficient, nitrogen-limited enological conditions. *Applied and Environmental Microbiology*, *78*(23), 8340–8352. https://doi.org/10.1128/AEM.02305-12

Agren, R., Mardinoglu, A., Asplund, A., Kampf, C., Uhlen, M., & Nielsen, J. (2014). Identification of anticancer drugs for hepatocellular carcinoma through personalized genome-scale metabolic modeling. *Molecular Systems Biology*, *10*(3), 1–13. https://doi.org/10.1002/msb.145122

Ahmad, A., Hartman, H. B., Krishnakumar, S., Fell, D. A., Poolman, M. G., & Srivastava, S. (2017). A Genome Scale Model of Geobacillus thermoglucosidasius (C56-YS93) reveals its biotechnological potential on rice straw hydrolysate. *Journal of Biotechnology*, *251*(December 2016), 30–37. https://doi.org/10.1016/j.jbiotec.2017.03.031

Akin, H., Brandam, C., Meyer, X. M., & Strehaiano, P. (2008). A model for pH determination during alcoholic fermentation of a grape must by Saccharomyces cerevisiae. *Chemical Engineering and Processing: Process Intensification*, *47*(11), 1986–1993. https://doi.org/10.1016/j.cep.2007.11.014

Alegría, E. G., López, I., Ruiz, J. I., Sáenz, J., Fernández, E., Zarazaga, M., Dizy, M., Torres, C., & Ruiz-Larrea, F. (2004). High tolerance of wild Lactobacillus plantarum and Oenococcus oeni strains to lyophilisation and stress environmental conditions of acid pH and ethanol. *FEMS Microbiology Letters*, *230*(1), 53–61. https://doi.org/10.1016/S0378-1097(03)00854-1

Angione, C. (2018). Integrating splice-isoform expression into genome-scale models characterizes breast cancer metabolism. *Bioinformatics*, *34*(3), 494–501. https://doi.org/10.1093/bioinformatics/btx562

Ansanay, V., Dequin, S., Blondin, B., & Barre, P. (1993). Cloning, sequence and expression of the gene encoding the malolactic enzyme from Lactococcus lactis. *FEBS Letters*, *332*(1–2), 74–80. https://doi.org/10.1016/0014-5793(93)80488-G

Ansanay, V., Dequin, S., Camarasa, C., Schaeffer, V., Grivet, J. P., Blondin, B., Salmon, J. M., & Barre, P. (1996). Malolactic fermentation by engineered Saccharomyces cerevisiae as compared with engineered Schizosaccharomyces pombe. *Yeast*, *12*(3), 215–225. https://doi.org/10.1002/(SICI)1097-0061(19960315)12:3<215::AID-YEA903>3.0.CO;2-M

Arena, M. E., & Manca De Nadra, M. C. (2005). Influence of ethanol and low pH on arginine and citrulline metabolism in lactic acid bacteria from wine. *Research in Microbiology*, *156*(8), 858–864. https://doi.org/10.1016/j.resmic.2005.03.010

Augagneur, Y., Ritt, J.-F., Linares, D. M., Remize, F., Tourdot-Maréchal, R., Garmyn, D., & Guzzo, J. (2007). Dual effect of organic acids as a function of

external pH in Oenococcus oeni. *Archives of Microbiology*, *188*(2), 147–157. https://doi.org/10.1007/s00203-007-0230-0

Aung, H. W., Henry, S. A., & Walker, L. P. (2013). Revising the Representation of Fatty Acid, Glycerolipid, and Glycerophospholipid Metabolism in the Consensus Model of Yeast Metabolism. *Industrial Biotechnology*, *9*(4), 215–228. https://doi.org/10.1089/ind.2013.0013

Badotti, F., Moreira, A. P. B., Tonon, L. A. C., de Lucena, B. T. L., de Gomes, F. C. O., Kruger, R., Thompson, C. C., de Morais, M. A., Rosa, C. A., & Thompson, F. L. (2014). Oenococcus alcoholitolerans sp. nov., a lactic acid bacteria isolated from cachaça and ethanol fermentation processes. *Antonie van Leeuwenhoek, International Journal of General and Molecular Microbiology*, *106*(6), 1259–1267. https://doi.org/10.1007/s10482-014-0296-z

Banks, J. L., Beard, H. S., Cao, Y., Cho, A. E., Damm, W., Farid, R., Felts, A. K., Halgren, T. A., Mainz, D. T., Maple, J. R., Murphy, R., Philipp, D. M., Repasky, M. P., Zhang, L. Y., Berne, B. J., Friesner, R. A., Gallicchio, E., & Levy, R. M. (2005). Integrated Modeling Program, Applied Chemical Theory (IMPACT). *Journal of Computational Chemistry*, *26*(16), 1752–1780. https://doi.org/10.1002/jcc.20292

Bartowsky, E. J. (2005). Oenococcus oeni and malolactic fermentation–moving into the molecular arena. *Australian Journal of Grape and Wine Research*, *11*, 174–187. https://doi.org/10.1111/j.1755-0238.2005.tb00286.x

Bartowsky, E. J. (2017). Oenococcus oeni and the genomic era. *FEMS Microbiology Reviews*, *41*(Supp_1), S84–S94. https://doi.org/10.1093/femsre/fux034

Bartowsky, E. J., & Borneman, A. R. (2011). Genomic variations of Oenococcus oeni strains and the potential to impact on malolactic fermentation and aroma compounds in wine. *Applied Microbiology and Biotechnology*, *92*(3), 441–447. https://doi.org/10.1007/s00253-011-3546-2

Bartowsky, E. J., Costello, P. J., & Chambers, P. J. (2015). Emerging trends in the application of malolactic fermentation. *Australian Journal of Grape and Wine Research*, *21*(Supplement 1), 663–669. https://doi.org/10.1111/ajgw.12185

Bartowsky, E. J., Francis, I. L., Bellon, J. R., & Henschke, P. A. (2002). Is buttery aroma perception in wines predictable from the diacetyl concentration? *Australian Journal of Grape and Wine Research*, *8*(3), 180–185. https://doi.org/10.1111/j.1755-0238.2002.tb00254.x

Bartowsky, E. J., & Henschke, P. A. (2004). The “buttery” attribute of wine--diacetyl--desirability, spoilage and beyond. *International Journal of Food Microbiology*, *96*(3), 235–252. https://doi.org/10.1016/j.ijfoodmicro.2004.05.013

Battermann, G., & Radler, F. (1991). A comparative study of malolactic enzyme and malic enzyme of different lactic acid bacteria. *Canadian Journal of Microbiology*, *37*(3), 211–217. https://doi.org/10.1139/m91-032

Bauer, R., & Dicks, L. (2004). Control of malolactic fermentation in wine. A review. *South African Journal of Enology and Viticulture*, *25*(2), 74–88. http://sasev.org.za/journal-sajev/sajev-articles/volume-25-2/Vol 25 (2) Paper 6.pdf

Beelman, R. B., Gavin, A., & Keen, R. M. (1977). A new strain of Leuconostoc oenos for induced malo-lactic fermentation in eastern wines. *American Journal of Enology and Viticulture*, *28*(3), 159–165.

Benito, Á., Calderón, F., Palomero, F., & Benito, S. (2015). Combine use of selected Schizosaccharomyces pombe and Lachancea thermotolerans yeast strains as an alternative to the traditional malolactic fermentation in red wine production. *Molecules*, *20*(6), 9510–9523.

Berbegal, C., Garofalo, C., Russo, P., Pati, S., Capozzi, V., & Spano, G. (2017). Use of Autochthonous Yeasts and Bacteria in Order to Control Brettanomyces bruxellensis in Wine. *Fermentation*, *3*(4), 65. https://doi.org/10.3390/fermentation3040065

Betteridge, A. L., Grbin, P., & Jiranek, V. (2015). Improving Oenococcus oeni to overcome challenges of wine malolactic fermentation. *Trends in Biotechnology*, *33*(9), 547–553. https://doi.org/10.1016/j.tibtech.2015.06.008

Betteridge, A. L., Sumby, K. M., Sundstrom, J. F., Grbin, P. R., & Jiranek, V. (2018). Application of directed evolution to develop ethanol tolerant Oenococcus oeni for more efficient malolactic fermentation. *Applied Microbiology and Biotechnology*, *102*(2), 921–932. https://doi.org/10.1007/s00253-017-8593-x

Bisson, L. F., & Walker, G. A. (2015). The microbial dynamics of wine fermentation. In W. Holzapfel (Ed.), *Advances in Fermented Foods and Beverages* (pp. 435–476). Elsevier. https://doi.org/10.1016/B978-1-78242-015-6.00017-7

Björkroth, J., & Holzapfel, W. (2006). Genera Leuconostoc, Oenococcus and Weissella. In M. Dworkin, S. Falkow, E. Rosenberg, K.-H. Schleifer, & E. Stackebrandt (Eds.), *The Prokaryotes: Volume 4: Bacteria: Firmicutes, Cyanobacteria* (pp. 267–319). Springer US. https://doi.org/10.1007/0-387-30744-3_9

Bleve, G., Tufariello, M., Vetrano, C., Mita, G., & Grieco, F. (2016). Simultaneous alcoholic and malolactic fermentations by Saccharomyces cerevisiae and Oenococcus oeni cells co-immobilized in alginate beads. *Frontiers in Microbiology*, *7*(JUN). https://doi.org/10.3389/fmicb.2016.00943

Bochevarov, A. D., Harder, E., Hughes, T. F., Greenwood, J. R., Braden, D. A., Philipp, D. M., Rinaldo, D., Halls, M. D., Zhang, J., & Friesner, R. A. (2013). Jaguar: A high-performance quantum chemistry software program with strengths in life and materials sciences. *International Journal of Quantum Chemistry*, *113*(18), 2110–2142. https://doi.org/10.1002/qua.24481

Bokulich, N. A., Ohta, M., Richardson, P. M., & Mills, D. A. (2013). Monitoring Seasonal Changes in Winery-Resident Microbiota. *PLoS ONE*, *8*(6).

https://doi.org/10.1371/journal.pone.0066437

Bon, E., Delaherche, A., Bilhère, E., De Daruvar, A., Lonvaud-Funel, A., & Le Marrec, C. (2009). Oenococcus oeni genome plasticity is associated with fitness. *Applied and Environmental Microbiology*, *75*(7), 2079–2090. https://doi.org/10.1128/AEM.02194-08

Bony, M., Bidart, F., Camarasa, C., Ansanay, V., Dulau, L., Barre, P., & Dequin, S. (1997). Metabolic analysis of S. cerevisiae strains engineered for malolactic fermentation. *FEBS Letters*, *410*(2–3), 452–456. https://doi.org/10.1016/S0014-5793(97)00637-6

Bordas, M., Araque, I., Bordons, A., & Reguant, C. (2015). Differential expression of selected Oenococcus oeni genes for adaptation in wine-like media and red wine. *Annals of Microbiology*, *65*(4), 2277–2285. https://doi.org/10.1007/s13213-015-1069-2

Bordbar, A., Monk, J. M., King, Z. A., & Palsson, B. O. (2014). Constraint-based models predict metabolic and associated cellular functions. *Nature Reviews Genetics*, *15*, 107. https://doi.org/10.1038/nrg3643

Borneman, A. R., McCarthy, J. M., Chambers, P. J., & Bartowsky, E. J. (2012). Comparative analysis of the Oenococcus oeni pan genome reveals genetic diversity in industrially-relevant pathways. *BMC Genomics*, *13*(1), 373. https://doi.org/10.1186/1471-2164-13-373

Boulton, R. B., Singleton, V. L., Bisson, L. F., & Kunkee, R. E. (1996). *Principles and Practices of Winemaking*. https://doi.org/10.1007/978-1-4615-1781-8

Bourdineaud, J. P., Nehmé, B., Tesse, S., & Lonvaud-Funel, A. (2003). The ftsH gene of the wine bacterium Oenococcus oeni is involved in protection against environmental stress. *Applied and Environmental Microbiology*, *69*(5), 2512–2520. https://doi.org/10.1128/AEM.69.5.2512-2520.2003

Brandam, C., Fahimi, N., & Taillandier, P. (2016). Mixed cultures of Oenococcus oeni strains: A mathematical model to test interaction on malolactic fermentation in winemaking. *LWT - Food Science and Technology*, *69*, 211–216. https://doi.org/10.1016/j.lwt.2016.01.045

Bravo-Ferrada, B. M., Hollmann, A., Brizuela, N., La Hens, D. V., Tymczyszyn, E., & Semorile, L. (2016). Growth and consumption of l-malic acid in wine-like medium by acclimated and non-acclimated cultures of Patagonian Oenococcus oeni strains. *Folia Microbiologica*, *61*(5), 365–373. https://doi.org/10.1007/s12223-016-0446-y

Bravo-Ferrada, B. M., Hollmann, A., Delfederico, L., Valdés La Hens, D., Caballero, A., & Semorile, L. (2013). Patagonian red wines: selection of Lactobacillus plantarum isolates as potential starter cultures for malolactic fermentation. *World Journal of Microbiology & Biotechnology*, *29*(9), 1537–1549. https://doi.org/10.1007/s11274-013-1337-x

Bridier, J., Claisse, O., Coton, M., Coton, E., & Lonvaud-Funel, A. (2010). Evidence of distinct populations and specific subpopulations within the species Oenococcus oeni. *Applied and Environmental Microbiology*, *76*(23), 7754–7764. https://doi.org/10.1128/AEM.01544-10

Brizuela, N. S., Bravo-Ferrada, B. M., Curilén, Y., Delfederico, L., Caballero, A., Semorile, L. C., Pozo-Bayon, M. A., & Tymczyszyn, E. E. (2018). Advantages of Using Blend Cultures of Native L. plantarum and O. oeni Strains to Induce Malolactic Fermentation of Patagonian Malbec Wine. *Frontiers in Microbiology*, *9*, 2109.

Brizuela, N. S., Tymczyszyn, E. E., Semorile, L. C., La Hens, D. V., Delfederico, L., Hollmann, A., & Bravo-Ferrada, B. (2018). Lactobacillus plantarum as a malolactic starter culture in winemaking: A new (old) player? *Electronic Journal of Biotechnology*, 1–9. https://doi.org/10.1016/j.ejbt.2018.12.002

Cabras, P., Angioni, A., Garau, V. L., Pirisi, F. M., Farris, G. A., Madau, G., & Emonti, G. (1999). Pesticides in fermentative processes of wine. *Journal of Agricultural and Food Chemistry*, *47*(9), 3854–3857. https://doi.org/10.1021/jf990005j

Cafaro, C., Bonomo, M. G., & Salzano, G. (2014). Adaptive changes in geranylgeranyl pyrophosphate synthase gene expression level under ethanol stress conditions in Oenococcus oeni. *Journal of Applied Microbiology*, *116*(1), 71–80. https://doi.org/10.1111/jam.12351

Campbell-Sills, H., El Khoury, M., Favier, M., Romano, A., Biasioli, F., Spano, G., Sherman, D. J., Bouchez, O., Coton, E., Coton, M., Okada, S., Tanaka, N., Dols-Lafargue, M., & Lucas, P. M. (2015). Phylogenomic Analysis of Oenococcus oeni Reveals Specific Domestication of Strains to Cider and Wines. *Genome Biology and Evolution*, *7*(6), 1506–1518. https://doi.org/10.1093/gbe/evv084

Campbell-Sills, H., El Khoury, M., Gammacurta, M., Miot-Sertier, C., Dutilh, L., Vestner, J., Capozzi, V., Sherman, D. J., Hubert, C., Claisse, O., Spano, G., De Revel, G., & Lucas, P. (2017). Two different Oenococcus oeni lineages are associated to either red or white wines in Burgundy: genomics and metabolomics insights. *OENO One*, *51*(3), 309–322. https://doi.org/10.20870/oeno-one.2017.51.4.1861

Capozzi, V., Russo, P., Lamontanara, A., Orrù, L., Cattivelli, L., & Spano, G. (2014). Genome Sequences of Five Oenococcus oeni Strains Isolated from Nero Di Troia Wine from the Same Terroir in Apulia, Southern Italy. *Genome Announcements*, *2*(5), 1–2. https://doi.org/10.1128/genomeA.01077-14

Cappello, M. S., Zapparoli, G., Logrieco, A., & Bartowsky, E. J. (2017). Linking wine lactic acid bacteria diversity with wine aroma and flavour. *International Journal of Food Microbiology*, *243*, 16–27. https://doi.org/10.1016/j.ijfoodmicro.2016.11.025

Capucho, I., & San Romao, M. V. (1994). Effect of ethanol and fatty acids on

malolactic activity ofLeuconostoc oenos. *Applied Microbiology and Biotechnology*, *42*(2–3), 391–395. https://doi.org/10.1007/BF00902747

Cardoso, J. G. R., Zeidan, A. A., Jensen, K., Sonnenschein, N., Neves, A. R., & Herrgård, M. J. (2018). MARSI: Metabolite analogues for rational strain improvement. *Bioinformatics*, *34*(13), 2319–2321. https://doi.org/10.1093/bioinformatics/bty108

Carre, E., Lafon-Lafourcade, S., & Ribéreau-Gayon, P. (1983). Occurrence of lactic Acid bacteria during the different stages of vinification and conservation of wines. *Applied and Environmental Microbiology*, *46*(4), 874–880. http://www.pubmedcentral.nih.gov/articlerender.fcgi?artid=239482&tool=pmcentrez&rendertype=abstract

Carreté, R., Vidal, M. T., Bordons, A., & Constantí, M. (2002). Inhibitory effect of sulfur dioxide and other stress compounds in wine on the ATPase activity of Oenococcus oeni. *FEMS Microbiology Letters*, *211*(2), 155–159. https://doi.org/10.1016/S0378-1097(02)00687-0

Caspi, R., Altman, T., Billington, R., Dreher, K., Foerster, H., Fulcher, C. A., Holland, T. A., Keseler, I. M., Kothari, A., Kubo, A., Krummenacker, M., Latendresse, M., Mueller, L. A., Ong, Q., Paley, S., Subhraveti, P., Weaver, D. S., Weerasinghe, D., Zhang, P., & Karp, P. D. (2014). The MetaCyc database of metabolic pathways and enzymes and the BioCyc collection of Pathway/Genome Databases. *Nucleic Acids Research*, *42*(D1), 459–471. https://doi.org/10.1093/nar/gkt1103

Caspritz, G., & Radlert, F. (1983). Malolactic Enzyme of Lactobacillus plantarum. *Journal of Biological Chemistry*, *258*(8), 4907–4910.

Cavin, J. F., Divies, C., & Guzzo, J. (1998). La fermentation malolactique. In C. Flanzy (Ed.), *Oenologie. Fondaments scientifiques et technologiques., Paris* (pp. 503–511). Technique et documentation Lavoisier.

Chelo, I. M., Zé-Zé, L., & Tenreiro, R. (2007). Congruence of evolutionary relationships inside the Leuconostoc-Oenococcus-Wiessella clade assessed by phylogenetic analysis of the 16S rRNA gene, dnaA, gyrB, rpoC and dnaK. *International Journal of Systematic and Evolutionary Microbiology*, *57*(2), 276–286. https://doi.org/10.1099/ijs.0.64468-0

Chidi, B. S., Bauer, F. F., & Rossouw, D. (2018). Organic Acid Metabolism and the Impact of Fermentation Practices on Wine Acidity-A Review. *S. Afr. J. Enol. Vitic*, *39*(2), 315–329. https://doi.org/10.21548/39-2-3172

Cho, A. E., Guallar, V., Berne, B. J., & Friesner, R. (2005). Importance of accurate charges in molecular docking: Quantum mechanical/molecular mechanical (QM/MM) approach. *Journal of Computational Chemistry*, *26*(9), 915–931. https://doi.org/10.1002/jcc.20222

Chu-Ky, S., Tourdot-Marechal, R., Marechal, P. A., & Guzzo, J. (2005). Combined cold, acid, ethanol shocks in Oenococcus oeni: Effects on membrane fluidity and

cell viability. *Biochimica et Biophysica Acta - Biomembranes*, *1717*(2), 118–124. https://doi.org/10.1016/j.bbamem.2005.09.015

Cibrario, A., Peanne, C., Lailheugue, M., Campbell-Sills, H., & Dols-Lafargue, M. (2016). Carbohydrate metabolism in Oenococcus oeni: a genomic insight. *BMC Genomics*, *17*(1), 984. https://doi.org/10.1186/s12864-016-3338-2

Ciezack, G., Hazo, L., Chambat, G., Heyraud, A., Lonvaud-Funel, A., & Dols-Lafargue, M. (2010). Evidence for exopolysaccharide production by Oenococcus oeni strains isolated from non-ropy wines. *Journal of Applied Microbiology*, *108*(2), 499–509. https://doi.org/10.1111/j.1365-2672.2009.04449.x

Conde, C., Silva, P., Fontes, N., Dias, A. C. P., Tavares, R. M., Sousa, M. J., Agasse, A., Delrot, S., & Gerós, H. (2007). Biochemical Changes throughout Grape Berry Development and Fruit and Wine Quality. *Food*, *1*(1), 1–22. https://doi.org/10.1093/jxb/ert395

Cook, D. J., & Nielsen, J. (2017). Genome-scale metabolic models applied to human health and disease. *Wiley Interdisciplinary Reviews: Systems Biology and Medicine*, *9*(6), 1–18. https://doi.org/10.1002/wsbm.1393

Cordente, A. G., Curtin, C. D., Varela, C., & Pretorius, I. S. (2012). Flavour-active wine yeasts. *Applied Microbiology and Biotechnology*, *96*(3), 601–618. https://doi.org/10.1007/s00253-012-4370-z

Costantini, A., Rantsiou, K., Majumder, A., Jacobsen, S., Pessione, E., Svensson, B., Garcia-Moruno, E., & Cocolin, L. (2015). Complementing DIGE proteomics and DNA subarray analyses to shed light on Oenococcus oeni adaptation to ethanol in wine-simulated conditions. *Journal of Proteomics*, *123*, 114–127. https://doi.org/10.1016/j.jprot.2015.04.019

Cotter, P. D., & Hill, C. (2003). Surviving the Acid Test : Responses of Gram-Positive Bacteria to Low pH Surviving the Acid Test : Responses of Gram-Positive Bacteria to Low pH. *Microbiology and Molecular Biology Reviews : MMBR*, *67*(3), 429–453. https://doi.org/10.1128/MMBR.67.3.429

Cousin, F. J., Le Guellec, R., Chagnot, C., Goux, D., Dalmasso, M., Laplace, J. M., & Cretenet, M. (2019). Oenococcus sicerae sp. nov., isolated from French cider. *Systematic and Applied Microbiology*, *42*(3), 302–308. https://doi.org/10.1016/j.syapm.2018.12.006

da Mota, R. V., Ramos, C. L., Peregrino, I., Hassimotto, N. M. A., Purgatto, E., de Souza, C. R., Dias, D. R., & Regina, M. D. A. (2017). Identification of the potential inhibitors of malolactic fermentation in wines. *Food Science and Technology*, 1–6.

da Silveira, M. G., Baumgärtner, M., Rombouts, F. M., & Abee, T. (2004). Effect of adaptation to ethanol on cytoplasmic and membrane protein profiles of Oenococcus oeni. *Applied and Environmental Microbiology*, *70*(5), 2748–2755. https://doi.org/10.1128/AEM.70.5.2748

da Silveira, M. G., Golovina, E. A., Folkert, A., Rombouts, F. M., Abee, T., Silveira, D., & Hoekstra, F. a. (2003). Membrane Fluidity Adjustments in Ethanol-Stressed Oenococcus oeni Cells. *Applied and Environmental Microbiology*, *69*(10), 5826–5832. https://doi.org/10.1128/AEM.69.10.5826

Dale, J. M., Popescu, L., & Karp, P. D. (2010). Machine learning methods for metabolic pathway prediction. *BMC Bioinformatics*, *11*(1), 15. https://doi.org/10.1186/1471-2105-11-15

Darias-Martín, J. J., Rodríguez, O., Díaz, E., & Lamuela-Raventós, R. M. (2000). Effect of skin contact on the antioxidant phenolics in white wine. *Food Chemistry*, *71*(4), 483–487. https://doi.org/10.1016/S0308-8146(00)00177-1

Darsonval, M., Alexandre, H., & Grandvalet, C. (2016). Genetically engineered Oenococcus oeni strains to highlight the impact of estA2 and estA7 esterase genes on wine ester profile. *Food Microbiology*, *60*, 21–28. https://doi.org/10.1016/j.fm.2016.06.012

Darsonval, M., Msadek, T., Alexandre, H., & Grandvalet, C. (2016). The antisense RNA approach: A new application for in vivo investigation of the stress response of Oenococcus oeni, a wine-associated lactic acid bacterium. *Applied and Environmental Microbiology*, *82*(1), 18–26. https://doi.org/10.1128/AEM.02495-15

Davis, C. R., Wibowo, D., Eschenbruch, R., Lee, T. H., & Fleet, G. H. (1985). Practical implications of malolactic fermentation: a review. *American Journal of Enology and Viticulture*, *36*(4), 290–301. http://www.ajevonline.org/content/36/4/290.short

Davis, C. R., Wibowo, D. J., Lee, T. H., & Fleet, G. H. (1986). Growth and Metabolism of Lactic Acid Bacteria during and after Malolactic Fermentation of Wines at Different pH. *Applied and Environmental Microbiology*, *51*(3), 539–545. https://aem.asm.org/content/51/3/539

de las Rivas, B., Marcobal, A. M., & Muñoz, R. (2004). Allelic diversity and population structure in Oenococcus oeni as determined from sequence analysis of housekeeping genes. *Applied and Environmental Microbiology*, *70*(12), 7210–7219. https://doi.org/10.1128/AEM.70.12.7210

De Man, J. C., Rogosa, M., & Sharpe, M. E. (1960). A Medium for the Cultivation of Lactobacilli. *Journal of Applied Bacteriology*, *23*(1), 130–135. https://doi.org/10.1111/j.1365-2672.1960.tb00188.x

De Vuyst, L., & Vandamme, E. J. (1994). Antimicrobial Potential of Lactic Acid Bacteria. In L. De Vuyst & E. J. Vandamme (Eds.), *Bacteriocins of Lactic Acid Bacteria* (pp. 92–129). Springer. https://doi.org/10.1007/978-1-4615-2668-1_3

Defilippi, B. G., Manríquez, D., Luengwilai, K., & González-Agüero, M. (2009). Aroma Volatiles. Biosynthesis and Mechanisms of Modulation During Fruit Ripening. *Advances in Botanical Research*, *50*, 1–37. https://doi.org/10.1016/S0065-2296(08)00801-X

Delaherche, A., Bon, E., Dupé, A., Lucas, M., Arveiler, B., De Daruvar, A., & Lonvaud-Funel, A. (2006). Intraspecific diversity of Oenococcus oeni strains determined by sequence analysis of target genes. *Applied Microbiology and Biotechnology*, *73*(2), 394–403. https://doi.org/10.1007/s00253-006-0487-2

Dicks, L., Dellaglio, F., & Collins, M. D. (1995). Proposal To Reclassify Leuconostoc oenos as Oenococcus oeni [corrig.] gen. nov., comb. nov. *International Journal of Systematic Bacteriology*, *45*(2), 395–397.

Dimopoulou, M., Hazo, L., & Dols-Lafargue, M. (2012). Exploration of phenomena contributing to the diversity of Oenococcus oeni exopolysaccharides. *International Journal of Food Microbiology*, *153*(1–2), 114–122. https://doi.org/10.1016/j.ijfoodmicro.2011.10.024

Dimopoulou, M., Vuillemin, M., Campbell-Sills, H., Lucas, P. M., Ballestra, P., Miot-Sertier, C., Favier, M., Coulon, J., Moine, V., Doco, T., Roques, M., Williams, P., Petrel, M., Gontier, E., Moulis, C., Remaud-Simeon, M., & Dols-Lafargue, M. (2014). Exopolysaccharide (EPS) synthesis by Oenococcus oeni: from genes to phenotypes. *PloS One*, *9*(6), e98898. https://doi.org/10.1371/journal.pone.0098898

Dols-Lafargue, M., Lee, H. Y., Le Marrec, C., Heyraud, A., Chambat, G., & Lonvaud-Funel, A. (2008). Characterization of gtf, a glucosyltransferase gene in the genomes of Pediococcus parvulus and Oenococcus oeni, two bacterial species commonly found in wine. *Applied and Environmental Microbiology*, *74*(13), 4079–4090. https://doi.org/10.1128/AEM.00673-08

Droste, P., Miebach, S., Niedenführ, S., Wiechert, W., & Nöh, K. (2011). Visualizing multi-omics data in metabolic networks with the software Omix: a case study. *Bio Systems*, *105*(2), 154–161. https://doi.org/10.1016/j.biosystems.2011.04.003

du Toit, M., Engelbrecht, L., Lerm, E., & Krieger-Weber, S. (2011). Lactobacillus: the Next Generation of Malolactic Fermentation Starter Cultures—an Overview. *Food and Bioprocess Technology*, *4*(6), 876–906. https://doi.org/10.1007/s11947-010-0448-8

du Toit, M., & Pretorius, I. S. (2000). Microbial Spoilage and Preservation of Wine: Using Weapons from Nature's Own Arsenal- A Review. *South African Journal of Enology and Viticulture*, *21*, 74–96.

Duar, R. M., Lin, X. B., Zheng, J., Martino, M. E., Grenier, T., Pérez-Muñoz, M. E., Leulier, F., Gänzle, M., & Walter, J. (2017). Lifestyles in transition: evolution and natural history of the genus Lactobacillus. *FEMS Microbiology Reviews*, *41*(Supp_1), S27–S48. https://doi.org/10.1093/femsre/fux030

Dunphy, L. J., & Papin, J. A. (2018). Biomedical applications of genome-scale metabolic network reconstructions of human pathogens. *Current Opinion in Biotechnology*, *51*, 70–79. https://doi.org/10.1016/j.copbio.2017.11.014

Edwards, J. S., & Palsson, B. O. (1999). Systems properties of the Haemophilus influenzae Rd metabolic genotype. *Journal of Biological Chemistry*, *274*(25),

17410–17416. https://doi.org/10.1074/jbc.274.25.17410

El Khoury, M., Campbell-Sills, H., Salin, F., Guichoux, E., Claisse, O., & Lucas, P. M. (2017). Biogeography of Oenococcus oeni reveals distinctive but nonspecific populations in wine-producing regions. *Applied and Environmental Microbiology*, *83*(3), 1–11. https://doi.org/10.1128/AEM.02322-16

Endo, A., & Okada, S. (2006). Oenococcus kitaharae sp. nov., a non-acidophilic and non-malolactic-fermenting oenococcus isolated from a composting distilled shochu residue. *International Journal of Systematic and Evolutionary Microbiology*, *56*(Pt 10), 2345–2348. https://doi.org/10.1099/ijs.0.64288-0

Fahimi, N., Brandam, C., & Taillandier, P. (2014). A mathematical model of the link between growth and L-malic acid consumption for five strains of Oenococcus oeni. *World Journal of Microbiology and Biotechnology*, *30*(12), 3163–3172. https://doi.org/10.1007/s11274-014-1743-8

Feist, A. M., Herrgard, M. J., Thiele, I., Reed, J. L., & Palsson, B. Ø. (2009). Reconstruction of Biochemical Networks in Microbial Organisms. *Nature Reviews Microbiology*, *7*(2), 129–143. https://doi.org/10.1038/nrmicro1949.Reconstruction

Feist, A. M., & Palsson, B. Ø. (2008). The Growing Scope of Application od Genome-scale Metabolic Reconstructions: the case of E. coli. *Nature Biotechnology*, *26*(6), 659–667. https://doi.org/10.1038/nbt1401.The

Flahaut, N. a L., Wiersma, A., van de Bunt, B., Martens, D. E., Schaap, P. J., Sijtsma, L., Dos Santos, V. a M., & de Vos, W. M. (2013). Genome-scale metabolic model for Lactococcus lactis MG1363 and its application to the analysis of flavor formation. *Applied Microbiology and Biotechnology*, *97*(19), 8729–8739. https://doi.org/10.1007/s00253-013-5140-2

Fleet, G. H. (1993). *Wine microbiology and biotechnology*. CRC Press.

Fleischmann, R. D., Adams, M. D., White, O., Clayton, R. A., Kirkness, E. F., Kerlavage, A. R., Bult, C. J., Tomb, J. F., Dougherty, B. A., Merrick, J. M., McKenney, K., Sutton, G., FitzHugh, W., Fields, C., Gocayne, J. D., Scott, J., Shirley, R., Liu, L. I., Glodek, A., … Venter, J. C. (1995). Whole-genome random sequencing and assembly of Haemophilus influenzae Rd. *Science*, *269*(5223), 496–512. https://doi.org/10.1126/science.7542800

Flesch, P. (1969). Über die Malat-Dehydrogenase-und Lactat-Dehydrogenase-Aktivität L-Äpfelsäure-abbauender Bakterien. *Archiv Für Mikrobiologie*, *68*(3), 259–277. https://doi.org/10.1007/BF00409918

Folger, O., Jerby, L., Frezza, C., Gottlieb, E., Ruppin, E., & Shlomi, T. (2011). Predicting selective drug targets in cancer through metabolic networks. *Molecular Systems Biology*, *7*(501), 1–10. https://doi.org/10.1038/msb.2011.35

Fourcassie, P., Belarbi, A., & Maujean, A. (1992). Growth, D-glucose utilization and malolactic fermentation by Leuconostoc œnos strains in 18 media deficient in

one amino acid. *Journal of Applied Bacteriology*, *73*, 489–496. http://onlinelibrary.wiley.com/doi/10.1111/j.1365-2672.1992.tb05010.x/full

Frezza, C., Zheng, L., Folger, O., Rajagopalan, K. N., MacKenzie, E. D., Jerby, L., Micaroni, M., Chaneton, B., Adam, J., Hedley, A., Kalna, G., Tomlinson, I. P. M., Pollard, P. J., Watson, D. G., Deberardinis, R. J., Shlomi, T., Ruppin, E., & Gottlieb, E. (2011). Haem oxygenase is synthetically lethal with the tumour suppressor fumarate hydratase. *Nature*, *477*, 225. https://doi.org/10.1038/nature10363

Friesner, R. A., Banks, J. L., Murphy, R. B., Halgren, T. A., Klicic, J. J., Mainz, D. T., Repasky, M. P., Knoll, E. H., Shelley, M., Perry, J. K., Shaw, D. E., Francis, P., & Shenkin, P. S. (2004). Glide: A New Approach for Rapid, Accurate Docking and Scoring. 1. Method and Assessment of Docking Accuracy. *Journal of Medicinal Chemistry*, *47*(7), 1739–1749. https://doi.org/10.1021/jm0306430

Gänzle, M. G. (2015). Lactic metabolism revisited: metabolism of lactic acid bacteria in food fermentations and food spoilage. *Current Opinion in Food Science*, *2*, 106–117. https://doi.org/https://doi.org/10.1016/j.cofs.2015.03.001

Garbay, S., Rozes, N., & Lonvaud-Funel, A. (1995). Fatty acid composition of Leuconostoc oenos, incidence of growth conditions and relationship with malolactic efficiency. *Food Microbiology*, *12*, 387–395. https://doi.org/10.1016/S0740-0020(95)80120-0

García-Quintáns, N., Magni, C., De Mendoza, D., & López, P. (1998). The citrate transport system of Lactococcus lactis subsp. lactis biovar diacetylactis is induced by acid stress. *Applied and Environmental Microbiology*, *64*(3), 850–857.

Garofalo, C., El Khoury, M., Lucas, P., Bely, M., Russo, P., Spano, G., & Capozzi, V. (2015). Autochthonous starter cultures and indigenous grape variety for regional wine production. *Journal of Applied Microbiology*, *118*(6), 1395–1408.

Garvie, E. I. (1967a). Leuconostoc oenos sp.nov. *Journal of General Microbiology*, *48*, 431–438.

Garvie, E. I. (1967b). The growth factor and amino acid requirements of species of the genus Leuconostoc, including Leuconostoc paramesenteroides (sp. nov.) and Leuconostoc oenos. *Journal of General Microbiology*, *48*, 439–447. https://doi.org/10.1099/00221287-48-3-439

Geng, J., & Nielsen, J. (2017). In silico analysis of human metabolism: Reconstruction, contextualization and application of genome-scale models. *Current Opinion in Systems Biology*, *2*, 29–38. https://doi.org/10.1016/j.coisb.2017.01.001

Gerlt, J. A., Bouvier, J. T., Davidson, D. B., Imker, H. J., Sadkhin, B., Slater, D. R., & Whalen, K. L. (2015). Enzyme function initiative-enzyme similarity tool (EFI-EST): A web tool for generating protein sequence similarity networks. *Biochimica et Biophysica Acta - Proteins and Proteomics*, *1854*(8), 1019–1037.

https://doi.org/10.1016/j.bbapap.2015.04.015

Gevorgyan, A., Poolman, M. G., & Fell, D. A. (2008). Detection of stoichiometric inconsistencies in biomolecular models. *Bioinformatics*, *24*(19), 2245–2251. https://doi.org/10.1093/bioinformatics/btn425

Gibson, D. G., Young, L., Chuang, R.-Y., Venter, J. C., Hutchison, C. a, Smith, H. O., Iii, C. A. H., & America, N. (2009). Enzymatic assembly of DNA molecules up to several hundred kilobases. In *Nature methods* (Vol. 6, Issue 5, pp. 343–345). https://doi.org/10.1038/nmeth.1318

Gockowiak, H., & Henschke, P. A. (2003). Interaction of pH, ethanol concentration and wine matrix on induction of malolactic fermentation with commercial 'direct inoculation' starter cultures. *Australian Journal of Grape and Wine Research*, *9*(3), 200–209. https://doi.org/10.1111/j.1755-0238.2003.tb00271.x

Grandvalet, C. (2017). Oenococcus oeni: Queen of the cellar, nightmare of geneticists. *Microbiology (United Kingdom)*, *163*(3), 297–299. https://doi.org/10.1099/mic.0.000456

Grandvalet, C., Assad-García, J. S., Chu-Ky, S., Tollot, M., Guzzo, J., Gresti, J., & Tourdot-Maréchal, R. (2008). Changes in membrane lipid composition in ethanol- and acid-adapted Oenococcus oeni cells: characterization of the cfa gene by heterologous complementation. *Microbiology (Reading, England)*, *154*(Pt 9), 2611–2619. https://doi.org/10.1099/mic.0.2007/016238-0

Grandvalet, C., Coucheney, F., & Guzzo, J. (2005). CtsR Is the Master Regulator of Stress Response Gene Expression in Oenococcus oeni. *Journal of Bacteriology*, *187*(16), 5614–5623. https://doi.org/10.1128/JB.187.16.5614

Grimaldi, A., Bartowsky, E. J., & Jiranek, V. (2005a). Screening of Lactobacillus spp. and Pediococcus spp. for glycosidase activities that are important in oenology. *Journal of Applied Microbiology*, *99*(5), 1061–1069. https://doi.org/10.1111/j.1365-2672.2005.02707.x

Grimaldi, A., Bartowsky, E. J., & Jiranek, V. (2005b). A survey of glycosidase activities of commercial wine strains of Oenococcus oeni. *International Journal of Food Microbiology*, *105*(2), 233–244. https://doi.org/10.1016/j.ijfoodmicro.2005.04.011

Groisillier, A., & Lonvaud-Funel, A. (1999). Comparison of partial malolactic enzyme gene sequences for phylogenetic analysis of some lactic acid bacteria species and relationships with the malic enzyme. *International Journal of Systematic Bacteriology*, *49 Pt 4*(1 999), 1417–1428. https://doi.org/10.1099/00207713-49-4-1417

Gudmundsson, S., Agudo, L., & Nogales, J. (2017). Applications of genome-scale metabolic models of microalgae and cyanobacteria in biotechnology. In *Microalgae-Based Biofuels and Bioproducts: From Feedstock Cultivation to End-Products*. Elsevier Ltd. https://doi.org/10.1016/B978-0-08-101023-5.00004-2

Guerrini, S., Bastianini, A., Blaiotta, G., Granchi, L., Moschetti, G., Coppola, S., Romano, P., & Vincenzini, M. (2003). Phenotypic and genotypic characterization of Oenococcus oeni strains isolated from Italian wines. *International Journal of Food Microbiology*, *83*(1), 1–14. https://doi.org/10.1016/S0168-1605(02)00323-9

Guerrini, S., Bastianini, A., Granchi, L., & Vincenzini, M. (2002). Effect of Oleic Acid on Oenococcus oeni Strains and Malolactic Fermentation in Wine. *Current Microbiology*, *44*(1), 5–9. https://doi.org/10.1007/s00284-001-0066-9

Gurobi Optimization Inc. (2016). *Gurobi Optimizer Reference Manual* (6.5). Gurobi Optimization, Inc. http://www.gurobi.com

Guzzo, J., Jobin, M.-P., Delmas, F., Fortier, L.-C., Garmyn, D., Tourdot-Maréchal, R., Lee, B., & Diviès, C. (2000). Regulation of stress response in Oenococcus oeni as a function of environmental changes and growth phase. *International Journal of Food Microbiology*, *55*(1), 27–31. https://doi.org/https://doi.org/10.1016/S0168-1605(00)00209-9

Guzzon, R., Poznanski, E., Conterno, L., Vagnoli, P., Krieger-Weber, S., & Cavazza, A. (2009). Selection of a new highly resistant strain for malolactic fermentation under difficult conditions. *South African Journal of Enology and Viticulture*, *30*(2), 133–141.

Hanly, T. J., Urello, M., & Henson, M. A. (2012). Dynamic flux balance modeling of S. cerevisiae and E. coli co-cultures for efficient consumption of glucose/xylose mixtures. *Applied Microbiology and Biotechnology*, *93*(6), 2529–2541. https://doi.org/10.1007/s00253-011-3628-1

Henick-Kling, T., Laurent, M.-H., & Acree, T. E. (1994). Changes in the aroma and odor of Chardonnay wine due to malolactic fermentation. *Wein-Wissenschaft*, *49*(1), 3–10. http://cat.inist.fr/?aModele=afficheN&cpsidt=3335414

Henríquez-Aedo, K., Durán, D., Garcia, A., Hengst, M. B., & Aranda, M. (2016). Identification of biogenic amines-producing lactic acid bacteria isolated from spontaneous malolactic fermentation of chilean red wines. *LWT - Food Science and Technology*, *68*, 183–189. https://doi.org/10.1016/j.lwt.2015.12.003

Henschke, P. A. (1993). An overview of malolactic fermentation research. *Australian-New Zealand Wine Industry Journal*, *8*, 69–79.

Ho Sui, S. J., Lo, R., Fernandes, A. R., Caulfield, M. D. G., Lerman, J. A., Xie, L., Bourne, P. E., Baillie, D. L., & Brinkman, F. S. L. (2012). Raloxifene attenuates Pseudomonas aeruginosa pyocyanin production and virulence. *International Journal of Antimicrobial Agents*, *40*(3), 246–251. https://doi.org/10.1016/j.ijantimicag.2012.05.009

Howell, G. (2016). Co-inoculation: The latest great development in malolactic fermentation. *Australian and New Zealand Grapegrower and Winemaker*, *630*, 74.

Husnik, J. I., Delaquis, P. J., Cliff, M. A., & van Vuuren, H. J. J. (2007). Functional Analyses of the Malolactic Wine Yeast ML01. *American Journal of Enology and Viticulture*, *58*(1), 42–52. http://www.ajevonline.org/content/58/1/42

Husnik, J. I., Volschenk, H., Bauer, J., Colavizza, D., Luo, Z., & van Vuuren, H. J. J. (2006). Metabolic engineering of malolactic wine yeast. *Metabolic Engineering*, *8*(4), 315–323. https://doi.org/10.1016/j.ymben.2006.02.003

Hutkins, R. W., & Nannen, N. L. (1993). pH Homeostasis in Lactic Acid Bacteria. *Journal of Dairy Science*, *76*(8), 2354–2365. https://doi.org/10.3168/jds.S0022-0302(93)77573-6

Ilabaca, C., Jara, C., & Romero, J. (2014). The rapid identification of lactic acid bacteria present in Chilean winemaking processes using culture-independent analysis. *Annals of Microbiology*, *64*(4), 1857–1859. https://doi.org/10.1007/s13213-014-0810-6

Ingraham, J. L., Vaughn, R. H., & Cooke, G. M. (1960). Studies on the Malo-Lactic Organisms Isolated from California Wines. *American Journal of Enology and Viticulture*, *11*(1), 1 LP – 4. http://www.ajevonline.org/content/11/1/1.abstract

Iorizzo, M., Testa, B., Lombardi, S. J., García-Ruiz, A., Muñoz-González, C., Bartolomé, B., & Moreno-Arribas, M. V. (2016). Selection and technological potential of Lactobacillus plantarum bacteria suitable for wine malolactic fermentation and grape aroma release. *LWT-Food Science and Technology*, *73*, 557–566.

Izquierdo-Cañas, P. M., García-Romero, E., Pérez-Martín, F., Seseña, S., & Llanos-Palop, M. (2015). Sequential inoculation versus co-inoculation in Cabernet Franc wine fermentation. *Food Science and Technology International*, *21*(3), 203–212. https://doi.org/10.1177/1082013214524585

Jain, R., & Srivastava, R. (2009). Metabolic investigation of host/pathogen interaction using MS2-infected Escherichia coli. *BMC Systems Biology*, *3*(121), 1–11. https://doi.org/10.1186/1752-0509-3-121

Jay, J. M. (1982). Antimicrobial properties of diacetyl. *Applied and Environmental Microbiology*, *44*(3), 525 LP – 532. http://aem.asm.org/content/44/3/525.abstract

Jiang, J., Sumby, K. M., Sundstrom, J. F., Grbin, P. R., & Jiranek, V. (2018). Directed evolution of Oenococcus oeni strains for more efficient malolactic fermentation in a multi-stressor wine environment. *Food Microbiology*, *73*, 150–159. https://doi.org/10.1016/j.fm.2018.01.005

Kanehisa, M. (2000). *Post-genome Informatics*. Oxford University Press. https://doi.org/10.1017/CBO9781107415324.004

Karp, P. D., Paley, S., & Romero, P. (2002). The Pathway Tools software. *Bioinformatics*, *18*(Suppl 1), S225–S232. https://doi.org/10.1093/bioinformatics/18.suppl_1.S225

Kim, H. U., Kim, S. Y., Jeong, H., Kim, T. Y., Kim, J. J., Choy, H. E., Yi, K. Y.,

Rhee, J. H., & Lee, S. Y. (2014). Integrative genome-scale metabolic analysis of Vibrio vulnificus for drug targeting and discovery. Mol. Syst. Biol. 7, 460. *Molecular Systems Biology*, *7*, 460.

Kim, W. J., Kim, H. U., & Lee, S. Y. (2017). Current state and applications of microbial genome-scale metabolic models. *Current Opinion in Systems Biology*, *2*, 10–18. https://doi.org/10.1016/j.coisb.2017.03.001

Klamt, S., Saez-Rodriguez, J., & Gilles, E. D. (2007). Structural and functional analysis of cellular networks with CellNetAnalyzer. *BMC Systems Biology*, *1*(1), 2. https://doi.org/10.1186/1752-0509-1-2

Klamt, S., & von Kamp, A. (2011). An application programming interface for CellNetAnalyzer. *Biosystems*, *105*(2), 162–168. https://doi.org/10.1016/j.biosystems.2011.02.002

Klitgord, N., & Segre, D. (2010). Environments that Induce Synthetic Microbial Ecosystems. *PLoS Computational Biology*, *6*(11), 1–17. https://doi.org/10.1371/journal.pcbi.1001002

Koduru, L., Kim, Y., Bang, J., Lakshmanan, M., Han, N. S., & Lee, D.-Y. (2017). Genome-scale modeling and transcriptome analysis of Leuconostoc mesenteroides unravel the redox governed metabolic states in obligate heterofermentative lactic acid bacteria. *Scientific Reports*, *7*(1), 15721. https://doi.org/10.1038/s41598-017-16026-9

König, H., Unden, G., & Fröhlich, J. (2009). *Biology of Microorganisms on Grapes, in Must and in Wine*. Springer.

Konings, W. N., Lolkema, J. S., Bolhuis, H., van Veen, H. W., Poolman, B., & Driessen, A. J. M. (1997). The role of transport processes in survival of lactic acid bacteria. *Antonie van Leeuwenhoek*, *71*(1–2), 117–128. https://doi.org/10.1023/A:1000143525601

Konings, Wil N. (2002). The cell membrane and the struggle for life of lactic acid bacteria. *Antonie van Leeuwenhoek*, *82*(3), 3–27. http://link.springer.com/chapter/10.1007/978-94-017-2029-8_2

Koonin, E. V. (2005). Orthologs, Paralogs, and Evolutionary Genomics. *Annual Review of Genetics*, *39*(1), 309–338. https://doi.org/10.1146/annurev.genet.39.073003.114725

Korkes, S., & Ochoa, S. (1948). Adaptive conversion of malate to lactate and carbon dioxide by Lactobacillus arabinosus. *The Journal of Biological Chemistry*, *176*(1), 463. http://www.ncbi.nlm.nih.gov/pubmed/18886184

Krueger, D. A. (2012). Composition of pomegranate juice. *Journal of AOAC International*, *95*, 163–168.

Kučerová, J., & Široký, J. (2011). Study of Changes Organic Acids in Red Wines During Malolactic Fermentation. *Acta Univ. Agric. Silvic. Mendel. Brun*, *59*(5), 145–150.

Kuepfer, L., Sauer, U., & Blank, L. M. (2005). Metabolic functions of duplicate genes in Saccharomyces cerevisiae. *Genome Research*, *15*(10), 1421–1430. https://doi.org/10.1101/gr.3992505.1

Kunkee, R. E. (1968). Malo-Lactic Fermentation. *Advances in Applied Microbiology*, *9*(C), 235–279. https://doi.org/10.1016/S0065-2164(08)70530-6

Kunkee, R. E. (1974). Malo-Lactic Fermentation and Winemaking. In A. D. Webb (Ed.), *Chemistry of Winemaking* (1st editio, Issue 137, pp. 151–170). American Chemical Society.

Kunkee, R. E. (1991). Some roles of malic acid in the malolactic fermentation in wine making. *FEMS Microbiology Letters*, *88*(1), 55–71. https://doi.org/10.1016/0378-1097(91)90696-8

Labarre, C., Diviès, C., & Guzzo, J. (1996). Genetic organization of the mle locus and identification of a mleR-like gene from Leuconostoc oenos. *Applied and Environmental Microbiology*, *62*(12), 4493–4498. http://www.pubmedcentral.nih.gov/articlerender.fcgi?artid=168275&tool=pmcentrez&rendertype=abstract

Labarre, C., Guzzo, J., Cavin, J. F., & Diviès, C. (1996). Cloning and characterization of the genes encoding the malolactic enzyme and the malate permease of Leuconostoc oenos. *Applied and Environmental Microbiology*, *62*(4), 1274–1282. http://www.pubmedcentral.nih.gov/articlerender.fcgi?artid=167893&tool=pmcentrez&rendertype=abstract

Lasik, M. (2013). The application of malolactic fermentation process to create good-quality grape wine produced in cool-climate countries: a review. *European Food Research and Technology*, *237*(6), 843–850. https://doi.org/10.1007/s00217-013-2083-x

Le Marrec, C., Bon, E., & Lonvaud-Funel, A. (2007). Tolerance to high osmolality of the lactic acid bacterium Oenococcus oeni and identification of potential osmoprotectants. *International Journal of Food Microbiology*, *115*(3), 335–342. https://doi.org/10.1016/j.ijfoodmicro.2006.12.039

Lechiancole, T., Blaiotta, G., Messina, D., Fusco, V., Villani, F., & Salzano, G. (2006). Evaluation of intra-specific diversities in Oenococcus oeni through analysis of genomic and expressed DNA. *Systematic and Applied Microbiology*, *29*(5), 375–381. https://doi.org/10.1016/j.syapm.2005.10.001

Lee, S. G., Lee, K. W., Park, T. H., Park, J. Y., Han, N. S., & Kim, J. H. (2012). Proteomic analysis of proteins increased or reduced by ethanol of Lactobacillus plantarum ST4 isolated from Makgeolli, traditional Korean rice wine. *Journal of Microbiology and Biotechnology*, *22*(4), 516–525.

Lerena, M. C., Rojo, M. C., Sari, S., Mercado, L. A., Krieger-Weber, S., & Combina, M. (2016). Malolactic fermentation induced by Lactobacillus plantarum in Malbec wines from Argentina. *South African Journal of Enology and*

Viticulture, *37*(2), 115–123.

Lerm, E., Engelbrecht, L., & Toit, M. (2011). Selection and characterisation of Oenococcus oeni and Lactobacillus plantarum South African wine isolates for use as malolactic fermentation starter cultures. *South African Journal of Enology and Viticulture*, *32*(2), 280–295. http://www.cabdirect.org/abstracts/20123076833.html

Letunic, I., & Bork, P. (2006). Interactive Tree Of Life (iTOL): an online tool for phylogenetic tree display and annotation. *Bioinformatics*, *23*(1), 127–128.

Levering, J., Fiedler, T., Sieg, A., van Grinsven, K. W. A., Hering, S., Veith, N., Olivier, B. G., Klett, L., Hugenholtz, J., Teusink, B., Kreikemeyer, B., & Kummer, U. (2016). Genome-scale reconstruction of the Streptococcus pyogenes M49 metabolic network reveals growth requirements and indicates potential drug targets. *Journal of Biotechnology*. https://doi.org/10.1016/j.jbiotec.2016.01.035

Lewis, N. E., & Abdel-Haleem, A. M. (2013). The evolution of genome-scale models of cancer metabolism. *Frontiers in Physiology*, *4*, 237.

Lewis, N. E., Nagarajan, H., & Palsson, B. O. (2012). Constraining the metabolic genotype-phenotype relationship using a phylogeny of in silico methods. *Nature Reviews Microbiology*, *10*(4), 291–305. https://doi.org/10.1038/nrmicro2737

Lewis, N. E., Schramm, G., Bordbar, A., Schellenberger, J., Andersen, M. P., Cheng, J. K., Patel, N., Yee, A., Lewis, R. A., Eils, R., König, R., & Palsson, B. Ø. (2010). Large-scale in silico modeling of metabolic interactions between cell types in the human brain. *Nature Biotechnology*, *28*, 1279. https://doi.org/10.1038/nbt.1711

Li, E., & Mira de Orduña, R. (2010). A rapid method for the determination of microbial biomass by dry weight using a moisture analyser with an infrared heating source and an analytical balance. *Letters in Applied Microbiology*, *50*(3), 283–288. https://doi.org/10.1111/j.1472-765X.2009.02789.x

Li, H., Zhang, C., & Liu, Y. (2006). Species attribution and distinguishing strains of Oenococcus oeni isolated from Chinese wines. *World Journal of Microbiology and Biotechnology*, *22*(5), 515–518. https://doi.org/10.1007/s11274-005-9065-5

Li, N., Duan, J., Gao, D., Luo, J., Zheng, R., Bian, Y., Zhang, X., & Ji, B. (2015). Mutation and selection of Oenococcus oeni for controlling wine malolactic fermentation. *European Food Research and Technology*, *240*(1), 93–100.

Liu, L., Zhang, H., Peng, S., Wang, T., Su, J., Liang, Y., Li, H., & Wang, H. (2017). Transcriptomic analysis of Oenococcus oeni SD-2a response to acid shock by RNA-seq. *Frontiers in Microbiology*, *8*(AUG), 1–12. https://doi.org/10.3389/fmicb.2017.01586

Liu, S.-Q. (2002). A review: malolactic fermentation in wine -- beyond deacidification. *Journal of Applied Microbiology*, *92*(4), 589–601.

http://www.ncbi.nlm.nih.gov/pubmed/11966898

Ljungh, Å., & Wadström, T. (2006). Lactic Acid Bacteria as Probiotics Further Reading. *Curr. Issues Intestinal Microbiol.*, *7*(2), 73–90. https://doi.org/10.1111/j.1574-6968.2010.02185.x

Loira, N., Dulermo, T., Nicaud, J.-M., & Sherman, D. (2012). A genome-scale metabolic model of the lipid-accumulating yeast Yarrowia lipolytica. *BMC Systems Biology*, *6*(1), 35. https://doi.org/10.1186/1752-0509-6-35

Lonvaud-Funel, A. (1999). Lactic acid bacteria in the quality improvement and depreciation of wine. *Antonie van Leeuwenhoek*, *76*(1–4), 317–331. http://www.ncbi.nlm.nih.gov/pubmed/10532386

Lonvaud-Funel, A., & Desens, C. (1990). Constitution en acides gras des membranes des bactéries lactiques du vin Incidences des conditions de culture. *Sciences Des Aliments*, *10*, 817–829.

Lonvaud-Funel, A., & Strasser de Saad, A. M. (1982). Purification and Properties of a Malolactic Enzyme from a Strain of Leuconostoc mesenteroides Isolated from Grapes. *Applied and Environmental Microbiology*, *43*(2), 357–361. http://www.pubmedcentral.nih.gov/articlerender.fcgi?artid=241831&tool=pmcentrez&rendertype=abstract

López, I., Santamaría, P., Tenorio, C., Garijo, P., Gutiérrez, A. R., & López, R. (2009). Evaluation of lysozyme to control vinification process and histamine production in Rioja wines. *Journal of Microbiology and Biotechnology*, *19*(9), 1005–1012. https://doi.org/10.4014/jmb.0811.602

Lorentzen, M. P. G., & Lucas, P. M. (2019). Distribution of Oenococcus oeni populations in natural habitats. *Applied Microbiology and Biotechnology*, *103*(7), 2937–2945. https://doi.org/10.1007/s00253-019-09689-z

Lucas, P. M., Claisse, O., & Lonvaud-Funel, A. (2008). High frequency of histamine-producing bacteria in the enological environment and instability of the histidine decarboxylase production phenotype. *Applied and Environmental Microbiology*, *74*(3), 811–817. https://doi.org/10.1128/AEM.01496-07

Lucio, O., Pardo, I., Heras, J. M., Krieger-Weber, S., & Ferrer, S. (2017). Use of starter cultures of Lactobacillus to induce malolactic fermentation in wine. *Australian Journal of Grape and Wine Research*, *23*(1), 15–21. https://doi.org/10.1111/ajgw.12261

Madden, T. (2002). The BLAST Sequence Analysis Tool. In J. McEntyre & J. Ostell (Eds.), *The NCBI Handbook* (pp. 1–15). National Center for Biotechnology Information (US). http://www.ncbi.nlm.nih.gov/books/NBK21097/

Magnúsdóttir, S., Heinken, A., Kutt, L., Ravcheev, D. A., Bauer, E., Noronha, A., Greenhalgh, K., Jäger, C., Baginska, J., Wilmes, P., Fleming, R. M. T., & Thiele, I. (2017). Generation of genome-scale metabolic reconstructions for 773 members of the human gut microbiota. *Nature Biotechnology*, *35*(1), 81–89.

https://doi.org/10.1038/nbt.3703

Magnúsdóttir, S., & Thiele, I. (2018). Modeling metabolism of the human gut microbiome. *Current Opinion in Biotechnology*, *51*, 90–96. https://doi.org/10.1016/j.copbio.2017.12.005

Maicas, S., Ferrer, S., & Pardo, I. (2002). NAD(P)H regeneration is the key for heterolactic fermentation of hexoses in Oenococcus oeni. *Microbiology*, *148*, 325–332. http://www.ncbi.nlm.nih.gov/pubmed/11782525

Maicas, S., González-Cabo, P., Ferrer, S., & Pardo, I. (1999). Production of Oenococcus oeni biomass to induce malolactic fermentation in wine by control of pH and substrate addition. *Biotechnology Letters*, *21*(4), 349–353. https://doi.org/10.1023/A:1005498925733

Maicas, S., Natividad, À., Ferrer, S., & Pardo, I. (2000). Malolactic fermentation in wine with high densities of non-proliferating Oenococcus oeni. *World Journal of Microbiology and Biotechnology*, *16*(8–9), 805–810. https://doi.org/10.1023/A:1008953504742

Makarova, K. S., & Koonin, E. V. (2007). Evolutionary genomics of lactic acid bacteria. *Journal of Bacteriology*, *189*(4), 1199–1208. https://doi.org/10.1128/JB.01351-06

Makarova, K. S., Slesarev, A., Wolf, Y. I., Sorokin, A., Mirkin, B., Koonin, E. V, Pavlov, A., Pavlova, N., Karamychev, V., Polouchine, N., Shakhova, V., Grigoriev, I., Lou, Y., Rohksar, D., Lucas, S., Huang, K., Goodstein, D. M., Hawkins, T., Plengvidhya, V., … Mills, D. A. (2006). Comparative genomics of the lactic acid bacteria. *Proceedings of the National Academy of Sciences of the United States of America*, *103*(42), 15611–15616. https://doi.org/10.1073/pnas.0607117103

Mardinoglu, A., Agren, R., Kampf, C., Asplund, A., Uhlen, M., & Nielsen, J. (2014). Genome-scale metabolic modelling of hepatocytes reveals serine deficiency in patients with non-alcoholic fatty liver disease. *Nature Communications*, *5*, 3083. https://doi.org/10.1038/ncomms4083

Marengo, F., Rantsiou, K., Torchio, F., Rolle, L., & Cocolin, L. (2015). Isolation, selection, and characterization of autochthonous Oenococcus oeni strains according to their oenological properties. *Oeno 2015 10 International Symposium of Enology of Bordeaux*, 166.

Margalef-Català, M., Araque, I., Bordons, A., & Reguant, C. (2016). Genetic and transcriptional study of glutathione metabolism in Oenococcus oeni. *International Journal of Food Microbiology*, *242*, 61–69. https://doi.org/10.1016/j.ijfoodmicro.2016.11.013

Marques, A. P., Duarte, A. J., Chambel, L., Teixeira, M. F., Romãeo, M. V. S., & Tenreiro, R. (2011). Genomic diversity of Oenococcus oeni from different winemaking regions of Portugal. *International Microbiology*, *14*(3), 155–162. https://doi.org/10.2436/20.1501.01.144

Martuscelli, M., Mastrocola, D., Jeanmonod, D. J., Rebecca, & Suzuki, K. et al. (2018). Biogenic Amines: A Claim for Wines. In C. Proestos (Ed.), *Biogenic Amines* (pp. 1–10). IntechOpen. https://doi.org/10.5772/intechopen.80362

Marty-Teysset, C., Posthuma, C., Lolkema, J. S., Schmitt, P., Divies, C., & Konings, W. N. (1996). Proton motive force generation by citrolactic fermentation in Leuconostoc mesenteroides. *Journal of Bacteriology*, *178*(8), 2178–2185. http://www.pubmedcentral.nih.gov/articlerender.fcgi?artid=177923&tool=pmcentrez&rendertype=abstract

Mateo, J. J., Jiménez, M., Pastor, A., & Huerta, T. (2001). Yeast starter cultures affecting wine fermentation and volatiles. *Food Research International*, *34*(4), 307–314. https://doi.org/https://doi.org/10.1016/S0963-9969(00)00168-X

Mato, I., Suárez-Luque, S., & Huidobro, J. F. (2005). A review of the analytical methods to determine organic acids in grape juices and wines. *Food Research International*, *38*(10), 1175–1188. https://doi.org/10.1016/j.foodres.2005.04.007

Matthews, A., Grbin, P. R., & Jiranek, V. (2006). A survey of lactic acid bacteria for enzymes of interest to oenology. *Australian Journal of Grape and Wine Research*, *12*(3), 235–244. https://doi.org/10.1111/j.1755-0238.2006.tb00063.x

Matthews, A., Grimaldi, A., Walker, M., Bartowsky, E. J., Grbin, P. R., & Jiranek, V. (2004). Lactic Acid Bacteria as a Potential Source of Enzymes for Use in Vinification. *Applied and Environmental Microbiology*, *70*(10), 5715–5731. https://doi.org/10.1128/AEM.70.10.5715

McCloskey, D., Palsson, B. Ø., & Feist, A. M. (2013). Basic and applied uses of genome-scale metabolic network reconstructions of Escherichia coli. *Molecular Systems Biology*, *9*(1), 661. https://doi.org/10.1038/msb.2013.18

McGinnis, S., & Madden, T. L. (2004). BLAST: At the core of a powerful and diverse set of sequence analysis tools. *Nucleic Acids Research*, *32*, 20–25. https://doi.org/10.1093/nar/gkh435

Megchelenbrink, W., Huynen, M., & Marchiori, E. (2014). optGpSampler: An improved tool for uniformly sampling the solution-space of genome-scale metabolic networks. *PLoS ONE*, *9*(2), e86587. https://doi.org/10.1371/journal.pone.0086587

Mendoza, S. N., Cañón, P. M., Contreras, A., Ribbeck, M., & Agosin, E. (2017). Genome-scale reconstruction of the metabolic network in Oenococcus oeni to assess wine malolactic fermentation. *Frontiers in Microbiology*, *8*(March), 1–15. https://doi.org/10.3389/FMICB.2017.00534

Mesas, J. M., Rodríguez, M. C., & Alegre, M. T. (2004). Tolerancia de Oenococcus oeni RS1 a las condiciones de estrés del vino. *Ciencia y Tecnología Alimentaria*, *4*(4), 278–282.

Mills, D. a, Rawsthorne, H., Parker, C., Tamir, D., & Makarova, K. S. (2005). Genomic analysis of Oenococcus oeni PSU-1 and its relevance to winemaking.

FEMS Microbiology Reviews, *29*(3), 465–475. https://doi.org/10.1016/j.femsre.2005.04.011

Mink, R., Kölling, R., Sommer, S., Schmarr, H., & Scharfenberger-schmeer, M. (2015). Diacetyl Formation by Oenococcus oeni during Winemaking Induced by Exogenous Pyruvate. *American Journal of Enology and Viticulture*, *66*(1), 85–90. https://doi.org/10.5344/ajev.2014.14056

Mtshali, P. S., Divol, B., Van Rensburg, P., & Du Toit, M. (2010). Genetic screening of wine-related enzymes in Lactobacillus species isolated from South African wines. *Journal of Applied Microbiology*, *108*(4), 1389–1397. https://doi.org/10.1111/j.1365-2672.2009.04535.x

Naouri, P., Chagnaud, P., Arnaud, A., & Galzy, P. (1990). Purification and properties of a malolactic enzyme from Leuconostoc oenos ATCC 23278. *Journal of Basic Microbiology*, *30*(8), 577–585. http://onlinelibrary.wiley.com/doi/10.1002/jobm.3620300813/abstract

Nielsen, J. (2017). Systems Biology of Metabolism: A Driver for Developing Personalized and Precision Medicine. *Cell Metabolism*, *25*(3), 572–579. https://doi.org/10.1016/j.cmet.2017.02.002

Nielsen, J. C., & Richelieu, M. (1999). Control of flavor development in wine during and after malolactic fermentation by Oenococcus oeni. *Applied and Environmental Microbiology*, *65*(2), 740–745. http://www.pubmedcentral.nih.gov/articlerender.fcgi?artid=91089&tool=pmcentrez&rendertype=abstract

Nilsson, A., & Nielsen, J. (2017). Genome scale metabolic modeling of cancer. *Metabolic Engineering*, *43*(October), 103–112. https://doi.org/10.1016/j.ymben.2016.10.022

Nookaew, I., Jewett, M., Meechai, A., Thammarongtham, C., Laoteng, K., Cheevadhanarak, S., Nielsen, J., & Bhumiratana, S. (2008). The genome-scale metabolic model iIN800 of Saccharomyces cerevisiae and its validation: a scaffold to query lipid metabolism. *BMC Systems Biology*, *2*(71). https://doi.org/10.1186/1752-0509-2-71

O'Sullivan, O., O'Callaghan, J., Sangrador-Vegas, A., McAuliffe, O., Slattery, L., Kaleta, P., Callanan, M., Fitzgerald, G. F., Ross, R. P., & Beresford, T. (2009). Comparative genomics of lactic acid bacteria reveals a niche-specific gene set. *BMC Microbiology*, *9*, 1–9. https://doi.org/10.1186/1471-2180-9-50

Oberhardt, M. a, Palsson, B. Ø., & Papin, J. a. (2009). Applications of genome-scale metabolic reconstructions. *Molecular Systems Biology*, *5*(320), 320. https://doi.org/10.1038/msb.2009.77

Ochoa, S., Mehler, A. H., & Kornberg, A. (1947). Reversible oxidative decarboxylation of malic acid. *The Journal of Biological Chemistry*, *167*(3), 871.

Ochoa, S., Mehler, A. H., & Kornberg, A. (1948). Biosynthesis of dicarboxylic acids by carbon dioxide fixation. *J. Biol. Chem.*, *174*(3), 979–1000.

Oddone, G. M., Mills, D. A., & Block, D. E. (2009). A dynamic, genome-scale flux model of Lactococcus lactis to increase specific recombinant protein expression. *Metabolic Engineering*, *11*(6), 367–381. https://doi.org/10.1016/j.ymben.2009.07.007

OIV. (2019). *2019 Statistical Report on World Vitiviniculture*. https://doi.org/64/19/6835 [pii]\n10.1158/0008-5472.CAN-04-1678

Olguín, N. T. (2010). *Molecular study of the mechanisms of Oenococcus oeni involved in its adaptation to wine conditions and in the development of malolactic fermentation* [Doctoral dissertation, Universitat Rovira i Virgili]. http://www.tesisenred.net/handle/10803/8682

Olguín, N. T., Bordons, A., & Reguant, C. (2009). Influence of ethanol and pH on the gene expression of the citrate pathway in Oenococcus oeni. *Food Microbiology*, *26*(2), 197–203. https://doi.org/10.1016/j.fm.2008.09.004

Olguín, N. T., Champomier-Vergès, M., Anglade, P., Baraige, F., Cordero-Otero, R., Bordons, A., Zagorec, M., & Reguant, C. (2015). Transcriptomic and proteomic analysis of Oenococcus oeni PSU-1 response to ethanol shock. *Food Microbiology*, *51*, 87–95. https://doi.org/10.1016/j.fm.2015.05.005

Olguín, N. T., Valdés La Hens, D., Delfederico, L., & Semorile, L. (2019). Relative expression of stress-related genes during acclimation at low temperature of psychrotrophic Oenococcus oeni strains from Patagonian wine. *World Journal of Microbiology and Biotechnology*, *35*(1), 5. https://doi.org/10.1007/s11274-018-2577-6

Oliveira, A. P., Nielsen, J., & Förster, J. (2005). Modeling Lactococcus lactis using a genome-scale flux model. *BMC Microbiology*, *5*(39). https://doi.org/10.1186/1471-2180-5-39

Opdam, S., Richelle, A., Kellman, B., Li, S., Zielinski, D. C., & Lewis, N. E. (2017). A Systematic Evaluation of Methods for Tailoring Genome-Scale Metabolic Models. *Cell Systems*, *4*, 318–329. https://doi.org/10.1016/j.cels.2017.01.010

Orth, J. D., Thiele, I., & Palsson, B. Ø. (2010). What is flux balance analysis? *Nature Biotechnology*, *28*(3), 245–248. https://doi.org/10.1038/nbt.1614

Park, J. M., Kim, T. Y., & Lee, S. Y. (2009). Constraints-based genome-scale metabolic simulation for systems metabolic engineering. *Biotechnology Advances*, *27*(6), 979–988. https://doi.org/10.1016/j.biotechadv.2009.05.019

Pastink, M. I., Teusink, B., Hols, P., Visser, S., De Vos, W. M., & Hugenholtz, J. (2009). Genome-scale model of Streptococcus thermophilus LMG18311 for metabolic comparison of lactic acid bacteria. *Applied and Environmental Microbiology*, *75*(11), 3627–3633. https://doi.org/10.1128/AEM.00138-09

Pereira, R., Nielsen, J., & Rocha, I. (2016). Improving the flux distributions

simulated with genome-scale metabolic models of Saccharomyces cerevisiae. *Metabolic Engineering Communications*, *3*, 153–163. https://doi.org/10.1016/j.meteno.2016.05.002

Piao, H., Hawley, E., Kopf, S., DeScenzo, R., Sealock, S., Henick-Kling, T., & Hess, M. (2015). Insights into the bacterial community and its temporal succession during the fermentation of wine grapes. *Frontiers in Microbiology*, *6*(JUL). https://doi.org/10.3389/fmicb.2015.00809

Poolman, M. G., Bonde, B. K., Gevorgyan, A. ., Patel, H. H., & Fell, D. A. (2006). Challenges to be faced in the reconstruction of metabolic networks from public databases. *IEE Proceedings - Systems Biology*, *153*(5), 379 – 384. https://doi.org/10.1049/ip-syb

Pozo-Bayón, M. Á., G-Alegría, E., Polo, M. C., Tenorio, C., Martín-Álvarez, P. J., Calvo de la Banda, M. T., Ruiz-Larrea, F., & Moreno-Arribas, M. V. (2005). Wine Volatile and Amino Acid Composition after Malolactic Fermentation: Effect of Oenococcus oeni and Lactobacillus plantarum Starter Cultures. *Journal of Agricultural and Food Chemistry*, *53*(22), 8729–8735. https://doi.org/10.1021/jf050739y

Raškevičius, V., Mikalayeva, V., Antanavičiūtė, I., Ceslevičienė, I., Skeberdis, V. A., Kairys, V., & Bordel, S. (2018). Genome scale metabolic models as tools for drug design and personalized medicine. *PLoS ONE*, *13*(1), 1–14. https://doi.org/10.1371/journal.pone.0190636

Remize, F., Gaudin, A., Kong, Y., Guzzo, J., Alexandre, H., Krieger-Weber, S., & Guilloux-Benatier, M. (2006). Oenococcus oeni preference for peptides: qualitative and quantitative analysis of nitrogen assimilation. *Archives of Microbiology*, *185*(6), 459–469. https://doi.org/10.1007/s00203-006-0116-6

Ren, Q., Chen, K., & Paulsen, I. T. (2007). TransportDB: a comprehensive database resource for cytoplasmic membrane transport systems and outer membrane channels. *Nucleic Acids Research*, *35*(Database issue), D274-9. https://doi.org/10.1093/nar/gkl925

Renouf, V., Miot-Sertier, C., Strehaiano, P., & Lonvaud-Funel, A. (2006). The wine microbial consortium: a real terroir characteristic. *Journal International Des Sciences de La Vigne et Du Vin*, *40*(4), 209–216.

Renouf, V., Vayssieres, L. C., Claisse, O., & Lonvaud-Funel, A. (2009). Genetic and phenotypic evidence for two groups of Oenococcus oeni strains and their prevalence during winemaking. *Applied Microbiology and Biotechnology*, *83*(1), 85–97. https://doi.org/10.1007/s00253-008-1843-1

Restuccia, D., Loizzo, M., & Spizzirri, U. (2018). Accumulation of Biogenic Amines in Wine: Role of Alcoholic and Malolactic Fermentation. *Fermentation*, *4*(1), 6.

Ribéreau-Gayon, P., Dubourdieu, D., Donèche, B., & Lovaud, A. (2006). *Handbook of Enology Volume 1 The Microbiology of Wine and Vinifications* (2nd ed.). John Wiley & Sons, Ltd.

Richter, H., De Graaf, A. A., Hamann, I., & Unden, G. (2003). Significance of phosphoglucose isomerase for the shift between heterolactic and mannitol fermentation of fructose by Oenococcus oeni. *Archives of Microbiology*, *180*(6), 465–470. https://doi.org/10.1007/s00203-003-0617-5

Richter, H., Vlad, D., & Unden, G. (2001). Significance of pantothenate for glucose fermentation by Oenococcus oeni and for suppression of the erythritol and acetate production. *Archives of Microbiology*, *175*(1), 26–31. https://doi.org/10.1007/s002030000233

Romero, J., Ilabaca, C., Ruiz, M., & Jara, C. (2018). Oenococcus oeni in Chilean Red Wines: Technological and genomic characterization. *Frontiers in Microbiology*, *9*, 90. https://doi.org/10.3389/FMICB.2018.00090

Rosario, D., Benfeitas, R., Bidkhori, G., Zhang, C., Uhlen, M., Shoaie, S., & Mardinoglu, A. (2018). Understanding the representative gut microbiota dysbiosis in metformin-treated Type 2 diabetes patients using genome-scale metabolic modeling. *Frontiers in Physiology*, *9*(JUN), 1–14. https://doi.org/10.3389/fphys.2018.00775

Russell, J. B., & Cook, G. M. (1995). Energetics of bacterial growth : balance of anabolic and catabolic reactions. *Microbiological Reviews*, *59*(1), 48–62.

SAG. (2018). *Informe Ejecutivo Producción de Vinos 2018*. Servicio Agrícola y Ganadero, Chile. https://www.sag.gob.cl/sites/default/files/infocosecha2018.pdf

Saguir, F., & Manca de Nadra, M. C. (1996). Organic acid metabolism under different glucose concentrations of Leuconostoc oenos from wine. *Journal of Applied Bacteriology*, 393–397. https://doi.org/10.1111/j.1365-2672.1996.tb03524.x

Sainz, J., Pizarro, F., Pérez-Correa, J. R., & Agosin, E. (2003). Modeling of yeast metabolism and process dynamics in batch fermentation. *Biotechnology and Bioengineering*, *81*(7), 818–828. https://doi.org/10.1002/bit.10535

Salema, M., Lolkema, J. S., San Romão, M. V., & Loureiro-Dias, M. C. (1996). The proton motive force generated in Leuconostoc oenos by L-malate fermentation. *Journal of Bacteriology*, *178*(11), 3127–3132. https://doi.org/10.1128/jb.178.11.3127-3132.1996

Salema, M., Poolman, B., Lolkema, J. S., Dias, M. C. L., & Konings, W. N. (1994). Uniport of Monoanionic L-malate in Membrane Vesicles from Leuconostoc Oenos. *European Journal of Biochemistry*, *225*(1), 289–295. https://doi.org/10.1111/j.1432-1033.1994.00289.x

Salou, P., Leroy, M. J., Goma, G., & Pareilleux, A. (1991). Influence of pH and malate-glucose ratio on the growth kinetics of Leuconostoc oenos. *Applied Microbiology and Biotechnology*, *36*(1), 87–91. https://doi.org/10.1007/BF00164704

Salou, P., Loubser, P., & Pareilleux, A. (1994). Growth and energetics of

Leuconostoc oenos during cometabolism of glucose with citrate or fructose. *Applied and Environmental Microbiology*, *60*(5), 1459–1466. http://www.pubmedcentral.nih.gov/articlerender.fcgi?artid=201503&tool=pmcentrez&rendertype=abstract

Sánchez, B. J., Pérez-Correa, J. R., & Agosin, E. (2014). Construction of robust dynamic genome-scale metabolic model structures of Saccharomyces cerevisiae through iterative re-parameterization. *Metabolic Engineering*, *25*, 159–173. https://doi.org/10.1016/j.ymben.2014.07.004

Sato, H., Yanagida, F., Shinohara, T., Suzuki, M., Suzuki, K., & Yokotsuka, K. (2001). Intraspecific diversity of Oenococcus oeni isolated during red wine-making in Japan. *FEMS Microbiology Letters*, *202*(1), 109–114. https://doi.org/10.1111/j.1574-6968.2001.tb10788.x

Schümann, C., Michlmayr, H., del Hierro, A. M., Kulbe, K. D., Jiranek, V., Eder, R., & Nguyen, T. H. (2013). Malolactic enzyme from Oenococcus oeni: Heterologous expression in Escherichia coli and biochemical characterization. *Bioengineered*, *4*(3), 147–152. https://doi.org/10.4161/bioe.22988

Schümann, C., Michlmayr, H., Eder, R., del Hierro, A. M., Kulbe, K. D., Mathiesen, G., & Nguyen, T.-H. (2012). Heterologous expression of Oenococcus oeni malolactic enzyme in Lactobacillus plantarum for improved malolactic fermentation. *AMB Express*, *2*(1), 19. https://doi.org/10.1186/2191-0855-2-19

Semon, M. J., Edwards, C. G., Forsyth, D., & Dinn, C. (2001). Inducing malolactic fermentation in Chardonnay musts and wines using different strains of Oenococcus oeni. *Australian Journal of Grape and Wine Research*, *7*(1), 52–59. https://doi.org/10.1111/j.1755-0238.2001.tb00194.x

Shelley, J. C., Cholleti, A., Frye, L. L., Greenwood, J. R., Timlin, M. R., & Uchimaya, M. (2007). Epik: A software program for pKa prediction and protonation state generation for drug-like molecules. *Journal of Computer-Aided Molecular Design*, *21*(12), 681–691. https://doi.org/10.1007/s10822-007-9133-z

Shen, Y., Liu, J., Estiu, G., Isin, B., Ahn, Y.-Y., Lee, D.-S., Barabási, A.-L., Kapatral, V., Wiest, O., & Oltvai, Z. N. (2010). Blueprint for antimicrobial hit discovery targeting metabolic networks. *Proceedings of the National Academy of Sciences USA*, *107*, 1082–1087. https://doi.org/10.1073/pnas.0909181107

Sievers, F., Wilm, A., Dineen, D., Gibson, T. J., Karplus, K., Li, W., Lopez, R., McWilliam, H., Remmert, M., Söding, J., Thompson, J. D., & Higgins, D. G. (2011). Fast, scalable generation of high-quality protein multiple sequence alignments using Clustal Omega. *Molecular Systems Biology*, *7*(539), 1–6. https://doi.org/10.1038/msb.2011.75

Smith, R. L. (1984). Efficient Monte Carlo Procedures for Generating Points Uniformly Distributed over Bounded Regions. *Operations Research*, *32*(6), 1296–1308. https://doi.org/10.1287/opre.32.6.1296

Soffritti, M., Belpoggi, F., Degli Esposti, D., Lambertini, L., Tibaldi, E., & Rigano,

A. (2006). First experimental demonstration of the multipotential carcinogenic effects of aspartame administered in the feed to Sprague-Dawley rats. *Environmental Health Perspectives*, *114*(3), 379–385. https://doi.org/10.1289/ehp.8711

Spettoli, P., Nuti, M. P., & Zamorani, A. (1984). Properties of Malolactic Activity Purified from Leuconostoc oenos ML34 by Affinity Chromatography. *Applied and Environmental Microbiology*, *48*(4), 900–901. http://www.pubmedcentral.nih.gov/articlerender.fcgi?artid=241643&tool=pmcentrez&rendertype=abstract

Stefanovic, E., Fitzgerald, G., & McAuliffe, O. (2017). Advances in the genomics and metabolomics of dairy lactobacilli: A review. *Food Microbiology*, *61*, 33–49. https://doi.org/10.1016/j.fm.2016.08.009

Sternes, P. R., & Borneman, A. R. (2016). Consensus pan-genome assembly of the specialised wine bacterium Oenococcus oeni. *BMC Genomics*, *17*(1), 308. https://doi.org/10.1186/s12864-016-2604-7

Sternes, P. R., Costello, P. J., Chambers, P. J., Bartowsky, E. J., & Borneman, A. R. (2017). Whole transcriptome RNAseq analysis of Oenococcus oeni reveals distinct intra-specific expression patterns during malolactic fermentation, including genes involved in diacetyl metabolism. *International Journal of Food Microbiology*, *257*(June), 216–224. https://doi.org/10.1016/j.ijfoodmicro.2017.06.024

Sumby, K. M., Grbin, P. R., & Jiranek, V. (2010). Microbial modulation of aromatic esters in wine: Current knowledge and future prospects. *Food Chemistry*, *121*(1), 1–16. https://doi.org/10.1016/j.foodchem.2009.12.004

Sun, S. Y., Gong, H. S., Liu, W. L., & Jin, C. W. (2016). Application and validation of autochthonous Lactobacillus plantarum starter cultures for controlled malolactic fermentation and its influence on the aromatic profile of cherry wines. *Food Microbiology*, *55*, 16–24. https://doi.org/10.1016/j.fm.2015.11.016

Suomalainen, H., & Lehtonen, M. (1979). The production of aroma compounds by yeast. *Journal of the Institute of Brewing*, *85*(3), 149–156. https://doi.org/10.1002/j.2050-0416.1979.tb06846.x

Suriano, S., Savino, M., Basile, T., Tarricone, L., & Di Gennaro, D. (2015). Management of malolactic fermentation and influence on chemical composition of Aglianico red wines. *Italian Journal of Food Science*, *27*, 310–319. https://doi.org/10.14674/1120-1770/ijfs.v273

Swiegers, J. H., Bartowsky, E. J., Henschke, P. A., & Pretorius, I. S. (2005). Yeast and bacterial modulation of wine aroma and flavour. *Australian Journal of Grape and Wine Research*, *11*(2), 139–173. https://doi.org/10.1111/j.1755-0238.2005.tb00285.x

Teixeira, H., Gonçalves, M. G., Rozès, N., Ramos, A., & San Romão, M. V. (2002). Lactobacillic acid accumulation in the plasma membrane of Oenococcus oeni: A

response to ethanol stress? *Microbial Ecology*, *43*(1), 146–153. https://doi.org/10.1007/s00248-001-0036-6

Terrade, N., & Mira de Orduña, R. (2009). Determination of the essential nutrient requirements of wine-related bacteria from the genera Oenococcus and Lactobacillus. *International Journal of Food Microbiology*, *133*(1–2), 8–13. https://doi.org/10.1016/j.ijfoodmicro.2009.03.020

Teusink, B., van Enckevort, F. H. J., Francke, C., Wiersma, A., Wegkamp, A., Smid, E. J., & Siezen, R. J. (2005). In Silico Reconstruction of the Metabolic Pathways of Lactobacillus plantarum: Comparing Predictions of Nutrient Requirements with Those from Growth Experiments. *Applied and Environmental Microbiology*, *71*(11), 7253–7262. https://doi.org/10.1128/AEM.71.11.7253

Teusink, B., Wiersma, A., Molenaar, D., Francke, C., de Vos, W. M., Siezen, R. J., & Smid, E. J. (2006). Analysis of growth of Lactobacillus plantarum WCFS1 on a complex medium using a genome-scale metabolic model. *The Journal of Biological Chemistry*, *281*(52), 40041–40048. https://doi.org/10.1074/jbc.M606263200

Thiele, I., & Palsson, B. Ø. (2010). A protocol for generating a high-quality genome-scale metabolic reconstruction. *Nature Protocols*, *5*(1), 93–121. https://doi.org/10.1038/nprot.2009.203

Tita, O., Bulancea, M., Pavelescu, D., & Martin, L. (2006). The Role of the Organic Acids in the Evolution of the Wine. *CHISA 2006–17th International Congress of Chemical and Process Engineering*, 27–31.

Toledo, M. S., Armijo, P., Godoy, L., Saavedra, J., & Ganga, M. A. (2018). Determination of Effects of Genetic Diversity of Oenococcus oeni and Physicochemical Characteristics on Malolactic Fermentation Across Chilean Vineyards, using Multivariate Methods. *Journal of Pure and Applied Microbiology*, *12*(1), 15–22. https://doi.org/10.22207/JPAM.12.1.03

Torriani, S., Felis, G. E., & Fracchetti, F. (2011). Selection criteria and tools for malolactic starters development: an update. *Annals of Microbiology*, *61*(1), 33–39. https://doi.org/10.1007/s13213-010-0072-x

Tourdot-Maréchal, R., Fortier, L. C., Guzzo, J., Lee, B., & Diviès, C. (1999). Acid sensitivity of neomycin-resistant mutants of Oenococcus oeni: A relationship between reduction of ATPase activity and lack of malolactic activity. *FEMS Microbiology Letters*, *178*(2), 319–326. https://doi.org/10.1016/S0378-1097(99)00377-8

Tracey, R. P., & Britz, T. J. (1989a). The effect of amino acids on malolactic fermentation by Leuconostoc oenos. *Journal of Applied Bacteriology*, *67*, 589–595.

Tracey, R. P., & Britz, T. J. (1989b). Cellular fatty acid composition of Leuconostoc oenos. *Journal of Applied Bacteriology*, *66*(5), 445–456. https://doi.org/10.1111/j.1365-2672.1989.tb05114.x

Tracey, R. P., & van Rooyen, T. J. (1988). Utilization of glucose, fructose and malic acid by malolactic bacteria: effect of ethanol and formation of mannitol and volatile acids. *Journal of Applied Bacteriology*, *65*(2), 113–118. https://doi.org/10.1111/j.1365-2672.1988.tb01499.x

Tristezza, M., di Feo, L., Tufariello, M., Grieco, F., Capozzi, V., Spano, G., Mita, G., & Grieco, F. (2016). Simultaneous inoculation of yeasts and lactic acid bacteria: Effects on fermentation dynamics and chemical composition of Negroamaro wine. *LWT - Food Science and Technology*, *66*, 406–412. https://doi.org/10.1016/j.lwt.2015.10.064

Tsakalidou, E., & Papadimitriou, K. (Eds.). (2011). *Stress responses of lactic acid bacteria*. Springer Science & Business Media.

Tzamali, E., Poirazi, P., & Tollis, I. G. (2011). A computational exploration of bacterial metabolic diversity identifying metabolic interactions and growth-efficient strain communities. *BMC Systems Biology*, *5*(167), 1–15. https://doi.org/10.1186/1752-0509-5-167.

Ugliano, M., & Moio, L. (2005). Changes in the concentration of yeast-derived volatile compounds of red wine during malolactic fermentation with four commercial starter cultures of Oenococcus oeni. *Journal of Agricultural and Food Chemistry*, *53*(26), 10134–10139. https://doi.org/10.1021/jf0514672

van de Guchte, M., Serror, P., Chervaux, C., Smokvina, T., Ehrlich, S., & Maguin, E. (2002). Stress responses in lactic acid bacteria. *Antonie van Leeuwenhoek*, *82*, 187–216. https://doi.org/10.1023/A:1020631532202

van der Ark, K. C. H., van Heck, R. G. A., Martins Dos Santos, V. A. P., Belzer, C., & de Vos, W. M. (2017). More than just a gut feeling: constraint-based genome-scale metabolic models for predicting functions of human intestinal microbes. *Microbiome*, *5*(78), 1–13. https://doi.org/10.1186/s40168-017-0299-x

Varela, C. A., Agosin, E., Baez, M. E., Klapa, M., & Stephanopoulos, G. (2003). Metabolic flux redistribution in Corynebacterium glutamicum in response to osmotic stress. *Applied Microbiology and Biotechnology*, *60*(5), 547–555. https://doi.org/10.1007/s00253-002-1120-7

Vargas, F. A., Pizarro, F., Pérez-Correa, J. R., & Agosin, E. (2011). Expanding a dynamic flux balance model of yeast fermentation to genome-scale. *BMC Systems Biology*, *5*(1), 75. https://doi.org/10.1186/1752-0509-5-75

Vaudano, E., Costantini, A., & Garcia-Moruno, E. (2016). An event-specific method for the detection and quantification of ML01, a genetically modified Saccharomyces cerevisiae wine strain, using quantitative PCR. *International Journal of Food Microbiology*, *234*, 15–23. https://doi.org/10.1016/j.ijfoodmicro.2016.06.017

Veith, N., Solheim, M., van Grinsven, K. W. A., Olivier, B. G., Levering, J., Grosseholz, R., Hugenholtz, J., Holo, H., Nes, I., Teusink, B., & Kummer, U. (2015). Using a genome-scale metabolic model of Enterococcus faecalis V583 to

assess amino acid uptake and its impact on central metabolism. *Applied and Environmental Microbiology*, *81*(5), 1622–1633. https://doi.org/10.1128/AEM.03279-14

Verce, M., De Vuyst, L., & Weckx, S. (2020). The metagenome-assembled genome of Candidatus Oenococcus aquikefiri from water kefir represents the species Oenococcus sicerae. *Food Microbiology*, *88*(September 2019), 103402. https://doi.org/10.1016/j.fm.2019.103402

Verouden, M. P. H., Notebaart, R. A., Westerhuis, J. A., van der Werf, M. J., Teusink, B., & Smilde, A. K. (2009). Multi-way analysis of flux distributions across multiple conditions. *Journal of Chemometrics*, *23*(7–8), 406–420. https://doi.org/10.1002/cem.1238

Versari, A., Parpinello, G. P., & Cattaneo, M. (1999). Leuconostoc oenos and malolactic fermentation in wine: a review. *Journal of Industrial Microbiology & Biotechnology*, *23*, 447–455. http://www.springerlink.com/index/8M7UKLWQNKU3XK0E.pdf

Vigentini, I., Praz, A., Domeneghetti, D., Zenato, S., Picozzi, C., Barmaz, A., & Foschino, R. (2016). Characterization of malolactic bacteria isolated from Aosta Valley wines and evidence of psychrotrophy in some strains. *Journal of Applied Microbiology*, *120*(4), 934–945. https://doi.org/10.1111/jam.13080

Volschenk, H., van Vuuren, H. J. J., & Viljoen-Bloom, M. (2017). Malic Acid in Wine: Origin, Function and Metabolism during Vinification. *South African Journal of Enology & Viticulture*, *27*(2), 123–136. https://doi.org/10.21548/27-2-1613

Volschenk, H., Viljoen, M., Grobler, J., Bauer, F., Lonvaud-Funel, A., Denayrolles, M., Subden, R. E., & Van Vuuren, H. J. J. (1997). Malolactic Fermentation in Grape Musts by a Genetically Engineered Strain of Saccharomyces cerevisiae. *American Journal of Enology and Viticulture*, *48*(2), 193–197. http://www.ajevonline.org/content/48/2/193

von Kamp, A., Thiele, S., Hädicke, O., & Klamt, S. (2017). Use of CellNetAnalyzer in biotechnology and metabolic engineering. *Journal of Biotechnology*, *261*, 221–228. https://doi.org/https://doi.org/10.1016/j.jbiotec.2017.05.001

Wagner, N., Tran, Q. H., Richter, H., Selzaer, P. M., & Unden, G. (2005). Pyruvate fermentation by Oenococcus oeni and Leuconostoc mesenteroides and role of pyruvate dehydrogenase in anaerobic fermentation. *Applied and Environmental Microbiology*, *71*(9), 4966–4971. https://doi.org/10.1128/AEM.71.9.4966

Wang, P., Li, A., Dong, M., & Fan, M. (2014). Induction, purification and characterization of malolactic enzyme from Oenococcus oeni SD-2a. *European Food Research and Technology*, *239*(5), 827–835. https://doi.org/10.1007/s00217-014-2276-y

Wells, a, & Osborne, J. P. (2012). Impact of acetaldehyde- and pyruvic acid-bound sulphur dioxide on wine lactic acid bacteria. *Letters in Applied Microbiology*,

54(3), 187–194. https://doi.org/10.1111/j.1472-765X.2011.03193.x

Williams, S. A., Hodges, R. A., & Strike, T. L. (1984). Cloning the gene for the malolactic fermentation of wine from Lactobacillus delbrueckii in Escherichia coli and yeasts. *Applied and Environmental Microbiology*, *47*(2), 288–293.

Wintermute, E. H., & Silver, P. A. (2010). Emergent cooperation in microbial metabolism. *Molecular Systems Biology*, *6*(407), 1–7. https://doi.org/10.1038/msb.2010.66

Wu, C., Huang, J., & Zhou, R. (2014). Progress in engineering acid stress resistance of lactic acid bacteria. *Applied Microbiology and Biotechnology*, *98*(3), 1055–1063. https://doi.org/10.1007/s00253-013-5435-3

Xu, N., Liu, J., Ai, L., & Liu, L. (2015). Reconstruction and analysis of the genome-scale metabolic model of Lactobacillus casei LC2W. *Gene*, *554*(2), 140–147. https://doi.org/10.1016/j.gene.2014.10.034

Xu, N., Ye, C., & Liu, L. (2018). Genome-scale biological models for industrial microbial systems. *Applied Microbiology and Biotechnology*, *102*(8), 3439–3451. https://doi.org/10.1007/s00253-018-8803-1

Yabaya, A., Bobai, M., & Adebayo, L. R. (2016). Production of wine from fermentation of Vitis vinifera (grape) juice using Saccharomyces cerevisiae strain isolated from palm wine. *International Journal of Information Research and Review*, *3*(10), 2834–2840.

Yizhak, K., Chaneton, B., Gottlieb, E., & Ruppin, E. (2015). Modeling cancer metabolism on a genome scale. *Molecular Systems Biology*, *11*(6), 817–817. https://doi.org/10.15252/msb.20145307

Zallot, R., Oberg, N., & Gerlt, J. A. (2019). The EFI Web Resource for Genomic Enzymology Tools: Leveraging Protein, Genome, and Metagenome Databases to Discover Novel Enzymes and Metabolic Pathways. *Biochemistry*, *58*(41), 4169–4182. https://doi.org/10.1021/acs.biochem.9b00735

Zamora, F. (2009). Biochemistry of Alcoholic Fermentation . In M. V. Moreno-Arribas & M. C. Polo (Eds.), *Wine Chemistry and Biochemistry* (pp. 3–26). Springer. https://doi.org/10.1097/mpg.0000000000001308

Zapparoli, G., Tosi, E., Azzolini, M., Vagnoli, P., & Krieger-Weber, S. (2009). Bacterial inoculation strategies for the achievement of Malolactic fermentation in high-alcohol wines. *South African Journal of Enology and Viticulture*, *30*(1), 49–55. https://doi.org/10.21548/30-1-1424

Zapparoli, G., Tosi, E., & Krieger, S. (2006). Influence of the pH of Chardonnay must on malolactic fermentation induced by bacteria co-inoculated with yeasts. *Vitis - Journal of Grapevine Research*, *45*(4), 197–198.

Zé-Zé, L., Chelo, I. M., & Tenreiro, R. (2008). Genome organization in “Oenococcus oeni” strains studied by comparison of physical and genetic maps. *International Microbiology*, *11*, 237–244. https://doi.org/10.2436/20.1501.01.67

Zé-Zé, L., Tenreiro, R., Brito, L., Santos, M. A., & Paveia, H. (1998). Physical map of the genome of Oenococcus oeni PSU-1 and localization of genetic markers. *Microbiology*, *144*, 1145–1156. http://mic.sgmjournals.org/content/144/5/1145.short

Zé-Zé, L., Tenreiro, R., & Paveia, H. (2000). The Oenococcus oeni genome: Physical and genetic mapping of strain GM and comparison with the genome of a "divergent" strain, PSU- 1. *Microbiology*, *146*(12), 3195–3204. https://doi.org/10.1099/00221287-146-12-3195

Zhang, D., & Lovitt, R. (2006). Performance assessment of malolactic fermenting bacteria Oenococcus oeni and Lactobacillus brevis in continuous culture. *Applied Microbiology and Biotechnology*, *69*(6), 658–664. https://doi.org/10.1007/s00253-005-0021-y

Zhang, D. S., & Lovitt, R. W. (2005). Studies on growth and metabolism of Oenococcus oeni on sugars and sugar mixtures. *Journal of Applied Microbiology*, *99*(3), 565–572. https://doi.org/10.1111/j.1365-2672.2005.02628.x

Zhang, G. (2013). The essential amino acids requirements for Oenococcus Oeni growth and organic acids metabolism. *African Journal of Microbiology Research*, *7*(16), 1591–1597. https://doi.org/10.5897/AJMR12.2235

Zheng, J., Wittouck, S., Salvetti, E., Franz, C. M. A. P., Harris, H. M. B., Mattarelli, P., O'toole, P. W., Pot, B., Vandamme, P., Walter, J., Watanabe, K., Wuyts, S., Felis, G. E., Gänzle, M. G., & Lebeer, S. (2020). A taxonomic note on the genus Lactobacillus: Description of 23 novel genera, emended description of the genus Lactobacillus beijerinck 1901, and union of Lactobacillaceae and Leuconostocaceae. *International Journal of Systematic and Evolutionary Microbiology*, *70*(4), 2782–2858. https://doi.org/10.1099/ijsem.0.004107

Zoecklein, B. W., Fugelsang, K. C., Gump, B. H., & Nury, F. S. (1999). Microbiology of Winemaking. In *Wine Analysis and Production* (pp. 280–302). Springer Science+Business Media. https://doi.org/http://dx.doi.org/10.1016/B978-0-12-384730-0.00356-6

7. SUPPLEMENTARY MATERIALS

S 2-1 Final restriction of iSM454 model.

Table 7-1: Final restriction of iSM424 model.

Reaction ID	Lower bound	Upper Bound
_R__lipoate_ex_	0	0
biotin_ex_	0	1000
folate_ex_	0	0
panthothenate_ex_	0	1000
thiamin_ex_	0	1000
nicotinamida_RNP_ex_	0	1000
riboflavin_ex_	0	1000
b_D_fructose_ex_	0	0
b_D_ribopyranose_ex_	0	1000
b_D_ribofuranose_ex_	0	0
D_mannose_ex_	0	0
D_xylose_ex_	0	0
cellobiose_ex_	0	0
a_D_glucose_ex_	0	0
b_D_galactose_ex_	0	0
a_D_galactose_ex_	0	0
melibiose_ex_	0	0
D_mannitol_ex_	0	1000
citrate_ex_	0	0
_R__lactate_ex_	0	1000
_S__lactate_ex_	0	1000
_S__malate_ex_	0	0
butanediol_ex_	0	1000
adenine_ex_	0	1000
guanine_ex_	0	1000
cytosine_ex_	0	1000
uracil_ex_	0	1000
xanthine_ex_	0	1000
L_ascorbate_ex_	0	0
D_gluconate_ex_	0	0
diacetyl_ex_	0	1000
trehalose_ex_	0	0
b_D_glucose_ex_	0	0
L_Arg_ex_	0	1000

L_Asn_ex_	0	1000
L_Ala_ex_	0	1000
L_Asp_ex_	0	1000
L_Cys_ex_	0	1000
L_Glu_ex_	0	1000
L_Gln_ex_	0	1000
Gly_ex_	0	1000
L_His_ex_	0	1000
L_Ile_ex_	0	1000
L_Leu_ex_	0	1000
L_Lys_ex_	0	1000
L_Met_ex_	0	1000
L_Phe_ex_	0	1000
L_Pro_ex_	0	1000
L_Ser_ex	0	1000
L_Thr_ex_	0	1000
L_Tyr_ex_	0	1000
L_Trp_ex_	0	1000
L_Val_ex_	0	1000
pyridoxine_ex_	0	1000
pyridoxal_ex_	0	0
pyridoxamine_ex_	0	0
SO4_ex_	0	1000
P_ex_	0	1000
oleate_ex_	0	1000
ethanol_ex_	0	1000
water_ex_	-1000	1000
oxygen_ex_	0	1000
CO2__ex_	0	1000
ammonium_ex_	0	0
acetate_ex_	0	1000
oligopeptide_ex_	0	0
glycerol_ex_	0	0
galactitol_ex_	0	0
L_arabinose_ex_	0	0
thymine_ex_	0	1000
Mn_ex_	0	1000
erythritol_ex_	0	1000
H+_ex	0	0
pyruvate_ex_	0	0

succinate_ex_	0	1000
lactate(R or D)_ex_	0	1000
3,5-dimethoxytoluene_ex_	0	1000
fucose_ex_	0	0
cyanate_ex_	0	0
4-aminobutanoate_ex_	0	0
Cd2+_ex_	0	0
K+_ex_	0	0
Cl_ex_	0	0
Mg2+_ex_	0	0
Fe2+_ex_	0	0
N-acetyl galactosamine_ex_	0	0
Na+_ex_	0	0
Ni2+_ex_	0	0
NO3_ex	0	0
Co2+_ex_	0	0
Zn2+_ex_	0	0
spermidine_ex_	0	1000
[FeS] cluster_ex_	0	0
Cu2+_ex_	0	0
(cellulose)n_ex_	0	0
taurine_ex_	0	0
sucrose_ex_	0	0
HCO3_ex_	0	0
dextran (glucose)n_ex_	0	1000
putrescine_ex_	0	1000
(cellulose)n-1_ex_	0	1000
heteropolysaccharide_ex_	0	0
H2S_exchange	0	1000

S 2-2 Genome-Scale Metabolic Model of *Oenococcus oeni*

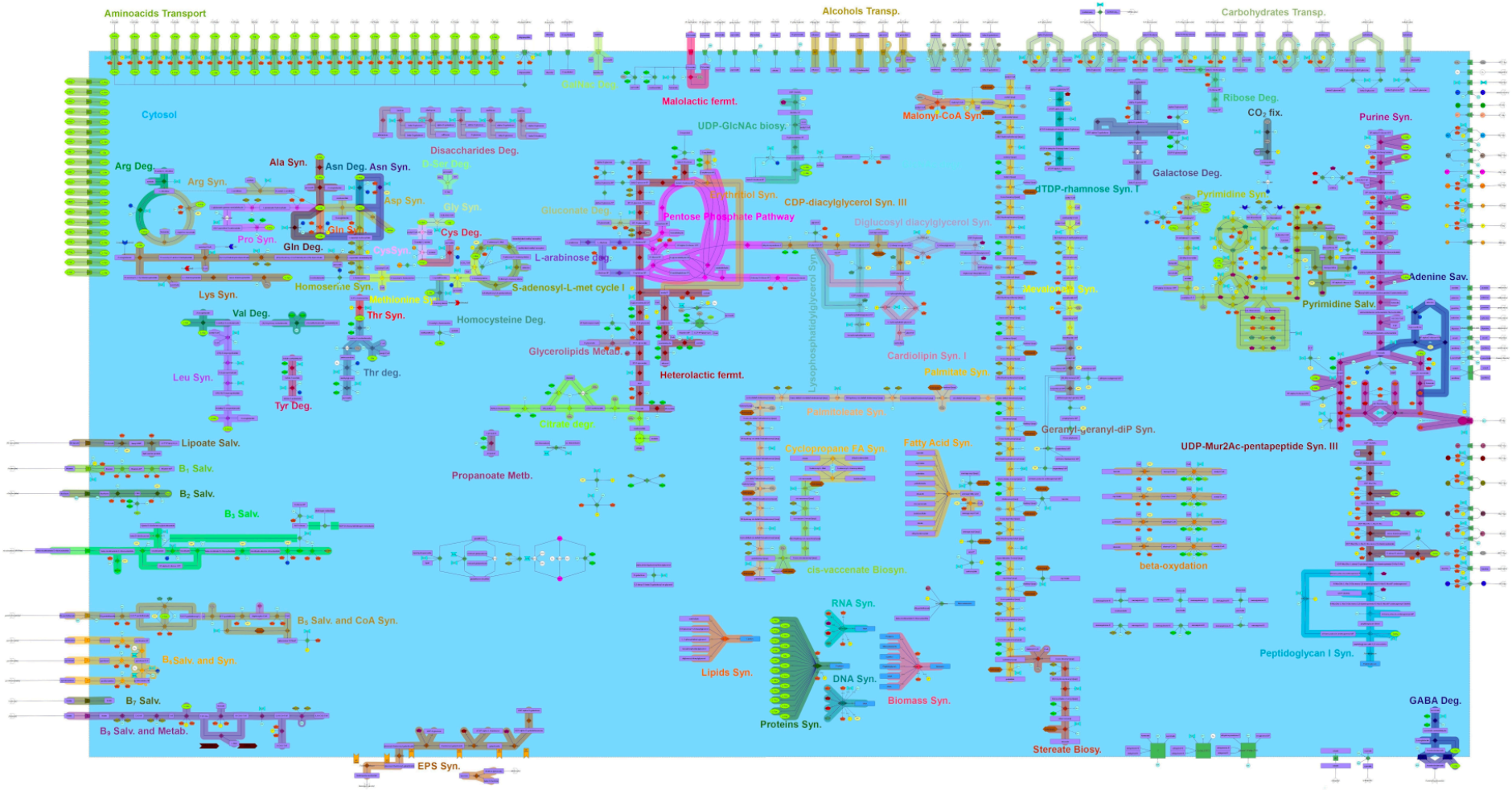

Figure 7-1: Genome-Scale Metabolic Model of *O. oeni* strain PSU-1. The metabolic map was developed using Omix 1.8 (Droste et al., 2011).

S 2-3 Connectivity of the iSM454 model

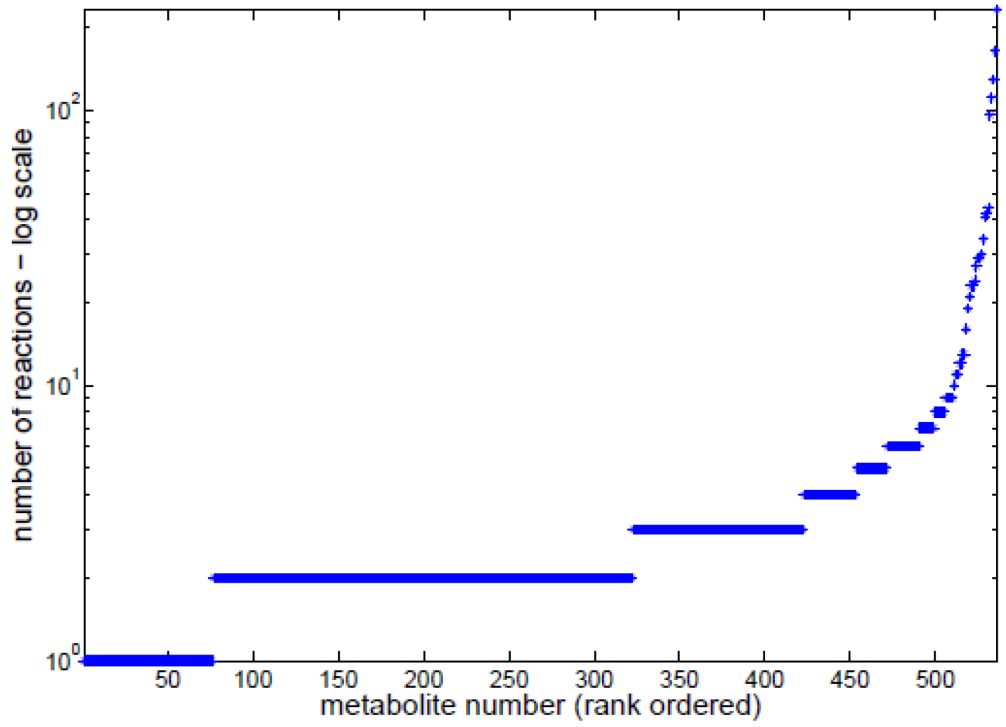

Figure 7-2: Connectivity of the iSM454 model. This figure shows in the x-axis the 536 metabolites of the model; ranked according to the numbre of connections they have (y-axis). Connections refers to the number of reactions in wich a metabolite participes.

S 3-1 Reactions contained in the reduced version of the iSM454 model.

Table 7-2: Reactions contained in the reduced version of the iSM454 model.

'_2PGADEHYDRAT_RXN'	'erythritol_ex_'
'PHOSACETYLTRANS_RXN'	'CO2__ex_'
'ACETATEKIN_RXN'	'oxygen_ex_'
'PEPDEPHOS_RXN'	'LCYSDESULF_RXN'
'GLUCOKIN_RXN'	'CYSTATHIONINE_BETA_LYASE_RXN'
'PHOSGLYPHOS_RXN'	'METHYL_GLYOXAL_DEHYDROG_RXN'
'PGLUCISOM_RXN'	'growth_rate'
'GAPOXNPHOSPHN_RXN'	'TRANS_ERITHRITOL_RXN'
'_3PGAREARR_RXN'	'TRANS_RXNK9E_520'
'GLU6PDEHYDROG_RXN'	'TRANS_RXNK9E_529'
'PHOSPHOKETOLASE_RXN'	'TRANS_RXNK9E_539'
'RXN66_3'	'TRANS_RXNK9E_540'
'ALCOHOL_DEHYDROG_RXN'	'TRANS_RXNK9E_542'
'DLACTDEHYDROGNADRXN'	'TRANS_RXNK9E_541'
'ACETALD_DEHYDROG_RXN'	'TRANS_RXNK9E_463'
'_6PGLUCONOLACT_RXN'	'TRANS_RXNK9E_524'
'ALDOSE_1_EPIMERASE_RXN'	'TRANSRXNK9E525'
'RXN_9952'	'TRANS_RXNK9E_434'
'ACETOLACTSYN_RXN'	'TRANS_RXNK9E_354'
'ACETOLACTATE_DECARBOXYLASE_RXN'	'TRANS_RXNK9E_535'
'RXN_11036'	'TRANS_RXNK9E_531'
'RR_BUTANEDIOL_DEHYDROGENASE_RXN'	'TRANS_RXNK9E_533'
'RXN_6081'	'TRANS_RXNK9E_530'
'CITLY_RXN'	'TRANS_RXNK9E_431'
'OXALODECARB_RXN'	'L_Cys_ex_'
'Mannitol_RXN'	'TRANS_RXNK9E_474'
'ERITHRITIOL_RXN'	'TRANS_RXNK9E_492'
'PHOSPHOKETOLASE2_RXN'	'L_Ser_ex_'
'_1_2_3_3_RXN'	'TRANS_RXNK9E_481'
'MALATE_DEH_RXN'	'TRANS_RXNK9E_500'
'FUMHYDR_RXN'	'L_Thr_ex_'
'PYRUVDEH_RXN'	'TRANS_RXNK9E_482'
'RXNK9E_163'	'TRANS_RXNK9E_490'
'TRANSALDOL-RXN'	'H2S_transport'
'PRPPSYN_RXN'	'H2S_exchange'
'RIBULP3EPIM_RXN'	'water_ex_'
'_1TRANSKETO_RXN'	'TRANS_RXNK9E_519'
'RIB5PISOM_RXN'	'ammonium_ex_'
'b_D_fructose_ex_'	'TRANS_RXNK9E_415'
'a_D_glucose_ex_'	'ATPSYN_RXN'
'D_mannitol_ex_'	'RXNK9E_225'
'citrate_ex_'	'CYSTATHIONINE_BETA_SYNTHASE_RXN'
'_R__lactate_ex_'	'AMACETOXID_RXN'
'_S__lactate_ex_'	'THREOSPON_RXN'
'_S__malate_ex_'	'THREODEHYD_RXN'
'butanediol_ex_'	'b_D_glucose_ex_'
'diacetyl_ex_'	'TRANS_RXNK9E_536'
'ethanol_ex_'	'TRANS_RXNK9E_534'
'ammonium_ex_'	'H__ex'
'acetate_ex_'	

S 3-2 Consume of fructose and glucose, and production of mannitol and erythritol.

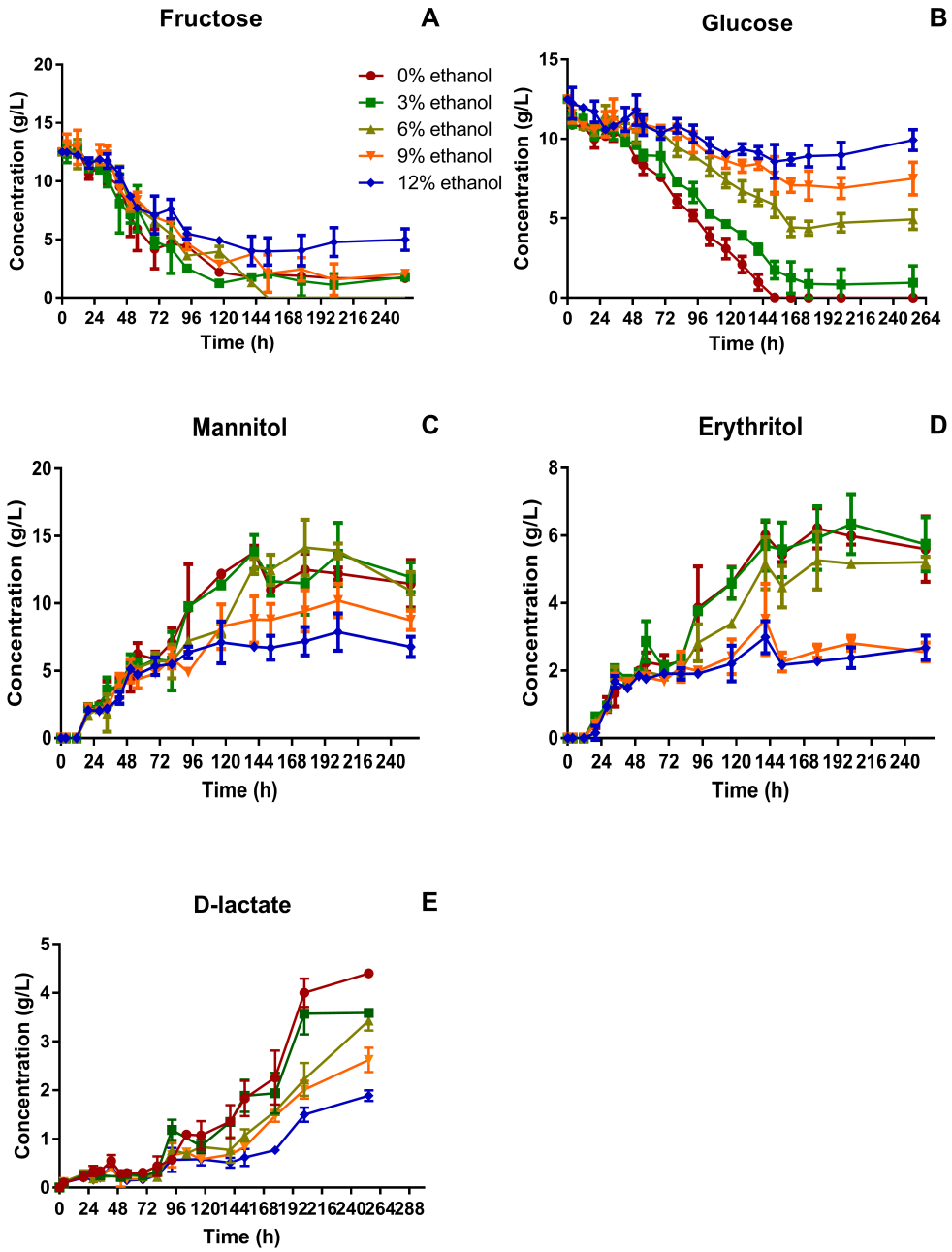

Figure 7-3: Time course of fructose consumption and metabolites production by *O. oeni* PSU-1, cultured at different ethanol concentrations. (A) Fructose consumption. (B) Glucose consumption. (C) Mannitol production. (D) Erythritol production and (E) D-lactate production.

S 3-3 Consume of L-malate and citrate, and production of L-lactate and acetate

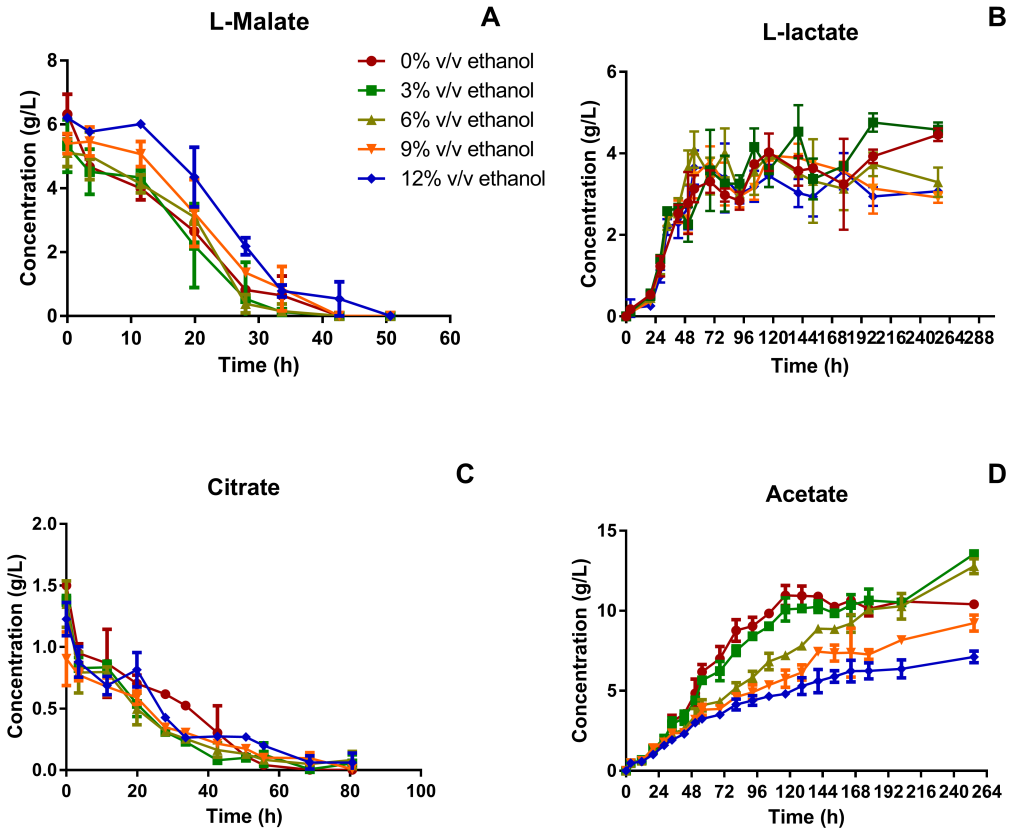

Figure 7-4: Time course of some of substrates and metabolites produced mainly by *O. oeni* PSU-1, cultured at different ethanol concentrations. (A) L-malate consumption. (B) L-lactate production. (C) Citrate consumption and (D) acetate production.

S 3-4 Specific amino acids consumption rate

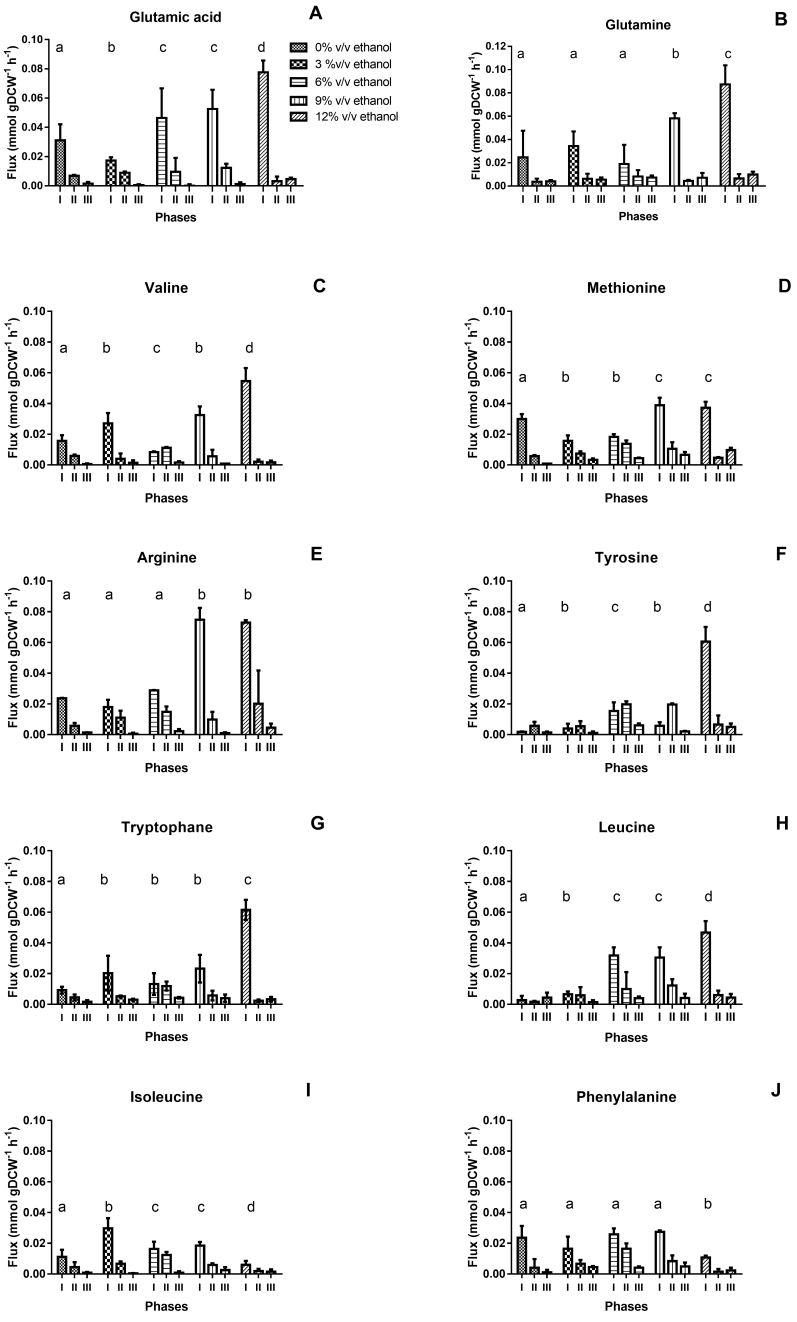

Figure 7-5: Specific amino acids consumption rate by *O. oeni* PSU-1, during cultivation under increasing ethanol contents. (A) Glutamic acid. (B) Glutamine. (C) Valine. (D) Methionine. (E) Arginine. (F) Tyrosine. (G) Tryptophan. (H) Leucine. (I) Isoleucine and (J) Phenylalanine. Statistical analysis only was performed in phase I and shared letters indicate no significant difference (Mood test, $p < 0.05$).

S 3-5 Sensitivity analisis of NGAM estimation

			_S__malate_ex_	lactate(R_or_D)_ex_	citrate_ex_	acetate_ex_	a_D_glucose_ex_	b_D_fructose_ex_	D_mannitol_ex_
Ethanol 0%	**phase 1**	**1%**	0,115	0,097	0,09	0,108	0,132	0,153	0,015
		-1%	0,079	0,098	0,104	0,086	0,062	0,041	0,179
	phase 2	**1%**	0,157	0,158	0,157	0,162	0,167	0,162	0,143
		-1%	0,157	0,157	0,157	0,152	0,148	0,152	0,172
	phase 3	**1%**	0,328	0,328	0,328	0,329	0,338	0,329	0,325
		-1%	0,328	0,329	0,328	0,328	0,318	0,328	0,331
Ethanol 3%	**phase 1**	**1%**	0,329	0,307	0,301	0,319	0,341	0,364	0,21
		-1%	0,286	0,308	0,314	0,296	0,274	0,251	0,406
	phase 2	**1%**	0,961	0,963	0,961	0,971	0,977	0,974	0,936
		-1%	0,961	0,96	0,961	0,951	0,945	0,948	0,986
	phase 3	**1%**	0,983	0,985	0,983	0,985	0,996	0,987	0,983
		-1%	0,983	0,982	0,983	0,982	0,97	0,98	0,983
Ethanol 6%	**phase 1**	**1%**	0,269	0,245	0,238	0,254	0,284	0,29	0,159
		-1%	0,221	0,245	0,253	0,236	0,206	0,2	0,331
	phase 2	**1%**	0,579	0,58	0,579	0,583	0,584	0,588	0,568
		-1%	0,579	0,578	0,579	0,575	0,574	0,57	0,59
	phase 3	**1%**	0,705	0,705	0,705	0,707	0,711	0,707	0,693
		-1%	0,705	0,704	0,705	0,702	0,698	0,702	0,716
Ethanol 9%	**phase 1**	**1%**	0,963	0,936	0,931	0,946	0,973	1,003	0,825
		-1%	0,91	0,937	0,942	0,927	0,9	0,87	1,048
	phase 2	**1%**	1,333	1,334	1,333	1,336	1,335	1,341	1,329
		-1%	1,333	1,332	1,333	1,329	1,331	1,324	1,337
	phase 3	**1%**	1,888	1,888	1,888	1,892	1,894	1,892	1,869
		-1%	1,888	1,887	1,888	1,883	1,881	1,883	1,907
Ethanol 12%	**phase 1**	**1%**	1,683	1,655	1,647	1,665	1,691	1,714	1,562
		-1%	1,628	1,656	1,664	1,646	1,62	1,596	1,749
	phase 2	**1%**	1,271	1,271	1,271	1,279	1,27	1,26	1,271
		-1%	1,271	1,271	1,271	1,263	1,272	1,282	1,271
	phase 3	**1%**	1,292	1,292	1,292	1,318	infeasible	infeasible	1,32
		-1%	1,292	1,292	1,292	infeasible	1,316	1,336	infeasible

Table 7-3: Sensitivity analysis of NGAM estimation with respect to the fixed specific consumption/production rates of compounds during growth of *O.oeni* PSU-1 at different ethanol concentrations in maxOeno medium.

*(continuation)

			L_Cys_ex_	L_Ser_ex_	L_Thr_ex_	L_Phe_ex_	L_Val_ex_	ethanol_ex_	_S__lactate_ex_	min	max
Ethanol 0%	**phase 1**	**1%**	0,097	0,097	0,097	0,063	0,063	0,09	0,094	0,015	0,153
		-1%	0,097	0,097	0,097	0,063	0,063	0,105	0,1	0,041	0,179
	phase 2	**1%**	0,157	0,157	0,157	0,157	0,182	0,157	0,158	0,143	0,182
		-1%	0,157	0,157	0,157	0,157	0,182	0,157	0,157	0,148	0,182
	phase 3	**1%**	0,328	0,328	0,328	0,271	0,328	0,325	0,328	0,271	0,338
		-1%	0,328	0,328	0,328	0,271	0,328	0,332	0,328	0,271	0,337
Ethanol 3%	**phase 1**	**1%**	0,308	0,308	0,308	0,301	0,301		0,304	0,21	0,364
		-1%	0,308	0,308	0,307	0,301	0,301		0,311	0,251	0,406
	phase 2	**1%**	0,961	0,961	0,961	1,044	1,044		0,961	0,936	1,044
		-1%	0,961	0,961	0,961	1,044	1,044		0,961	0,945	1,044
	phase 3	**1%**	0,983	0,983	0,983	1,297	1,297		0,983	0,968	1,297
		-1%	0,983	0,983	0,983	1,297	1,297		0,983	0,97	1,297
Ethanol 6%	**phase 1**	**1%**	0,245	0,245	0,245	0,51	0,51		0,241	0,159	0,51
		-1%	0,245	0,245	0,245	0,51	0,51		0,249	0,2	0,51
	phase 2	**1%**	0,579	0,579	0,579	1,253	1,253		0,579	0,568	1,253
		-1%	0,579	0,579	0,579	1,253	1,253		0,579	0,57	1,253
	phase 3	**1%**	0,705	0,705	0,705	1,322	1,322		0,705	0,693	1,322
		-1%	0,705	0,704	0,705	1,322	1,322		0,705	0,698	1,322
Ethanol 9%	**phase 1**	**1%**	0,937	0,937	0,937	1,052	1,052		0,932	0,825	1,052
		-1%	0,936	0,936	0,936	1,052	1,052		0,94	0,87	1,052
	phase 2	**1%**	1,333	1,333	1,333	2,222	2,222		1,334	1,327	2,222
		-1%	1,332	1,333	1,333	2,222	2,222		1,332	1,324	2,222
	phase 3	**1%**	1,888	1,888	1,888	2,782	2,782		1,889	1,869	2,782
		-1%	1,888	1,888	1,888	2,782	2,782		1,886	1,881	2,782
Ethanol 12%	**phase 1**	**1%**	1,656	1,656	1,656	1,741	1,741		1,651	1,562	1,741
		-1%	1,655	1,655	1,655	1,741	1,741		1,66	1,596	1,749
	phase 2	**1%**	1,271	1,271	1,271	2,492	2,492		1,272	1,26	2,492
		-1%	1,271	1,271	1,271	2,492	2,492		1,27	1,263	2,492
	phase 3	**1%**	1,292	1,292	1,292	3,114	3,114		1,292	1,292	3,114
		-1%	1,292	1,292	1,292	3,114	3,114		1,292	1,29	3,114

S 4-1 Structural stability of the model after 50 ns

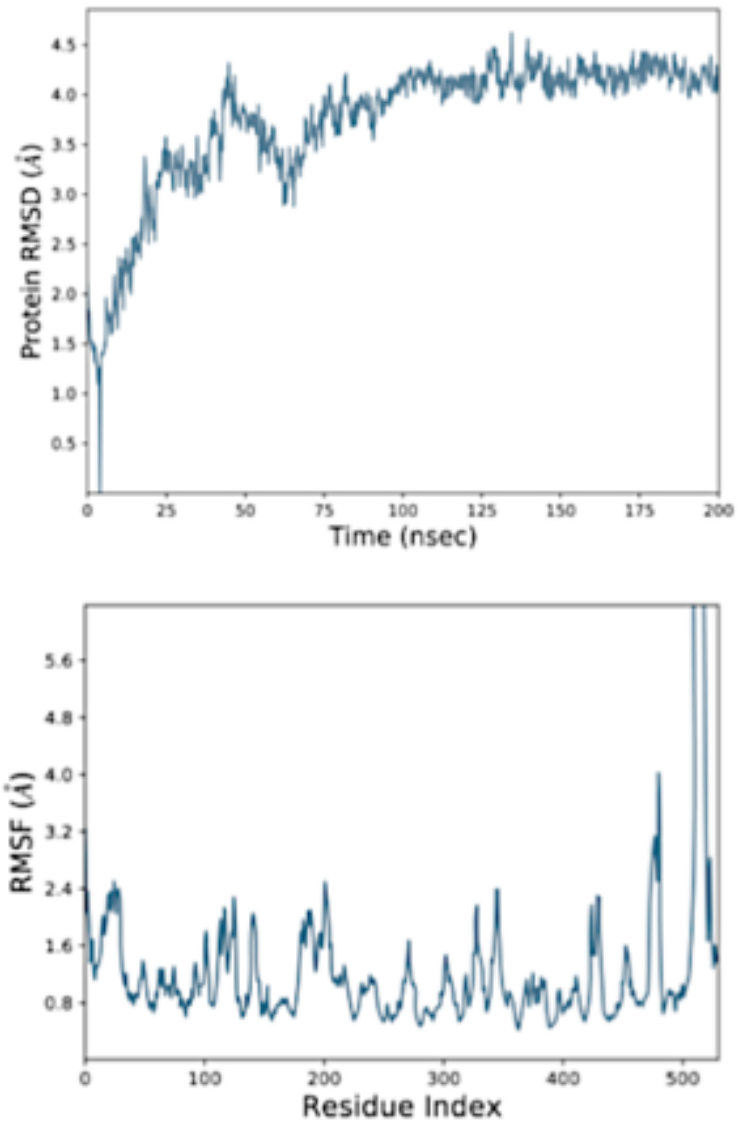

Figure 7-6: The monomeric model of MLE was submitted to 200 ns simulation, reaching structural stability after 50 ns, by the structural rearrangement of the carboxyl-term. (A) RMSD values show the conformational stability of MLE; (B) Conformational changes of MLE with the corresponding RMSF values.

S 4-2 Interactions and contacts of MLE with MAL− and MAL2−

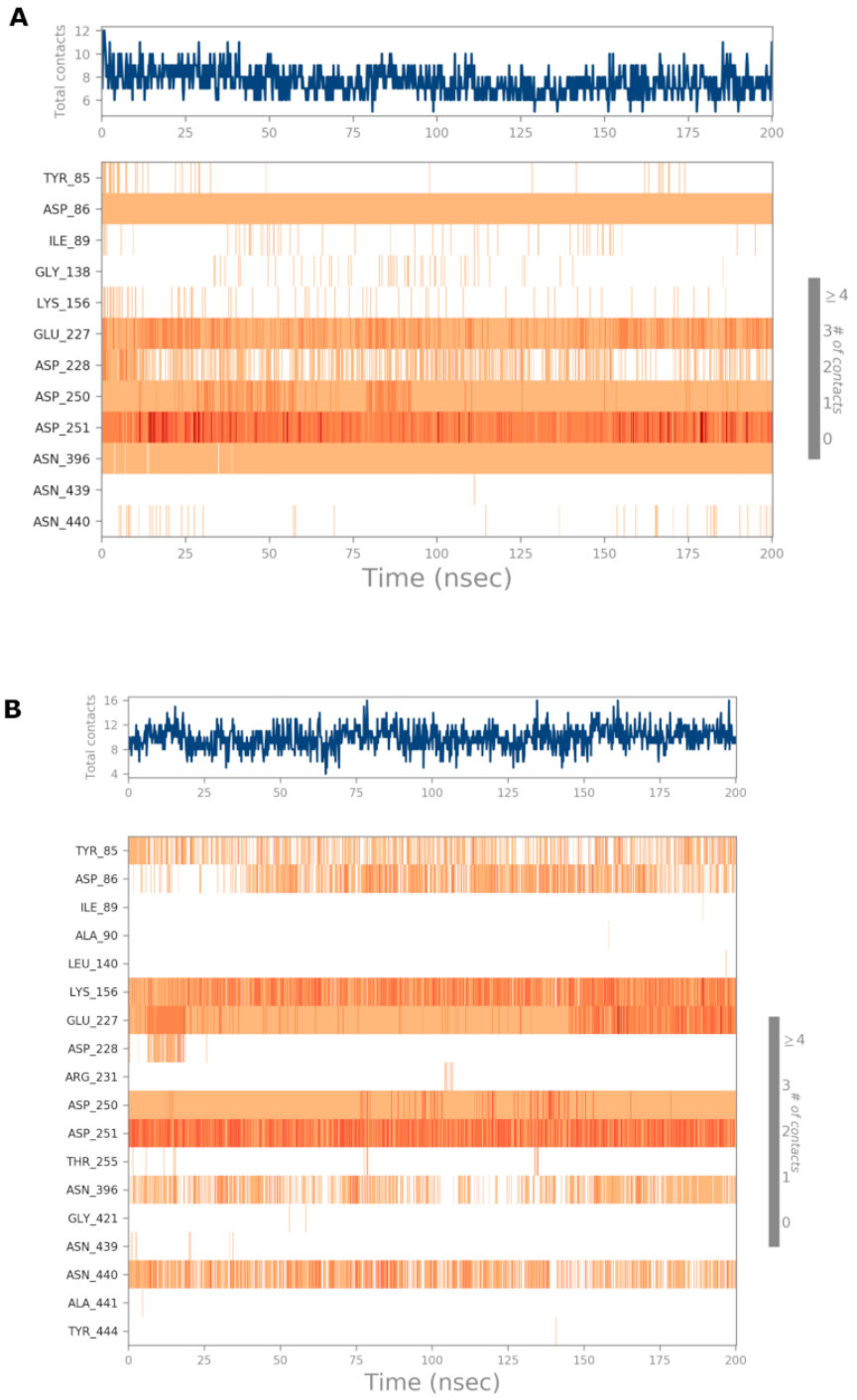

Figure 7-7: Interactions and contacts of MLE with MAL− (A) and MAL2− (B). The total number of interactions is depicted on the upper panels, while bottom panels show residues that interact with the ligand in each trajectory frame.

S 4-3 pET28a-MLE expression vector

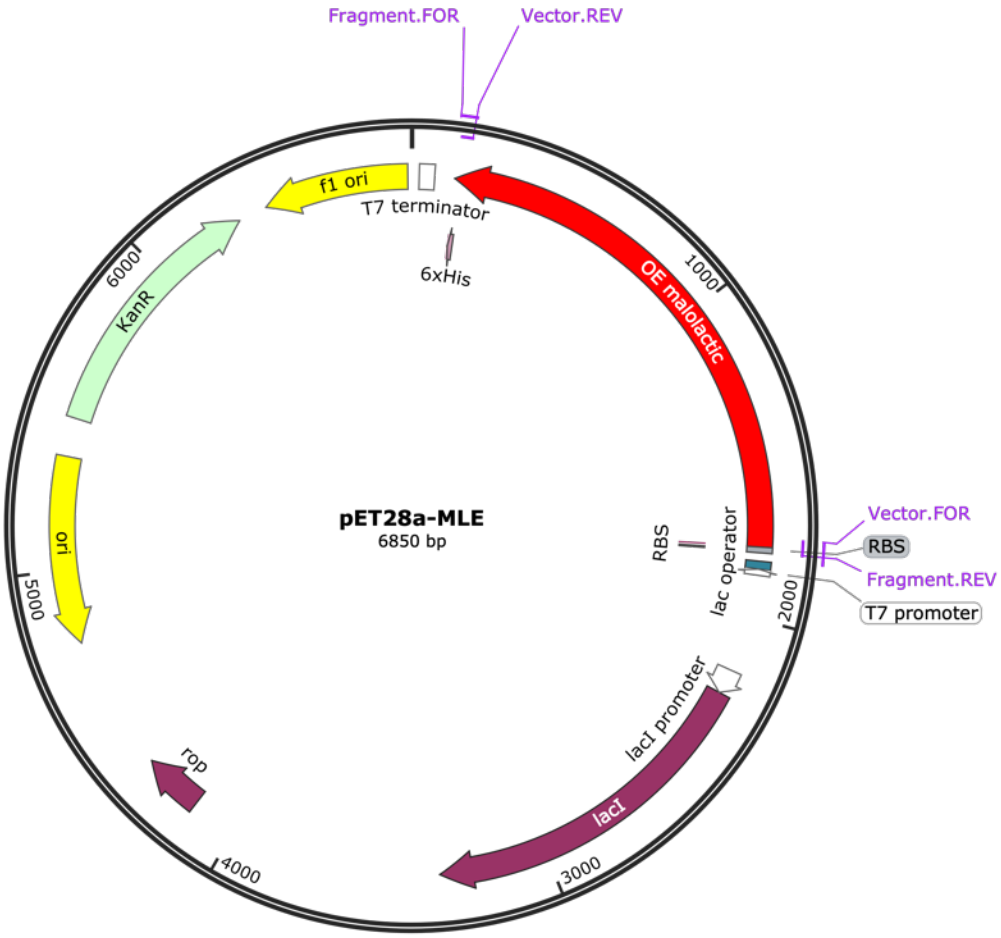

Figure 7-8: Map of pET28a-MLE expression vector. The purple solid arrow indicates the site of MLE gene of *O. oeni* strain DSM 20255 (OE malolactic).